Performance evaluation of a low-emissions stove using a biomass and coal blend

M Maass

orcid.org/ 0000-0003-0541-7078

Dissertation accepted in fulfilment of the requirements for the degree *Master of Engineering in Chemical Engineering* at the North-West University

Supervisor:	Prof HWJP Neomagus
Co- Supervisor:	Prof JR Bunt
Co- Supervisor:	Dr FH Conradie

Graduation: April 2024

DECLARATION

I, Maritz Maass, hereby declare that this dissertation titled: ”Performance evaluation of a low-emissions stove using a biomass and coal blend”, submitted in fulfilment of the requirements for the degree Master of Chemical Engineering, is my own work and that where the published work of others has been consulted, appropriate references have been provided. Furthermore, this work has not been submitted to any other tertiary institution, and copies submitted for examination are the property of the University.

ABSTRACT

Anthropogenic activities, particularly coal combustion for industrial and domestic purposes, contribute significantly to air pollution, posing severe health risks. In developing countries like South Africa, indoor air pollution from coal combustion is a pressing concern. Identified pollutants from coal combustion include particulate matter (PM), carbon oxides (CO_x), nitrogen oxides (NO_x), and sulphur dioxide (SO_2). A significant global population relies on solid fuels like coal for energy, especially in rural South Africa. Transitioning to cleaner energy sources and advanced stove technologies is crucial to mitigate health risks associated with domestic coal combustion, as studies reveal challenges in reducing emissions even with improved designs of open fires and braziers.

The NWU semi-continuous stove underwent combustion experiments using coal discards and torrefied wood blended extrudates under high-power and low-power conditions. Higher biomass content in fuels leads to decreased ignition times in both high and low-power experiments. High-power settings accelerate combustion, resulting in shorter ignition times. Burn rates increased with increased biomass content in pellets. 0% biomass pellets displayed an average burn rate of 23 g/min, and 100% biomass pellets displayed an average burn rate of 77 g/min. The stove shows higher biomass consumption rates but maintains similar coal consumption rates compared to other stoves. Power output increases with biomass content, mainly corresponding to higher burn rates. 0% biomass pellets displayed a peak power output of 10 kW, and 100% biomass pellets displayed a peak power output of 30 kW. Differences from similar research on coal stoves are attributed to stove design and fuel characteristics. The mass of fuel needed to raise water temperature increases with biomass content in high-power experiments but decreases beyond 50% in low-power experiments. Cooking efficiencies, the ratio between the energy output of the stove and energy absorbed by the cooking pot, ranged from 1.5% to 5.5%. An inverse relationship between the energy output during the cooking phase and cooking efficiency was observed, indicating diminishing returns at higher energy outputs. System efficiency decreases with increasing biomass content, and it is sensitive to combustion dynamics and excess oxygen in high-power experiments. The system efficiency ranged from 77% to 96%. Low-power experiments generally displayed higher system efficiency.

In high-power experiments, CO and CO_2 emission factors were higher compared to low-power experiments, decreasing with pellets with low biomass content and increasing with higher biomass content. CO emission factors ranged from 0.9 g/MJ to 4.4 g/MJ, and CO_2 emission factors ranged from 87 g/MJ to 97 g/MJ. NO_x emission factors decreased with decreasing nitrogen content in the fuel. NO_x emissions also decreased at high temperatures, attributed to flue gas

recycling reducing NO_x through reactions with hydrocarbons. NOx emission factors ranged from 0.03 g/MJ to 0.11 g/MJ. SO_2 emission factors initially decreased with biomass content up to 50%, then increased due to limited reactions with calcium species in the parent coal, decreasing sulphur retention. Low-power experiments generally exhibited lower SO_2 emission factors. SO_2 emission factors ranged from 0.11 g/MJ to 0.22 g/MJ. The particulate matter emissions initially decreased with biomass addition and increased with higher biomass content, with high-power experiments showing higher PM emissions influenced by flue gas velocity and weak pellet integrity. PM emission factors ranged from 0.04 g/MJ to 5.2 g/MJ.

The NWU semi-continuous stove effectively burned blended fuel with up to 25% biomass.

Keywords: Emission offsets, Biomass, Coal, Co-combustion, Pellets, Semi-continuous, Low-emissions stove

ACKNOWLEDGEMENTS

- My supervisors, Prof. Hein Neomagus, Prof. John Bunt, and Dr. Frikkie Conradie, for their advice, guidance, and moral support.
- A special thanks to Prof. Hein Neomagus for spending many hours proofreading this report and meeting with me over weekends.
- My former supervisor Prof. Burgert Hattingh, for crucial advice and guidance.
- Prof. Hattingh's UETS strategic funds and Prof. Bunt's SARChI chair for funding this project.
- Ms René Bekker for conducting various analyses on the raw materials used in this study.
- Sasol for their financial support during my studies.

CONFERENCES

Part of this work was presented at the Forum on Renewable Energy Promotion in Developing Countries (2022) hosted by China Agricultural University. The virtual conference was held on 22 September 2022 on a virtual platform.

TABLE OF CONTENTS

CHAPTER 1: INTRODUCTION 1

1.1 Background and Rationale 1

1.1.1 Significance of coal 1

1.1.2 Health concerns 2

1.1.3 Clean cook stove technology 3

1.1.4 Transition to biomass 3

1.1.5 Torrefaction 4

1.1.6 Coal and biomass waste 5

1.2 Research problem, Objectives, and Scope 7

1.2.1 Aim and Objectives 7

1.3 Scope 7

CHAPTER 2: LITERATURE REVIEW 9

2.1 Coal Consumption (Industrial versus Domestic) 9

2.2 Properties of Coal 9

2.3 Properties of Wood/Biomass 10

2.4 Co-firing of Biomass and Coal 11

2.4.1 Emissions from Blended Fuel Stock 12

2.4.2 Blending Ratios 12

2.5 Torrefaction of Wood 13

2.5.1 Advantages of torrefaction 13

2.5.2 Cost of Torrefaction 14

2.6 Combustion in Household Devices 15

2.6.1 Stove classification 15

2.6.2 Ignition methods for domestic combustion devices 17

2.6.3 Requirements for household combustion 18

2.7 Measuring of Stove Emissions 20

2.7.1 Hood-method 20

2.7.2 Dilution Tunnel Method 20

2.8 Thermal Efficiency of Domestic Stoves 21

2.8.1 Water boiling test 21

2.9 Formation of Pollutants during Combustion 22

2.9.1 Gaseous pollutants 22

2.9.2 Formation of particulate matter 26

2.9.3 Summary of Pollutants Formation 27

CHAPTER 3: MATERIAL PREPARATION AND CHARACTERISATION 28

3.1 Materials 28

3.2 Sample Preparation 29

3.2.1 Coal preparation 29

3.2.2 Biomass Preparation 29

3.2.3 Blending 32

3.2.4 Pelletisation of blends 32

3.3 Chemical and Physical analysis 34

3.4 Characterisation Results 35

3.4.1 Coal Characterisation 35

3.4.2 Biomass Characterisation 38

3.4.3 Pellet Characterisation 41

3.5 Summary 45

CHAPTER 4: EXPERIMENTAL METHODS FOR COMBUSTION TESTS 47

4.1 Materials 47

4.2 Stove Characterisation and Operation 48

4.2.1 Characterisation of stove 48

4.2.2 Stove Operation 48

4.3 Experimental Setup and Data Acquisition Procedures 50

4.3.1 Standard Operating Procedures 51

4.3.2 Emissions Monitoring 53

4.3.3 Temperature monitoring 54

4.3.4 Mass monitoring 55

4.4 Data Processing and Analysis 56

4.4.1 Thermal Performance 56

4.4.2 Emissions Performance 60

CHAPTER 5: RESULTS AND DISCUSSION 63

5.1 Stove Operation 63

5.1.1 Fuel Consumption and Run-time 63

5.1.2 Flue gas velocity 64

5.1.3 Stove Temperature 65

5.1.4 Observed Flue Gas Composition 71

5.1.5 Combustion Temperature and $CO/SO_2/NO_x$ Concentration 74

5.2 Thermal Performance 76

5.2.1 Ignition Times 76

5.2.2 Fuel Burning Rates and Peak Temperatures 77

5.2.3 Power Output 79

5.2.4 Water Boiling Test 81

5.2.5 Energy Efficiencies 82

5.3 Emissions Performance 85

5.3.1 CO and CO_2 Emission Factors 85

5.3.2 NO_x Emission Factors 88

5.3.3 SO_2 Emission Factors 90

5.3.4 Particulate Matter Emission Factors 92

CHAPER 6: CONCLUSION AND RECOMMENDATIONS 95

6.1 Summary of Findings 95

6.2 Conclusion 97

6.3 Recommendations 98

APPENDIX A TORREFACTION PRE-TESTS 116

APPENDIX B PELLETISATION PRE-TESTS 119

APPENDIX C CARBON BALANCE 120

APPENDIX D MASS BALANCE 123

APPENDIX E ASH BEHAVIOUR 124

APPENDIX F EXPERIMENTAL UNCERTAINTY 126

APPENDIX G CALIBRATION CURVES 132

APPENDIX H COMBUSTION EXPERIMENT TEMPERATURE DATA 133

APPENDIX I OBSERVED FLUE GAS COMPOSTION 145

APPENDIX J COMBUSTION TEMPERATURE AND CO/SO_2/NO_X 151

LIST OF TABLES

Table 3-1: Material and equipment list 28

Table 3-2: Particle size distribution of wood chips 30

Table 3-3: Instrument list of Torrefaction rig 31

Table 3-4: Coal – Biomass blend ratios 32

Table 3-5: Overview of analyses 34

Table 3-6: Proximate analysis of parent coal (a.d) 35

Table 3-7: Ultimate analysis of parent coal (d.a.f) 35

Table 3-8: Calorific value of parent coal (a.d) 36

Table 3-9: XRD analysis of parent coal 37

Table 3-10: Summary of XRF analysis of parent coal 38

Table 3-11: Proximate analysis of raw pine wood and torrefied pine wood (a.d) 39

Table 3-12: Ultimate analysis of raw pine wood and torrefied pine wood (d.a.f) 40

Table 3-13: Calorific value of raw wood and torrefied wood (a.d) 40

Table 3-14: Summary of fibre analysis conducted on biomass and torrefied biomass 41

Table 3-15: Summary of analysis on pellet blends 45

Table 4-1: Materials used during combustion experiments 47

Table 4-2: Component list of NWU semi-continuous stove 49

Table 4-3: Instrument list of stove experimental setup 50

Table 5-1: Average flue gas volumetric flowrate and velocity of pellets through the chimney 64

Table 5-2: Ignition times of pellets at high- and low-power 76

Table 5-3: Water boiling test results 81

Table 5-4: Thermal efficiencies of pellet blends 83

Table 5-5: CO_2 and CO emission factors of pellets 86

Table 5-6: Summary of CO and CO_2 emission factors from literature 87

Table 5-7: NO_x emission factors of pellets 89

Table 5-8: Summary of NO_x emission factors from literature 89
Table 5-9: SO_2 emission factors of pellets 91
Table 5-10: Summary of SO_2 emission factors from literature 91
Table 5-11: PM_{10} emission factors of pellets 93
Table 5-12: Summary of PM emission factors from literature 94

Table A-1: Valve and instrument list of pyrolysis oven 117
Table A-2: Residence time and mass loss correlation 118

Table B-1: Compressive strength of drum coal pellets and coal extrudates 119

Table C-1: Carbon balance over the fuel, ash, and flue gas example 122

Table D-1: Mass balance recovery through flue 123

Table E-1: Proximate analysis of pellet ash post-combustion (d.b) 125
Table E-2: Mass unreacted carbon in post-combustion ash for each pellet blend 125

Table F-1: Ignition times of repeated experiments 128
Table F-2: Water boiling test times of repeated experiments 129
Table F-3: Deviation of CO_2 emission factors 129
Table F-4: Deviation of CO emission factors 130
Table F-5: Deviation of SO_2 emission factors 130
Table F-6: Deviation of NO_x emission factors 130
Table F-7: Deviation of PM emission factors 131

Table G-1: Calibration data of two consecutive experiments 132

LIST OF FIGURES

Figure 1-1: NWU semi-continuous stove (Designed by Mr. Crispin Pemberton-Pigott)..... 8

Figure 2-1: Heat transfer mechanism: A) Conduction; B) Radiation; C) Convection 17

Figure 2-2: Ignition methods: A) BLUD; B) TLUD 18

Figure 2-3: Combustion triangle 19

Figure 2-4: Reaction routes for the formation of sulphur (Adapted from Fleig et al., 2009) 24

Figure 2-5: Combustion products of coal 27

Figure 3-1: Sample preparation overview 29

Figure 3-2: Torrefaction rig schematic 31

Figure 3-3: Picture of extrudates 33

Figure 3-4: Proximate analysis of pellet blends (a.d) 42

Figure 3-5: Ultimate analysis of pellet blends 43

Figure 3-6: Calorific value of pellet blends 43

Figure 3-7: Compressive strength of pellet blends 44

Figure 4-1: a) Stove drawing b) Grate 48

Figure 4-2: Stove experimental setup schematic 50

Figure 4-3: Thermocouple placement in stove 54

Figure 5-1: Fuel consumption as a function of combustion time and pellet composition (High-power experiments) 63

Figure 5-2: Fuel consumption as a function of combustion time and pellet (Low-power experiments)…….. 64

Figure 5-3: Combustion chamber temperatures (0% biomass, high-power experiment) 65

Figure 5-4: Combustion chamber temperatures (100% biomass, high-power experiment) 66

Figure 5-5: Hopper temperatures (0% biomass, high-power experiment) 68

Figure 5-6: Hopper temperatures (100% biomass, high-power experiment) 68

Figure 5-7: Combustion chamber temperatures (0% biomass, low-power experiment)..... 69

Figure 5-8: Hopper temperatures (0% biomass, low-power experiment) 70

Figure 5-9: CO_2, O_2, and CO concentrations over time (0% biomass, high-power experiment)…….. 71

Figure 5-10: CO_2, O_2, and CO concentrations over time (0% biomass, low-power experiment)…….. 72

Figure 5-11: CO_2, O_2, and CO concentrations over time (90% biomass, high-power experiment)……..... 73

Figure 5-12: CO concentration and combustion zone temperature over time (0% biomass, high-power experiment)..... 74

Figure 5-13: SO_2 concentration and combustion zone temperature over time (0% biomass, high-power experiment)..... 74

Figure 5-14: NO_x concentration and combustion zone temperature over time (0% Biomass, High-power experiment)..... 75

Figure 5-15: Burn rates of pellet blends during high-power and low-power experiments..... 77

Figure 5-16: Peak temperatures of pellet blends during high-power and low-power experiments……..... 77

Figure 5-17: Power output of pellet blends versus mass loss (a.f.b), High-power experiments…….. 79

Figure 5-18: Power output of pellet blends versus mass loss (a.f.b), Low-power experiments…….. 80

Figure 5-19: System efficiency of pellets during high-power combustion experiments (a.f.b)…….. 82

Figure 5-20: CO_2 emission factors of pellet blends (g/MJ) 85

Figure 5-21: CO emission factors of pellet blends (g/MJ) 86

Figure 5-22: NO_x emission factors of pellet blends (g/MJ) 88

Figure 5-23: SO_2 emission factors of pellet blends (g/MJ) 90

Figure 5-24: PM emission factors of pellet blends (g/MJ) 92

Figure A-1: Schematic of pyrolysis oven..... 116

Figure A-2: DTG analysis of raw pine sawdust..... 117

Figure A-3: Mass loss of raw pine sawdust during TGA..... 118

Figure C-1: dm/dt raw data 120
Figure C-2: Mass carbon consumption rate of fuel 120
Figure C-3: Mol carbon consumption rate of fuel 121
Figure C-4: Mol flow rate of flue gas 121
Figure C-5: Molar flow rates of CO_2, CO, NO_x, and SO_2 in flue gas 122

Figure E-1: Ash tray after high-power combustion experiments using 0%, 25%, and 75% biomass pellets…… 124

Figure F-1: Fuel consumption of 10% biomass pellets as a function of time at high-power 126
Figure F-2: Fuel consumption of 10% biomass pellets as a function of time at low-power 126
Figure F-3: Fuel bed temperature of high-power experiment using 0% biomass pellets. 127
Figure F-4: Power output of 0% biomass pellets over mass loss (a.f.b) 128

Figure H-1: Combustion chamber temperatures (0% biomass, high-power experiment)..... 133
Figure H-2: Combustion chamber temperatures (0% biomass, Low-power experiment)..... 133
Figure H-3: Combustion chamber temperatures (10% biomass, high-power experiment)..... 134
Figure H-4: Combustion chamber temperatures (10% biomass, low-power experiment) 134
Figure H-5: Combustion chamber temperatures (25% biomass, high-power experiment)..... 135
Figure H-6: Combustion chamber temperatures (25% biomass, low-power experiment) 135
Figure H-7: Combustion chamber temperatures (50% biomass, high-power experiment)..... 136
Figure H-8: Combustion chamber temperatures (50% biomass, low-power experiment) 136
Figure H-9: Combustion chamber temperatures (75% biomass, high-power experiment)..... 137
Figure H-10: Combustion chamber temperatures (75% biomass, low-power experiment) 137
Figure H-11: Combustion chamber temperatures (90% biomass, high-power experiment).... 138
Figure H-12: Combustion chamber temperatures (90% biomass, low-power experiment) 138
Figure H-13: Hopper temperatures (0% biomass, high-power experiment)..... 139
Figure H-14: Hopper temperatures (0% biomass, low-power experiment) 139

Figure H-15: Hopper temperatures (10% biomass, high-power experiment)..... 140
Figure H-16: Hopper temperatures (10% biomass, low-power experiment)..... 140
Figure H-17: Hopper temperatures (25% biomass, high-power experiment)..... 141
Figure H-18: Hopper temperatures (25% biomass, low-power experiment)..... 141
Figure H-19: Hopper temperatures (50% biomass, high-power experiment)..... 142
Figure H-20: Hopper temperatures (50% biomass, low-power experiment)..... 142
Figure H-21: Hopper temperatures (75% biomass, high-power experiment)..... 143
Figure H-22: Hopper temperatures (75% biomass, low-power experiment)..... 143
Figure H-23: Hopper temperatures (90% biomass, high-power experiment)..... 144
Figure H-24: Hopper temperatures (90% biomass, low-power experiment)..... 144

Figure I-1: CO_2, O_2, and CO concentrations over time (0% biomass, high-power experiment)…….. 145
Figure I-2: CO_2, O_2, and CO concentrations over time (0% biomass, low-power experiment)…… 145
Figure I-3: CO_2, O_2, and CO concentrations over time (10% biomass, high-power experiment)…… 146
Figure I-4: CO_2, O_2, and CO concentrations over time (10% biomass, low-power experiment)……..... 146
Figure I-5: CO_2, O_2, and CO concentrations over time (25% biomass, high-power experiment)……..... 147
Figure I-6: CO_2, O_2, and CO concentrations over time (25% biomass, low-power experiment)……..... 147
Figure I-7: CO_2, O_2, and CO concentrations over time (50% biomass, high-power experiment)…… 148
Figure I-8: CO_2, O_2, and CO concentrations over time (50% biomass, low-power experiment)……..... 148
Figure I-9: CO_2, O_2, and CO concentrations over time (75% biomass, high-power experiment)……..... 149

Figure I-10: CO_2, O_2, and CO concentrations over time (75% biomass, low-power experiment)……..... 149

Figure I-11: CO_2, O_2, and CO concentrations over time (90% biomass, high-power experiment)…….. 150

Figure I-12: CO_2, O_2, and CO concentrations over time (90% biomass, low-power experiment)…….. 150

Figure J-1: CO, SO_2, and NO_x concentration and combustion zone temperature over time (0% biomass, high-power experiment) 151

Figure J-2: CO, SO_2, and NO_x concentration and combustion zone temperature over time (0% biomass, low-power experiment)..... 152

Figure J-3: CO, SO_2, and NO_x concentration and combustion zone temperature over time (10% biomass, high-power experiment) 153

Figure J-4: CO, SO_2, and NO_x concentration and combustion zone temperature over time (10% biomass, low-power experiment)..... 154

Figure J-5: CO, SO_2, and NO_x concentration and combustion zone temperature over time (25% biomass, high-power experiment) 155

Figure J-6: CO, SO_2, and NO_x concentration and combustion zone temperature over time (25% biomass, low-power experiment)..... 156

Figure J-7: CO, SO_2, and NO_x concentration and combustion zone temperature over time (50% biomass, high-power experiment) 157

Figure J-8: CO, SO_2, and NO_x concentration and combustion zone temperature over time (50% biomass, low-power experiment)..... 158

Figure J-9: CO, SO_2, and NO_x concentration and combustion zone temperature over time (75% biomass, high-power experiment) 159

Figure J-10: CO, SO_2, and NO_x concentration and combustion zone temperature over time (75% biomass, low-power experiment)..... 160

Figure J-11: CO, SO_2, and NO_x concentration and combustion zone temperature over time (90% biomass, high-power experiment) 161

Figure J-12: CO, SO_2, and NO_x concentration and combustion zone temperature over time (90% biomass, low-power experiment)..... 162

LIST OF ABBREVIATIONS

Abbreviation	Description
BMMS	Brick Management and Manufacturing Supplies
BLUD	Bottom lit up-draft
CV	Calorific value
GHG	Greenhouse gas
HHV	Higher heating value
LHV	Lower heating value
NWU	North-West University
PAHs	Poly-aromatic hydrocarbons
PM	Particulate matter
PVA	Polyvinyl alcohol
TGA	Thermogravimetric analysis
TLUD	Top lit up-draft
VOCs	Volatile organic compounds

CHAPTER 1: INTRODUCTION

1.1 Background and Rationale

1.1.1 Significance of coal

Coal is the world's most utilised energy source, primarily due to its abundant availability and high carbon content, making it the leading fossil fuel in global energy production (WCA, 2021). In South Africa, coal is significant among the array of energy sources, alongside crude oil, renewables, natural gas, and nuclear power. Coal accounts for 65% of the country's primary energy supply (Department of Energy, 2021), emphasising its vital role in the nation's energy landscape.

Globally, approximately 1.4 billion people, with a significant portion residing in Africa, lack access to electricity. These communities, often marginalised and underserved, rely on traditional energy sources for their basic needs (Makonese *et al.*, 2018). Coal, owing to its affordability and high energy output, remains a lifeline in such areas, enabling heat generation and cooking activities, especially in regions where alternatives are scarce or financially unfeasible (Buthelezi *et al.*, 2019; Munawer, 2018).

Within South Africa, coal's influence extends deeply into the domestic sphere, constituting 7% of the total energy consumption in 2018 (Department of Energy, 2019). This extensive reliance is particularly notable in rural areas where coal serves as a preferred fuel for heating, mainly due to its widespread availability and cost-effectiveness. These areas are typically close to coal mines. Notably, informal settlements in South Africa heavily rely on coal or wood for both heating and cooking purposes, underscoring its indispensable role in everyday life (Adesina *et al.*, 2022).

The extensive use of coal raises environmental concerns, particularly in industrial applications where large quantities are consumed, contributing significantly to air pollution and greenhouse gas emissions. Domestic use of coal is substantially less than industrial use, making the environmental impact relatively smaller (Department of Energy, 2021). Despite this, domestic coal use profoundly impacts human health, leading to concerns about air quality and related health issues (Barnes *et al.*, 2006). As discussions around climate change and environmental sustainability intensify, addressing the significant health implications of domestic coal use becomes an aspect of fostering a healthier environment for communities. Consequently, alongside the pursuit of renewable energy sources, there is a pressing need to prioritise solutions that improve indoor air quality and safeguard human well-being, especially in regions heavily reliant on coal for domestic purposes (Adesina *et al.*, 2022).

1.1.2 Health concerns

Anthropogenic activities, particularly coal combustion for both industrial and domestic purposes, significantly contribute to air pollution, posing grave risks to human health (Kampa & Castanas, 2008). Indoor air pollution, especially from coal combustion, remains a pressing concern, particularly in developing countries like South Africa. Although domestic coal combustion is vital for heating and cooking in rural South Africa, it releases combustion gases, contributing significantly to indoor air pollution (Thurston, 2022; Zhou *et al.*, 2020). Despite WHO guidelines specifying $PM_{2.5}$ and PM_{10} concentrations not exceeding 5 µg/m^3 and 10 µg/m^3 annually (WHO, 2021a), South Africa exceeds these levels regularly, posing severe health risks (Adesina *et al.*, 2022). Millions face premature deaths from illnesses caused by indoor air pollution from solid fuel combustion in South Africa and other developing countries (WHO, 2021b).

The World Health Organization (WHO) has identified key pollutants arising from coal combustion, including particulate matter (PM), carbon oxides (CO_x), nitrogen oxides (NO_x), sulphur dioxide (SO_2), and volatile organic compounds (VOCs) (Kampa & Castanas, 2008; WHO, 2021b). PM, a diverse mixture of suspended particles, contains minerals, organic materials, biological substances, reactive gases, and carbon, with fine and ultrafine particles capable of reaching lung alveoli, causing severe cardiovascular and respiratory problems (Kampa & Castanas, 2008). Carbon oxides heighten the risks of diseases like malaria and cardiovascular diseases, which are prevalent in malaria-prone regions of South Africa (Munawer, 2018). NO and NO_2, significant nitrogen oxides, are linked to increased cardiovascular mortality upon chronic exposure (Lippmann & Leikauf, 2020). Nitrogen oxide exposure in infants can lead to methemoglobinemia and potentially cancer (Hakeem et al., 2016), while SO_2 in the air causes breathing difficulties, asthma, and increased mortality rates (Khaniabadi *et al.*, 2017). VOCs in ambient air pose severe health risks, such as damage to the liver, kidneys, and nervous system. Less severe symptoms include eye and nose irritation and headaches (Kampa & Castanas, 2008).

A substantial global population relies on solid fuels, including coal, for energy, utilising conventional devices such as open fires and braziers (Barnes *et al.*, 2006). Studies in rural South Africa show over 98% reliance on biomass and coal combustion for energy, using basic open fires and coal-burning braziers, which emit high levels of pollutants (Makonese *et al.*, 2017a). Comparisons between basic and improved open fires reveal that while improved designs emit less smoke, reducing emissions persists, underlining the need for cleaner technologies (Ballard-Tremeer & Jawurek, 1996). These findings underscore the importance of transitioning to cleaner energy sources and advanced technologies to mitigate the significant health risks associated with domestic coal combustion.

1.1.3 Clean cookstove technology

Enhancing fuel ignition procedures, selecting appropriate fuel types, and employing improved stove designs play a pivotal role in mitigating the effects of emissions on human health, especially in regions heavily reliant on domestic coal combustion (WHO, 2021b; World Bank, 2014, 2015).

Implementing advanced ignition techniques and selecting cleaner fuel options decrease the emission of harmful pollutants such as PM, CO_x, NO_x, SO_2, and VOCs (Glasius *et al.*, 2006; Nussbaumer, 2003; Ozgen *et al.*, 2014). These measures result in lower indoor air pollution levels, ensuring a healthier living environment for households. Cleaner fuel-burning methods and optimised stove designs reduce particles and toxic gases released during combustion (Glasius *et al.*, 2006; Ozgen *et al.*, 2014). By minimising exposure to these pollutants, individuals, especially vulnerable populations like children and the elderly, experience fewer respiratory problems, including asthma and chronic obstructive pulmonary disease (COPD) (Neuberger *et al.*, 2004).

Advanced stove designs optimise the combustion process, ensuring more efficient and complete burning of fuels (Nussbaumer, 2003). This efficiency reduces the emission of harmful by-products, improving indoor air quality. Ventilation mechanisms further aid in dispersing residual pollutants, making indoor spaces safer for occupants (Penttinen *et al.*, 2001). Homes with these improvements are less prone to illnesses related to indoor air pollution, leading to reduced healthcare expenses and an overall improvement in their quality of life (Brandelet *et al.*, 2018; Neuberger *et al.*, 2004; Penttinen *et al.*, 2001). These improvements are particularly relevant in communities with limited access to medical facilities.

Clean stove technology is a potential solution to mitigate the pollution caused by solid fuel combustion in rural developments worldwide. The issues associated with conventional cooking devices used in rural villages and urban households are mitigated by researching various stove designs. These designs are specifically designed for a region and purpose (fuel availability, cooking, space heating, etc.) (Taylor, 2009). Tailoring ignition techniques, fuel choices, and stove designs to specific regional needs ensures a customised approach to minimising emissions. By understanding local preferences and lifestyles, interventions can be designed to effectively address the unique challenges faced by different communities, making the adoption of cleaner technologies more practical and sustainable (Ahmed *et al.*, 2019; Njenga *et al.*, 2016; Prasad *et al.*, 1985).

1.1.4 Transition to biomass

While the long-term goal remains the phasing out of non-renewable coal, interim strategies are imperative to mitigate the environmental and health impact of coal combustion. A promising transitional solution involves co-firing coal with biomass, marking a shift towards renewable energy

sources. Unlike coal, biomass is renewable and offers a sustainable alternative for domestic combustion uses (Durix *et al.*, 2016; Sh *et al.*, 2019; World Bank, 2014).

Combining coal with biomass presents a potential mitigation strategy. Studies by Ahn et al., (2014); Hein & Bemtgen, (1998); Madanayake et al., (2017); Mock et al., (2017); Sahu et al., (2014); Sami et al., (2001); Sondreal et al., (2001) indicate that co-firing results in reduced emissions of sulphur oxides (SO_x) and nitrogen oxides (NO_x) during combustion, thus lessening the potential impact on both the environment and human health.

Moreover, research by Zhang et al., (2022) demonstrates that incorporating biomass into coal combustion inhibits particulate matter (PM) production, further enhancing the environmental benefits of this approach. Wood, a common biomass source, proves preferable in specific regions due to its availability, while other forms, like animal dung, are also frequently used, depending on the region (Misra *et al.*, 2018). This transition decreases reliance on non-renewable resources and promotes the utilisation of sustainable biomass, paving the way for a greener and healthier future.

1.1.5 Torrefaction

Biomass often lags behind coal in calorific value for energy production, rendering coal more thermally efficient (Forest Research, 2022). This inherent disparity poses a challenge for the widespread use of biomass. However, a potential solution emerges in the form of torrefaction, a thermochemical process designed to enhance the chemical and physical properties of biomass (Tumuluru *et al.*, 2011).

Torrefaction involves subjecting biomass to mild temperatures, reducing its moisture and volatile content. Among its many advantages is that torrefaction increases the energy density of biomass (Galanakis, 2017). Studies, such as the one conducted by Maxwell et al., (2020), have confirmed the effectiveness of torrefaction in the energy densification of wood, a common biomass source.

This innovation holds promise and is actively being explored for large-scale implementation. Torrefying biomass has become a more viable and competitive option for domestic use (European Commission, 2016). Additionally, torrefaction simplifies biomass processing, making it more convenient and cost-effective. In essence, torrefaction addresses the calorific disparity between biomass and coal and streamlines biomass utilisation, making it a more efficient, accessible, and environmentally friendly energy source (Basu, 2018).

1.1.6 Coal and biomass waste

Coal waste

Coal processing operations generate substantial amounts of coarse and fine coal processing wastes due to in-seam and out-of-seam dilution mining practices. Clean coal recovery values typically range between 50% and 80% (Chugh & Behum, 2014), and these waste materials may contain trace metals and sulphur, potentially resulting in leachate water with corrosive characteristics (Fečko *et al.*, 2013). Adequate measures, such as liners, collection systems, and treatment processes, are necessary to manage water discharges and neutralise acid drainage. The production and quality of coal waste vary depending on mining or processing methods and long-term waste placement strategies. Practical, economical, and environmentally acceptable coal waste management necessitates a multidisciplinary approach, incorporating geology, soil mechanics, hydrology, hydraulics, geochemistry, soil science, agronomy, and environmental sciences (Chugh & Behum, 2014; Taha *et al.*, 2017).

On a global scale, coal mining activities for industrialisation result in massive waste stockpiles, exemplified by China stockpiling 5 billion tons (Taha *et al.*, 2017). Risks associated with coal waste include geotechnical instability, spontaneous combustion leading to explosions, acid generation affecting soil and water quality, air pollution causing ecosystem alterations, and visible impacts on landscape aesthetics (Walker, 1999). Closing coal mines, as seen in South Africa, can lead to illegal and unsafe mining activities with hazardous conditions (Brown, 2022). The prevalent hazards of fire in coal production and transport cycles, driven by natural oxidation and spontaneous combustion, pose substantial challenges (Taha *et al.*, 2017). The high cost of fire prevention and the potential for mine abandonment or loss of cargo at sea underscores the need for comprehensive detection, prevention, and control measures (Walker, 1999).

Wood waste

Waste sawdust is primarily generated by timber industries globally, with annual production reaching significant volumes. In the USA alone, approximately 3 million tons of sawdust are produced annually, often ending up in landfills (Mallakpour *et al.*, 2021). In South Africa, sawmills produce an estimated 376,000 tonnes of sawdust annually (Andrew *et al.*, 2016). Improper disposal of wood waste, primarily through open burning, poses serious health-related problems and environmental challenges (Kim & Song, 2014). Developing countries like Bangladesh and Pakistan face more severe consequences, leading to pollution when sawdust is burnt off (Batool *et al.*, 2021). Effective management of sawdust waste is a significant challenge worldwide, particularly in developing nations.

Sawdust, a by-product of woodworking operations, is a lignocellulosic compound abundantly obtained from sawing, planing, sanding, and wood milling (Mallakpour *et al.*, 2021). While historically used in livestock farms and paper mills, the disposal of sawdust without treatment into the surrounding environment is typical (Obata *et al.*, 2006). However, the versatile nature of sawdust has led to increased research and applications, covering various fields such as chemistry, pollution remediation, oil-water separation, activated carbon production, energy storage, fuel usage, bio-plastics production, cellulose nanocrystal extraction, and more (Mishra & Mohanty, 2018; Montiano *et al.*, 2013).

Recycling and reusing sawdust is pivotal in addressing waste treatment challenges and resource scarcity. The recycling of wood waste is particularly encouraged due to limited landfill space and restrictions on waste incineration (Obata *et al.*, 2006). Utilising wood as a renewable resource for products and energy production helps decrease environmental burdens, offering an alternative to virgin raw materials and reducing expenses related to logging, transportation, and disposal. Given the current environmental challenges, recycling methods for wood waste are deemed necessary for sustainable practices (Batool *et al.*, 2021; Obata *et al.*, 2006).

1.2 Research problem, Objectives, and Scope

The escalating issue of indoor air pollution in rural communities arises from the use of coal due to its cost-effectiveness and wide availability. Combustion of coal leads to the emission of hazardous pollutants, including carbon oxides (CO_x), nitrogen oxides (NO_x), sulphur dioxide (SO_2), and particulate matter (PM), posing severe health risks to inhabitants. Inefficient combustion processes contribute significantly to unintended emissions, like carbon monoxide (CO) and PM. The NWU semi-continuous stove has been developed to improve coal combustion efficiency. While emissions from efficient coal combustion are unavoidable, this study aims to explore the stove's adaptability towards fuel type by introducing wood as an alternative fuel. Wood combustion is known to produce fewer harmful emissions, making it a potential solution to mitigate indoor air pollution in rural communities and urban households. The study investigates the stove's performance when loaded with wood, evaluating its flexibility regarding fuel type and capability to reduce indoor air pollution associated with fossil fuel use.

1.2.1 Aim and Objectives

The study aims to investigate the effect of co-firing coal and torrefied wood fines, in pellet form, on the thermal and emissions performance of the NWU semi-continuous coal stove.

- Source a representative sample of waste coal fines and wood.
- Characterise the coal, raw wood, and torrefied wood.
- Investigate torrefaction conditions for raw pine wood.
- Evaluate and select a suitable agglomeration technique to produce fuel pellets with adequate integrity.
- Perform stove combustion experiments with the produced fuel pellets to evaluate the effect of different blending ratios and power ratings.
- Benchmark performance with previously used fuels and comment on the effectiveness of using biomass for the NWU semi-continuous stove.

1.3 Scope

This study investigates the effect of adding torrefied wood to coal on the emissions and thermal performance of the NWU semi-continuous stove. The study's primary goal is to determine the correlation between the biomass content of the fuel (pellets) and the emissions and thermal performance of the stove.

The raw materials are discarded grade D Highveld coal waste and pine woodchips from a paper mill. The report addresses the need to dispose of waste effectively by repurposing coal fines while

transforming a financial liability into a valuable resource. Furthermore, the adoption of low-quality coal aligns with similar investigations documented in literature, allowing for meaningful result comparisons (Guo *et al.*, 2022; Kalembkiewicz & Chmielarz, 2012; Paraschiv *et al.*, 2020; Vershinina *et al.*, 2021).

The woodchips are torrefied to increase energy density and crushability. The entire sample is torrefied in the same batch to ensure uniform composition throughout the entire sample. The coal and torrefied wood are mixed into blends ranging from 0 – 100 wt% biomass, and the mixtures are pelletised.

Thermogravimetric analysis is conducted on the wood to determine the operating conditions of the torrefaction process. The wood is characterised before and after torrefaction to investigate the effect of torrefaction on the wood.

Combustion experiments are conducted on the NWU semi-continuous stove using the produced pellets. The emissions and thermal efficiency resulting from the combustion of the fuel blends are compared and used to comment on the stove's flexibility regarding fuel type. The blended fuel's performance is compared to other domestic fuels used in literature.

Figure 1-1: NWU semi-continuous stove (Designed by Mr. Crispin Pemberton-Pigott)

CHAPTER 2: LITERATURE REVIEW

2.1 Coal Consumption (Industrial versus Domestic)

Coal remains the largest source of electricity generation globally, maintaining its dominance in the energy landscape. However, its utilisation extends beyond electricity production, playing a vital role in industrial applications such as steel, cement, and petrochemical industries (WCA, 2021).

Industrial coal consumption is necessary for many production processes. Because of its stability and dependability, coal remains the primary fuel source for global energy production. Approximately 72% of the country's primary energy needs are met by coal (Eskom, 2021). While the cement industry depends on coal for high-temperature requirements, the steel sector largely depends on it for smelting and coke manufacturing. 70% of the world's steel production relies on coal, and roughly 60% of the energy required for aluminium production is produced from coal (WCA, 2021). The petrochemical sector also uses coal as a feedstock and energy source (Department of Energy, 2019, 2021).

In domestic areas with few options, coal is utilised to generate power for home purposes. However, its contribution is far less than for industrial purposes. Traditional use of coal in domestic areas is for heating and cooking. The coal used in various industries accounts for 98% of the total coal usage. Whereas domestic accounts for 2% on average (Department of Energy, 2019, 2021).

2.2 Properties of Coal

Coal is a combustible sedimentary rock used as a significant energy source for centuries. Understanding coal's properties, characteristics, and composition is necessary for efficient utilisation, environmental considerations, and technological advancements.

Coal can be classified into different types based on its geological origin and carbon content. The main types of coal are anthracite, bituminous, sub-bituminous, and lignite. The classification of coal is closely related to its rank, which is determined by the coalification process and the carbon content. Anthracite has the highest carbon content and is the highest rank of coal, while lignite has the lowest carbon content and is considered the lowest rank of coal (Bowen & Irwin, 2008; Kopp, 2022; Miller & Tillman, 2008; Roberts *et al.*, 2015; Zeng, 2009).

Coal primarily consists of two main components: inorganic minerals and organic carbonaceous macerals (Davidson, 1982; Kopp, 2022; Miller & Tillman, 2008). The organic macerals form the combustible part of the coal, while the inorganic minerals are incombustible.

The organic macerals are divided into vitrinite, liptinite, and inertinite. Macerals consist primarily of carbon, oxygen, hydrogen, and small amounts of sulphur and nitrogen (Bowen & Irwin, 2008; Miller & Tillman, 2008). The maceral groups have different quantities of these primary components (Winans & Crelling, 1983). The maceral groups differ in origin and rank (Davidson, 1982). The chemical properties, physical properties, and reactivity of the various coal macerals change as the rank of the coal changes (Winans & Crelling, 1983).

The inorganic component of coal consists of a wide range of ash-forming minerals (Davidson, 1982; Miller & Tillman, 2008). These minerals mainly consist of Si, Al, and Fe, with trace elements that exclude C, H, O, N, and S. The inorganic substances can be classified into three types according to their origin: plant, detrital, and chemical. They can further be classified based on their environment and human health effects (Zeng, 2009).

Different physical and chemical traits that coal possesses impact how it is used. Calorific value, caking and swelling characteristics, grindability, and ash fusion temperature are a few of them. The calorific value of coal indicates its energy content and establishes its market value. Its caking and swelling qualities influence the behaviour of coal during combustion and its appropriateness for particular applications. The term "grindability" describes how easily coal can be ground, which impacts how effectively it can be pulverised. The temperature at which coal ash turns into molten slag during combustion is known as the "ash fusion temperature" (Bowen & Irwin, 2008; Davidson, 1982; Wagner, 2021; Winans & Crelling, 1983).

2.3 Properties of Wood/Biomass

Woody biomass, herbaceous biomass, biomass derived from straw, aquatic biomass, and waste biomass (like manure, sewage, and biological waste) can all be classified according to their unique features. Typically, the category to which a particular type of biomass belongs determines how it is used. The moisture content of the biomass has a significant role in determining the best energy conversion method. In general, biochemical processes like fermentation and anaerobic digestion are better suited for biomass with a high moisture content, such as waste and aquatic biomass. Herbaceous biomass has an intermediate moisture content, while woody biomass has the lowest (Di Blasi, 1997; Demirbas, 2004; Parmar, 2017).

Wood is primarily composed of cellulose, hemicellulose, lignin, and extractives. They contribute to the fibre properties of the wood, which impacts the fuel properties (Biorefinery Edu, 2018; Havstad, 2020).

Cellulose is the most abundant component of fibre wall and contributes to 40 – 45% of wood’s dry mass. Cellulose consists of linear chains of glucose bonded to a degree of polymerisation

(Biorefinery Edu, 2018; Brigham, 2018). The molecular structure of cellulose is responsible for its characteristic properties such as hydrophilicity, chirality, degradability, and chemical inconstancy instigated by the high reactivity of hydroxyl groups (Biorefinery Edu, 2018; Singh *et al.*, 2020).

Hemicellulose is a heterogeneous polymer that is comprised of different sugars. In some cases, it is the second most abundant component material in wood, depending on the amount of lignin, with a composition ranging from 25 – 35% dry weight of wood (Abu Ghalia & Dahman, 2017; Ahmad & Zakaria, 2019). Hemicellulose differs from cellulose in linearity and degree of polymerisation. Hemicellulose has a side group on the chain molecule and has a much lower degree of polymerisation than cellulose. Hemicellulose is amorphous (Biorefinery Edu, 2018; Patel & Parsania, 2018). The main hemicellulose in softwood is galactoglucomannans and arabinoglucuronoxylan, while the hemicellulose in hardwood is glucuronoxylans (Biorefinery Edu, 2018). Hardwood and softwood are not distinguished by their appearance or physical attributes. Generally, deciduous trees, which lose their leaves annually, are classified as hardwood and conifer trees as softwood, which remain evergreen. Hardwood is generally denser than softwood because deciduous trees have a lower growth rate than conifer trees (Middleton, 2020).

Lignin mainly consists of three kinds of alcohols: coumaryl, coniferyl, and sinapyl. These subunits together form the phenylpropanoid units (Kumar & Dixit, 2021). In some cases, lignin is the second most abundant component in plant mass, comprising 27 – 32% of the dry weight of wood (Calvo-Flores, 2020). Lignin is a class of hydrocarbon polymers consisting of aromatic and aliphatic structures. Lignin is an amorphous polymer with a high molecular weight (Abu Ghalia & Dahman, 2017).

Extractives in wood are natural products originating from lignocellulose cell walls. They are present in the cell walls but not chemically bonded to them. Extractives can be divided into three major subgroups: aliphatic compounds (fats and waxes), aromatic phenolic compounds, and terpenes and terpenoids (Chateigner-Boutin & Saulnier, 2022).

2.4 Co-firing of Biomass and Coal

Fossil fuel combustion has long been the primary energy source for power generation, transportation, and industrial processes. However, the burning of fossil fuels releases significant amounts of harmful gaseous emissions, such as nitrogen oxides (NO_x), sulphur dioxide (SO_2), and carbon dioxide (CO_2), which contribute to air pollution and climate change. Numerous techniques and methods have been proposed to mitigate these emissions and reduce associated costs in response to these environmental challenges. One such technique gaining popularity among coal-fired plants is co-firing, which involves combusting a renewable fuel, typically biomass, alongside the primary fossil fuel (Easterly & Burnham, 1996; Hein & Bemtgen, 1998; Hughes & Tillman, 1998).

Co-firing biomass with coal can be useful to reduce emissions by substituting a measure of the base fuel (coal) with a carbon-neutral fuel (biomass). Wood is considered a carbon-neutral fuel because it releases the same amount of CO_2 that was absorbed by the plants during their growth (Grainger & Smith, 2021).

2.4.1 Emissions from Blended Fuel Stock

Co-firing's ability to reduce net CO_2 emissions is one of the primary drivers behind its popularity. The reduction in CO_2 emissions is due to biomass being a carbon-neutral fuel source. Biomass is considered carbon-neutral because burning biomass results in net CO_2 emissions of zero. Biomass co-firing appears to be a viable option for CO_2 mitigation when the cost of CO_2 avoidance is considered. Co-firing is a more researched and secure technology than other options (Basu *et al.*, 2011; Farrelly *et al.*, 2013; Nocito & Dibenedetto, 2020). In addition, it has been demonstrated that the co-firing of biomass and coal consistently reduces both SO_x and NO_x emissions (Basu *et al.*, 2011; Leckner & Karlsson, 1993; Maxwell *et al.*, 2020a; Pedersen *et al.*, 1997; Skodras *et al.*, 2002). This reduction is because biomass contains lower sulphur concentrations than coal. However, it is anticipated that the alkali and alkaline earth components (such as Ca and K) in biomass fuels retain sulphur from coal, leading to a more significant reduction in SO_x emissions (Agbor *et al.*, 2014; Jiang *et al.*, 2022; Mitchell *et al.*, 2016). Thermal NO from the N_2 in the air and fuel NO from coal are the primary sources of NO_x emissions during biomass co-firing. However, NO_x emissions from biomass combustion are comparatively low. In contrast to the HCN generally produced by coal combustion, the nitrogen component of biomass is primarily converted into NH_3 during combustion, which has a reduced potential for conversion to NO (Jiang *et al.*, 2022; Leckner & Karlsson, 1993; Mitchell *et al.*, 2016).

2.4.2 Blending Ratios

Considering costs and plant performance, ideal co-firing ratios for coal and biomass blends must be established. Based on energy content, co-firing is possible with blends consisting of more than 20% biomass. The configuration of the plant and the co-firing technique determines how much coal may be substituted, if at all (more than 50%) (Bhuiyan *et al.*, 2018; Tillman, 2000). The compatibility of the fuels is to be considered when combining coal and biomass for co-firing. The parameters of combustion and overall performance can be affected by factors such as fuel particle size, density, moisture content, and chemical makeup. For effective and stable co-firing, a complete understanding of the fuel characteristics and how they interact is essential (Ahn *et al.*, 2014; Madanayake *et al.*, 2017). Coal and biomass combustion properties differ regarding burnout efficiency, ash behaviour, and ignition temperature. The proportion of coal to biomass in the mixture can have an impact on the stability of the flame, combustion behaviour, and emission levels. Experimental investigations

and modelling techniques are applied to evaluate the effects of fuel mixing on combustion processes and improve the co-firing operation (Priyanto *et al.*, 2016; Sami *et al.*, 2001).

2.5 Torrefaction of Wood

Torrefaction is a thermal treatment at relatively low temperatures ranging from 225 to 300 °C. The process aims to produce a fuel with increased energy density by decomposing the reactive hemicellulose and depolymerising the lignin. The cellulose partially depolymerises, producing a more porous and energy-dense material (Prins *et al.*, 2006a). The process can improve the fuel characteristics of biomass for better co-combustion with coal (Gent *et al.*, 2017; Kartal & Özveren, 2022). The bulk of the depolymerisation of biomass occurs at this stage. The degree of depolymerisation depends on the torrefaction temperature and the resistance time (Basu, 2018).

2.5.1 Advantages of torrefaction

Torrefaction improves biomass's physical and chemical properties regarding combustion (Gent *et al.*, 2017; Kartal & Özveren, 2022; Prins *et al.*, 2006a). Agricultural waste, such as maise stalks and animal dung, do not have favourable heating properties. These properties generally include high moisture content and low energy density. Torrefaction can remedy these shortcomings of fuel sources (Nunes *et al.*, 2018; Shah, 2018).

Physical advantages

The grindability of torrefied biomass is improved compared to raw biomass. The improvement is due to torrefaction disrupting biomass's cell structure, thereby increasing brittleness (Nunes *et al.*, 2018; Shah, 2018). Brittleness is essential when producing pellets since the biomass needs to be fine. The energy consumption for the milling of torrefied biomass is three to seven times lower than that of raw biomass (Nunes *et al.*, 2018).

The bulk density of the biomass is increased due to the released moisture and volatile matter during the torrefaction process (Shah, 2018). The increase makes transport and storage easier since the large volume of biomass is decreased (Nunes *et al.*, 2018).

Chemical advantages

The energy density of the biomass is increased through the torrefaction process (Shah, 2018). Tumuluru *et al.*, (2011) found that the calorific value of biomass typically increases from 11,6 – 16,3 MJ/kg to 19,8 – 24,4 MJ/kg. The reactivity of the biomass increases due to the increase in porosity after torrefaction (Nunes *et al.*, 2018).

According to research, torrefaction lowers biomass's sulphur and chlorine content while barely affecting the alkali level. Refractory elements, such as Mg, Ca, and Fe, remain mostly unaffected. Torrefaction transforms alkali and alkaline earth metals into less reactive forms. As a result, alkaline earth metals are retained in aluminosilicates, and the production of PM_1 is decreased (Han *et al.*, 2023). It also decreases alkalis, S, and Cl vaporisation during biomass burning. PM emissions during the co-combustion of coal and torrefied biomass are influenced by elemental vaporisation, competitive interactions between alkalis and other elements (Mg, Ca, and Fe), metal retention in aluminosilicates, and chloride sulfation. Torrefaction prevents mineral vaporisation, which lessens PM_1 generation. However, due to the encouraged retention of metals in coarse particles, the emission of PM_{10} may increase or it may decrease as larger particles (PM_{10}+) clump together (Basu, 2018; Han *et al.*, 2023; Kartal & Özveren, 2022; Shah, 2018).

2.5.2 Cost of Torrefaction

Biomass torrefaction is a process that involves the thermal treatment of biomass under inert conditions. Constructing torrefaction plants on a commercial scale necessitates large capital expenditures. The facility's scale, the feedstock type, the torrefaction conditions, and the potential use of heat or volatile organic compounds (VOCs) for secondary purposes, such as offsetting heating costs, impact the operating costs of a torrefaction plant. The reported cost of torrefaction per ton of torrefied biomass varies greatly, from 300 ZAR to 1300 ZAR per tonne (Bergman *et al.*, 2005).

1. Investment: Due to the need for specialised reactors, process equipment, and infrastructure, the building of commercial-scale torrefaction facilities requires a sizeable upfront capital investment. The capital expense varies according to the torrefaction system's complexity and intended production capacity (Bergman *et al.*, 2005; Demirbas, 2004; Nunes *et al.*, 2014; Sermyagina *et al.*, 2016).
2. Operating Costs: The operational expenses of torrefaction are influenced by several factors. Costs are primarily influenced by a facility's size, with larger installations typically benefiting from economies of scale. Operating expenses are also influenced by the availability and type of feedstock used. Torrefaction operating conditions, such as temperature and residence time, impact energy usage and process effectiveness (Bergman *et al.*, 2005; Nunes *et al.*, 2014; Sermyagina *et al.*, 2016).
3. Utilisation of Heat and VOCs: Torrefaction economics considers the potential use of heat and VOCs produced during the process. These by-products can be used for other purposes or to offset the facility's heating expenditures, which lowers operating costs and boost overall energy efficiency (Bergman *et al.*, 2005; Demirbas, 2004; Nunes *et al.*, 2014; Sermyagina *et al.*, 2016).

4. Environmental: During the torrefaction process, the devolatilisation of wood releases volatile organic compounds (VOCs) that can pose environmental and health risks to the surrounding environment and individuals close to the torrefaction reactor. Consequently, flue gas treatment becomes an expenditure to mitigate these potential hazards. VOC Capture and Removal: Flue gas treatment systems are designed to capture and remove VOCs emitted during torrefaction. Techniques such as condensation, adsorption, and thermal oxidation can effectively remove and treat these pollutants (Bergman *et al.*, 2005; Nunes *et al.*, 2014; Sermyagina *et al.*, 2016; Tillman, 2000).

2.6 Combustion in Household Devices

The majority of coal in South Africa is used for electricity generation. However, high levels of household coal use still exist in rural/urban developments, especially in areas close to coal mines. An estimated 950,000 households use coal as an energy source (Balmer, 2007). In many cases, biomass is the preferred source of fuel. Between one-third and one-half of the world rely on biomass to meet their energy needs (Bailis, 2004).

2.6.1 Stove classification

Taylor, (2009) specifies the base classifications for household combustion devices: Fuel type, feeding procedure, combustion regime, ignition and draft direction, heat transfer mechanism, and exhaust area.

Fuel type

Mitchell et al., (2016) tested different fuels in a single-chamber stove and reported that the fuel type influenced the emission production. The particulate matter production during the burning of wood was heavily dependent on the volatile matter content of the wood, while coal showed a different trend. NO_x formation was found to be dependent on the nitrogen content of the fuel.

Mitchell et al., (2016) also found that the torrefied wood had the lowest emissions from all the fuel types. Trubetskaya et al., (2021) found that wood logs generated the most PM, whereas the torrefied fuel produced the lowest PM.

Feeding procedure

Domestic stoves have three main fuel-feeding procedures: continuous-feed, batch-feed, and mixed-feed. Continuous-feed stoves allow fuel to be added at any time during combustion, for example, an open fire. This procedure requires direct access to the combustion chamber. Continuous-feed stoves can be extinguished by cutting off the fuel supply. Batch-feed stoves are fed once before ignition and

can only be refuelled after the burn-cycle. Batch-feed stoves are extinguished either by burnout or cutting the oxygen supply. Mixed-feed stoves are batch-feed stoves but allow discreet quantities of fuel to be added throughout the burn cycle (Taylor, 2009).

Combustion regime

The combustion regime indicates the degree of coupling between primary and secondary combustion. Primary combustion is the initial burning of the fuel in the fuel bed, including the pyrolysis of the fuel and the reactions with carbon in the solid phase. Secondary combustion occurs when the primary combustion superheats the surrounding air, causing gas-phase reactions (Taylor, 2009). The combustion regime of a stove can be classified as one of three categories: gasifier, non-gasifier, and semi-gasifier. Gasifier stoves can separate the gas generation from the gas combustion. The fuel undergoes pyrolysis, and the solid fuel is converted into gas. The gas is transported to a different chamber where it is combusted, usually with a secondary oxygen supply (Energypedia, 2018; Taylor, 2009). Njenga et al. (2016) tested gasifier stoves against conventional stoves and reported that gasifier stoves use less time and fuel to cook a meal and produce less CO and PM than the conventional stove and the basic three-stone stove. The difference is due to primary combustion relying mainly on the exothermic reaction from the conversion of char to CO and CO_2, and the secondary combustion converting unreacted CO to CO_2 with an abundance of oxygen, which is also an exothermic reaction, resulting in more heat generated and less CO pollution (Taylor, 2009).

Ignition direction versus draft

An important classification is the direction of the ignition in the fuel bed compared to the direction of the draft. Three main classifications describe the airflow direction: concurrent-flow, counter-flow, and cross-flow. Concurrent-flow describes combustion where the ignition travel and airflow are in the same direction and are the most common (e.g., open fires).

Counter-flow describes combustion, where the ignition and airflow travel in opposite directions. This design is typical with top-lit updraft (TLUD) combustion devices. TLUD devices are lit at the top of the bed, and the air inlet is at the bottom of the device. Obi et al., (2016) found that the TLUD stove was significantly influenced by fuel type. The TLUD stove performed better than a conventional stove in all performance parameters investigated. Obi et al., (2016) also tested the TLUD stove with different biomass fuels and found that woodchips offered better stove performance. Ahmed et al., (2019) found that wood chips and corn cobs had similar performance in a TLUD stove, but peanut shell pellets had the highest system efficiency.

Cross-flow describes combustion where the airflow travels perpendicular to the ignition direction. These stoves are uncommon in the domestic setting and are rarely researched.

Heat transfer mechanism

The heat transfer mechanism between the stove and the cooking pot significantly influences thermal efficiency. Heat can be transferred to the cooking pot from the stove via convection, conduction, and radiation (Taylor, 2009; Thomas, 2003). Convection stoves place the cookpot directly in the path of the hot combustion gas. The heat from the gas is used to heat the cooking pot (Agenbroad *et al.*, 2011; Taylor, 2009). Conduction stoves use a boundary layer between the combustion zone and the cooking pot (usually a material with high thermal conductivity and weak insulative properties) that heats the pot (Prasad *et al.*, 1985; Taylor, 2009). Combustion devices that use radiation as a heat transfer mechanism to cook usually work by suspending the cooking pot over the bed of coals (Taylor, 2009). Radiation and convection stoves usually exhaust the combustion products in the surrounding area, making conduction stoves the preferred mechanism regarding human health.

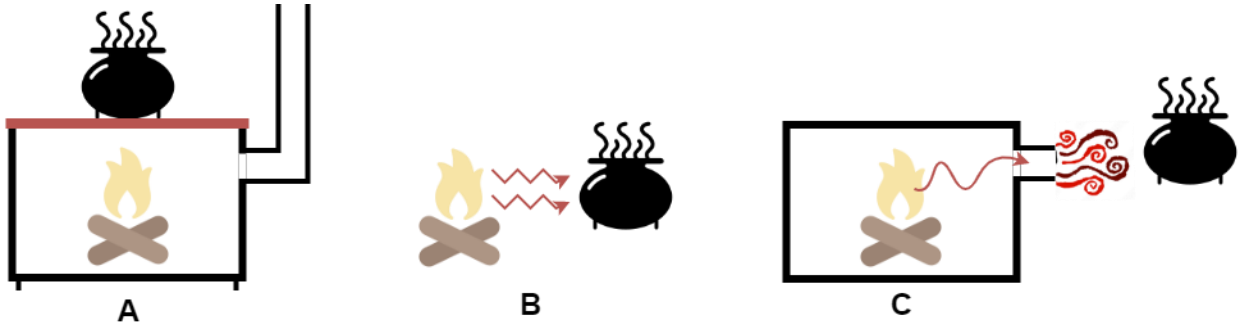

Figure 2-1: Heat transfer mechanism: A) Conduction; B) Radiation; C) Convection

Exhaust-area

An important classification regarding human health is the area where the combustion products are exhausted. The two main criteria for classification are room-exhausted and outside-exhausted (Taylor, 2009). Chimneyed stoves are reliant on a draft to guide the flue gas. Stoves can rely on natural drafts or forced drafts.

2.6.2 Ignition methods for domestic combustion devices

Two ignition methods are used to ignite the fuel bed of cooking stoves. The most common method used by most combustion devices is the bottom-lit updraft (BLUD) method. This method entails lighting the fuel bed from the bottom (Figure 2-2a). The top-lit updraft ignition method entails lighting the fuel bed from the top (Figure 2-2b).

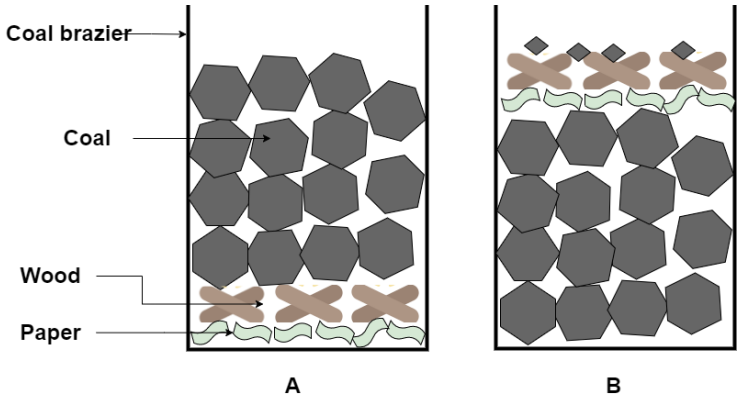

Figure 2-2: Ignition methods: A) BLUD; B) TLUD

Makonese et al., (2017) conducted experiments to determine the difference between the two ignition methods regarding emissions and reported that the BLUD method produced four to five times the PM compared to the TLUD method, slightly less CO and NO_x, and relatively the same amount of CO_2.

The reasoning behind this is due to the draft direction compared to the direction of ignition travel. Using the BLUD method generally implies a concurrent-flow. The heat generated from initial combustion travels through the fuel bed and pyrolyses the fuel, causing spikes in VOCs and PM. Makonese et al., (2015) conducted experiments to determine the effect of the ignition methods in coal-burning braziers and reported similar results. Pemberton-Pigott, (2010) reported that a TLUD Vesto gasifier stove produces a low CO/CO_2 ratio and a high thermal efficiency. Azom *et al.*, (2017) reported that when using the TLUD method, the ignition was highly sensitive to the moisture content of the fuel and that wet fuel would sometimes not ignite. A survey reported that it takes time to size the fire-starting biomass when using the TLUD ignition method. Persons must also be educated to use the TLUD ignition method since it is not commonly used in rural communities.

2.6.3 Requirements for household combustion

There are three requirements for combustion to take place (Figure 2-3): fuel, air, and an initial ignition source (heat) to initiate the reaction (Thomas, 2003).

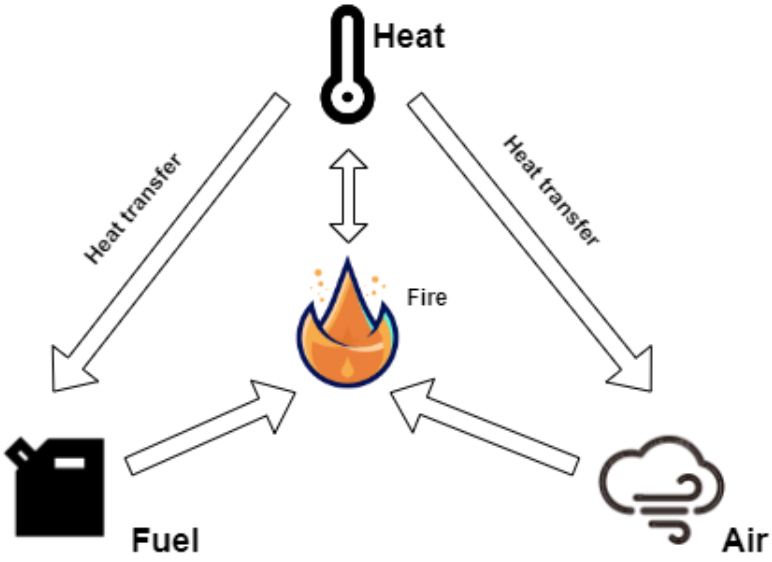

Figure 2-3: Combustion triangle

The combustion is firstly fuel-limited until the ignition process is complete. After ignition, the combustion is draft-limited, meaning that the heat can be controlled by controlling the air supply to the combustion zone. After the fuel has been sufficiently depleted, the combustion is fuel-limited once again (Thomas, 2003).

For a household, these parameters must be suitable for specific activities that the community relies on. The two primary uses for solid-fuel stoves are generally cooking and space heating. Many stoves possess the ability for both. Stoves that serve the purpose of space heating are generally indoors. These stoves are preferably required to exhaust outside due to health concerns. These stoves generally use conduction as a heat transfer method to cook (Taylor, 2009).

Fuel consumption paired with thermal efficiency is essential in rural communities. Bolaji & Olalusi, (2009) tested an improved coal stove against a traditional coal stove and a kerosene stove. The study found that the improved stove had a coal burning rate of 0.15 $kg.h^{-1}$ whereas the traditional stove had a coal burning rate of 0.20 $kg.h^{-1}$. This difference could be due to ineffective draft control (Thomas, 2003). Furthermore, Bolaji & Olalusi, (2009) found that the thermal efficiency of the improved stove, kerosene stove, and traditional stove were 42.6%, 40.5%, and 28.2%, respectively. The high fuel consumption of the traditional stove contributes to its low thermal efficiency since the two parameters are inversely proportional to each other (Bolaji & Olalusi, 2009). Adeyemi et al., (2017) reported similar findings running an improvised stove on high-power. The stove fuel consumption and thermal efficiency resulted in 0.31 $kg.h^{-1}$ and 35%, respectively. The comparatively low thermal efficiency is a result of the higher fuel consumption.

2.7 Measuring of Stove Emissions

2.7.1 Hood-method

The Hood Method is a technique for carefully collecting coal stove emissions. By using this technique, the pollution that results from burning coal is lessened. The Hood Method involves covering the stove with a hood or canopy that collects emissions as they are produced (Ballard-Tremeer & Jawurek, 1999; González *et al.*, 2008; Witt *et al.*, 2006).

The hood or canopy is made to fit entirely around the stove to ensure that all emissions are collected. A duct system connects the hood, often made of metal, to a filtering system. The filtering system is made to take out harmful gases and particles that coal combustion releases (Ballard-Tremeer & Jawurek, 1999; González *et al.*, 2008; Witt *et al.*, 2006).

Because it captures emissions at the source, the Hood Method effectively captures combustion emissions. This trait suggests that pollutants are not dispersed into the atmosphere, where they might endanger people and the environment. The Hood Method is a realistic option for experimentation because it is inexpensive and easy to implement (Ballard-Tremeer & Jawurek, 1999; González *et al.*, 2008; Witt *et al.*, 2006).

2.7.2 Dilution Tunnel Method

The dilution tunnel method is a standard method for determining the emissions from coal stoves. By diluting the sample with either nitrogen or clean air, this technique can calculate the amount of pollutants in the exhaust gas (Allen *et al.*, 2022).

A tube with sampling openings at both ends makes up the dilution tunnel. One end of the tube is used to collect the sample, while the other is used to pump clean air or nitrogen through the tunnel. As a result, the exhaust gases become diluted, lowering the concentration of pollutants and facilitating accurate measurement (Allen *et al.*, 2022; Hildemann *et al.*, 1989).

A probe is put into the chimney or exhaust pipe of the stove to collect the sample. The probe is attached to the sample port at one end of the dilution tunnel. The diluter feed is activated, drawing fresh air or nitrogen into the tunnel to saturate the exhaust gases. At the other end of the tunnel, samples of the diluted gases are taken, and various instruments, such as gas analysers, are used to measure the concentrations of pollutants (Allen *et al.*, 2022; Hildemann *et al.*, 1989).

The dilution ratio, a component of the Dilution Tunnel Method, determines the precision of the measurement. The dilution ratio is determined by dividing the diluter flow rate by the exhaust gas

flow rate. The measurement accuracy is increased by a lower concentration of contaminants caused by a larger dilution ratio (Hueglin *et al.*, 1997).

2.8 Thermal Efficiency of Domestic Stoves

Domestic stoves are frequently used in homes worldwide for heating and cooking. Many of these stoves are inefficient, leading to higher fuel consumption, which increases indoor air pollution and harms the environment. So, it is necessary to evaluate the thermal efficiency of household stoves and find measures to enhance their performance (Trubetskaya *et al.*, 2021).

A residential stove's thermal efficiency is evaluated by comparing the amount of heat it produces to the amount of fuel it consumes. Careful calculations of the fuel consumption, fuel heating value, and stove output are necessary for this process. The thermal efficiency of domestic stoves has been measured using a variety of techniques (Islam *et al.*, 2022; Mekonnen, 2022).

The heating value of the fuel, the stove's ability to transfer heat, and thermal losses are only a few of the variables that calculate household stoves' thermal efficiency. Depending on the type and quality of the fuel, the heating value may vary. Several elements, such as the stove's design, the combustion process, and insulation usage, affect the stove's ability to transmit heat efficiently. Radiation, conduction, and convection are three ways heat losses can occur (Kole *et al.*, 2022a; Pasha *et al.*, 2023).

Reducing the fuel consumption, indoor air pollution, and greenhouse gas emissions of household stoves can all result from increasing their thermal efficiency. The efficiency of stoves can be increased in several ways, including stove design, fuel quality, and user behaviour. For instance, better stove designs can increase the efficacy of heat transfer, while utilising higher-quality fuels can enhance the heating value and reduce emissions (Mekonnen, 2022).

In conclusion, figuring out how to increase the performance of domestic stoves requires monitoring and analysing their thermal efficiency. Stove efficiency has been measured using both direct and indirect approaches. Numerous steps may be taken to enhance performance, and increasing stove efficiency can result in considerable advantages.

2.8.1 Water boiling test

The water boiling method is a commonly employed technique to assess the thermal efficiency of a residential coal-burning stove. This method involves measuring the quantity of heat generated by the stove and the amount of water that can be heated by that heat (Islam *et al.*, 2022; Mekonnen, 2022; Pundle *et al.*, 2019). The stove's efficiency can be evaluated by employing the following formula:

$$Efficiency = \left(\frac{Heat\ output}{Heat\ input}\right) \times 100\% \quad \text{(E2-1)}$$

The calculation of heat input involves the measurement of the weight of the coal utilised and determining its calorific value, which represents the amount of heat released when one unit mass of fuel is burned. Calorific value is typically quantified in joules per kilogram (J/kg). The formula for computing heat input is as follows:

$$Heat\ input = m_{fuel} \times CV \quad \text{(E2-2)}$$

In Equation 2.2, m_{fuel} represents the mass of fuel burned, and CV represents the calorific value.

Heat output is calculated by measuring the temperature of the water before and after the stove heats it. The amount of heat absorbed by the water can be calculated using the following formula:

$$Heat\ output = m_w \times cp_w \times \Delta T \quad \text{(E2-3)}$$

In Equation 2-3, m_w, cp_w, and ΔT represents the mass of water boiled in the pot during the test, the specific heat capacity of water, and the temperature difference of the water in the pot. The specific heat of water is the amount required to raise the temperature of one unit of water by one degree Celsius. It is typically measured in joules per kilogram-degree Celsius (J/kg-°C). The formula for calculating the amount of heat absorbed by the water assumes no heat loss to the surroundings (Islam *et al.*, 2022; Mekonnen, 2022; Pundle *et al.*, 2019).

2.9 Formation of Pollutants during Combustion

Burning coal and wood is typical for producing energy and providing heat. However, these processes release many pollutants into the atmosphere, raising severe environmental and health issues. It is essential to comprehend how these pollutants are formed to mitigate their production.

2.9.1 Gaseous pollutants

Several gaseous pollutants are produced during combustion. The incomplete combustion of carbon-containing fuels results in carbon monoxide (CO) formation. The oxidation of nitrogen in the combustion air produces nitrogen oxides (NO_x). When the oxygen and sulphur in the fuel react, sulphur dioxide (SO_2) is produced. There is also the production of particulate matter, which comprises different chemical species (Leckner & Karlsson, 1993; Makonese *et al.*, 2017b; Shen *et al.*, 2021).

Sulphur oxides

Coal contains sulphur in various forms, including sulphides, sulphates, organic sulphur compounds, and traces of elemental sulphur. There is very little sulphur in biomass, such as wood. Most of the sulphur linked to the fuel is released into the gas phase during combustion. The organically bound component of sulphur in coal is another sizeable fraction. Coal generally has little sulphate (Fleig *et al.*, 2009; Zaugg *et al.*, 1989). Sulphides in the form of pyrite are usually the main fraction released according to the reactions:

$$2\ FeS_2(s) \rightarrow 2\ FeS\ (s) + S_2\ (g) \quad \text{(R2-1)}$$

$$2\ FeS\ (s) \rightarrow 2\ Fe + S_2\ (g) \quad \text{(R2-2)}$$

$$S_2 + 2\ O_2 \rightarrow 2\ SO_2 \quad \text{(R2-3)}$$

Sulphur dioxide (SO_2) is the thermodynamically preferred sulphur oxide at high temperatures (>1000°C) in oxygen-rich environments. Hydrogen sulphide (H_2S) is created in the gas phase during sub-stoichiometric conditions in the flame or is released from organic sulphur compounds. When the temperature and oxygen content are higher, SO_2 is significantly favoured in the equilibrium. Therefore, the concentration of H_2S in the released gas is low when there is an excess of oxygen, as is often the case in pulverized coal combustors and fuels containing biomass (Fleig *et al.*, 2009; Zaugg *et al.*, 1989). The most prevalent SO_3 formation occurs according to the following reactions:

$$SO_2 + {}^1/_2\ O_2 \rightarrow SO_3 \quad \text{(R2-4)}$$

$$SO_2 + OH \rightarrow HOSO_2 \quad \text{(R2-5)}$$

$$HOSO_2 + O_2 \rightarrow SO_3 + HO_2 \quad \text{(R2-6)}$$

At lower temperatures, the equilibrium tends toward sulphur trioxide (SO_3), while the reaction rate reduces with temperature. As a result, the concentration of SO_3 in the released gas is much lower than that of SO_2 by several orders of magnitude. About 0.1% to 1% of the SO_2 in air-fired pulverized coal combustion is converted to SO_3 by oxidation (Fleig *et al.*, 2009; Pisupadti, 2003; Sarbassov *et al.*, 2018).

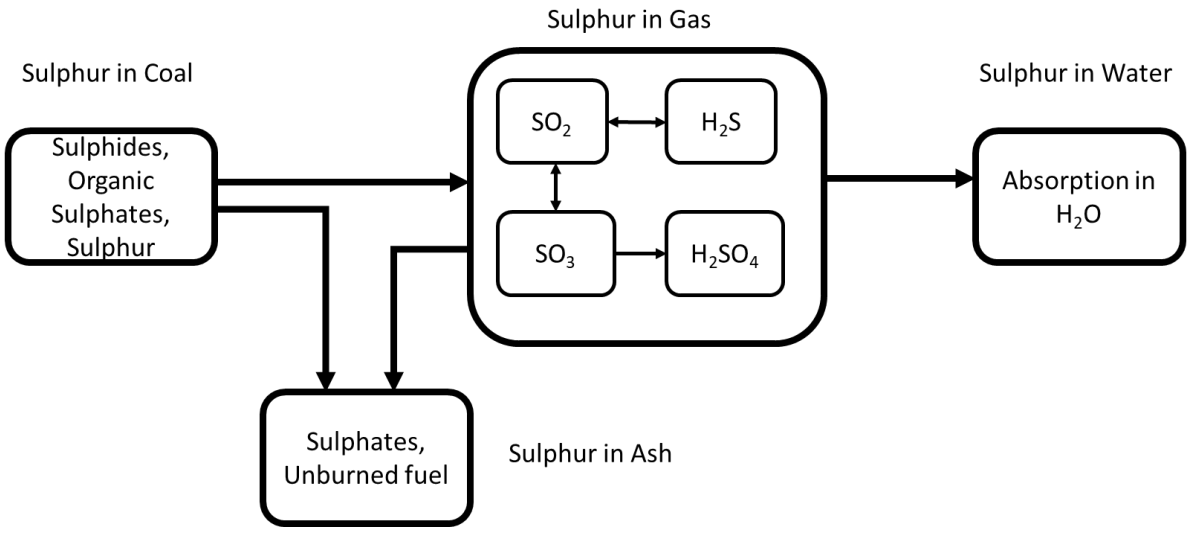

Figure 2-4: Reaction routes for the formation of sulphur (Adapted from Fleig et al., 2009**)**

Figure 2-4 displays the reaction routes that the sulphur in the coal can follow during the combustion process. In addition to creating gaseous sulphur products, reactions between sulphur and alkali and alkaline earth metals (Na, K, Mg, and Ca) in the ash can trap sulphur. Sulphur can, therefore, be bonded to minerals and remain there without being released. Reactions with calcium (Ca) dominate the sulphate retention in the ash. The degree of sulphur retention in the ash mostly depends on the coal's molar ratio of Ca to S (Fleig *et al.*, 2009). With enough Ca present in the combustion zone, sulphur is retained according to the following reactions:

$$CaCO_3 \rightarrow CaO + CO_2 \qquad \text{(R2-7)}$$

$$2\,CaO + 2\,SO_2 + O_2 \rightarrow 2\,CaSO_4 \qquad \text{(R2-8)}$$

Calcination (Reaction 2-7) is inhibited in pressurized combustion conditions and prohibited in atmospheric pressure conditions (Fleig *et al.*, 2009).

Nitric oxides

In the context of combustion, the formation of NO_x can occur through three distinct mechanisms: Thermal NO_x, Fuel NO_x, and Prompt NO_x.

The molar concentrations of nitrogen and oxygen and the combustion temperature affect the concentration of thermal NO_x. The production of thermal NO_x is significantly reduced when combustion occurs at temperatures lower than 1,300°C (Hill & Smoot, 2000; Pisupadti, 2003; Zaugg *et al.*, 1989).

$$N_2 + O \rightarrow NO + N \qquad \text{(R2-9)}$$

$$N + O_2 \rightarrow NO + O \quad \text{(R2-10)}$$

$$N + OH \rightarrow NO + H \quad \text{(R2-11)}$$

Reactions 2-9 – 2-11 are referred to as the Zeldovich mechanism. Reaction 2-11 is included in the mechanism when combustion occurs in fuel-rich conditions.

Fuel NO_x is the most significant contributor to NO_x production. Fuel NO_x is a by-product of the oxidation of nitrogen already present in fuels containing nitrogen, such as coal. The common occurrence of fuel NO in coal systems can be attributed to the fuel-rich conditions and moderate temperatures (1500–2000 K) in coal flames. Due to the significantly weaker N-H and N-C bonds in nitrogen attached to the fuel, the creation of fuel NO occurs more frequently than thermal NO. In contrast, the triple bond in molecular nitrogen must be broken for thermal NO to form. This difference emphasizes why fuel NO is prevalent in coal systems (Hill & Smoot, 2000; Pisupadti, 2003; Zaugg *et al.*, 1989).

In fuel-rich conditions, which are present to some extent in all combustion processes, prompt NO_x is produced when molecular nitrogen from the air reacts with the fuel. Then, as the nitrogen oxidizes with the fuel, NO_x is created during combustion, comparable to fuel NO_x (Hill & Smoot, 2000; Pisupadti, 2003; Zaugg *et al.*, 1989).

$$CH + N_2 \rightarrow HCN + N \quad \text{(R2-12)}$$

$$C + N_2 \rightarrow CN + N \quad \text{(R2-13)}$$

Understanding these three pathways of NO_x formation in combustion processes is for effective management and control of nitrogen oxide emissions.

Carbon monoxide

Carbon monoxide is produced due to the incomplete combustion of carbon-based fuels. Various factors contribute to incomplete combustion (Gadsby *et al.*, 1948; Makonese *et al.*, 2017a).

The appropriate ratio of oxygen to fuel may not be reached in some regions of the combustion process due to insufficient mixing of the air and fuel. Insufficient mixing prevents the fuel's complete oxidation, producing carbon monoxide (Pisupadti, 2003).

A lack of air delivered to the flame can reduce the oxygen needed for complete combustion. In these circumstances, the fuel might not be completely oxidized, which would cause carbon monoxide to be produced (Bolaji & Olalusi, 2009; Pisupadti, 2003).

Insufficient residence time for the fuel in combustion systems can prevent complete combustion. Carbon monoxide is produced because the fuel is only partially reacted by the high temperatures and oxygen-rich environment (Bolaji & Olalusi, 2009; Pisupadti, 2003).

Flame temperature reduction before combustion is finished can cause incomplete combustion. The combustion process can be stopped before all of the fuel molecules have been oxidized if the flame temperature drops too quickly, either from heat loss or an insufficient fuel-air mixture. The generation of carbon monoxide may be aided by early cooling (Greiner, 1997; Pisupadti, 2003).

2.9.2 Formation of particulate matter

Particulate matter (PM) emissions from coal combustion can occur through various mechanisms, each contributing to the formation of different types and sizes of particles. Black carbon, or soot, is a kind of PM created when coal is burned partially (Li *et al.*, 2016). Poly-aromatic hydrocarbons (PAHs), or primary carbon-enriched particles, are aggregated together in chains. Soot particles are created by transforming a hydrocarbon fuel with a few carbon atoms into a carbonaceous collection with millions of carbon atoms. Soot particle composition and size distribution are influenced by combustion temperature, residence length, and aromatic hydrocarbons (Liang *et al.*, 2023). The parent coal's rank-related aromatic hydrocarbons contribute to the increased soot output. If not oxidized within the flame zone, soot particles have been reported to increase heat transfer by radiation and can be released in the flue gas. This solid-vapour-particle pathway forms articulate agglomerates in the 1-2 μm size range and is associated with volatile elements in the PM (Luan *et al.*, 2022).

Ash, previously disregarded as a pollutant, is now understood to be a transporter of harmful trace elements. It can be found as fly ash (smaller particles entrained in the gas flow) or bottom ash (larger particles left over after burning). Ash particles are entrained due to airflow across the coal bed (Liu *et al.*, 2022; Xu *et al.*, 2011).

2.9.3 Summary of Pollutants Formation

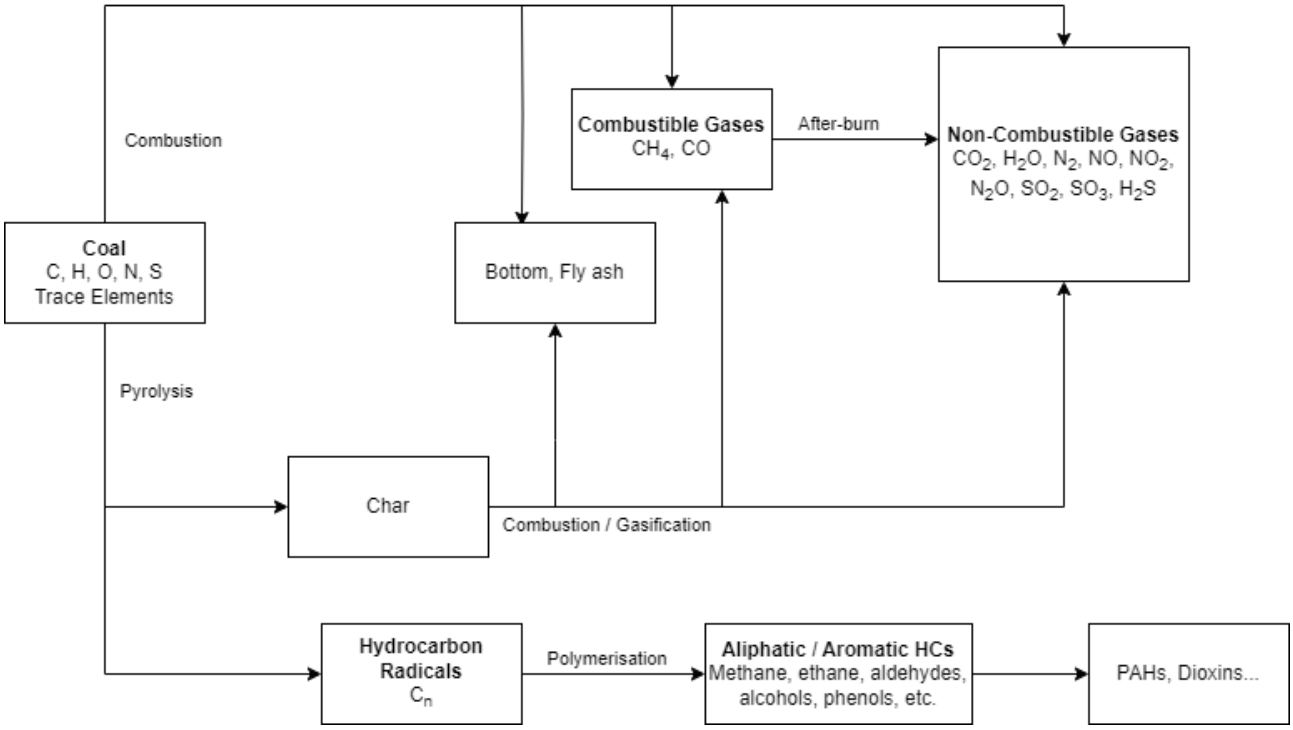

Figure 2-5: Combustion products of coal
(Adapted from Sumbane-Prinsloo et al., (2021) and Krawczyk & Zajemska, (2013))

Figure 2-5 provides an overview of the outcomes resulting from coal combustion. This process yields products categorized into three distinct groups: combustible gases, non-combustible gases, and ash. Combustible gases can undergo further combustion, transforming into non-combustible gases. When coal undergoes pyrolysis, it gives rise to char and hydrocarbon radicals. Char is particularly suitable for combustion or gasification processes, following a similar pathway as coal during combustion. CO_2 and H_2O are formed during the complete combustion of the fuel. CO is formed during incomplete combustion due to insufficient oxygen. CO can be further oxidised to CO_2 if the temperature is high enough.

CHAPTER 3: MATERIAL PREPARATION AND CHARACTERISATION

This section presents how the materials were prepared and the results obtained from the chemical and mechanical analyses.

3.1 Materials

This study uses discarded Grade D coal fines and pine wood chips. Grade D Highveld coal fines were selected to emulate the utilization of low-quality coal in coal-burning stoves commonly found in rural and urban households. Additionally, pine wood chips were chosen due to their widespread usage in construction, leading to an abundance of pine wood waste. The selection of pine wood in the form of chips offers advantages such as simplified storage and transportation logistics. **Table 3-1** summarises the material and equipment used to prepare the samples.

Table 3-1: Material and equipment list

Description	Supplier	Detail	Use
Materials and gasses			
Coal	CoalTech	Highveld grade D waste coal	Raw material
Wood	Sappi	Waste pine wood chips	Raw material
Nitrogen	Afrox	Purity: > 99.999%	Torrefaction, TGA
Polyethylene glycol	Pennywise distributors	-	Binding agent
Equipment			
Three-phase horizontal tube furnace	NWU	Custom made	Torrefaction trial run
TGA instrument	NWU	SDT Q600 TGA from TA instruments	Thermogravimetric analysis (TGA)
Hammer mill	NWU	-	Pulverising
Grinder	NWU	-	Grinding
Rotary kiln	Thermopower furnaces	Indirectly fired, electrically heated	Bulk torrefaction
Steele stiff extruder	BMMS	-	Extrusion of fines

3.2 Sample Preparation

This section details the methods for preparing the raw materials for combustion experiments.

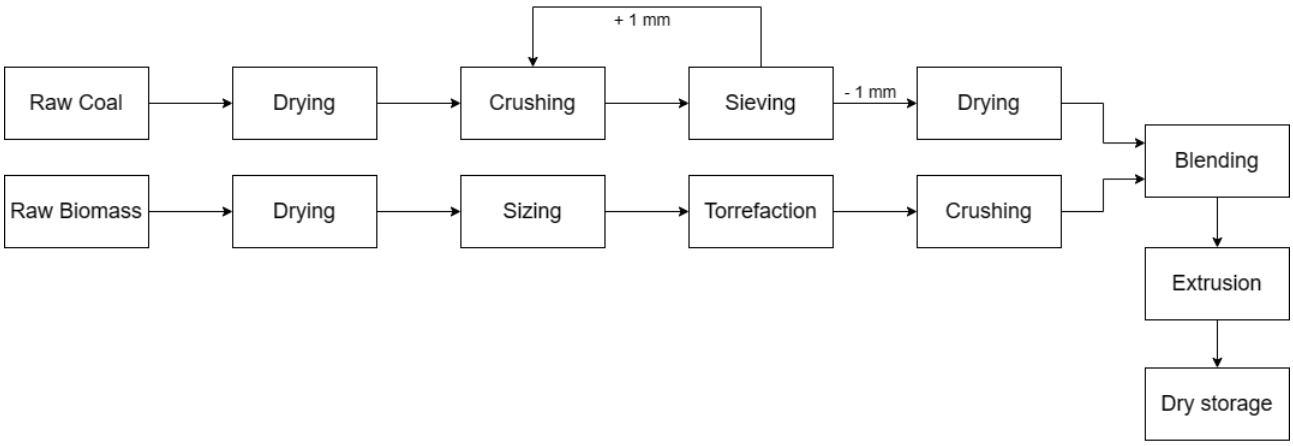

Figure 3-1: Sample preparation overview

Figure 3-1 displays an overview of the preparation route followed for the samples used in the combustion experiments.

3.2.1 Coal preparation

The key stages of this coal preparation process are visually depicted in **Figure 3-1**, summarising the consecutive and correlated steps undertaken to facilitate the preparation of the raw coal samples.

The initial state of the acquired coal was fine (- 1 mm), containing some large clumps formed due to high moisture content. The coal was stored indoors under controlled conditions to gradually reduce its moisture content and prevent the agglomeration of coal particles during subsequent size reduction procedures. The coal was air-dried indoors for 14 days until further processing.

The dried coal was finely crushed using a grinder, and the crushed coal was then sieved and separated into + 1 mm and - 1 mm particles. The + 1 mm particles were subjected to a further pass through the hammer mill, ensuring that any remaining coarse particles were uniformly reduced to the desired fineness. Meanwhile, the - 1 mm particles were dried indoors once more until they were needed for the blending procedure, approximately 5 weeks.

3.2.2 Biomass Preparation

The key stages of this biomass preparation process are visually depicted in **Figure 3-1**, summarising the consecutive and correlated steps undertaken to facilitate the preparation of the raw wood samples. These waste wood chips were obtained from a paper factory, and as a prerequisite to their use, they underwent a washing procedure before being discarded by the paper mill. Upon

acquisition, the wood chips were arranged indoors for controlled drying to reduce the moisture content. The wood chips were left to dry for 14 days in a controlled environment under atmospheric temperature and pressure before further processing. During this period, the average temperature and atmospheric pressure of Potchefstroom, South Africa, was 11 °C and 87 kPa, respectively.

Table 3-2: Particle size distribution of wood chips

Size	Composition wt%
Fines (- 2 mm)	1.3
- 2 + 4 mm	11.5
- 4 + 6 mm	59.3
- 6 + 8 mm	21.7
- 8 + 10 mm	3.9
+ 10 mm	2.2
Bark	0.1

Table 3-2 summarises the particle size distribution of the wood chips received from the paper mill. The wood chips underwent a sieving process, separating the larger chips (+ 6 mm) from the overall stockpile. The + 6 mm particles were then subjected to a hammermill with a 6 mm sieve for size reduction, ensuring they fell within the desired size range (+2 mm -6 mm). The woodchips were stored within sealed containers. The fines (- 2 mm) were discarded, and the +2 mm -6 mm particles were subjected to further processing.

Torrefaction process

The rotary kiln used for the torrefaction process was set up at Thermopower Furnaces, Olifantsfontein, South Africa. **Figure 3-2** and **Table 3-3** display the torrefaction rig schematic and instrument list used to torrefy the wood chips, respectively. The pre-determination of the torrefaction operating conditions, temperature and residence time, can be seen in **Appendix A Torrefaction pre-tests**.

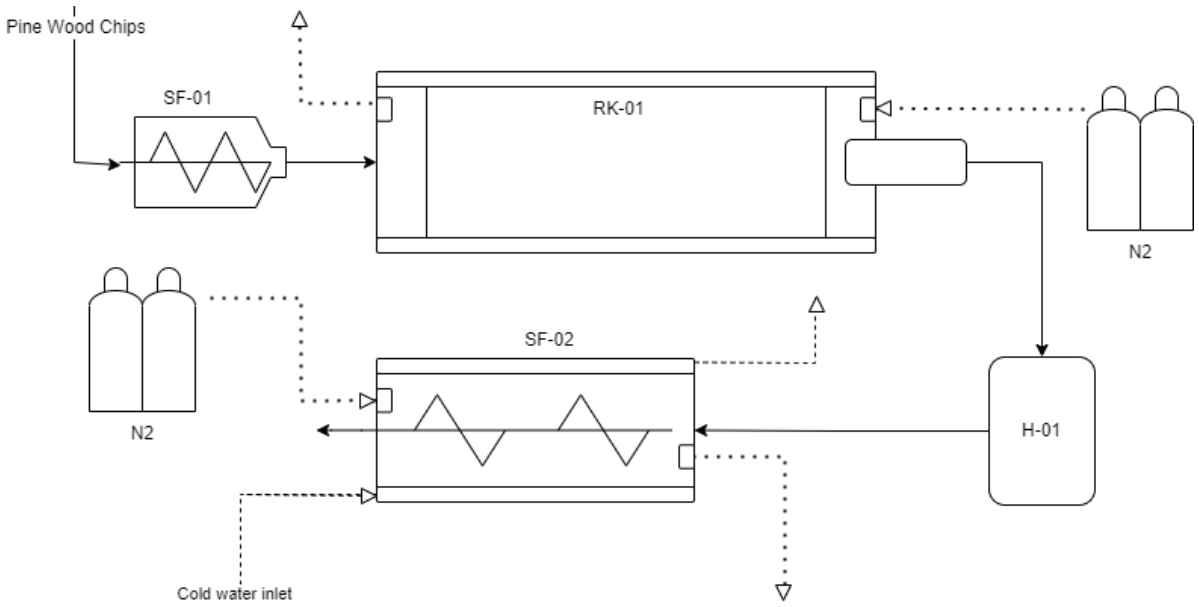

Figure 3-2: Torrefaction rig schematic

Table 3-3: Instrument list of Torrefaction rig

Displayed Text	Description
SF-01	Screw feeder
SF-02	Insulated screw feeder
RK-01	Rotary kiln
H-01	Hopper
N2	Nitrogen gas cylinders

The wood chips were introduced into a hopper directly from dry storage containers. Subsequently, these wood chips were conveyed through a screw feeder rotating with the driving motor set to 19.2 Hz, delivering a consistent feed rate of 30 $kg.hr^{-1}$ into an indirectly fired, electrically heated rotary kiln. The rotary kiln has a 5 m length and a 960 mm internal diameter tube. The rotary kiln's driving motor was set to 8.0 Hz, resulting in an observed rotational speed of 5 r.p.m. to guarantee a controlled residence time of one hour within the kiln. The wood chips travelled at a rate of 5 $m.hr^{-1}$ in the kiln. The rotary kiln was operated at 278 °C (± 3 °C). A nitrogen flow was continuously introduced into the rotary kiln at 30 $NL.min^{-1}$.

Upon exiting the rotary kiln, the processed wood chips descended into a secondary hopper, where a second screw feeder further transported them. Similar to the initial stage, nitrogen was employed within the second screw feeder at 17 $L.min^{-1}$ to maintain an inert atmosphere. The entire system, from the feedstock to the final product, is sealed to prevent air from entering and causing the wood to combust.

Furthermore, a cooling system was integrated into the second screw feeder. Cold water circulated through the feeder's insulation, facilitating the rapid and thorough cooling of the wood chips. This cooling process ensured that once the wood chips emerged from the system, they remained entirely inert and resistant to combustion upon contact with ambient air.

3.2.3 Blending

The coal and biomass were blended into different ratios in preparation for pelletisation. The seven ratios selected are given in **Table 3-4**:

Table 3-4: Coal – Biomass blend ratios

Sample	Biomass weight %	Coal weight %
1	0	100
2	10	90
3	25	75
4	50	50
5	75	25
6	90	10
7	100	0

The blending process involved mixing coal and torrefied wood fines following the specified ratios. The components were weighed on a scale before being added to a drum. After the coal and torrefied wood had been added to the drum in a specific ratio, 5 wt% polyvinyl alcohol (PVA) was used as a binder. The drum was then sealed and tumbled for 30 minutes to ensure homogeneity. The sealed drums prevent contamination and protect the samples from moisture adsorption.

3.2.4 Pelletisation of blends

Lab-scale pelletisation techniques were investigated before mass pelletisation was started. Extrusion was preferred because the drum method could not produce pellets with the desired biomass-coal ratios. Refer to **Appendix B: Pelletisation pre-tests**.

Extrusion

Moisture was introduced into the blends until a moisture content between 18 wt% and 20 wt% was achieved to produce a semi-slurry. The added moisture activates the adhesive properties of the materials without lowering the viscosity to the extent that the materials flow out of the extruder. The prepared blend was conveyed into the extruder with the assistance of a screw feeder. The extruder

was equipped with a 19 mm die. This pellet size was selected based on its suitability for the stove's dimensions and performance characteristics. The extruder operates at ambient temperature and a 15 - 22 bar pressure. Following the extrusion process, the freshly formed pellets were set aside for air drying, given that a proximate analysis confirmed that their moisture content was 20 – 25 wt% due to the water added pre-extrusion. **Figure 3-3** shows the extrudates produced from the coal-biomass blends containing 0% biomass to 100% biomass.

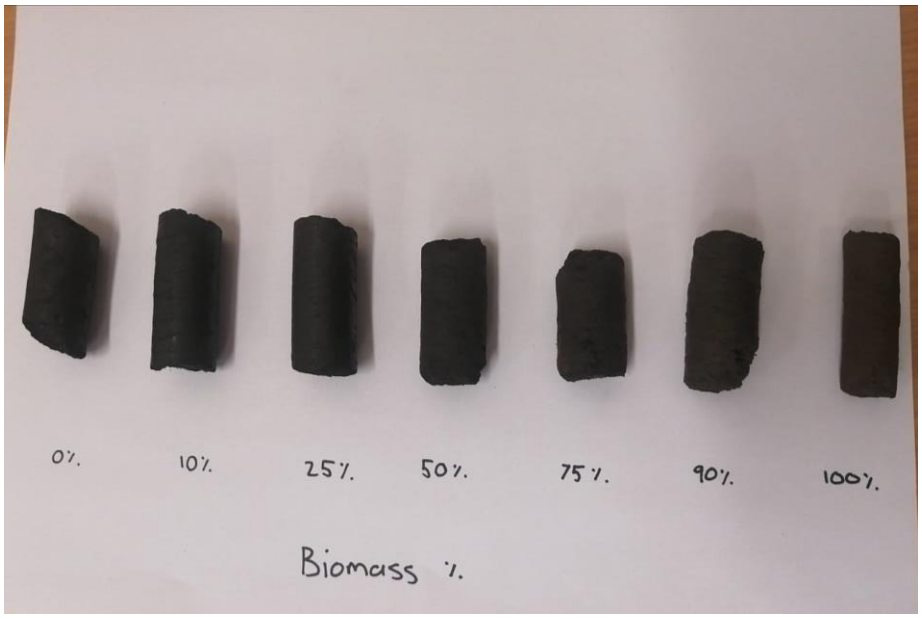

Figure 3-3: Picture of extrudates

3.3 Chemical and Physical Analysis

Table 3-5 summarises the analyses conducted on the raw and processed material.

Table 3-5: Overview of analyses

Property	Standard	Laboratory	Material
Proximate analysis			
Moisture content (wt%)	ISO 11722:1999	Bureau Veritas Testing and Inspections South Africa	Coal, Torrefied wood, Raw wood, Pellet blends
Ash (wt%)	ISO 1171:2010		
Volatile matter (wt%)	ISO 562:2010		
Fixed carbon (wt%)	Difference		
Ultimate analysis			
Carbon (wt%)	ISO 12902 – CHN	Bureau Veritas Testing and Inspections South Africa	Coal, Torrefied wood, Raw wood, Pellet blends
Hydrogen (wt%)	ISO 12902 – CHN		
Nitrogen (wt%)	ISO 12902 – CHN		
Oxygen (wt%)	Difference		
Total Sulphur (wt%)	ISO 13909-4: 2001		
Mineral analysis			
X-Ray diffraction analysis	Rietveld method	XRD Analytics	Coal
X-ray fluorescence analysis	ISO 13909-4: 2001		
Fibre analysis			
Fibre analysis	ASM 060	NWU	Raw wood, Torrefied wood
Calorific value			
HHV	ISO 1928:2009	NWU	Coal, Raw wood, Torrefied wood, Pellet blends
Structural integrity			
Compressive strength	-	NWU	Pellets blends

The compressive strength was determined using an LRXplus instrument from Loyd Instruments. A pellet is placed on the press between two plates. The instrument applies increasing force until the pellet cracks or brakes. The force applied before the pellet broke is the force recorded. Equation 3-1 is used to determine the compressive strength ($\sigma\ [MPa]$) of the pellet:

$$\sigma = \frac{F_{max}}{A_p} \quad \text{(E3-1)}$$

Where F_{max} is the max force applied measured in Newton and $A_p\ [mm^2]$ is the contact area between the pellet and the instrument's press.

3.4 Characterisation Results

This section contains the results from sample preparation and analyses conducted on the raw materials and products.

3.4.1 Coal Characterisation

Proximate Analysis

Table 3-6 summarises the proximate analysis of the parent coal in comparison to other typical Highveld coals.

Table 3-6: Proximate analysis of parent coal (a.d)

	This study	(Kühn *et al.*, 2017)	Sumbane-Prinsloo et al., (2021)	Wagner & Hlatshwayo, (2005)
% Moisture	4.7	2.1	2.6	4.2
% Volatile matter	22.3	20.4	24.4	21.5
% Ash	29.9	30.6	24.0	26.9
% Fixed carbon	43.1	46.9	49.0	47.5

The parent coal is compared to coals from the same origin. The proximate analysis of the parent coal compares to proximate analyses of different Highveld coal samples used in studies by Sumbane-Prinsloo et al., (2021), Wagner & Hlatshwayo, (2005), and Kühn et al., (2017). The composition of the parent coal suggests that the coal is classified as a highly volatile, high-ash bituminous coal (Mastalerz *et al.*, 2011).

Ultimate Analysis

Table 3-7 summarises the ultimate analysis of the parent coal on a dried ash-free basis.

Table 3-7: Ultimate analysis of parent coal (d.a.f)

	This study	(Kühn *et al.*, 2017)	Sumbane-Prinsloo et al., (2021)	Wagner & Hlatshwayo, (2005)
% Hydrogen	4.7	4.0	4.4	4.1
% Nitrogen	1.8	1.9	1.9	1.9
% Carbon	74.9	79.0	79.0	79.9
% Oxygen (calculation)	17.3	14.1	14.2	12.4
% Total sulphur	1.2	0.9	0.5	1.5

The ultimate analysis of the parent coal compares to ultimate analyses of different Highveld coal samples used in studies by Sumbane-Prinsloo et al., (2021), Wagner & Hlatshwayo, (2005), and Kühn et al., (2017). The parent coal contains relatively low carbon content compared to other Highveld coal samples and relatively high oxygen content. The hydrogen, nitrogen, and sulphur content compare to other Highveld coals. Chen et al., (2017) reported that the degree of surface oxidation of coal increases with an increase in surface area. The parent coal used in this study possibly oxidised to a greater degree due to its particle size consisting of fines and prolonged exposure to the environment.

Calorific Value

Table 3-8 shows the calorific value of the parent coal on an air-dried basis.

Table 3-8: Calorific value of parent coal (a.d)

	Parent coal	Kühn et al., (2017)	Sumbane-Prinsloo et al., (2021)	Wagner & Hlatshwayo, (2005)
Gross Calorific Value (MJ/kg)	20.4	22.4	22.8	22.6

The calorific value is relatively lower than typical highveld coal. The calorific value is directly related to the composition of the coal. The findings by Kühn et al., (2017), Sumbane-Prinsloo et al., (2021), and Wagner & Hlatshwayo, (2005) suggest that the low gross calorific value of the parent coal (air-dried basis), in comparison, is due to its low carbon content (49.0%), high ash content (29.9%), and relatively high oxygen content (11.3%). Secondary factors may include the mineral composition of the coal.

X-Ray Diffraction analysis (XRD)

Table 3-9 summarises the XRD analysis of the parent coal.

Table 3-9: XRD analysis of parent coal

Mineral species	Composition by weight (%)	
	This study	Sumbane-Prinsloo et al., (2021)
Organic C	62.9	75.9
Quartz	8.5	7.9
Kaolinite	23.0	12.8
Calcite	0.9	1.3
Dolomite	0.9	2.0
Diopside	0.6	n.r
Muscovite	3.2	n.r
Gypsum	0.0	n.r
Siderite	n.r	0.1
Pyrite	n.r	0.1
Total	**100**	**100**

n.r = not reported

The composition of the coal sample is predominantly composed of organic carbon. The presence of clay minerals (kaolinite), mica (muscovite), and small amounts of quartz, calcite, dolomite, and diopside is not unusual in coal samples and can vary depending on the coal's geological origin (Kühn *et al.*, 2017; Sumbane-Prinsloo *et al.*, 2021). The kaolinite content in the parent coal is relatively high, typical for Highveld coals, and the organic carbon is relatively low compared to coal from the same region (Sumbane-Prinsloo *et al.*, 2021).

X-ray Fluorescence analysis (XRF)

Table 3-10 displays the results from the XRF analysis conducted on the parent coal.

Table 3-10: Summary of XRF analysis of parent coal

Ash Species	Composition by weight (%)		
	This study	Sumbane-Prinsloo et al., (2021)	Kühn et al., (2017)
Al_2O_3	22.4	23.3	31.4
CaO	11.4	11.9	5.7
Cr_2O_3	0.04	0.03	n.r
Fe_2O_3	4.6	1.1	1.2
K_2O	0.9	0.4	2.1
MgO	2.3	3.8	0.8
MnO	0.2	0.04	0.03
Na_2O	0.6	n.r	0.2
P_2O_5	0.7	0.6	0.9
SiO_2	46.9	55.2	49.0
SO_3	6.5	2.3	6.7
TiO_2	2.5	1.3	1.9
V_2O_5	0.02	0.03	n.r
ZrO_2	0.1	n.r	n.r
BaO	0.2	n.r	n.r
SrO	0.3	n.r	n.r
ZnO	0.04	n.r	n.r
Total	99.62	99.99	99.99

n.r = not reported

High levels of Al_2O_3 and SiO_2 indicate the presence of Al-containing species and silica in the parent coal. The parent coal has relatively low aluminium and silica and relatively high ferrous and titanium content compared to coals from the same region (Kühn *et al.*, 2017; Sumbane-Prinsloo *et al.*, 2021).

3.4.2 Biomass Characterisation

The total mass loss through torrefaction was determined by using an ash balance over the process.

$$Mass\ loss\% = \left(1 - \frac{x_{ash,0}}{x_{ash}}\right) \cdot 100 \qquad \text{(E3-2)}$$

Equation 3-2 is used to determine the mass loss from the torrefaction process where x_{ash} is the ash yield of the torrefied pine wood and $x_{ash,0}$ is the ash yield in the raw pine wood (See **Table 3-11)**. The total mass loss from the torrefaction process was determined as 36.4%. This value slightly deviates from the small-scale torrefaction test (See Appendix A: **Torrefaction pre-test results**). This difference can be attributed to the scale difference of the two processes. Variables such as particle-

particle interactions and temperature differences over the larger equipment may explain the slight difference in mass loss.

The following observations were made following the completion of the torrefaction process on wood chips: The wood exhibited increased brittleness post-torrefaction, significantly enhancing its grindability. This brittleness facilitated the conversion of the wood into finer particles, simplifying the crushing step before the pelletisation process.

Proximate Analysis

Table 3-11 shows the proximate analysis of the raw and torrefied pine wood.

Table 3-11: Proximate analysis of raw pine wood and torrefied pine wood (a.d)

	Current study		(McNamee *et al.*, 2016)	
	Raw Pine wood	Torrefied Pine wood	Raw Pine wood	Torrefied pine wood
% Moisture	7.5	4.5	7.1	1.2
% Volatile matter	79.6	78.3	77.9	75.5
% Ash	0.7	1.1	0.3	0.5
% Fixed carbon	12.2	16.1	14.7	22.8

Upon observation, torrefaction mitigated the inherent hygroscopic nature of the wood, reducing its tendency to absorb moisture (Chen *et al.*, 2018, 2019). A substantial amount of volatile matter and moisture were released during torrefaction, reducing by 37% and 62%, respectively. Although the composition of fixed carbon in the sample increased (due to the greater mass loss of volatile matter compared to fixed carbon), the mass of fixed carbon in the original material was reduced by 16%. The ash yield of the wood increased by 57.1%. The mineral matter remains unreacted at this low torrefaction temperature while moisture and volatile matter are released. McNamee et al., (2016) conducted torrefaction experiments on pine wood with similar operating conditions of 270 °C and 60 minutes residence time and reported a total mass loss of 40.0%, similar to this study. Furthermore, an 89% reduction in moisture, 38% reduction in volatile matter, and 1% reduction in the mass fixed carbon in the sample was reported.

Ultimate Analysis

Table 3-12 summarises the proximate analysis of the raw pine wood and the torrefied pine wood on a dried ash-free basis.

Table 3-12: Ultimate analysis of raw pine wood and torrefied pine wood (d.a.f)

	Current study		(McNamee *et al.*, 2016)	
	Raw Pine wood	Torrefied Pine wood	Raw Pine wood	Torrefied Pine wood
% Hydrogen	7.5	7.0	5.7	5.7
% Nitrogen	0.2	0.1	0.1	0.1
% Carbon	52.2	54.8	49.7	54.1
% Oxygen (calculation)	48.3	42.6	44.5	40.1
% Total sulphur	0.1	0.1	0.1	-

The hydrogen, nitrogen, and oxygen content of the wood decreased by 39%, 41%, and 42% during the torrefaction, respectively. The carbon content and total sulphur content decreased by 31% and 4.6% during the torrefaction, respectively. McNamee et al., (2016) conducted torrefaction experiments on pine wood with similar operating conditions of 270 °C and 60 minutes residence time and reported a hydrogen reduction of 35%, a nitrogen reduction of 51%, a carbon content reduction of 30%, and an oxygen reduction of 43%. These are similar to the findings of this study.

Calorific Value

Table 3-13 reports the calorific value of the raw pine wood and torrefied pine wood on an air-dried basis.

Table 3-13: Calorific value of raw wood and torrefied wood (a.d)

	Current Study		(Liao *et al.*, 2021)	
	Raw Pine Wood	Torrefied Pine Wood	Raw Pine Wood	Torrefied Pine Wood
Gross Calorific Value (MJ/kg)	18.5	19.5	17.7	18.2

The torrefaction of the pine wood resulted in a 5% increase in calorific value due to the increased fixed carbon content. A study by Liao et al., (2021) noticed a 3% increase in calorific value after torrefaction of pine wood at 280 °C.

Fibre Analysis

Fibre analyses were done on the raw and torrefied wood chips. **Table 3-14** summarises the fibre analysis results obtained.

Table 3-14: Summary of fibre analysis conducted on biomass and torrefied biomass

	Raw Pine Wood	Torrefied Pine Wood	Raw Pine Wood	Torrefied Pine Wood
	% Dry, ash free, extractive free			
	This study		(De Oliveira Brotto *et al.*, 2023)	
% Hemicellulose	14.7	4.4	16.8	2.5
% Cellulose	46.5	45.3	42.4	39.3
% Lignin	38.8	50.3	38.5	55.8
% Extractives	ND	ND	2.3	2.4

ND = not detected

An 81% breakdown of hemicellulose occurred at a temperature of 275 °C. The cellulose decreased by 38%, and lignin decreased by 17%, causing the weight percentage to increase. These findings concur with the initial TGA tests (Refer to **Appendix A Torrefaction pre-tests**). De Oliveira Brotto et al., (2023) studied the torrefaction of pine wood chips at an operating temperature of 290 °C and residence time of 30 minutes. The study showed a 91% reduction of hemicellulose, 41% reduction of cellulose, and 7% decrease in lignin content. This reduction in hemicellulose is higher than reported in this study due to the elevated operating temperature.

3.4.3 Pellet Characterisation

Extrusion

The pellets produced held their form after exiting the extruder. Their integrity can be attributed to the extrusion process, which relies on compression to shape the pellets. The compression exerted during extrusion ensured that the pellets possessed the necessary structural integrity for their intended applications. Notably, including biomass significantly compromised the structural integrity of the resulting pellets, rendering them too fragile for practical use in the absence of a binding agent. Conversely, the coal component did not exhibit such a requirement for an additional binder. The PVA was added to all blends, including the 0% and 100% biomass samples, for consistency. The 90% and 100% biomass pellets needed 3 wt% of starch to pelletise with sufficient structural integrity.

Proximate analysis

Figure 3-4 shows the proximate analysis results of the pellet blends.

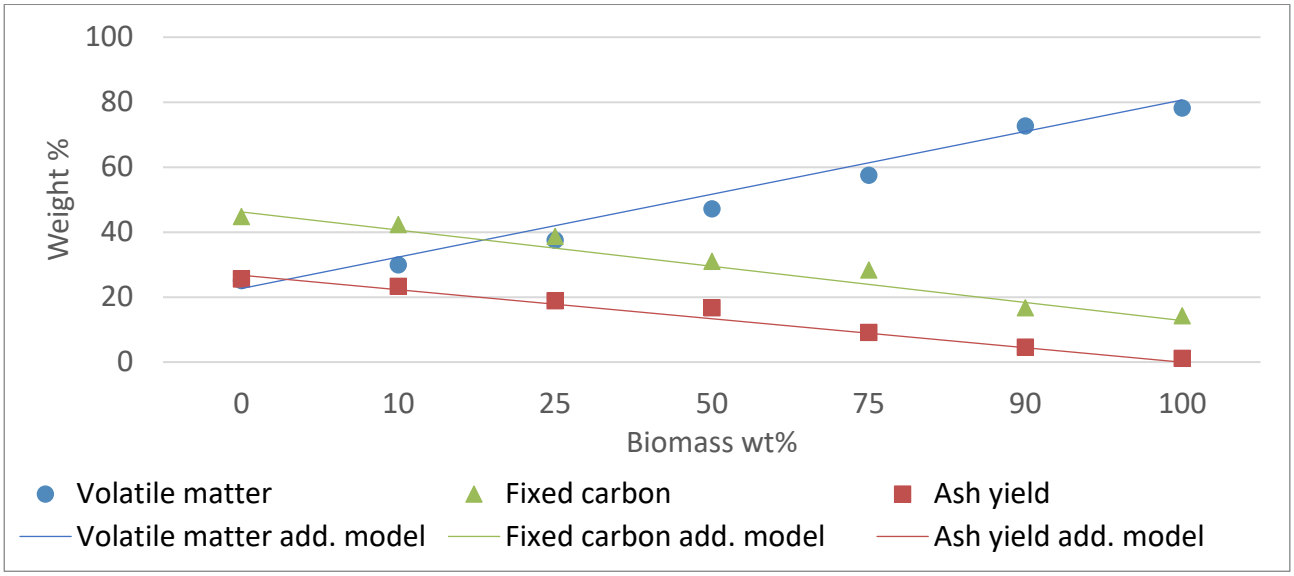

Figure 3-4: Proximate analysis of pellet blends (a.d)

Figure 3-4 depicts the volatile matter, fixed carbon, and ash yield of the pellet blends. Fixed carbon and ash yield steadily decreases with rising biomass content, while volatile matter shows a reciprocal rapid increase. These trends are because biomass inherently has lower ash content, lower fixed carbon, and higher volatile content. An additive model for the pellet composition is determined using the following equation:

$$Component_i\ wt\% = (x_{i,Coal} \cdot y_C + x_{i,Biomass} \cdot y_B) \cdot 100 \qquad \text{(E3-3)}$$

In Equation 3-3, the weight percentage of component *i* is determined as a function of the inherent weight percentage of component *i* of the parent coal ($x_{i,Coal}$) and the inherent weight percentage of component *i* of the torrefied biomass ($x_{i,Biomas}$). y_C and y_B represent the fraction of coal and the fraction of biomass in the pellet, respectively.

The compositions of the pellet blends correlate with the respective additive models. This correlation suggests that the pellet blends are homogeneous since the compositions follow a linear function with the biomass content used as the independent variable. The ash yield in the 100% coal pellet is lowered by 4.3% from the parent coal while the volatile matter slightly increases. These trends are due to the added polyvinyl alcohol binder, which consists of C-OH polymers. The 100% biomass pellets showed a slight reduction in volatile matter due to adding 5 wt% polyvinyl alcohol and 3 wt% starch as binder. The binders are suspected to contain inherently less volatile matter than the wood, reducing the overall volatile matter content.

Ultimate analysis

Figure 3-5 shows the ultimate analysis of the pellet blends.

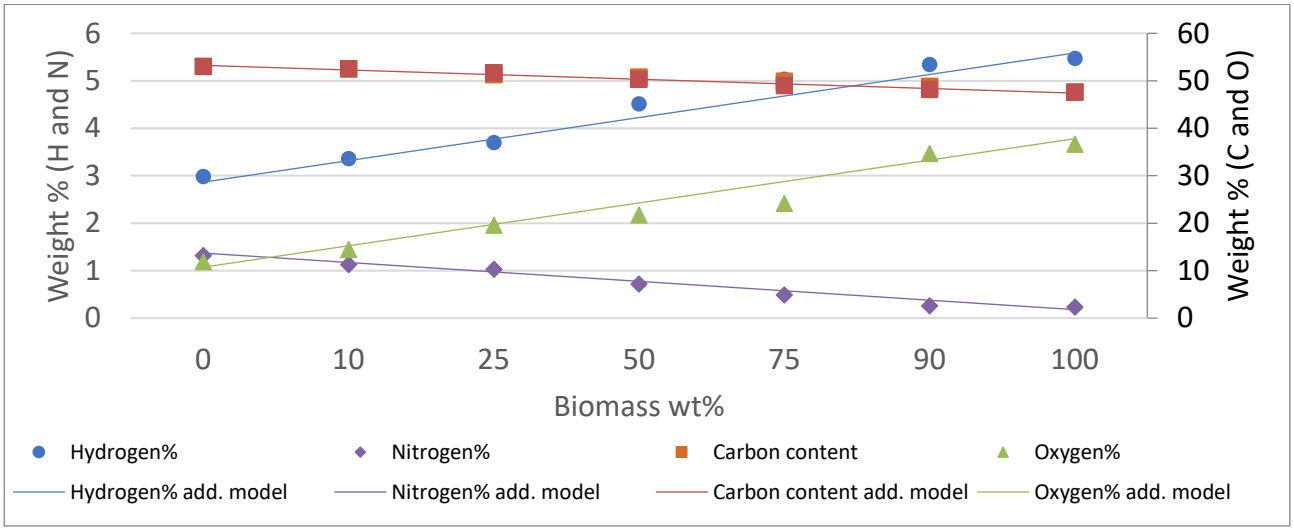

Figure 3-5: Ultimate analysis of pellet blends

The analyses show that the compositions of the pellet blends correlate with the respective additive models determined using Equation 3-3. This correlation speaks to the homogeneity of the blends since the composition is a linear function of the biomass and coal percentages.

Calorific Value

Figure 3-6 shows the outcome of the gross calorific values obtained for the pellet blends.

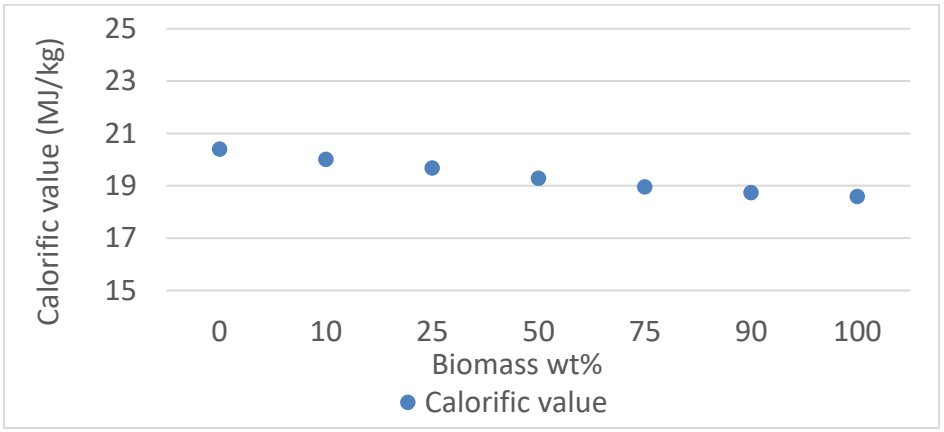

Figure 3-6: Calorific value of pellet blends

A steady decrease in CV is noticed with an increase in biomass composition. This trend is due to biomass inherently having a lower CV than coal. In the coal–biomass blending range, 0% to 100% biomass, a CV decrease of 9% is measured, consistent with the ash contents and carbon contents of the samples.

Compressive Strength

The pellets obtained through the extrusion processes were subjected to compressive strength testing to assess the structural durability of the pellets. The experimental deviation for the compressive strength was determined by repeating the compressive strength test for each pellet blend 5 times.

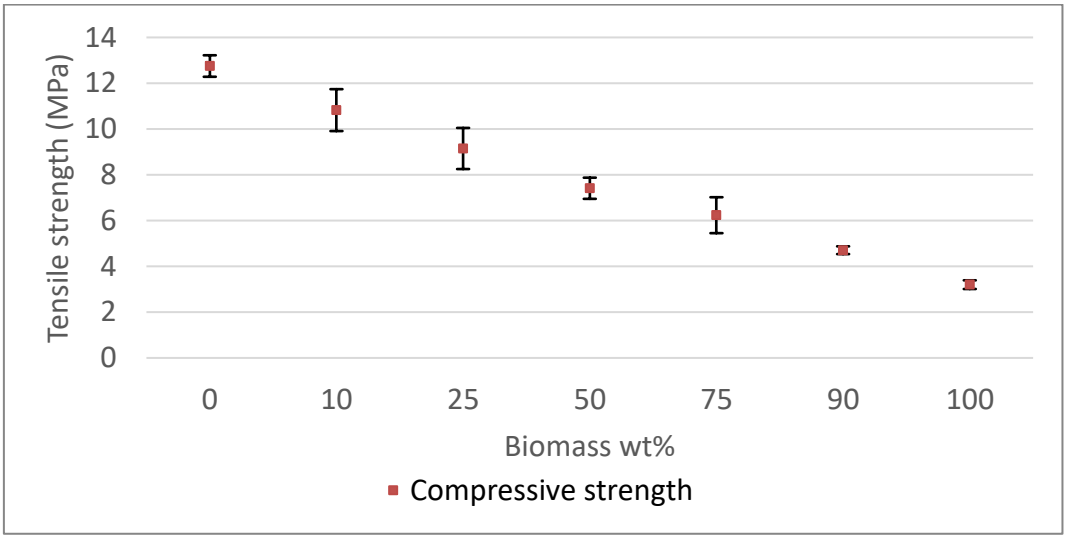

Figure 3-7: Compressive strength of pellet blends

Figure 3-7 shows the compressive strength of the different pellet blends. The compressive strength (MPa) steadily decreases with increased biomass content. The compressive strength decreases from 12.8 MPa (0 wt% biomass) to 4.7 MPa (90 wt% biomass). It becomes evident that coal particles generally tend to agglomerate, leading to higher compressive strength with higher coal content. This characteristic is often attributed to the cohesive properties of coal, including its higher carbon content and inherent binding capabilities (Yuan *et al.*, 2022). Sawdust particles tend to have lower agglomeration tendencies due to their composition primarily consisting of wood fibres, which lack the same adhesive properties found in coal (Yuan *et al.*, 2022).

3.5 Summary

Table 3-15 summarises the analysis results reported on the raw materials and pellet blends.

Table 3-15: Summary of analysis on pellet blends

	% Biomass	Torrefied wood	Parent coal	0	10	25	50	75	90	100
Proximate analysis (air-dried)	% Moisture	4.5	4.7	4.5	4.5	4.9	5.1	5.1	5.1	5.5
	% Volatile matter	79.5	22.3	25.1	29.9	37.5	47.2	57.5	72.7	78.2
	% Ash	0.9	29.9	25.6	23.3	18.9	16.7	9.1	4.6	1.1
	%Fixed carbon	15.3	43.1	44.8	42.3	38.7	31	28.3	17.7	15.2
Ultimate analysis (air-dried)	% Hydrogen	6.6	3.1	3.0	3.4	3.7	4.5	5.0	5.3	5.5
	% Nitrogen	0.1	1.2	1.3	1.1	1.0	0.7	0.5	0.3	0.2
	% Carbon	51.8	49.0	53.0	52.6	51.3	50.8	49.9	48.9	47.7
	% Oxygen (calculation)	40.3	11.3	11.9	14.5	19.6	21.7	24.2	34.7	36.7
	% Total sulphur	0.09	0.8	0.72	0.7	0.58	0.43	0.25	0.2	0.13
Gross calorific value (air-dried basis) (MJ/kg)		19.5	20.4	20.4	20.0	19.7	19.3	19.0	18.7	18.6
Gross calorific value (ash-free basis) (MJ/kg)		19.7	29.1	27.4	26.1	24.3	23.2	20.9	19.6	18.8
Lower heating value (ash-free basis) (MJ/kg)		18.5	28.4	26.7	25.4	23.4	22.1	19.7	18.4	17.6
Compressive strength (MPa)		NA	NA	12.7	10.8	9.2	7.4	6.2	4.7	4.1

This study focused on preparing and analysing coal-biomass blends in coal-burning stoves commonly used in households. Grade D coal fines and pine wood chips were chosen for their availability and ease of handling. Preparation methods were employed to ensure consistent sample quality. Torrefaction of wood chips was performed to modify specific characteristics for producing pellets with adequate integrity. Various blending ratios, ranging from 0% to 100% biomass, were tested, and polyvinyl alcohol (PVA) was added as a binder. Lab-scale techniques were used to make pellets, with extrusion being the preferred method for combustion experiments. The study found that as biomass content increased, the calorific value (CV) decreased due to the lower heating value of biomass. Coal exhibited higher agglomeration tendencies compared to wood, as the compressive strength of the pellets decreased as the biomass percentage increased.

CHAPTER 4: EXPERIMENTAL METHODS FOR COMBUSTION TESTS

The experimental methods used during the experimentation are discussed in this chapter. Section 4.1 summarises the material used during combustion experiments. Section 4.2 discusses the NWU semi-continuous stove and its operation. Section 4.3 Discusses the experimental setup and data capture. Section 4.4 discusses the processing of the experimentally obtained data.

4.1 Materials

Table 4-1 summarises the materials and gases used during combustion experiments.

Table 4-1: Materials used during combustion experiments

Description	Supplier	Detail	Use
Materials			
0% – 100% Biomass pellets	NWU	Produced with raw materials **Table 3-15: Summary of analysis on pellet blends**	Combustion experiments
Paraffin	Redspot chemicals	-	Fire-starter
Wood-chips	Sappi	Pine wood chips	Fire-starter
Acetone	Redspot chemicals	-	Cleaning sample lines
Ice	NWU	-	Moisture traps
Gases			
Nitrogen	Afrox	Purity: > 99.999%	Zero calibration, dilution of flue gas
CO	Afrox	991 ppm	Span calibration
CO_2	Afrox	20.4 vol%	Span calibration
NO	Afrox	288 ppm	Span calibration
SO_2	Afrox	525 ppm	Span calibration
Dry air	Afrox	21.2 vol% O2	Span calibration

4.2 Stove Characterisation and Operation

In this study, the combustion experiments were conducted using the NWU semi-continuous stove. This stove is primarily constructed from mild steel, except for the insulating material inside, which consists of refractory brick. It is designed to implement clean stove technology to ensure low emissions.

4.2.1 Characterisation of stove

The stove is operated based on how the stove is characterised. Taylor, (2009) used various criteria to characterise a solid fuel stove (Section 2.6.1: **Stove classification**). The NWU semi-continuous stove is characterised using the same criteria as a semi-continuous coal-burning stove. It features a mixed-feed system, essentially a batch-feed system that allows fuel to be added to the combustion zone during the burn cycle. This feature is possible due to the separate fuel hopper and combustion chamber. The stove operates under a non-gasifier combustion regime, which does not distinguish gas generation from gas combustion. Regarding ignition direction versus draft, the stove follows a cross-flow configuration, where the air supply flows perpendicular to the ignition direction. Heat transfer between the stove and cooking pot is primarily through conduction, with a steel plate between the combustion zone and the cooking pot. The combustion products are exhausted outside via a stack, making it an outside-exhausted stove, which improves indoor air quality and human health.

4.2.2 Stove Operation

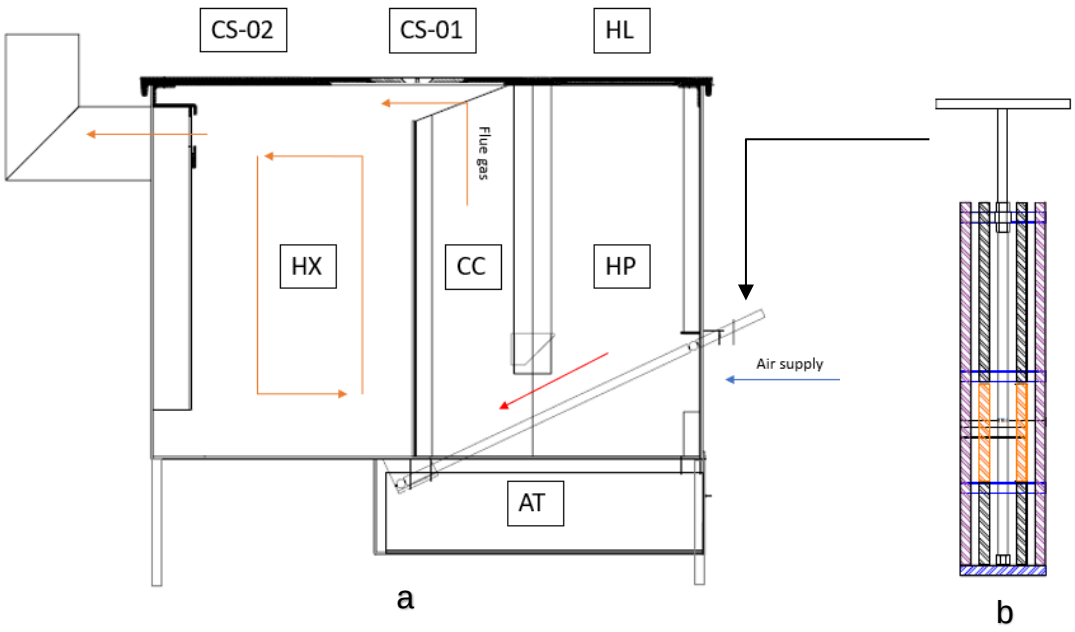

Figure 4-1: a) Stove drawing b) Grate

Table 4-2: Component list of NWU semi-continuous stove

Displayed Text	Description
CS-01	Main cooking surface
CS-02	Additional cooking surface
HL	Hopper lid
HX	Heat exchanger
CC	Combustion chamber
HP	Hopper
AT	Ashtray

Figure 4-1a provides a side-view illustration of the stove, featuring three distinct compartments: the hopper, the combustion chamber, and the heat exchanger. The hopper functions as a fuel container, with the fuel resting on the grate depicted in **Figure 4-1b**. The grate, positioned at a 30° angle towards the combustion chamber, facilitates automatic fuel feeding. The hopper is insulated with refractory brick lining from the combustion chamber. Similarly, the combustion chamber is lined with refractory brick to isolate it from the heat exchanger. An opening in the refractory brick between the combustion chamber and the heat exchanger allows combustion gases to flow into the heat exchanger. Here, the combustion gas circulates, enabling the heat exchanger to recycle the combustion gases, allowing the stove more time to absorb the heat from these gases. The grate is situated directly above the ashtray, ensuring that ash generated in the combustion chamber and the hopper is gathered in the removable ash tray for convenient cleaning. The grate is positioned in the stove with a 15 mm leeway parallel to the grate (opposite to the direction of fuel movement). This gap allows for a grate-shake. This shaking action becomes necessary when the fuel becomes stagnant and fails to move toward the combustion chamber. Moving the grate back and forth puts the fuel in motion and dislodges accumulated ash, causing it to fall into the ashtray. The grate also has a rotating action to dislodge further if necessary. The stove has a cooking surface directly above the combustion chamber (CS-01) and another above the heat exchanger (CS-02). The air supply opening is not fixed, which can be manipulated to control the air supply to the combustion chamber. Sliding a steel sheet over the opening can adjust the opening size. This function is used to manage fuel consumption and heat output. A mostly closed air supply (low-power) causes a slower burn, resulting in smaller heat output. This setting is convenient for space heating. An open air-supply (high-power) causes higher fuel consumption, producing more heat. This setting is convenient for cooking.

4.3 Experimental Setup and Data Acquisition Procedures

In preparation for the combustion experiment, the following steps were undertaken for emissions monitoring, temperature monitoring, and mass monitoring processes. **Figure 4-2** represents a schematic of the complete experimental setup for emissions, temperature, and mass monitoring. **Table 4-3** is an instrument list of the equipment used in the experimental setup.

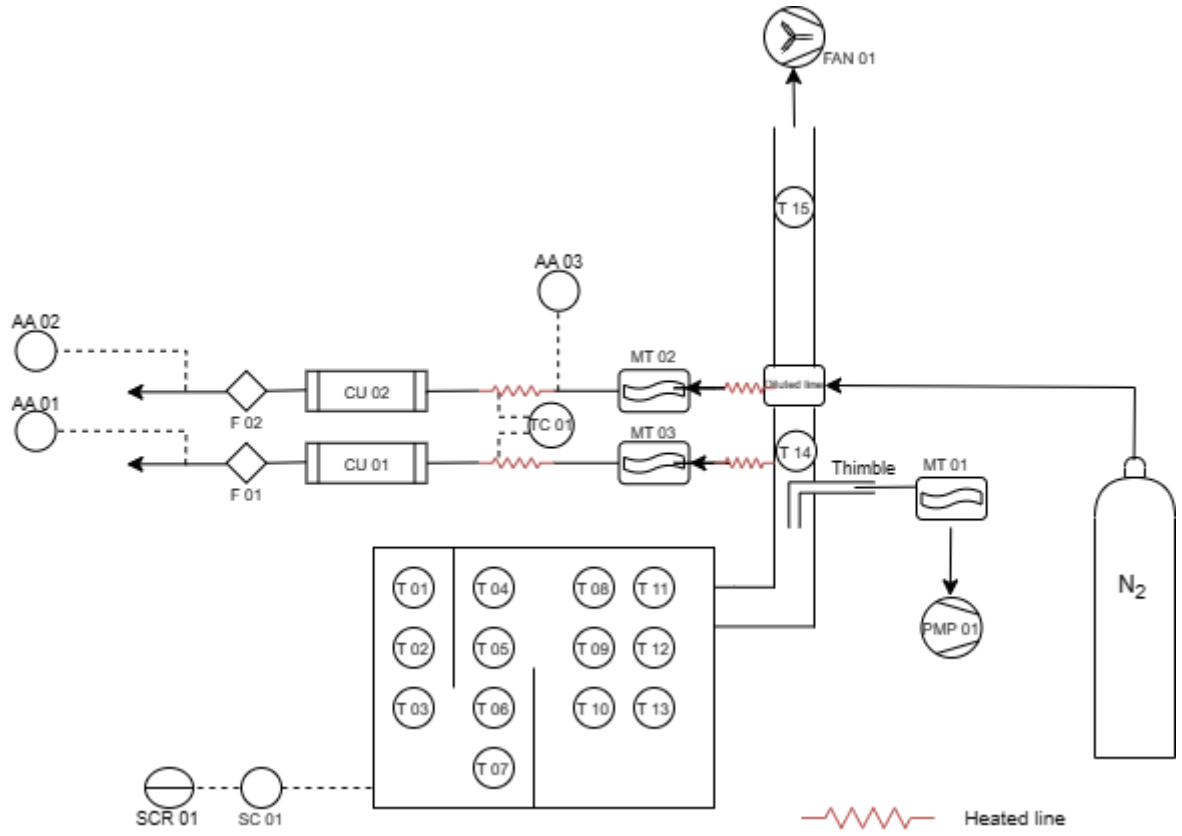

Figure 4-2: Stove experimental setup schematic

Table 4-3: Instrument list of stove experimental setup

Displayed text	Description	Displayed text	Description
T 01 - 15	K-type thermocouple	MT 01 - 03	Moisture trap
AA 01	Horiba PG 350 analyser (undiluted)	PMP 01	Aquaria CF20 pump
AA 02	Horiba PG 350 analyser (diluted)	FAN 01	Extractor fan
AA 03	DustTrak II	TC 01	Temperature controller
CU 01	Conditioning unit	SC 01	Sartorius platform scale
CU 02	Conditioning unit	SCR 01	Combix 2
F 01 - 02	Filter	COMP	Computer

4.3.1 Standard Operating Procedures

Cleaning Procedure

In preparation for the combustion experiment, the experimental setup undergoes cleaning. The ash buildup inside the stove is cleaned. This buildup does not necessarily occur in the ashtray only since the fly ash from the previous combustion experiment can accumulate in the heat exchanger section of the stove. The sampling lines are purged with acetone and nitrogen. This procedure is carried out to eliminate residual soot and prevent moisture buildup within the lines, which could compromise the accuracy of subsequent measurements.

Equipment Safeguard Procedure

The temperature controller (TC-01) of the insulated sampling lines is set to 90 °C to safeguard against moisture-related issues. This precaution is taken to prevent the moisture present in the flue gas from condensing, which might lead to blockages and potentially harm the gas analysers. The conditioning units (CU-01, CU-02) feature filters that undergo cleaning in an ultrasonic bath with acetone to eliminate accumulated soot buildup. These filters are dried before they are installed into the conditioning units. The in-line filters are swapped with clean filters. The moisture traps (MT-01, MT-02, MT-03) are drained and filled with ice.

Instrument Calibration

The warmup procedure for the gas analysers is started. This procedure takes 30 minutes to complete. The gas analysers underwent zero calibration using nitrogen and span calibration for CO, CO_2, NO, SO_2, and O_2. The DustTrak particulate matter analyser is zero-calibrated with a zero-filter that does not allow particulate matter to enter the sampling line.

Instrument Response Delay

The flue gas sampled by the gas analysers undergoes a travel time from the combustion zone. A temporal gap exists between the mass loss recorded on the scale and the corresponding readings captured by the gas analysers at that specific moment of mass loss. During commissioning experiments, it was observed that the effects following a grate shake were registered by the gas analysers five seconds after the initiation of the shake. The gas analyser data is adjusted to address the delay between the real-time measurements.

Start-up Procedure

The scale is tared so that the initial mass reading is zero. The ignition process is prepared by adding fuel to the hopper until the grate is covered from the combustion zone to the hopper, approximately 1 to 1.5 kg (depending on fuel density). Approximately 150 g of pine wood chips are placed on the fuel bed in the stove, above the 1.5 kg of fuel. Two wood chips soaked in paraffin are placed on the wood chips as fire starters. The air controller is closed (irrespective of the power setting of the experiment). The fire is started with a matchstick directly after all loggers are activated and logging has started. After the ignition phase is completed (fuel bed reaches 500 °C), the air controller is set to the intended power setting (completely open for high-power experiments and 2 mm open for low-power experiments), and the hopper is filled with pellets and left until burnout. The experiments are done using a constant initial volume of fuel. This decision is based on the target demographic generally using the stove for cooking rather than heating, which entails a shorter run-time.

Water Boiling Test Procedure

The water boiling test procedure is standardized to isolate the manipulated variables outlined in this study as the sole factors affecting the boiling time of water. This method is consistent with previous studies conducted on the NWU semi-continuous stove. The procedure differs throughout literature due to factors such as stove size and atmospheric pressure, influencing the accuracy of the water boiling test. Before each experiment, the cooking pot is cleaned, and one litre of water is added. The cooking pot is placed on the cooking surface CS-01 (refer to **Figure 4-1a**) immediately following the initial grate-shake in each experiment. The pot is removed when the water reaches a temperature of 95 °C.

Grate Shake Procedure

The grate-shake procedure is necessary due to ash accumulation in the combustion zone and fuel stagnation in the hopper. This procedure effectively resolved both issues through a dual-action motion, as detailed in Section 4.1.2. It remained consistent across all experiments. The grate-shake involves parallel and twist motions. Both motions are applied twice at high intensity to prevent procedure failure and the need for repetition. The grate-shake procedure is considered to have failed if the fuel and accumulated ash have not been sufficiently agitated. This procedure significantly impacted stove emissions performance, causing a sharp increase in fly ash and carbon monoxide production due to the disturbance of the fuel bed. The necessity for a grate shake was determined by two variables: the combustion zone temperature (T-07) drops below 600 °C, the oxygen content in the flue gas exceeds 12 vol%, or visible dead zones in the fuel bed are observed.

Handling of Ash

The ash produced from combustion experiments was allowed to cool and was collected the day after the experiment. The ash was subjected to crushing and mixing in a ball mill to ensure a uniform mixture. The ash was then stored in sealed bags awaiting analysis.

4.3.2 Emissions Monitoring

Three distinct sample lines are deployed as the flue gas flows through the stack. Two of these lines allow the unaltered flue gas (without diluting the flue gas with nitrogen) to flow through. The first of these two lines incorporated a thimble filter designed to capture particulate matter. The flue gas is then directed to a moisture trap (MT-01) and a thimble filter pump (PMP-01). The second unaltered flue gas line leads to the second moisture trap (MT-02). The moisture traps are ice baths with the sample line leading through them. The condensed moisture leaks into a reservoir while the cool flue gas flows to the conditioning unit (CU-01)

Higher up in the chimney, a diluter is positioned to blend the flue gas with nitrogen, thereby diluting it. The third sample line is connected to the diluter and guides the diluted flue gas to a third moisture trap (MT-03). This line is diluted because the PM concentration in the flue gas exceeded the DustTrak analyser's detection range. To prevent condensation within the sample lines leading to the moisture traps, they are equipped with electrically heated lines that are wrapped around the sample lines. The sample lines and heated lines are wrapped in thermal foam for insulation, ensuring the preservation of the gas state until reaching the moisture traps.

Two conditioning units (CU-01 and CU-02) are downstream from the moisture traps, each corresponding to a gas analyser. The primary function of these conditioning units is to eliminate residual moisture from the flue gas before analysis. Further downstream, just before reaching the gas analysers, in-line filters (F-01 and F-02) provide additional protection against moisture and particulate matter. These measures collectively ensured the safety of the gas analysers. An extraction fan (FAN-01) is directly above the chimney to extract the flue gas outside.

Horiba PG-300 Series Portable Gas Analyser

The gas analyser PG-300 utilizes different detection methods for various gases: NO_x detection employs cross-modulation Chemiluminescence Detection (CLD) Method, while SO_2 and CO detection use cross-modulation Non-Dispersive Infrared Absorption (NDIR) Method. CO_2 detection utilizes Non-Dispersive Infrared Absorption (NDIR) Method, and O_2 detection utilizes a Paramagnetic method. The cross-modulation mechanism alternates sample and reference gases in the same cell, reducing drift and enhancing stability. The device features a user-friendly LCD touchscreen,

advanced functions, and reduced warm-up time (30 minutes). The NO_x converter ensures 95% efficiency, and the analyser is energy-efficient (35% reduced power consumption) and equipped with SD™ memory card slot and ethernet interface for data storage and real-time communication.

DustTrak™ II Aerosol Monitor 8532

The DustTrak™ II Aerosol Monitor 8532 is a handheld, battery-operated device utilizing light-scattering laser photometry to provide real-time aerosol mass readings. Its sheath air system isolates aerosols in the optics chamber, ensuring clean optics, improved reliability, and low maintenance. Suitable for various environments, including clean offices and harsh industrial sites, it measures contaminants like dust, smoke, fumes, and mists. The device offers manual and programmable data logging, covers aerosol concentrations from 0.001 to 150 mg/m³, and detects particles corresponding to PM_1, $PM_{2.5}$, respirable, or PM_{10} size fractions. It is lightweight, portable, and is a single-channel, handheld unit.

4.3.3 Temperature monitoring

The internal and external surface temperatures of the stove are monitored during combustion experiments. The internal temperatures of the stove are measured in real-time, with 10-second intervals, using fixed K-type thermocouples placed inside the stove. A laser pyrometer measures The external temperature at specific intervals throughout the combustion experiment. **Figure 4-3** shows an isolated stove schematic with temperature monitoring equipment.

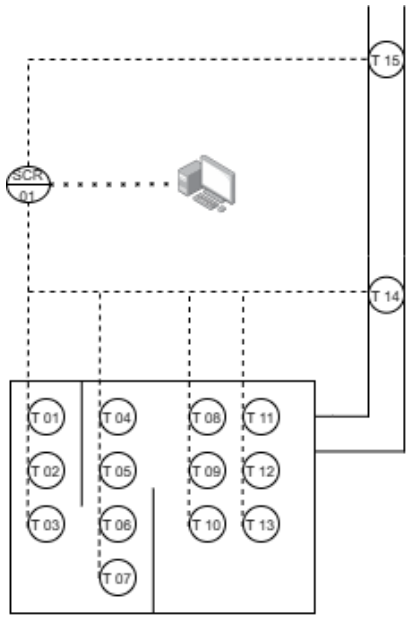

Figure 4-3: Thermocouple placement in stove

A network of thermocouples monitors various temperature points within the stove. Three thermocouples (T-01, T-02, T-03) are positioned in the stove hopper (as indicated in **Figure 4-1** section HP) to measure the feed fuel temperature. This section feeds the combustion chamber. However, due to its proximity to the combustion chamber, temperature rises are anticipated during prolonged combustion.

Within the combustion chamber (refer to **Figure 4-1a** section CC), four thermocouples (T-04, T-05, T-06, T-07) are deployed. T-07 is located directly above the grate in the fuel bed. T-04 monitors the temperature of the combustion gas entering the heat exchanger, while T-05 and T-06 are positioned to record the temperature of the fuel bed and flames.

Moving into the heat exchanger section of the stove (refer to **Figure 4-1a** section HX), six thermocouples (T-08, T-09, T-10, T-11, T-12, T-13) are placed to outline the temperature profile of the flue gas movement within this area. Here, the flue gas circulates to dissipate heat, and the arrangement of thermocouples allowed for an analysis of the temperature variations throughout the heat exchanger.

Additionally, to estimate the total heat loss through the chimney, two thermocouples (T-14, T-15) are positioned within the chimney to measure the temperature of the exiting flue gas. Each thermocouple is individually connected to a Combix unit (SCR-01), enabling the computer to record the temperature readings from the thermocouples.

The surface temperature of the cooking surface is measured with a laser pyrometer at 30-minute intervals throughout the combustion experiment. This measurement is intended to give insight into when the stove surface is ready for cooking since all experiments are cold-started.

4.3.4 Mass monitoring

The stove is positioned on a platform scale (SC-01) to measure the mass throughout the combustion experiments at 10-second intervals. This data gives insight into the burning rate of the fuel and serves as the foundation for establishing the carbon balance. The scale is connected to a Combix unit (SCR-01), enabling the computer to monitor the mass of the setup as the experiment progresses. The ashtray is also on the scale, meaning the mass loss due to fuel combustion is ash-free.

4.4 Data Processing and Analysis

The methods used to determine the specific thermal and emissions performance of the semi-continuous stove are discussed in this section.

4.4.1 Thermal Performance

The various thermal performance indicators use the temperature and mass data obtained from the combustion experiments. The thermal efficiency of the system is evaluated based on energy output. It includes the system efficiency (η_{system}), which gives the fraction of total usable energy delivered, cooking efficiency (η_{cook}), indicating the fraction of energy released by the burning fuel delivered to the pot and heating efficiency (η_{heat}), describing the energy delivered into the room for space heating. Another parameter is combustion efficiency (η_{comb}), which accounts for the combustible fraction remaining in the residue after the fire has been extinguished.

Ignition Time

In the study conducted by Le Roux, (2009), ignition was characterized using an *imbaula*, which was defined as an elevation in temperature directly above the fuel bed. Similarly, Sumbane-Prinsloo et al., (2021) and Kühn et al., (2017) employed a conventional Union stove, defining ignition as a temperature increase within the fuel bed up to 500 °C. This study defines ignition as the temperature directly above the fuel bed, measured by the K-type thermocouple (T-06), attaining 500 °C (Refer to **Figure 4-3**). The time elapsed from the initiation of the ignition process to the point of achieving ignition is recorded for analysis.

Fuel Burn Rate

The fuel burn rate is the rate at which fuel is consumed in the stove on an air-dried basis. The ash produced by the burning fuel is factored into the mass loss. The energy output and heat transfer efficiencies in the stove's thermal performance context necessitate knowledge of the fuel burn rate. This parameter is derived from mass loss data obtained via the scale (SC-01) positioned beneath the stove (Refer to **Figure 4-2**) and the composition of the fuel.

Data logging on the scale initiates after the experiment startup procedure is completed. This precaution is needed as any interactions with the stove cause fluctuations in mass loss readings. Some interactions are unavoidable, such as placing the cooking pot on the stove for the water-boiling test. To mitigate these fluctuations, holding one litre of water, the cooking pot is weighed before and after being placed on the stove. When the water temperature reaches 95 °C, the pot is removed, ensuring water evaporation does not impact the mass loss data.

During the experiment startup procedure, where fuel is added in two stages, the mass of the stove increases while data logging is ongoing. The mass of the second batch of fuel is weighed before being added to the stove to note the total mass of fuel used during the experiment, as mass loss occurred during the ignition of the first batch. Additionally, the grate-shake procedure, taking approximately two seconds to complete, has minimal impact on the data, given that its duration is smaller than the 10-second intervals between data logging points. The mass recordings (m_t) are altered to 1-minute intervals (Δt) to minimise the noise in the data using Equation 4-1. The mean burn rate is determined with Equation 4-2:

$$\frac{dm_{a.f}}{dt} \approx \frac{m_t - m_{t-1}}{\Delta t} \quad \text{(E4-1)}$$

$$R_{mean} = \frac{dm_{a.f}/dt}{(1 - x_{ash})} \quad \text{(E4-2)}$$

$\frac{dm_{a.f}}{dt}\left[\frac{g}{min}\right]$ is the mass loss recorded from fuel combustion on an ash-free basis in a 1-minute interval, and x_{ash} is the ash yield of the fuel obtained from the proximate analysis.

Power Output

The power output (P) of the stove refers to the rate at which the stove generates thermal energy or heat. In scientific terms, it can be described as the stove's heat output per unit of time. The lower heating value ($LHV_{a.f}$) on an ash-free basis is used to determine the power output. The lower heating value is determined using the calorific value and compensating for the heat lost to moisture formation and evaporation. The LHV can be calculated using the following equation (EPA, 2007):

$$LHV_{a.f} = CV_{a.f} - H_{v,water} \cdot (x_{moist} + 9 \cdot x_H) \quad \text{(E4-3)}$$

$$P\ [kW] = \frac{m_{a.f} \cdot LHV_{a.f}}{60} \quad \text{(E4-4)}$$

Where $CV_{a.f}\left[\frac{MJ}{kg}\right]$, $H_{v,water}\left[\frac{MJ}{kg}\right]$, x_{moist}, and $m_{a.f}\ [g]$ represents the calorific value of the fuel on an ash-free basis, the heat of evaporation of water (2.24 $[MJ/kg]$), the moisture content of the fuel, and the mass loss recorded from fuel burned on an ash-free basis throughout the experiment, respectively.

System Efficiency

The overall system efficiency determines the effective heat output provided by the system. This assessment encompasses the stove's dual heating and cooking device functionality. Specifically, it focuses on the heat lost through the stack as the only heat lost, given that the heat dispersed within the house environment is utilized for heating purposes. The system efficiency can be defined as the ratio of energy delivered to both the cooking pot and the room and the energy released during fuel combustion. The system efficiency also accounts for the heat lost through incomplete combustion. The CO_2 to CO ratio indicates the degree of incomplete fuel combustion. The Siegert method is used to calculate the heat loss through the stack (Kumar & Singh, 2016; TSI, 2004; Verma *et al.*, 2012):

$$S_L[\%] = k_s \cdot \frac{T_{fg} - T_a}{yCO_2} \quad \text{(E4-5)}$$

Where the flue losses are represented by S_L. T_{fg} and T_a are the flue gas temperature and the ambient temperature, respectively. yCO_2 is the fraction of carbon dioxide in the flue gas and k_s is the Siegert constant. The value of the Siegert constant is 0.63 $\left[\frac{1}{°C}\right]$ for coal and 0.64 $\left[\frac{1}{°C}\right]$ for pine wood (Kumar & Singh, 2016). T_{fg} is the temperature at the chimney exit measured by thermocouple T-15. The heat loss due to incomplete combustion is given through the following equation:

$$S_{CO}[\%] = \frac{\alpha \cdot yCO}{yCO + yCO_2} \quad \text{(E4-6)}$$

Where S_{CO} represents the heat lost due to incomplete combustion. yCO is the fraction of carbon monoxide in the flue gas, and $\alpha = 0.75$ is a coefficient based on the enthalpy of formation difference between CO_2 and CO.

The usable power output of the stove incorporates system efficiency (η_{system}) determined with the heat loss factors S_L and S_{CO}:

$$\eta_{system} = 100 - S_L - S_{CO} \quad \text{(E4-7)}$$

$$P_U = P \cdot \frac{\eta_{system}}{100} \quad \text{(E4-8)}$$

Where P is the power output (E4-4) and P_U is the usable power output of the stove.

Cooking Efficiency

The cooking efficiency (η_{cook}) is the relation between the energy used to boil water in the cooking pot and the total energy released from fuel combustion. Equation 4-8 is used:

$$\eta_{cook} = \frac{m_W \cdot Cp_W \cdot \Delta T}{\Delta m_{a.f} \cdot LHV_{a.f}} \cdot 100 \quad \text{(E4-9)}$$

Where m_W, $\Delta m_{a.f}$, Cp_W, and $LHV_{a.f}$ represent the mass of water in the cooking pot, the mass loss recorded from fuel burned (ash-free) to raise the water to the desired temperature, the specific heat capacity of water, and the lower heating value of the fuel on an ash-free basis, respectively. The variable ΔT denotes the temperature variation experienced by the water in the cooking pot. The designated temperature endpoint for the water in the cooking pot was set at 95 °C. This choice was made to prevent the heat energy from vaporising the water, thereby avoiding additional mass loss recorded on the stove.

Heating Efficiency

The heating efficiency (η_{heat}) is the relation between the energy used to heat the room and the total energy released from fuel combustion. Mathematically, the heating efficiency is the cooking efficiency subtracted from the system efficiency (Deng, Nie, Yuan, *et al.*, 2022; Kühn *et al.*, 2017; Sumbane-Prinsloo *et al.*, 2021). Equation 4-9 is used:

$$\eta_{heat} = \eta_{system} - \eta_{cook} \quad \text{(E4-10)}$$

The heat transferred to the room for heating corresponds to the residual thermal energy remaining after deducting the heat losses through the stack and the heat absorbed by the cooking pot and water from the total heat generated during fuel combustion.

Combustion efficiency

The combustion efficiency (η_{comb}) is defined as the ratio between the energy lost due to carbon in the ash that has not combusted as intended and the total energy released due to fuel combustion. Kühn et al., (2017) and Sumbane-Prinsloo et al., (2021) used a similar method during stove-combustion experiments. Equation 4-10 is used:

$$\eta_{comb} = \frac{32.8 \cdot m_A \cdot \left(\frac{LOI}{100}\right)}{m_{a.f} \cdot LHV_f} \cdot 100 \quad \text{(E4-11)}$$

In the equation, the numerator signifies the overall energy loss attributable to unreacted carbon in the stove's ash chamber, where 32.8 represents the calorific value of fixed carbon, m_A denotes the ash mass, and LOI represents the loss of ignition. The loss of ignition is defined as the difference in mass before and after the ash is exposed to high temperatures (850 °C) for a prolonged period to burn the remaining combustible material in the ash. The denominator represents the complete

energy output resulting from the fuel combustion during the experimental process, where $m_{a.f}$ denotes the mass loss recorded from fuel burned (ash-free) from ignition to burnout and $LHV_{a.f}$ denotes the lower heating value of the fuel on an ash-free basis.

4.4.2 Emissions Performance

The gas analysers sample the flue gas in the stack and record the concentration of each pollutant (CO, CO_2, NO_x, SO_2, and O_2) in volume percentage (vol%) on a dry basis.

Carbon Balance

A carbon balance is done over the combustion process to quantify the pollutants in the flue gas. The mass loss data acquired from the mass monitoring equipment is used to determine the combusted carbon with the following:

$$\frac{dm_C}{dt} = \frac{dm_{a.f}}{dt} \cdot x_{C,a.f} \tag{E4-12}$$

Where $\frac{dm_C}{dt}\left[\frac{g}{min}\right]$ is the carbon mass loss recorded from fuel combustion in a 1-minute interval. $\frac{dm_{a.f}}{dt}\left[\frac{g}{min}\right]$ and $x_{C,a.f}$ is the mass loss recorded from fuel burned on an ash-free basis in a 1-minute interval and the carbon content of the fuel on an ash-free basis, respectively. The mass carbon is converted to mole carbon.

$$\frac{dn_C}{dt} = \frac{{dm_C}/{dt}}{MW_C} \tag{E4-13}$$

Where ${dn_c}/{dt}\left[\frac{mol}{min}\right]$ is the molar flow rate of carbon burned in the fuel in a 1-minute interval, and MW_C is the molar mass of carbon. With the change in mass in the stove being monitored, the CO_2 + CO fraction is known. The following equation represents the carbon balance over the combustion process:

$$\frac{dn_{fg}}{dt} = \frac{\frac{dn_C}{dt}}{(1 - y_{H_2O}) \cdot (y_{CO} + y_{CO_2})} \tag{E4-14}$$

Where ${dn_{fg}}/{dt}\left[\frac{mol}{min}\right]$ is the molar flow rate of the flue gas in the stack on a dry-basis measured in a 1-minute interval. y_{CO} and y_{CO_2} is the molar gas fraction of carbon monoxide and carbon dioxide in the flue gas on a dry-basis. y_{CO} and y_{CO_2} are obtained from the gas analyser data. y_{H_2O} is the fraction of H_2O in the flue gas used to convert the flue gas interpretations to a wet basis. The fraction of H_2O

in the flue gas is assumed to be 5 vol% (Luo *et al.*, 2023). The molar flow rates of carbon monoxide (CO), carbon dioxide (CO_2), nitrogen oxides (NO_x), and sulphur dioxide (SO_2) in the flue gas can be determined using Equation 4-15:

$$\frac{dn_i}{dt} = \frac{dn_{fg}}{dt} \cdot y_i \cdot (1 - y_{H_2O}) \quad \text{(E4-15)}$$

Where ${dn_i}/{dt}\ \left[\frac{mol}{min}\right]$ and y_i represent the molar flow rate on a wet-basis and gas fraction of component i in the flue gas on a dry-basis, respectively. The gas fraction is converted to a wet basis with the fraction of H_2O (y_{H_2O}) in the flue gas. The molar flow rate of the pollutants is then converted to mass flow rates with their respective molar mass:

$$\frac{dm_i}{dt} = \frac{dn_i}{dt} \cdot MW_i \quad \text{(E4-16)}$$

Where ${dm_i}/{dt}\ \left[\frac{g}{min}\right]$ and MW_i represent the mass flow rate in 1-minute intervals and the molar weight of component i in the flue gas, respectively.

Emission Factors

The emissions performance of the stove is defined by the emission factors of the pollutants that contribute to the composition of the flue gas. These include CO_2, CO, NO_x, SO_2, and PM. The emission factors are calculated on an energy basis since the fuels used in this study vary in composition and energy content.

$$EF_i = \frac{\int_0^t m_i}{E_{UH}} \quad \text{(E4-17)}$$

$$E_{UH} = m_{a.f} \cdot LHV_{a.f} \cdot \eta_{system} \quad \text{(E4-18)}$$

where EF_i is the emission factor of component i in the flue gas determined by integrating the mass of component i (m_i) detected in the flue gas in 1-minute intervals over the total duration of the combustion experiment ($t\ [min]$) and dividing by the usable heat energy released from the burned fuel ($E_{UH}\ [MJ]$). E_{UH} is determined with the mass fuel burned on an ash-free basis ($m_{a.f}$), the lower heating value of the fuel on an ash-free basis ($LHV_{a.f}$), and the system efficiency (η_{system}) of the stove. An example of the carbon balance and overall mass balance can be seen in **Appendix C: Carbon Balance**.

Flue gas flow rate

The flue gas flow rate is the flue gas volume flowing through the chimney. The flue gas volume encompasses the combustion products and the excess oxygen and nitrogen entering the stove air supply. Equation 4-19 is used to determine the volumetric flow rate (V_0 $\left[\frac{m^3}{s}\right]$) of the flue gas:

$$V_o = \frac{dn_{fg}}{dt} \cdot \frac{R \cdot T_{chimney}}{P_{atm}} \quad \text{(E4-19)}$$

Where R $\left[\frac{J}{mole \cdot K}\right]$ is the ideal gas constant, $T_{chimney}$ $[K]$ is the temperature of the chimney, and P_{atm} $[kPa]$ is the atmospheric pressure. The atmospheric pressure in Potchefstroom, South Africa, is 87.5 kPa.

The velocity of the flue gas (v $\left[\frac{m}{s}\right]$) through the chimney is determined with Equation 4-20:

$$v = \frac{V_o}{A} \quad \text{(E4-20)}$$

$$A = \pi \cdot \left(\frac{d}{2}\right)^2 \quad \text{(E4-21)}$$

Where A $[m^2]$ is the cross-sectional area of the inner chimney determined with the inner diameter of the chimney (d $[m]$). The chimney has a cross-sectional diameter of 96 mm.

CHAPTER 5: RESULTS AND DISCUSSION

This chapter discusses the results of the combustion experiments, as detailed in Chapter 4. Section 5.1 discusses the **qualitative** observations resulting from the combustion experiments, focusing on the operation of the stove. Section 5.2 discusses the **quantitative** measurements done regarding the thermal performance of the fuel and stove. Section 5.3 discusses the **quantitative** measurements done regarding the emissions performance of the fuel and stove.

5.1 Stove Operation

This section discusses the **qualitative** observations from the combustion experiments with the pellet blends.

5.1.1 Fuel Consumption and Run-time

Figure 5-1 displays the fuel consumption rate and burnout times for the pellet blends during high-power experiments.

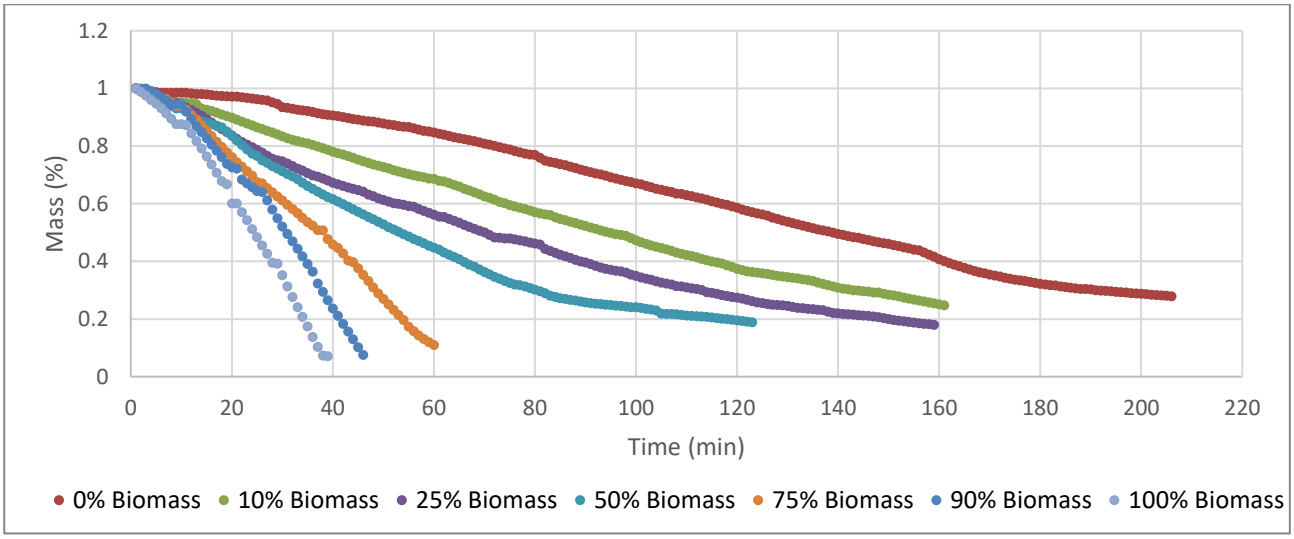

Figure 5-1: Fuel consumption as a function of combustion time and pellet composition (High-power experiments)

The pellet blends exhibit an increased fuel consumption proportional to the increase in biomass content. Pellets with 0% biomass (100% coal) display the lowest fuel consumption rate. Pellets containing 10% and 25% biomass demonstrate comparable run times. Pellets containing 75% and higher biomass exhibit a significant increase in burn rate, resulting in a prominent decrease in runtime. Onuegbu et al., (2011) reported similar results when conducting combustion experiments on a stove using coal and biomass blends. Yuan et al., (2022) reported that biomass pellets burned faster than coal pellets during thermogravimetric analysis of the two samples.

Figure 5-2 displays the fuel consumption rate and burnout times for the pellet blends during low-power experiments.

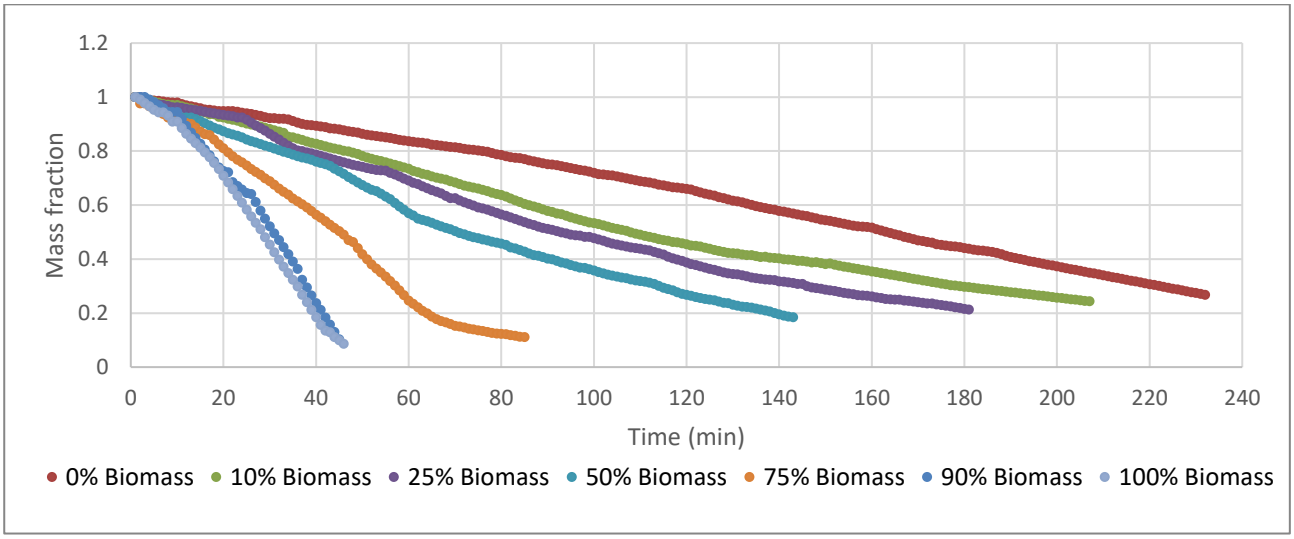

Figure 5-2: Fuel consumption as a function of combustion time and pellet (Low-power experiments)

The low-power experiments demonstrate a consistent trend with the high-power experiments concerning the correlation between burn rate and biomass content. The low-power experiments showcase an extended runtime when the fuel hopper is fully loaded compared to the high-power experiments. The 10% biomass pellets exhibit the largest increase in runtime of 31%. Consistent with the high-power experiments, a significant increase in burn rate and reduction in runtime is observed from a biomass content of 75% and higher in the low-power experiments. Deng et al., (2020) reported that increased air supply flow rates initiated increased burn rates, similar to this study, after conducting combustion experiments on a forced-draft stove with varying air supply flow rates.

5.1.2 Flue gas velocity

Table 5-1 shows the average volumetric flow rate and velocity of the flue gas through the chimney during combustion experiments. The experimental uncertainty is based on the deviation determined in **Appendix F** for the burn rate, as the volumetric flow rate is a function of the mass loss rate.

Table 5-1: Average flue gas volumetric flowrate and velocity of pellets through the chimney

% Biomass	0	10	25	50	75	90
Average volumetric flowrate through chimney (L/s)						
High-power	6.8 ± 0.4	5.9 ± 0.4	5.7 ± 0.4	9.1 ± 0.6	9.6 ± 0.6	10.3 ± 0.7
Low-power	5.4 ± 0.4	4.4 ± 0.4	5.6 ± 0.5	4.7 ± 0.4	5.8 ± 0.5	5.8 ± 0.5
Average flue gas velocity in chimney (m/s)						
High-power	1.0 ± 0.1	0.8 ± 0.1	0.8 ± 0.1	1.3 ± 0.1	1.3 ± 0.1	1.4 ± 0.1
Low-power	0.8 ± 0.1	0.6 ± >0.1	0.7 ± 0.1	0.7 ± 0.1	0.8 ± 0.1	0.8 ± 0.1

The volumetric flow rate and velocity of the flue gas display an initial decrease with the addition of biomass at low quantities, 25% during high-power experiments and 50% during low-power experiments. Pellets with a higher biomass content significantly increased volumetric flow rate and chimney velocity. The burn rate is the main factor influencing the flue gas volume and velocity. The more fuel burned in a time interval, the greater the volume of combustion gas is formed in that time interval. However, the composition of the flue gas can influence the volume thereof (Felder *et al.*, 2017).

5.1.3 Stove Temperature

Figure 5-3 displays the temperature measurements of the combustion chamber inside the stove during a high-power combustion experiment using 0% biomass pellets. The four thermocouple readings are from T-04, T-05, T-06, and T-07 (**Figure 4-3**). The thermocouple T-07 is situated directly within the fuel bed (layer of fuel resting on the combustion zone surface), while T-04, T-05, and T-06 are uniformly spaced above the fuel bed, with T-04 positioned farthest up from it.

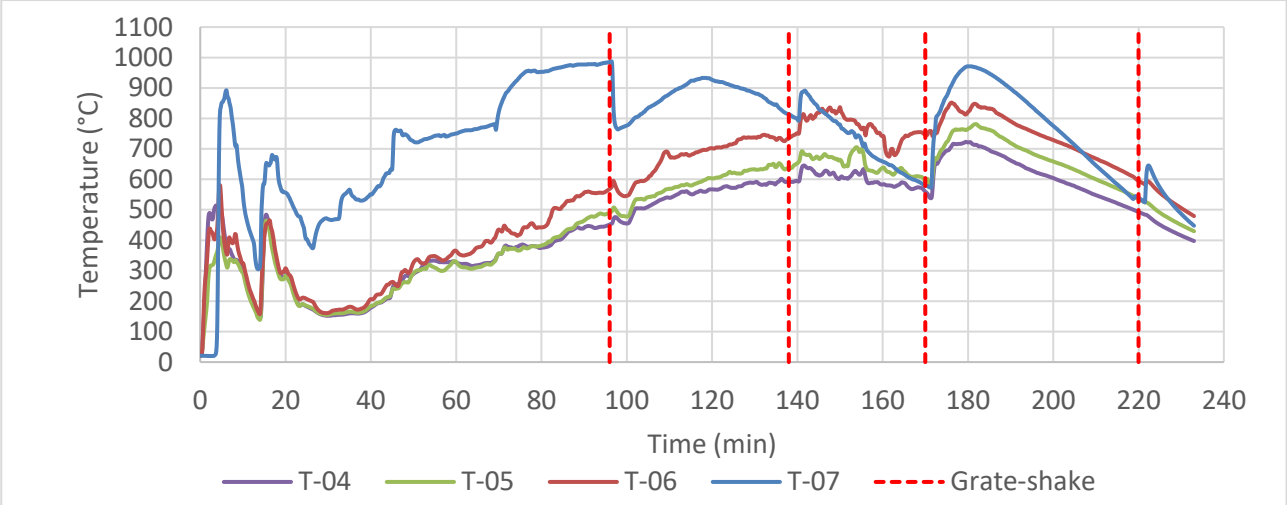

Figure 5-3: Combustion chamber temperatures (0% biomass, high-power experiment)

During ignition, the thermocouples above the fuel bed initially display similar temperatures. The temperature profile within the fuel bed demonstrates an initial delay, as the temperature only starts to increase 5 minutes after ignition. This delay is attributed to the top-lit ignition method employed in the fuel bed, necessitating additional time to reach the temperature in the centre. The combustion chamber temperature experiences an initial peak linked to the ignition of paraffin-soaked wood chips utilized as fire starters. Subsequently, a second peak is observed upon opening the air controller supplying air to the combustion zone. The temperature of the fuel bed (T-07) shows higher temperatures than the temperature above the fuel bed throughout the experiment. During the combustion phase, roughly 40 minutes after ignition, the temperature above the fuel bed. The temperature trend within the fuel bed diverges from the observed temperature trends above the fuel

bed. The temperatures above the fuel bed follow the same trend with minor temperature differences, primarily influenced by fluid dynamics (gas flow). Distinct temperature fluctuations are evident in T-07 at approximately 96, 138, 170, and 220 minutes into the experiment, coinciding with the implementation of grate-shake procedures, while the temperature fluctuations above are less noticeable. These intervals are marked by a temperature reduction followed by an immediate increase. Following the grate-shake procedure executed 170 minutes into the experiment, the temperature within the fuel bed corresponds with the temperatures recorded above the fuel bed. Noticeably, the temperature of the fuel bed (T-07) decreases at approximately 120 minutes after ignition starts while the temperatures above the fuel bed increase. A possible cause for this is the formation of ash between the pellets. Ash build-up around the thermocouple inhibits heat transfer and redirects the airflow between the pellets (Strandberg *et al.*, 2018). At approximately 140 minutes after ignition, the fuel bed temperature decreases below the temperatures above the fuel bed (T-06, T-05, and T-04) and increases to a higher temperature immediately after the grate-shake procedure is implemented. The grate shake procedure agitates the fuel bed, causing the accumulated ash to detach from the pellets, thereby increasing the reactive surface area of the pellets and the reaction rate. Öhman et al., (2000) reported that during the combustion of pellets, a homogenous layer of ash is formed, coating the particles. The ash coat inhibits combustion due to reducing the reactive surface area of the pellet.

Figure 5-4 displays the temperature measurements of the combustion chamber inside the stove during a high-power combustion experiment using 100% biomass pellets.

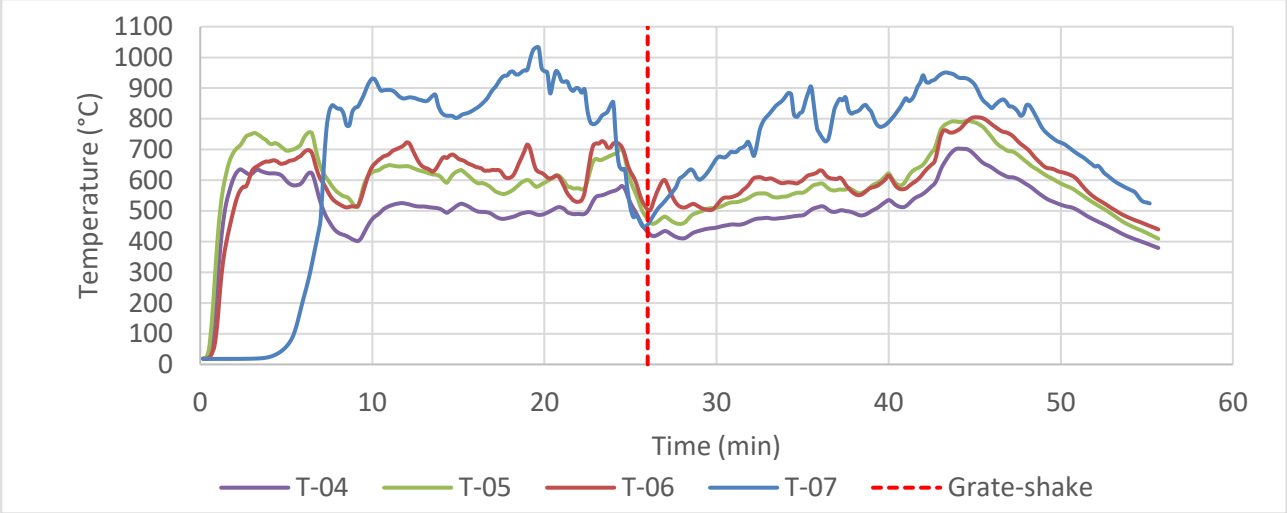

Figure 5-4: Combustion chamber temperatures (100% biomass, high-power experiment)

The temperatures within the combustion chamber display similar trends to those observed during the 0% biomass pellets regarding the ignition and combustion phase. An initial peak is evident during the ignition phase, corresponding to the ignition of paraffin-soaked wood chips utilized as fire

starters. This peak correlates with the initial peak observed in the combustion of 0% biomass pellets (100% coal). The temperature decrease after the initial peak is smaller than that observed during the combustion of 0% biomass pellets, suggesting swift ignition after the initiation of the paraffin-soaked wood chips. Onuegbu et al., (2011) conducted combustion experiments using coal and biomass blended pellets and reported shorter ignition times with increasing biomass content.

Following the second peak, induced by the opening of the air controller allowing airflow to the combustion chamber, there is no discernible decrease in temperature until the execution of the grate-shake procedure at approximately 26 minutes into the experiment. Due to the increased burn rate, the first grate-shake procedure was necessary earlier than the combustion of the 0% biomass pellets. Due to the short run time compared to the 0% biomass pellets, the conditions that dictate whether a grate-shake is necessary are only met once during the experiment. In contrast to the combustion of 0% biomass pellets, the temperature trend of the fuel bed demonstrates less divergence from the temperatures recorded above the fuel bed. A plausible explanation for this phenomenon is the elevated combustion rate associated with 100% biomass pellets. This higher combustion rate results in an increased flow rate of combustion gases and elevated flames, yielding combustion chamber temperatures similar to those observed within the fuel bed. The fuel bed temperature decreases below the temperatures above the fuel bed only once during the experiment. Similar to the 0% biomass pellets, this could be due to ash build-up within the fuel bed. However, this occurs less frequently in the 100% biomass pellets due to their significantly lower ash yield (Öhman *et al.*, 2000).

Increasing biomass content reduces the frequency at which the fuel bed temperature drops below the temperatures above the fuel bed. However, the magnitude of the temperature drops increases with an increase in biomass content in the pellets. Refer to **Appendix H** for the combustion chamber temperatures for all combustion experiments. The magnitude of temperature drops increases with the addition of biomass due to the thermal degradation of the pellets at high temperatures. Strandberg et al., (2018) conducted combustion experiments on biomass pellets and reported that rapid devolatilization compromises the structural integrity of the pellets and creates internal cavities. These trends hold for pellets with increasing biomass content.

Figure 5-5 displays the temperature measurements of the hopper inside the stove during a high-power combustion experiment using 0% biomass pellets (100% coal). The three thermocouple readings are from T-01, T-02, and T-03 (**Figure 4-3**). The thermocouple T-03 is on the grate supporting the fuel directly next to the combustion zone. T-01 and T-02 are uniformly placed above the grate, with T-01 the farthest up.

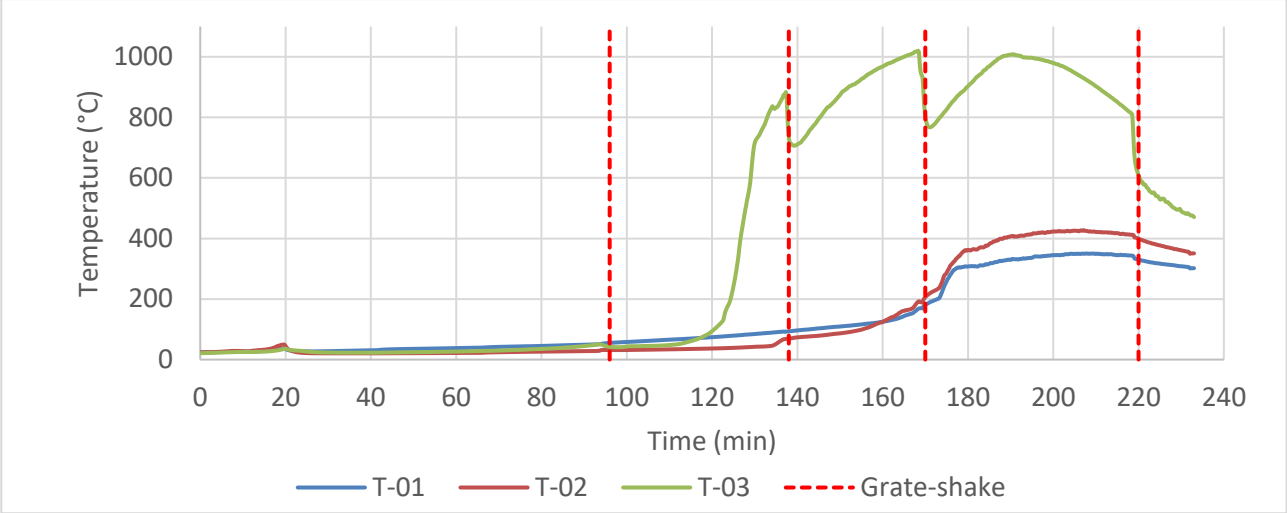

Figure 5-5: Hopper temperatures (0% biomass, high-power experiment)

The temperatures within the hopper persist below 100 °C for most of the combustion experiment. Approximately 120 minutes into the experiment, the fuel in the hopper nearest to the combustion zone underwent ignition. The fuel resting directly on the grate experiences full ignition, facilitated by its proximity to the air inlet. Temperature spikes observed directly above the grate (T-03) coincide with the grate-shake procedures implemented 138 and 170 minutes into the combustion experiment. Ignition of the fuel within the mid-section and top of the hopper occurs gradually, as it is in contact with the burning fuel on the grate. However, the temperatures attained by this section do not reach the elevated levels observed in the fuel resting directly on the grate. This difference is due to a deficit in air supply, impeding the full combustion potential of the fuel within the hopper.

Figure 5-6 displays the temperature measurements of the hopper inside the stove during a high-power combustion experiment using 100% biomass pellets.

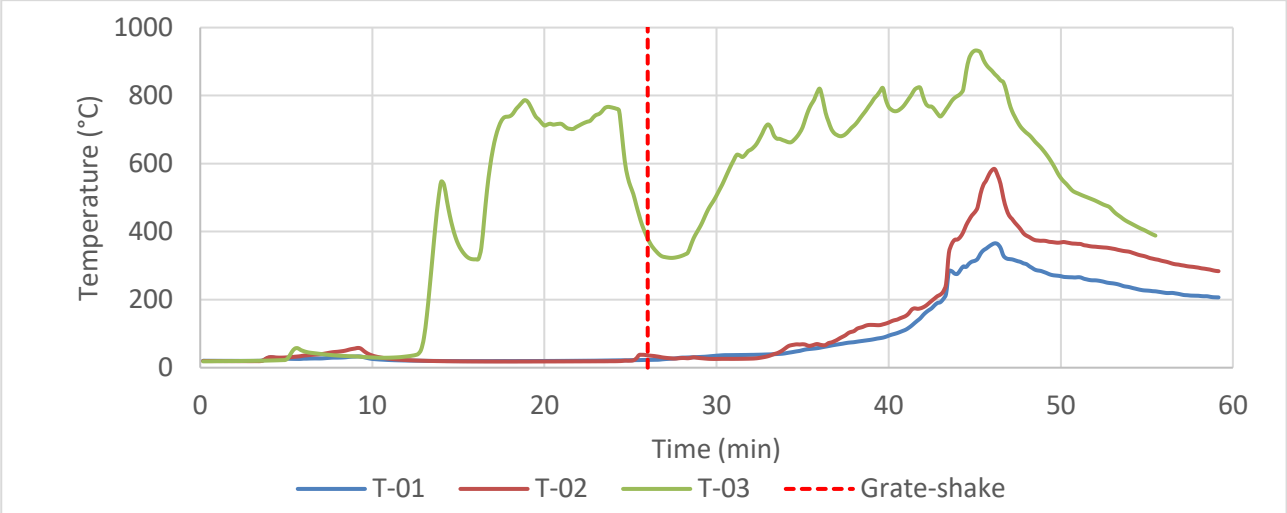

Figure 5-6: Hopper temperatures (100% biomass, high-power experiment)

The temperature profile of the fuel situated on the grate within the hopper closest to the combustion zone resembles the temperature curve observed for the fuel bed in the combustion zone (T-07), as illustrated in **Figure 5-4**. This correspondence suggests simultaneous fuel ignition on the grate and the fuel bed within the combustion chamber. The remaining fuel within the hopper undergoes a gradual ignition process due to a limited air supply. In the mid-section (T-02) of the hopper, a notable peak temperature of 600°C is reached, surpassing the temperatures observed during the combustion of 0% biomass pellets. The noticeable decrease in temperature observed in the T-03 curve aligns with the grate-shake procedure executed at approximately 26 minutes into the experiment.

Figure 5-7 displays the temperature measurements of the combustion chamber inside the stove during a low-power combustion experiment using 0% biomass pellets.

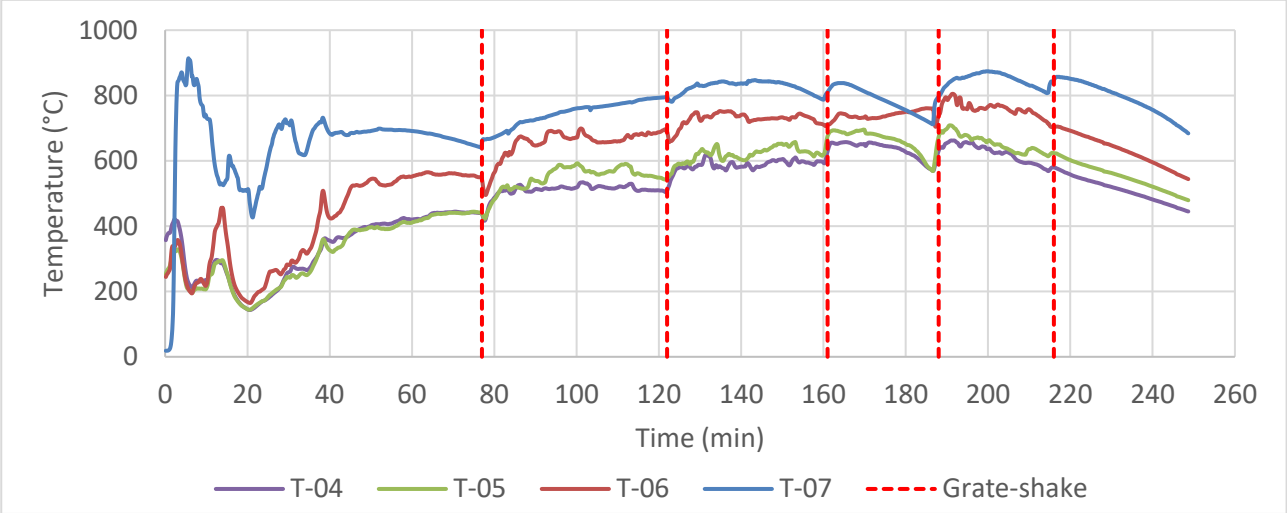

Figure 5-7: Combustion chamber temperatures (0% biomass, low-power experiment)

The temperature profile of the fuel bed (T-07) consistently exhibits elevated temperatures compared to the region above the fuel bed throughout the experiment. Initially, the thermocouples positioned above the fuel bed register similar temperatures. However, approximately 15 minutes after ignition, noticeable temperature differences emerge in the upper region. These differences can be attributed to the large flame from the paraffin fire starters prevalent during the start of ignition. Proximity to the fuel bed is associated with higher temperatures in the thermocouples. The temperatures of the fuel bed and the region above it exhibit parallel trends with minor temperature differentials, predominantly influenced by the dynamics of combustion gases. Notably, distinctive temperature fluctuations manifest around 77, 122, 161, 188, and 216 minutes into the experiment, corresponding with the implementation of the grate-shaking procedures. These instances are characterized by a temperature decrease followed by an immediate increase. Similar to the high-power experiments, the grate-shake agitates the fuel bed, causing the ash coating the pellets to detach, creating more

surface reactions (Öhman *et al.*, 2000). The fuel bed temperature (T-07) does not drop below the temperatures above the fuel bed due to the grate-shake procedure being implemented because of a combination of temperature decreases, oxygen surplus in the flue gas, and visible dead zones in the combustion zone. After the second grate-shake, the frequency of the procedure becomes more pronounced, resembling the pattern observed in the high-power experiments.

The frequency of temperature drops during low-power experiments is similar to that of high-power experiments. However, the magnitude of the drops decreased compared to high-power experiments. Refer to **Appendix H** for the combustion chamber temperatures for all combustion experiments.

Figure 5-8 displays the temperature measurements of the hopper inside the stove during a low-power combustion experiment using 0% biomass pellets.

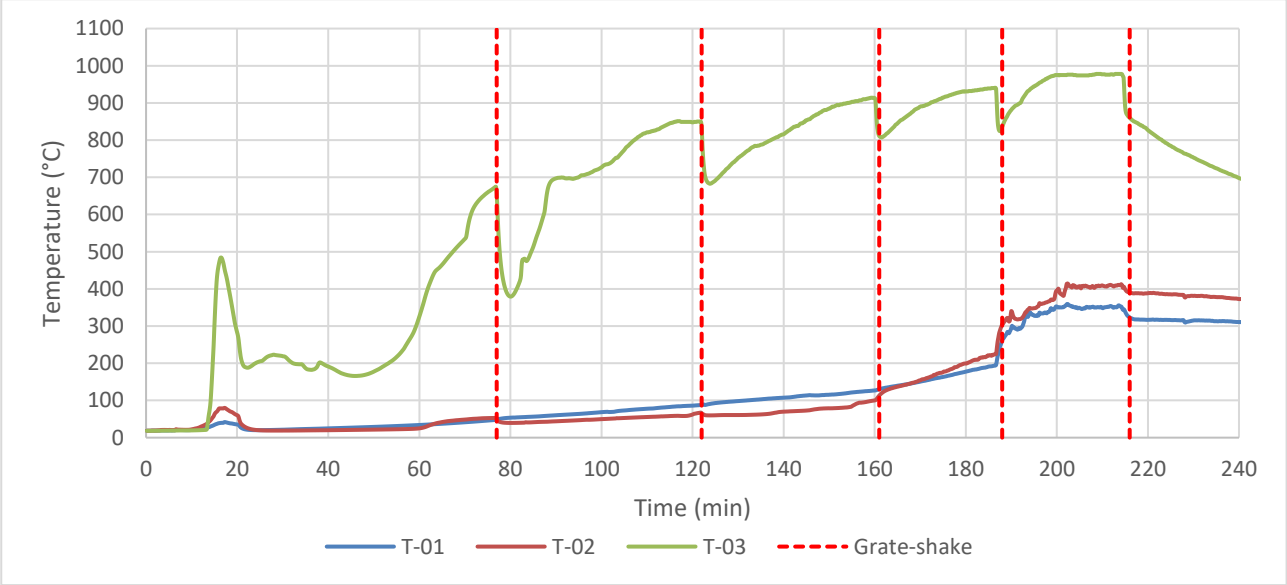

Figure 5-8: Hopper temperatures (0% biomass, low-power experiment)

The temperature profile of the fuel situated on the grate within the hopper closest to the combustion zone exhibits a high temperature similar to that of the combustion zone. This correlation suggests fuel ignition on the grate and the fuel bed within the combustion chamber. Ignition of the fuel within the mid-section and top of the hopper occurs gradually, as it is in contact with the burning fuel on the grate. However, the temperatures in this section do not reach the elevated levels observed in the fuel resting directly on the grate. This difference is due to a deficit in air supply, impeding the full combustion potential of the fuel within the hopper, similar to the high-power experiments.

5.1.4 Observed Flue Gas Composition

The 0% biomass pellets and 90% biomass experiments are discussed in this section to compare the two extremes of the blends used in this study, while the intermediate blend ratios are available in **Appendix I**.

Figure 5-9 displays the CO_2, O_2, and CO concentrations in the flue gas during the high-power combustion experiment of the 0% biomass pellets.

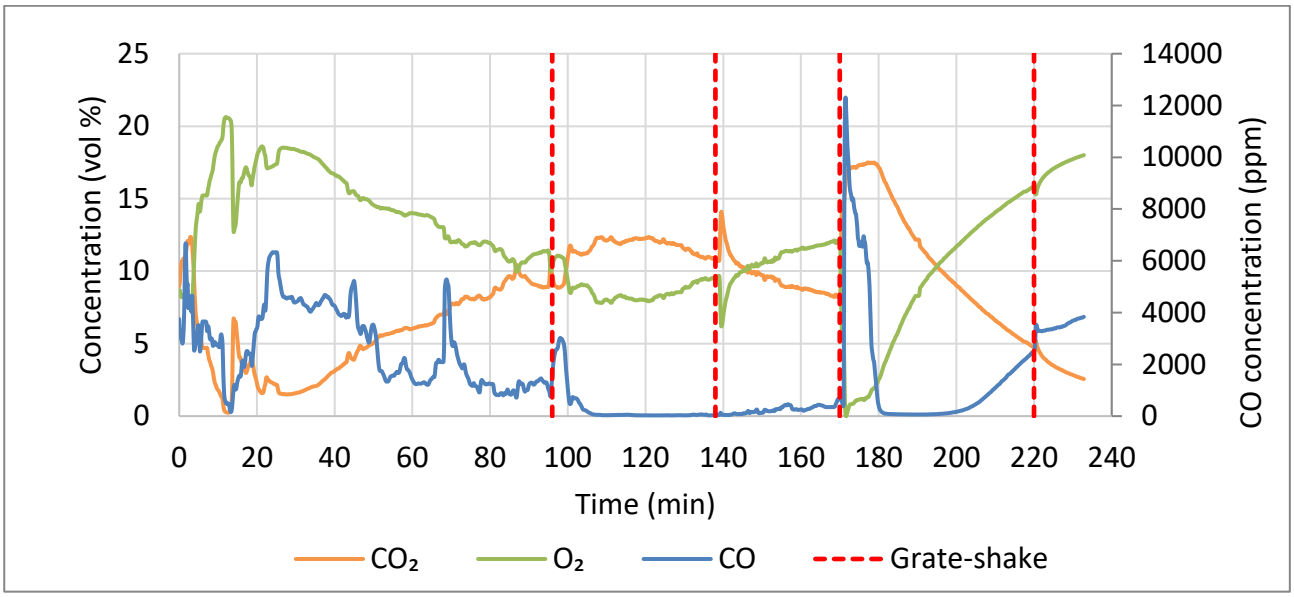

Figure 5-9: CO_2, O_2, and CO concentrations over time (0% biomass, high-power experiment)

The CO_2 and O_2 concentrations follow inverse trends throughout the experiment. This trend would suggest that O_2 is predominantly converted to CO_2 throughout the combustion experiment, while other oxidised species have little influence. The grate-shake procedures promote the oxidation of carbon in the fuel. The spikes in CO concentration correspond with the grate-shake procedures. This correlation suggests that the disturbance of the fuel bed promotes a rapid reaction between oxygen and the carbon in the fuel, causing an increased consumption and rapid depletion of O_2. The O_2 deficiency causes an increased production of CO. Deng, Nie, Yuan, et al., (2022) investigated the effect of oxygen content available in the combustion zone on the emissions performance of a biomass stove and reported that the stove has a range of oxygen concentration at which minimal CO is formed. Falling out of this range, whether it be over this range or under, would lead to increased production of CO. Deng, Nie, Yuan, et al., (2022) reported an oxygen concentration ranging from 19 vol% to 20 vol% producing the lowest CO emissions, compared to an oxygen concentration ranging from 9 vol% to 12 vol% found in this study. These differences can be attributed to the stove design and fuel type.

Figure 5-10 displays the CO_2, O_2, and CO concentrations in the flue gas during the low-power combustion experiment of the 0% biomass pellets.

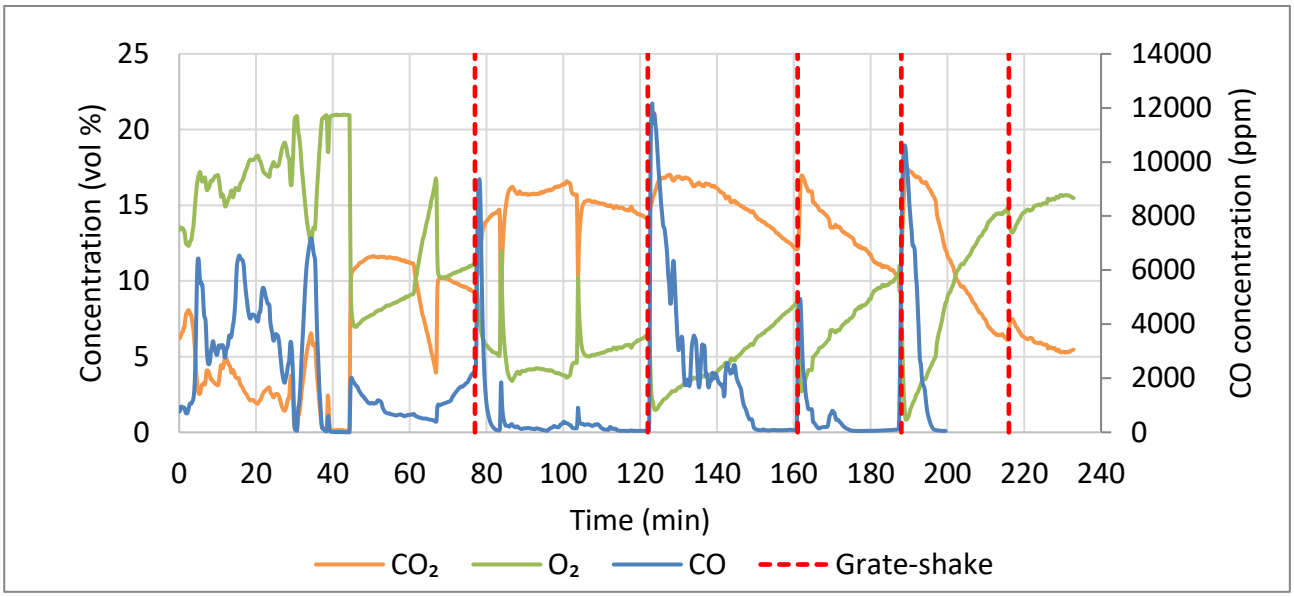

Figure 5-10: CO_2, O_2, and CO concentrations over time (0% biomass, low-power experiment)

The CO_2 and O_2 concentrations follow inverse trends throughout the experiment. This trend would suggest that similar to the high-power experiment, O_2 is predominantly converted to CO_2 throughout the combustion experiment, while other oxidised species have little influence. The grate-shake procedures promote the oxidation of carbon in the fuel. The dips in O_2 and increases in CO_2, initiated by the grate-shake procedure, are more profound than the high-power experiments. The CO concentration follows the inverse trend seen by the concentration of oxygen in the flue gas, indicating that more CO is produced when the O_2 is less abundant in the combustion zone. The spikes in CO concentration correspond with the grate shake procedures, where the O_2 is rapidly consumed, leading to an O_2 shortage. The grate-shake procedures during the experiment resulted in greater O_2 dips than the high-powered experiment. The overall O_2 concentration is lower than the high-power experiments. The CO concentration was lowest during an O_2 concentration of 5 vol% to 10 vol%. Similar to the high-power experiment and the findings of Deng, Nie, Yuan, et al., (2022), falling out of the favourable oxygen range leads to increased production of CO.

The average O_2 concentration in the low-power experiments is higher than in the high-power experiments during the ignition phase and lower during the combustion phase. These differences are due to ignition being slower during low-power experiments. During the combustion phase, the air supply is less during low-power experiments, causing lower O_2 concentrations. The average CO concentration is also higher for low-power experiments compared to high-power experiments. This

trend correlates with the lower O_2 concentrations. Noticeably, the magnitude of the CO spikes correlating with a grate-shake is greater during low-power experiments. This correlation is due to the O_2 taking longer to replenish after rapid oxidation of carbon in the fuel, caused by agitation of the fuel bed, thereby depleting the available oxygen in the combustion zone. All pellet blends follow this trend. Refer to **Appendix I** for the observed flue gas compositions for all combustion experiments.

Figure 5-11 displays the CO_2 and O_2 concentration in the flue gas during the high-power combustion experiment of the 90% biomass pellets.

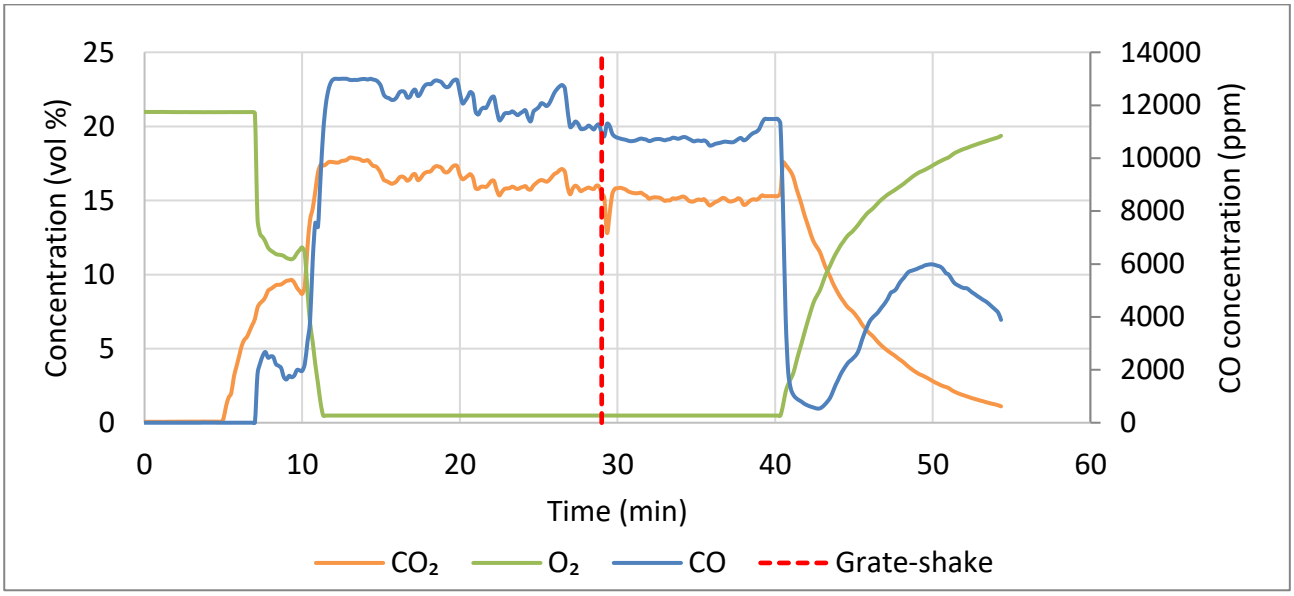

Figure 5-11: CO_2, O_2, and CO concentrations over time (90% biomass, high-power experiment)

Throughout the majority of the 90% biomass high-power experiment, the oxygen concentration is very low. The O_2 falls below the range of the gas analysers (1 vol %), causing the data to produce a straight line. Only during ignition and burnout is the oxygen concentration not depleted. This phenomenon can be seen in pellets containing 75% biomass and higher (refer to Appendix I: **Figure I-9**). This oxygen deficiency is the cause of the elevated CO production (Deng, Nie, Yuan, *et al.*, 2022). The CO_2 and O_2 concentrations follow inverse trends throughout the experiment. This trend would suggest that, similar to the 0% biomass pellets, O_2 is predominantly converted to CO_2 throughout the combustion experiment. The CO concentration follows an inverse trend of the O_2 concentration. This trend is due to the O_2 in the combustion zone being depleted. The cause of this could be attributed to the high burn rate of the 90% biomass pellets (refer to **Figure 5-1**).

The average O_2 concentration decreases with increased biomass content in the pellets. This trend can be attributed to the increased burn rate of the fuel. O_2 deficiency can be observed during combustion experiments using pellets containing 75% and higher biomass. Refer to **Appendix I** for the observed flue gas composition for all combustion experiments.

5.1.5 Combustion Temperature and CO/SO_2/NO_x Concentration

Figure 5-12 displays the CO concentration and the combustion zone temperature throughout the high-power combustion experiments using 0% biomass pellets.

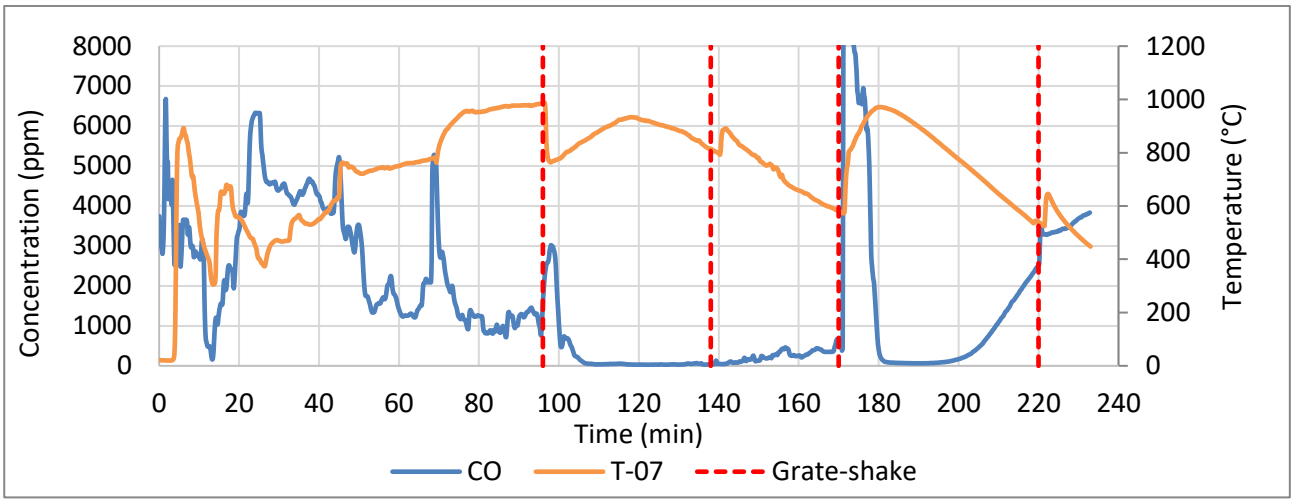

Figure 5-12: CO concentration and combustion zone temperature over time (0% biomass, high-power experiment)

The fuel bed temperature decreases with an increase in the CO concentration. This trend is due to CO_2 having a higher heat of formation than CO. The more carbon in the fuel is oxidised to CO_2, resulting in less CO formation, the more heat is released (Senneca, 2017). Sumbane-Prinsloo et al., (2021) reported similar findings during coal combustion in a coal-burning stove.

Figure 5-13 displays the SO_2 concentration and the combustion zone temperature throughout the high-power combustion experiments using 0% biomass pellets.

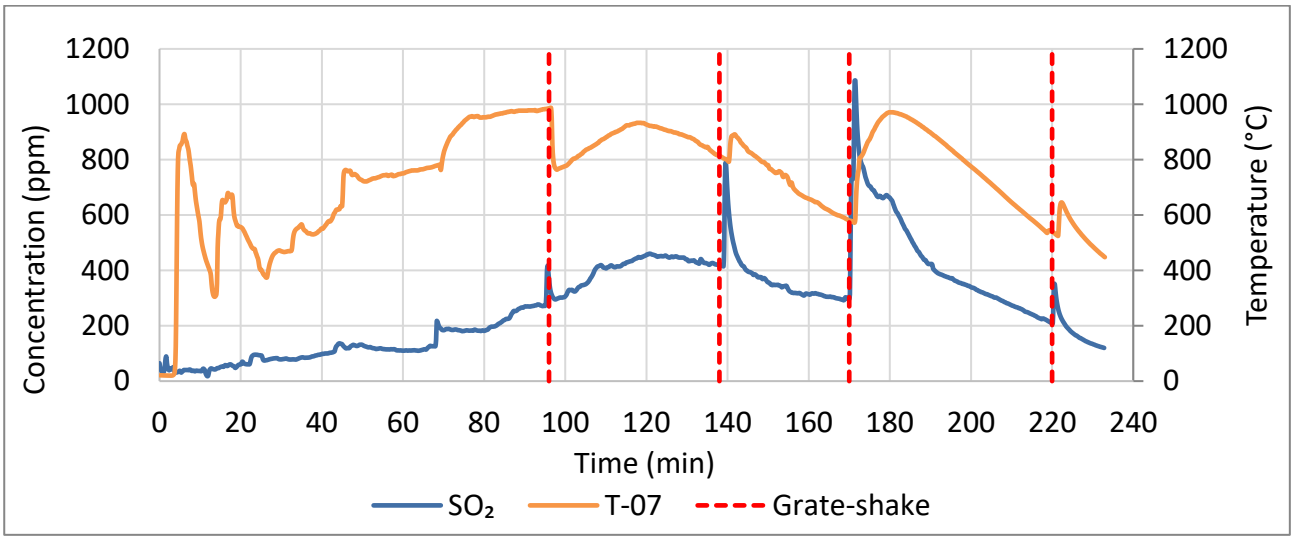

Figure 5-13: SO_2 concentration and combustion zone temperature over time (0% biomass, high-power experiment)

SO_2 formation mirrors the temperature of the combustion zone, where an increase in temperature corresponds with an increase in SO_2 concentration in the flue gas. Wang et al., (2022) and Sumbane-Prinsloo et al., (2021) reported similar findings from the combustion of coal in coal-burning stoves. This trend can be attributed to insufficient contact time between SO_2 and Ca-containing species due to the rapid generation of SO_2, leading to insufficient sulphur retention (Wang *et al.*, 2022).

Figure 5-14 displays the NO_x concentration and the combustion zone temperature throughout the high-power combustion experiments using 0% biomass pellets.

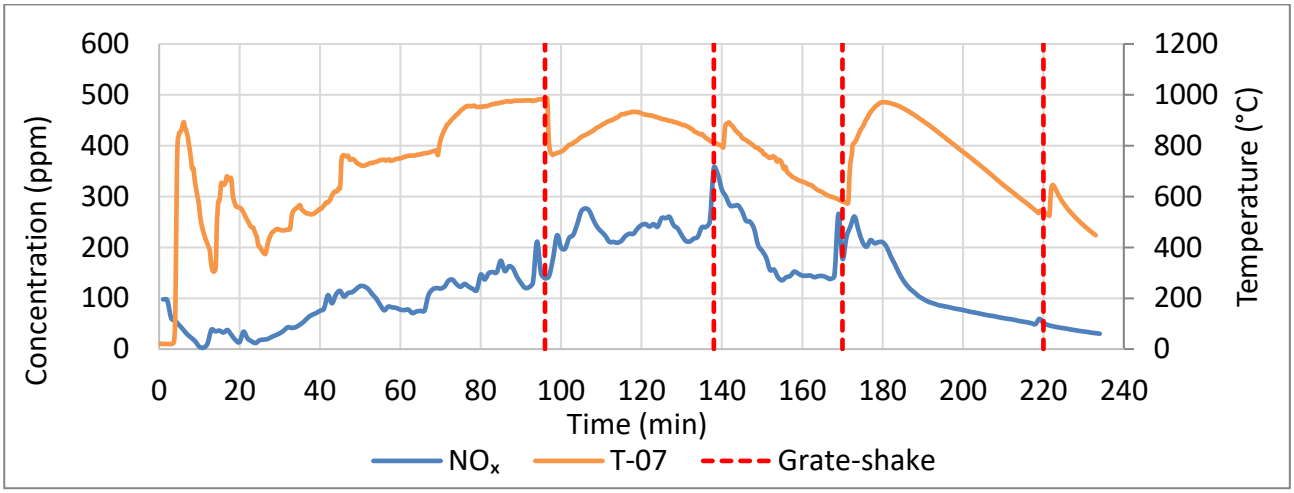

Figure 5-14: NO_x concentration and combustion zone temperature over time (0% Biomass, High-power experiment)

The formation of NO_x correlates with the temperature of the combustion zone, where an increase in temperature corresponds with an average increase in NO_x concentration in the flue gas. However, at temperatures above 800 °C, the NOx concentration shows fluctuations that do not correspond to temperature. Wang et al., (2022) reported similar findings in a coal-burning stove. A possible explanation for this is variation pattern is a result of competition between the oxidation of fuel-N and the heterogeneous reduction of NO to other N-species such as HCN (Smoot *et al.*, 1998; Wang *et al.*, 2022).

5.2 Thermal Performance

5.2.1 Ignition Times

Table 5-2 displays the average ignition times for the different fuels. Refer to **Appendix F** for the experimental uncertainty.

Table 5-2: Ignition times of pellets at high- and low-power

	Average Ignition Time (min)						
% Biomass	0	10	25	50	75	90	100
High-power	36 ± 4	24 ± 2	18 ± 2	10 ± 1	6 ± 1	3 ± 1	3 ± 1
Low-power	47 ± 5	38 ± 4	25 ± 3	16 ± 2	11 ± 1	5 ± 1	3 ± 1

The ignition times (until the fuel bed reaches 500 °C) of the fuels decrease with increased biomass content in both high and low-power experiments. The ignition times in the combustion experiments show correlations with several factors. Higher levels of volatile matter result in quicker ignition as easily combustible materials vaporize and burn readily (Jeguirim & Khiari, 2022). Sumbane-Prinsloo et al., (2021) reported similar findings regarding the correlation between volatile matter and ignition time. Onuegbu *et al.*, (2011) investigated the ignition times of briquettes produced with coal and biomass blends and reported a decrease in ignition time as biomass content increased and attributed this finding to the increased volatile matter in the fuel, similar to the findings of this study. Lower ash content correlates with shorter ignition times, indicating that the absence of non-combustible materials facilitates faster combustion (Jeguirim & Khiari, 2022).

High-power, characterized by open air supplies and increased oxygen, accelerates combustion, leading to significantly shorter ignition times across biomass compositions. Deng, Nie, Yuan, et al., (2022) reported that increased airflow to the combustion zone resulted in faster ignition. Low-power, involving closed air supplies and reduced oxygen, slows combustion, resulting in comparatively longer ignition times. However, the compressive strength of biomass pellets introduces complexity. The pellets with higher compressive strength resist breaking down and igniting during the initial stages of combustion, potentially leading to prolonged ignition times (Ferreira *et al.*, 2023). The interplay between composition, structural factors, and power settings impacts pellet ignition times. Sumbane-Prinsloo et al., (2021) studied the effect of coal particle size on a coal stove and found ignition times ranging from 23 minutes to 50 minutes, depending on the particle size. The fuel closest to the fuel used in this study is the 20 mm coal particles, which resulted in an ignition time of 38 minutes, closely resembling the ignition time seen from the 0% biomass (100% coal) pellets during a high-power experiment.

5.2.2 Fuel Burning Rates and Peak Temperatures

Figure 5-15 displays the mean burn rates of the pellet blends during high-power and low-power experiments. Refer to **Appendix F** for the relevant experimental uncertainty analysis.

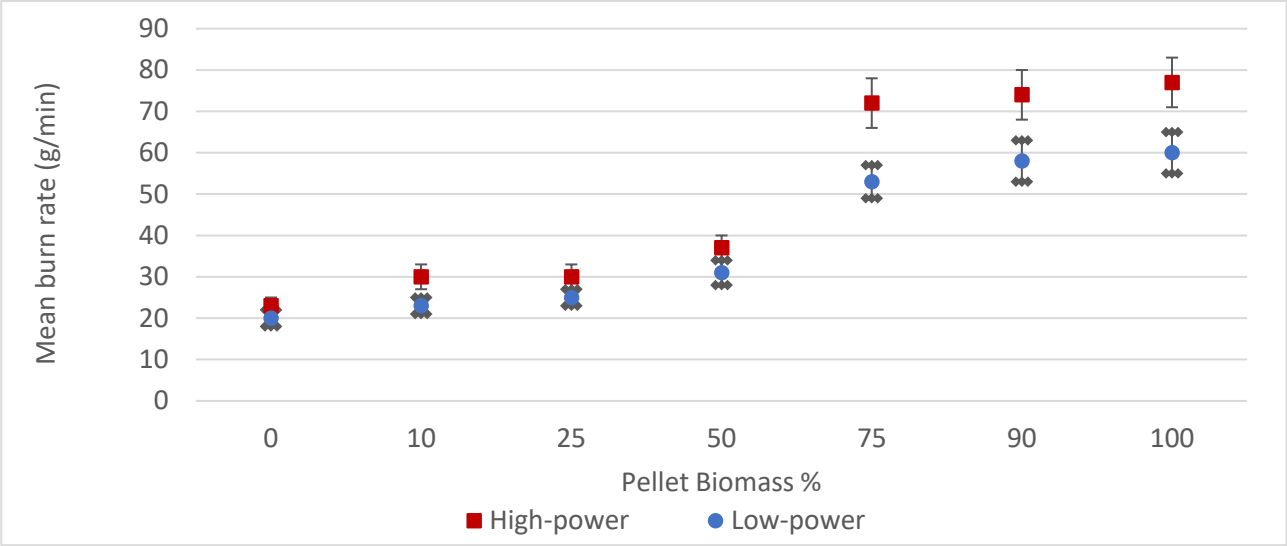

Figure 5-15: Burn rates of pellet blends during high-power and low-power experiments

Mean burn rates increased with higher biomass content, peaking at 100% in both high-power and low-power experiments, with a marginal decrease in mean burn rate afterwards. The slight difference between the 75%, 90%, and 100% biomass pellets could be due to the oxygen-depleted combustion zone (refer to **Appendix I**), causing mass transfer limitations.

Figure 5-16 displays the peak temperatures of the pellet blends during high-power and low-power experiments. Refer to **Appendix F** for the relevant experimental uncertainty analysis.

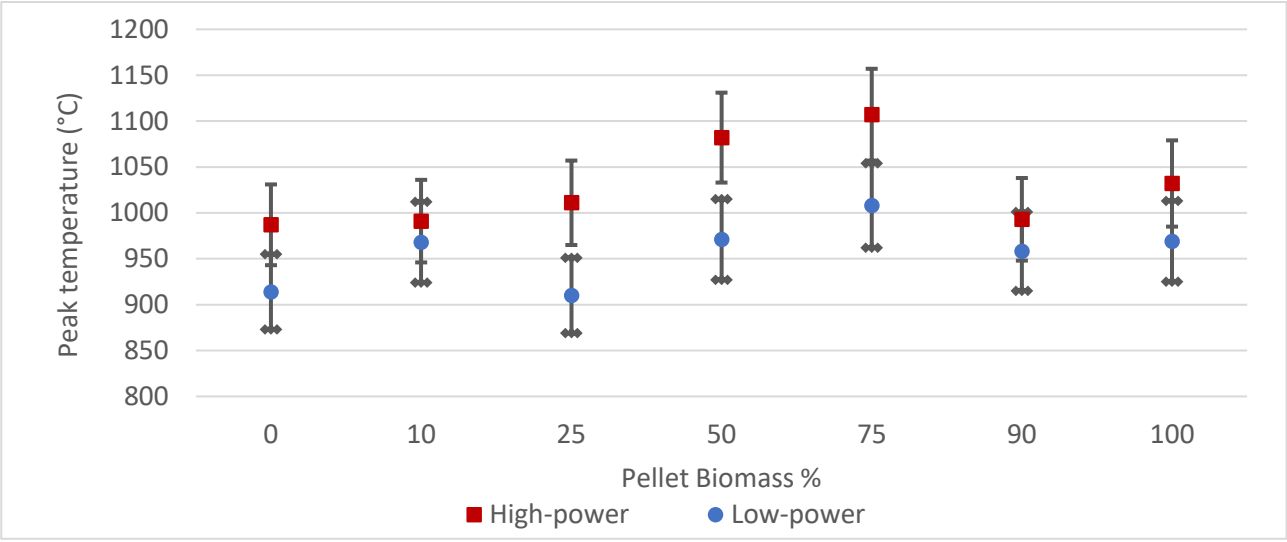

Figure 5-16: Peak temperatures of pellet blends during high-power and low-power experiments

Increasing biomass content led to a rising peak temperature until reaching a maximum at 75% biomass. Subsequently, there was a decline in peak temperature at this composition for both high-power and low-power experiments. Transitioning from 90% to 100% biomass showed a slight temperature increase. Low-power experiments consistently exhibited a 7% to 10% reduction in peak temperature compared to high-power experiments.

Burn rates increased with an increase in volatile matter, contributing to higher peak temperatures, particularly in high-power experiments. Onuegbu *et al.*, (2011) reported similar findings when investigating the burn rate of briquettes produced with coal and biomass blends. The peak temperatures of the pellets increase as the ash yield decreases (Aich *et al.*, 2020). Jayanti et al., (2007) investigated the effect of fuel ash yield on combustion and reported that peak temperatures increased as ash yield decreased, similar to the findings of this study. The increased temperatures also affect the burn rate (Ferreira *et al.*, 2023). Similarly, burn rates and peak temperature increased with a decrease in the fixed carbon content of the fuel, suggesting that fuels with stable compounds require more ignition energy, resulting in slower combustion and lower mean burn rates (Aich *et al.*, 2020; Ferreira *et al.*, 2023; Sumbane-Prinsloo *et al.*, 2021). Compressive strength negatively correlates with burn rates and peak temperatures. Pellets with higher compressive strength resist breaking down and igniting, potentially resulting in slower combustion, lower peak and mean burn rates, and peak temperatures (Biswas *et al.*, 2014; Cheng *et al.*, 2018).

Sumbane-Prinsloo et al., (2021) reported a burn rate of 0.4 – 0.6% per minute during experiments conducted on a coal stove using Highveld coal. This finding closely aligns with the results of this study's combustion experiments utilizing 0% biomass pellets. Furthermore, Sumbane-Prinsloo et al., (2021) identified a peak temperature of 837 °C, which is approximately 15% lower than the peak temperature observed in the 0% biomass, high-power experiments and approximately 8% lower than in the 0% biomass, low-power experiments conducted in this study. In the investigation by Deng et al., (2020), a wood-burning stove was examined under low-power and high-power settings, using unspecified wood pellets as fuel. The reported burn rates were 20 $g.min^{-1}$ and 18 $g.min^{-1}$ for high-power and low-power experiments, respectively. These rates are notably lower than the burn rates observed in this study when using 100% biomass pellets. Contributing factors to this difference are the larger stove used in this study and the fact that this stove was designed specifically for coal combustion. Kole et al., (2022) evaluated the performance of a smaller husk biomass stove, observing an average burn rate of 32 $g.min^{-1}$, significantly lower than the burn rate recorded in this study during the combustion of 100% biomass pellets. In a study by Deng et al., (2022), on a biomass stove using maize-produced pellets at high-power and low-power conditions, burn rates of 17 $g.min^{-1}$ and 10 $g.min^{-1}$ were found, respectively. These rates are remarkably lower than the burn rate

observed during this study using 100% biomass pellets and exhibit a closer similarity to the burn rates of 0% biomass pellets.

The stove utilized in our study demonstrates a notably higher biomass consumption rate than other biomass stoves while maintaining a relatively standard coal consumption rate. Specifically, the NWU semi-continuous stove exhibits a burn rate for biomass pellets comprising 50% biomass or less that aligns with conventional biomass stoves.

5.2.3 Power Output

An investigation of the stove's usable power output with the different pellet blends was conducted at high-power and low-power. The findings are illustrated in **Figure 5-17** and **Figure 5-18**, respectively, depicting the usable energy generation concerning mass loss percentage (calculated on an ash-free basis) for the stove utilizing distinct fuel blends during high-power and low-power combustion experiments, respectively. Note that the figures are not lines but individual points, with only outliers removed.

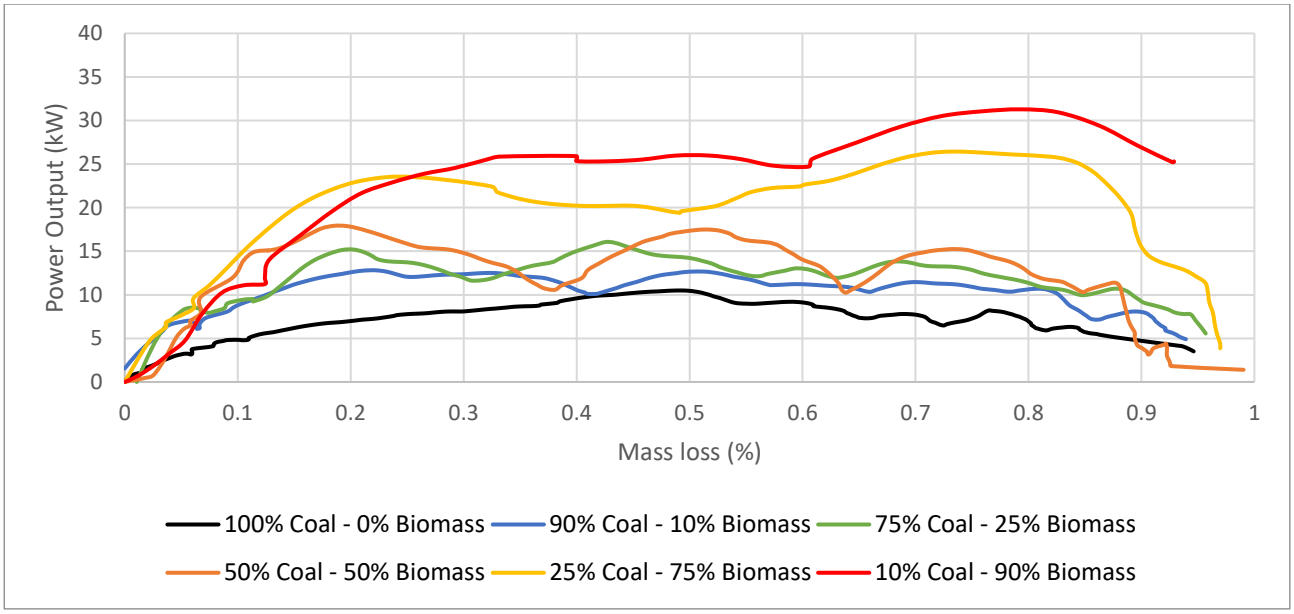

Figure 5-17: Power output of pellet blends versus mass loss (a.f.b), High-power experiments

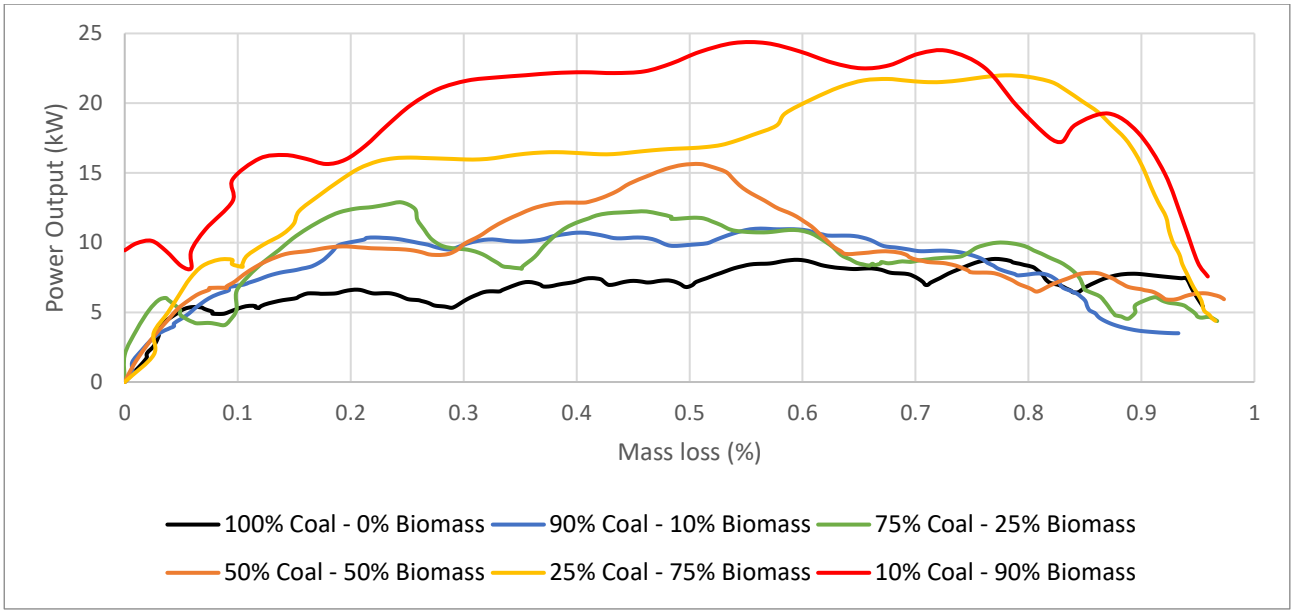

Figure 5-18: Power output of pellet blends versus mass loss (a.f.b), Low-power experiments

In both high-power and low-power experiments, the power output of the pellets increases with increased biomass content. In high-power experiments, pellets composed mainly of biomass (90% biomass) achieve a peak power output of approximately 30 kW, while in low-power experiments, the corresponding value is approximately 25 kW. Conversely, pellets devoid of biomass (0% biomass) exhibit a peak power output of around 10 kW in high-power experiments and approximately 8 kW in low-power experiments. Intermediate biomass compositions within the pellet blends fall within this power output range for both high-power and low-power experiments, with power output increasing with biomass composition.

The rise in power output corresponds with a decrease in calorific value, indicating that the higher burn rates contributed to the increased power output. Grimsby et al., (2016) reported similar results when conducting combustion experiments on a biomass stove with different biomass fuels. Sumbane-Prinsloo et al., (2021) found the average power output of a coal-burning stove to be 10 kW, which is similar to the power output noticed in this study during the 0% biomass pellets, high-power experiments and slightly higher than the 0% biomass pellets, low-power experiments. Kole et al., (2022) evaluated the power output of a husk biomass stove and found a power output of 7.5 kW, which is remarkably lower than the power output seen from the 100% biomass pellets combustion experiments. However, this was strongly related to the size of the stove and the initial mass fuel loaded.

5.2.4 Water Boiling Test

Table 5-3 shows the results from the water boiling test.

Table 5-3: Water boiling test results

% Biomass	Mass Burned (kg)	Fuel CV (MJ/kg)	Boiling Time (min)
High-power			
0	0.33	20.2	11 ± 2
10	0.48	20.1	8 ± 1
25	0.49	19.9	9 ± 1
50	0.53	19.7	6 ± 1
75	0.64	19.5	10 ± 2
90	1.01	19.4	10 ± 2
Low-power			
0	0.40	20.2	17 ± 2
10	0.41	20.1	14 ± 2
25	0.52	19.9	11 ± 2
50	0.37	19.7	8 ± 1
75	0.80	19.5	10 ± 2
90	0.38	19.4	10 ± 2

In the high-power experiments, it was observed that the mass of fuel necessary to raise the water temperature to 95 °C exhibited an increase corresponding to the rise in biomass content within the pellets. Similarly, the low-power experiments demonstrated a consistent pattern, aligning with the trend observed in the high-power experiments up to a 50% biomass content threshold. Beyond this point, there was a decrease in the mass of fuel required to reach the same temperature, excluding the 75% biomass content. Onuegbu et al., (2011) conducted a water boiling test on a stove using briquettes made from coal and biomass blends and reported faster boiling times as the biomass content in the briquettes increased. Kole et al., (2022) conducted water boiling tests on a biomass stove using husk biomass as fuel and reported a time to bring 3.5 L of water of 9 minutes. This time is faster than the boiling times reported in this study due to the increased water in the pot compared to this study. Sumbane-Prinsloo et al., (2021) conducted water boiling tests on a coal stove and reported a boiling time between 17 minutes and 28 minutes for different size coal particles using 2 L water in a pot. The coal samples closest to the coal pellets used in this study displayed a boiling time of 23 minutes. This time is comparable to the 0% biomass, low-power experiments boiling time exhibited in this study, as boiling 2 L would take twice as long. Grimsby et al., (2016) conducted water boiling tests on a biomass stove using different biomass fuels and reported boiling times of 36, 18, and 10 minutes using the different fuels. Grimsby et al., (2016) also reported an increase in boiling time when conducting low-power experiments compared to high-power experiments. These findings align with the results of this study.

5.2.5 Energy Efficiencies

Energy efficiencies indicate how efficiently the stove transfers energy expended from the fuel.

System Efficiency

Figure 5-19 summarises the system efficiency observed for each pellet blend in the context of high-power combustion experiments. This analysis incorporates stack temperature, as it affects the system efficiency substantially. The system efficiency is presented over the mass loss fractions on an ash-free basis.

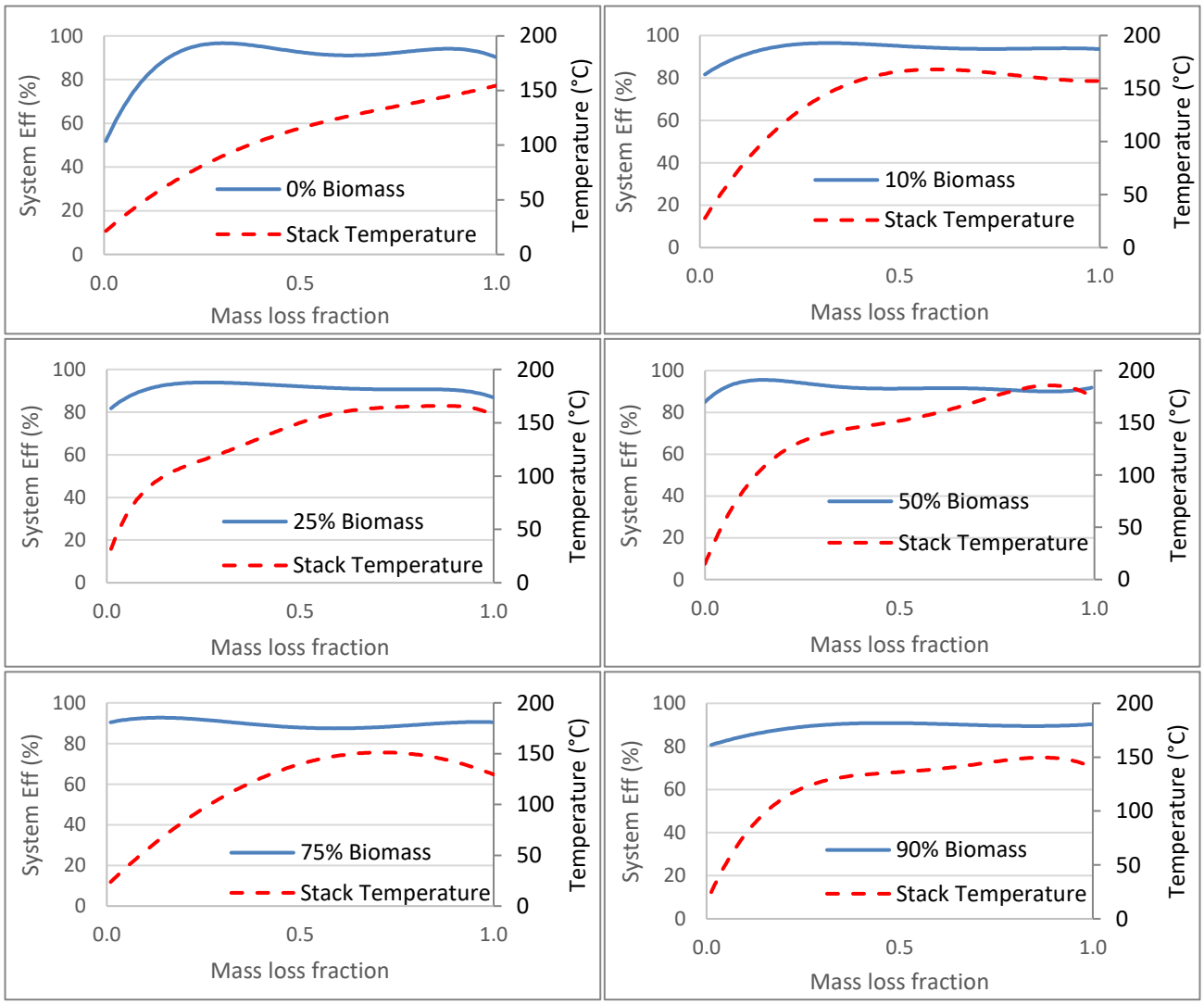

Figure 5-19: System efficiency of pellets during high-power combustion experiments (a.f.b)

The system efficiency for all high-power experiments shows an initial peak. This trend can be attributed to the heat absorbed by the stove. Once the stove has reached temperature, the stack temperature increases and lowers the system efficiency. At roughly 60% conversion, the system efficiency starts to increase slightly. This increase can be attributed to the combustion efficiency

reaching its peak, where CO production is at its lowest. The dips can also be attributed to the grate-shake procedure, which significantly lowers CO_2 production and increases CO production. The 10% biomass pellets exhibited the highest system efficiency, showing steady efficiency with minimal decreases, while the 75% and 90% biomass pellets exhibited the lowest system efficiency.

Sumbane-Prinsloo et al., (2021) assessed the system efficiency of a Union coal-burning stove employing methodologies similar to those applied in this study. Their results yielded a system efficiency of approximately 70%, which is approximately 10%-15% less efficient than the outcomes observed in our study.

In a study conducted by Vitoussia et al., (2020), the performance of a biomass stove utilizing pellets derived from three distinct biomasses—palm nut shells, palm nut fibres, and coffee husk was evaluated. The reported system efficiencies were 69%, 80%, and 78%, respectively. Notably, palm-nut shell pellets exhibited a substantial deviation from the efficiency observed in the current study, while palm nut fibre and coffee husk pellets displayed minor deviations.

Thermal Efficiency

The thermal efficiencies, such as cooking efficiency, system efficiency, heating efficiency, and combustion efficiency, were determined, and the results are summarised in **Table 5-4**.

Table 5-4: Thermal efficiencies of pellet blends

% Biomass	Cooking Efficiency (%)	System Efficiency (%)	Heating Efficiency (%)	Combustion Efficiency (%)
		High-power		
0	4.5	89	79	92
10	3.6	93	91	98
25	3.3	90	87	99
50	5.5	89	83	99
75	2.8	80	77	97
90	1.7	77	72	96
		Low-power		
0	3.9	83	84	91
10	3.8	96	92	97
25	4.1	91	90	99
50	4.6	94	90	99
75	2.1	95	89	97
90	2.4	95	88	96

The data reveals trends between energy output and cooking efficiency. In the high-power category, as energy output increases, cooking efficiency decreases. The 90% biomass pellets exhibit the highest energy output during the cooking phase but the lowest cooking efficiency. Conversely, the

50% biomass pellets have the lowest energy output during the cooking phase but a relatively higher cooking efficiency. This inverse relationship suggests diminishing returns concerning efficiency at higher energy outputs in the high-power category. In the low-power category, a similar trend is observed. The 75% biomass pellets produced the highest energy output but lowest efficiency. The 50% biomass pellets, with the lowest energy output, demonstrate the highest efficiency regarding low-power experiments. This trend also indicates a consistent pattern of decreasing efficiency with increasing energy output in the low-power category. Sumbane-Prinsloo et al., (2021) determined the cooking efficiency through a water boiling test on a coal stove and found a cooking efficiency of 1.4% - 2.6%, slightly lower than the thermal efficiency exhibited by the stove and pellets used in this study.

As for the system efficiency, a general pattern emerges in the high-power experiments where system efficiency experiences an initial increase with lower percentages of biomass, reaching its peak at 10% biomass. However, a gradual decline in efficiency is observed with increasing biomass content, with the most substantial drop occurring at 75% and 90% biomass concentrations. This trend suggests that the combustion dynamics at higher power levels are more sensitive to changes in biomass content, leading to diminishing efficiency as biomass concentration increases. A possible explanation is that an oxygen surplus occurs due to the increased inherent oxygen content of biomass. Kole et al., (2022) conducted combustion experiments while manipulating the oxygen content in the stove air supply and reported that an oxygen deficit and surplus inhibits combustion, producing more CO. As the system efficiency in this study is sensitive to heat lost through incomplete combustion, this would cause fluctuations. In contrast, low-power experiments exhibit a different trend, improving system efficiency as biomass content increases. The highest efficiency is observed at 10% biomass, and while there is a decline at higher biomass percentages, it is less pronounced compared to high-power experiments. This difference suggests that air supply influences the system efficiency. Incorporating biomass into pellet blends at a 10% concentration yields an initial increase in heating efficiency, as observed in both high-power and low-power experiments. However, beyond this initial enhancement, heating efficiency experiences a subsequent decline with increasing biomass content in the pellets. This trend can be attributed to the high velocity of the flue gas, resulting in substantial heat loss through the stack. Notably, in experiments conducted at low-power, the heating efficiency surpasses that of high-power experiments at corresponding biomass percentages. In high-power experiments, pellet blends containing 10%, 25%, and 50% biomass exhibit greater heating efficiency than pellets devoid of biomass (0%). Conversely, in low-power experiments, all biomass-containing pellet blends exhibit larger heating efficiency than the 0% biomass pellets. The combustion efficiency increases with the addition of biomass. This trend could be due to the biomass creating cavities in the pellets, leading to larger reactive surface areas within the pellets and thorough combustion, as seen by Strandberg et al., (2018). The proximate analysis

results on the ash can be found in Appendix E: **Table E-1**. The fixed carbon remaining in the ash after burnout supports the findings regarding combustion efficiency, as the two are closely related.

5.3 Emissions Performance

The emission factors of the combustion pollutants are presented in mass per unit energy $[g/MJ]$. Note that the 100% biomass pellets are not included because the gas analysers cannot analyse the high flue gas flow rate caused by the high burn rate.

5.3.1 CO and CO_2 Emission Factors

Figure 5-20 and **Figure 5-21** show the CO_2 and CO emission factors resulting from the combustion of the different pellet blends, respectively.

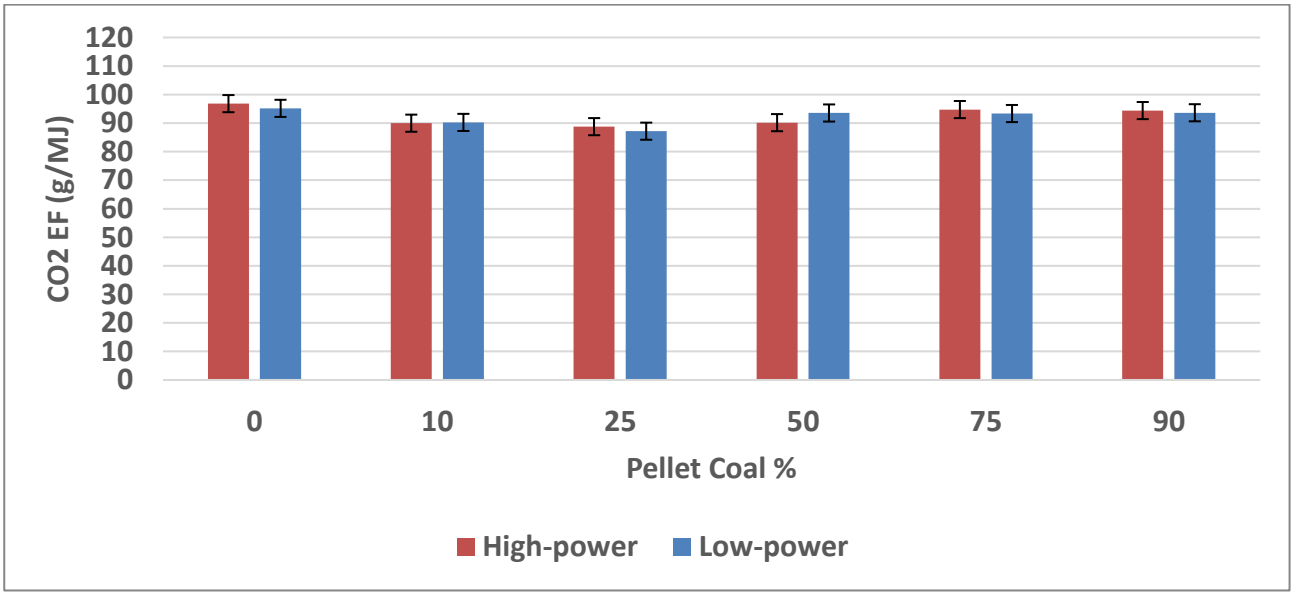

Figure 5-20: CO_2 emission factors of pellet blends (g/MJ)

The high-power experiments produced more CO_2 than the low-power experiments, except for the 50% biomass pellets. There is a slight decrease in CO_2 emission factors with increasing biomass content, with 25% biomass pellets exhibiting the lowest CO_2 emission factors, after which the emission factors increase with rising biomass content. The 0% biomass pellets displayed the highest CO_2 emission factors.

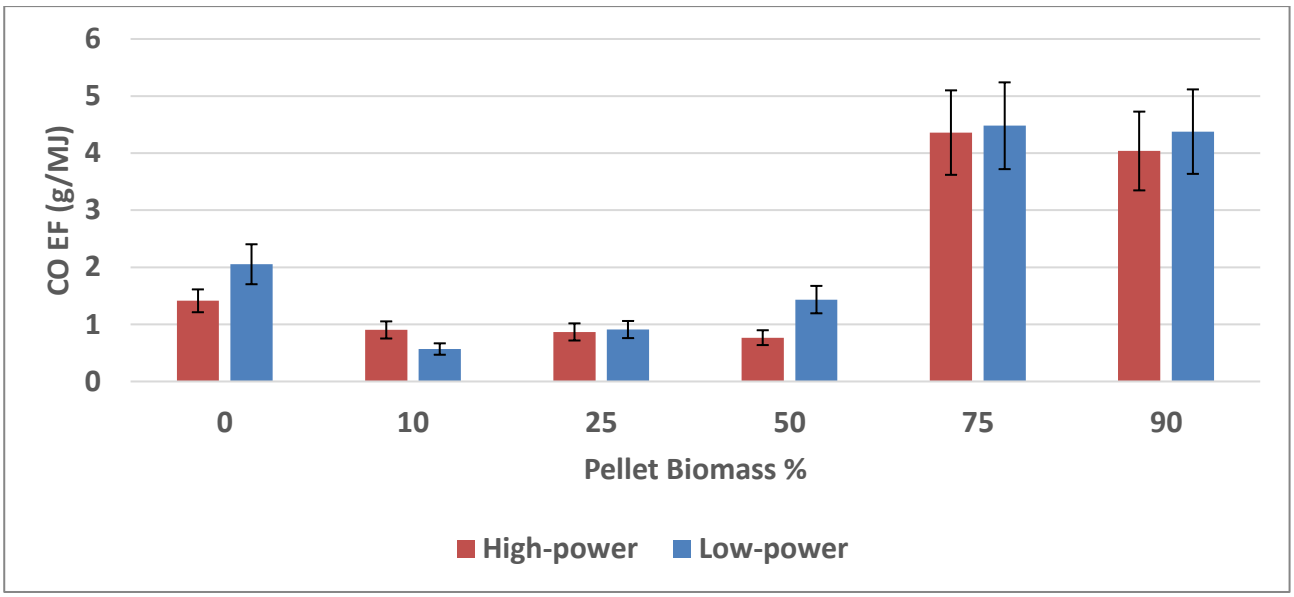

Figure 5-21: CO emission factors of pellet blends (g/MJ)

In contrast to the CO_2 emission factors, the low-power experiments generally produced more CO than high-power experiments (refer to **Figure 5-9** and **Figure 5-10**). CO emission factors initially decreased with the addition of biomass and increased significantly at higher biomass content during both high-power and low-power experiments.

The CO_2 and CO emission factors are quantified in **Table 5-5** in $[g/MJ]$ and emission rates in $[g/min]$. Refer to **Table F-3** and **Table F-4** in Appendix F for the respective uncertainty analysis.

Table 5-5: CO_2 and CO emission factors of pellets

CO_2						
% Biomass	0	10	25	50	75	90
			High-power			
EF (g/MJ)	97 ± 3	90 ± 3	89 ± 3	90 ± 3	95 ± 3	94 ± 3
ER (g/min)	47 ± 2	55 ± 2	56 ± 2	85 ± 3	123 ± 4	129 ± 4
			Low-power			
EF (g/MJ)	95 ± 3	90 ± 3	87 ± 3	94 ± 3	93 ± 3	94 ± 3
ER (g/min)	43 ± 2	42 ± 2	46 ± 2	53 ± 2	79 ± 3	95 ± 3

CO						
			High-power			
EF (g/MJ)	1.41 ± 0.20	0.90 ± 0.15	0.87 ± 0.15	0.77 ± 0.13	4.36 ± 0.74	4.04 ± 0.69
ER (g/min)	1.02 ± 0.17	0.54 ± 0.09	0.54 ± 0.09	0.74 ± 0.13	5.83 ± 1.00	5.34 ± 0.91
			Low-Power			
EF (g/MJ)	2.05 ± 0.35	0.57 ± 0.10	0.91 ± 0.15	1.43 ± 0.24	4.48 ± 0.76	4.38 ± 0.74
ER (g/min)	0.62 ± 0.11	0.26 ± 0.04	1.02 ± 0.17	0.80 ± 0.14	3.64 ± 0.62	4.37 ± 0.74

The CO_2 emission factors for the different pellets only differ slightly, while the emission rate increases with increased biomass content. This trend is due to the increase in burn rate as the biomass content increases. Sumbane-Prinsloo et al., (2021) reported CO_2 emission factors ranging from 85 g/MJ to 106 g/MJ and CO emission factors ranging from 2.9 g/MJ to 5.4 g/MJ during combustion of different-sized coal in a coal-burning stove. The CO_2 emission factors are comparable to the results from this study, where the CO emission factors are comparable to the 0% biomass pellets and 75%+ biomass pellets used in this study. Deng, Nie, Lu, et al., (2022) reported CO emission factors ranging from 0.5 g/MJ to 3.4 g/MJ with coal and emission factors ranging from 0.1 g/MJ to 1.2 g/MJ with the biomass used as fuel in combustion experiments on a domestic stove. These CO emission factors closely align with the results of this study. Shrestha et al., (2021) investigated the emissions performance of four different biomass stoves using biomass pellets as fuel and reported CO_2 emission factors ranging from 99 g/MJ to 107 g/MJ and CO emission factors ranging from 0.86 g/MJ to 1.74 g/MJ, which closely aligns with the results from this study, excluding the 75% and 90% biomass pellets. **Table 5-6** summarises emission factors of CO_2 and CO from similar studies.

Table 5-6: Summary of CO and CO_2 emission factors from literature

Study	Fuel	Power setting	CO_2 EF [g/MJ]	CO EF [g/MJ]
This study	0% - 90% biomass pellets	High-power	89 - 97	0.77 – 4.36
		Low-power	87 - 95	0.57 – 4.48
(Meyer *et al.*, 2020)	Grade A and D Lump coal	High-power	90 – 92	0.16 – 0.53
		Low-power	88 – 92	0.57 – 0.68
(Bentson *et al.*, 2022)	Unspecified biomass	High-power	-	0.7 – 2.7
		Low-power	-	2.4 – 11.2
(Sumbane-Prinsloo *et al.*, 2021)	15 mm – 40 mm lump coal	-	85 - 106	2.27 – 5.35
(Himanshu *et al.*, 2022)	Unspecified biomass	High-power	-	0.91
		Low-power	-	0.98
(Kole et al., 2022)	Coffee husk and rice husk	-	-	4.2 - 5.0
(Chen *et al.*, 2016)	Cornstalk pellets	-	-	0.86 – 2.36
(Deng, Nie, Lu, *et al.*, 2022)	Biomass pellets	High-power	-	0.11 – 0.30
		Low-power	-	0.85 – 1.18
	Lump coal and coal briquettes	High-power	-	0.46 – 1.25
		Low-power	-	2.19 – 3.36

The CO_2 emission factors are comparable to other studies, the CO emission factors on the lower end are comparable to most studies, and the higher end is only comparable to the study conducted by Kole et al., (2022).

5.3.2 NO_x Emission Factors

Figure 5-22 shows the levels of NO_x emission factors resulting from the combustion of the different pellet blends.

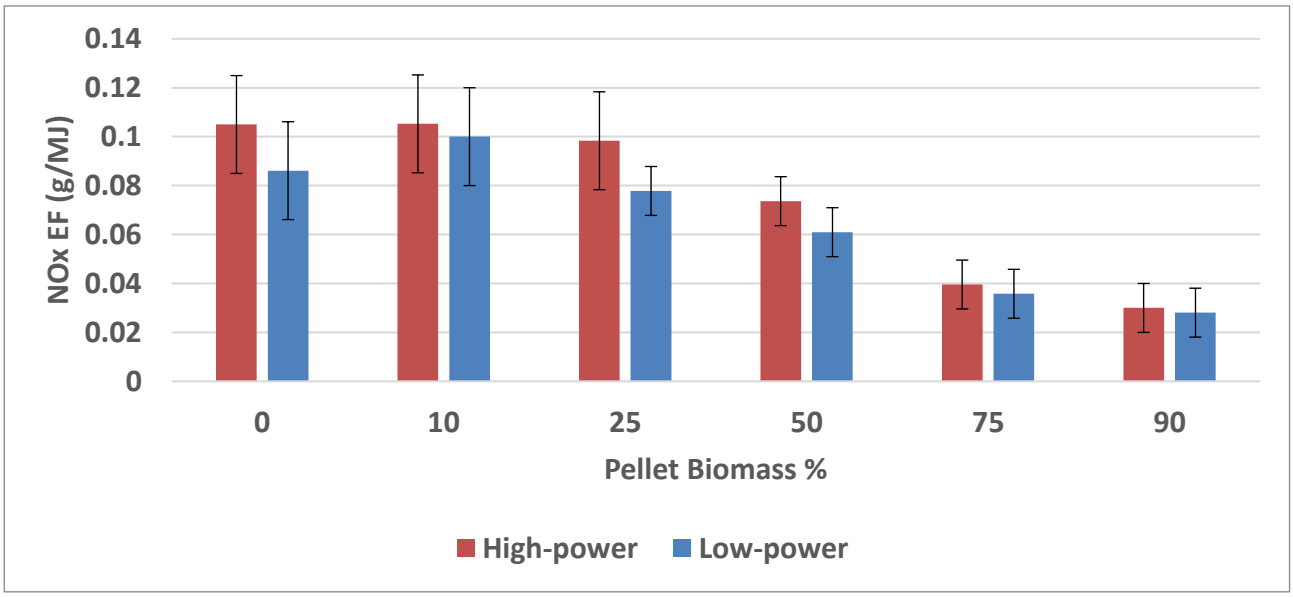

Figure 5-22: NO_x emission factors of pellet blends (g/MJ)

The NO_x emission factors show a decrease with increasing biomass content except for the 0% biomass pellets during the low-power experiment, which shows a lower NO_X emission factor compared to the 10% biomass pellets. The low-power experiments also exhibit lower NO_x emission factors than the high-power ones. The 10% biomass pellets displayed the largest NO_x emission factors of both high-power and low-power experiments. This trend would suggest that oxygen deficiency inhibits the oxidation of the nitrogen in the fuel. There is a positive correlation between the NO_x emission factors and the nitrogen content of the fuel. Deng, Nie, Lu, et al., (2022) conducted a study on the performance of a solid fuel stove at high-power and low-power settings using bituminous coal and biomass, including wood, as fuel. The NO_x emission factors resulting from the experiments decreased under low-power conditions compared to the high-power conditions, similar to the results in this study. The NO_x emission factors of the fuels are proportional to the nitrogen content in the fuel. Rahman et al., (2022) found that at temperatures lower than 1500 °C, fuel-NO is the only contribution to the NO formed (thermal-NO formation does not occur). This trend would correspond with the correlation between the NO_x emission factors and the nitrogen content of the fuel.

The NO_x emission factors and recovery are quantified in **Table 5-7** in $[g/MJ]$. Refer the **Table F-6** in Appendix F for the respective uncertainty analysis and the mass balance of the combustion experiments.

Table 5-7: NO_x emission factors of pellets

% Biomass	0	10	25	50	75	90
High-power						
Recovery (%)	8	8	10	11	9	9
EF (g/MJ)	0.11 ± 0.02	0.11 ± 0.02	0.10 ± 0.02	0.07 ± 0.01	0.04 ± 0.01	0.03 ± 0.01
Low-Power						
Recovery (%)	6	8	8	8	7	10
EF (g/MJ)	0.09 ± 0.02	0.10 0.02	0.08 ± 0.01	0.06 ± 0.01	0.04 ± 0.01	0.03 ± 0.01

EF = Emission factor

Meyer et al., (2020) reported emission factors of 0.13 g/MJ to 0.15 g/MJ while conducting combustion experiments on the same stove used in this study using lump coal. These results closely align with the results reported in this study. Deng, Nie, Lu, et al., (2022) reported NO_x emission factors of 0.26 g/MJ for bituminous coal and 0.19 g/MJ for wood pellets. Sumbane-Prinsloo et al., (2021) reported NO_x emission factors ranging from 0.25 g/MJ to 0.55 g/MJ during coal combustion in a coal stove. These emission factors are higher than the results of this study. This difference can be attributed to the lower nitrogen content of the fuel used in this study. Zeng et al., (2022) and Smoot et al., (1998) reported that reburning could reduce the NO_x in a flue gas. This result is a possible explanation for the low NO_x emission factors in this study. The NWU semi-continuous stove recycles the flue gas in the heat exchanger compartment of the stove. Any hydrocarbons released by the fuel in the hopper while it undergoes pyrolysis due to the hopper's high temperature and oxygen-deficient conditions would produce nitrogen compounds from the NO in the heat exchanger (Gil, 2002). **Table 5-8** summarises emission factors of NO_x from similar studies.

Table 5-8: Summary of NO_x emission factors from literature

Study	Fuel	Power setting	NO_x EF [g/MJ]
This study	0% - 90% biomass pellets	High-power	0.03 – 0.11
		Low-power	0.03 – 0.10
(Sumbane-Prinsloo *et al.*, 2021)	15 mm – 40 mm lump coal	-	0.25 – 0.52
(Li *et al.*, 2020)	Lump coal from 7 regions	-	0.04 – 0.09
(Meyer *et al.*, 2020)	Grade A and D Lump coal	High-power	0.14 – 0.15
		Low-power	0.11 – 0.13
(Maxwell *et al.*, 2020b)	7 different wood species	-	0.05 – 0.14
(Deng, Nie, Lu, *et al.*, 2022)	Biomass pellets	High-power	0.19 – 0.46
		Low-power	0.16 – 0.43
	Lump coal and coal briquettes	High-power	0.14 – 0.26
		Low-power	0.14 – 0.25

The NO_x emission factors observed in this study align with the studies of Li et al., (2020), Meyer et al., (2020), and Maxwell et al., (2020b), who reported relatively low NO_x emission factors.

5.3.3 SO_2 Emission Factors

Figure 5-23 shows the levels of SO_2 emission factors resulting from the combustion of the different pellet blends.

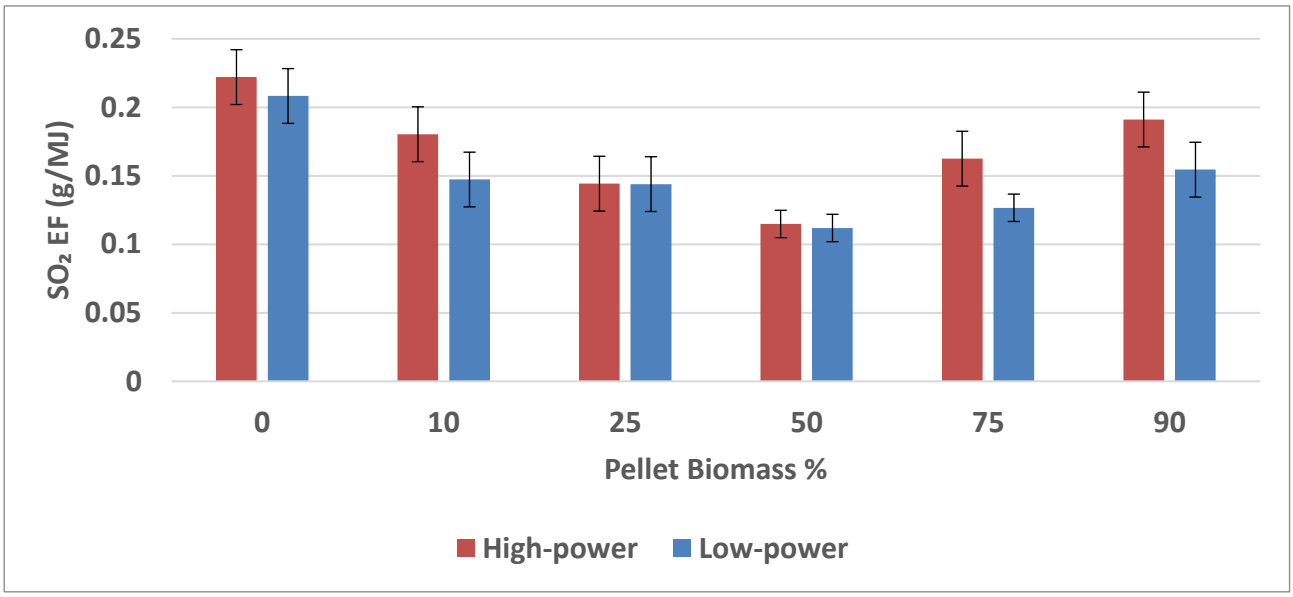

Figure 5-23: SO_2 emission factors of pellet blends (g/MJ)

SO_2 emission factors initially decrease with rising biomass in pellets until reaching a minimum at 50% biomass. Afterwards, SO_2 factors increase with higher biomass content. Emission factors decrease with a decrease of fuel sulphur content up to 50% biomass, then show the inverse beyond 50% biomass. The ash yield of the pellets decreases with increased biomass content, and subsequently, the calcium species also decreases. A possible explanation for the increasing SO_2 emission factors seen during the combustion of high biomass content pellets is the reaction between calcium species, which is abundant in the parent coal, and sulphur to form $CaSO_4$, which would remain in the ash after combustion (Xiao & Song, 2011). This correlation could explain why, with a biomass content of 75% and greater, more of the sulphur content in the fuel is formed into SO_2 since there are fewer calcium species to react with. According to the mass balance of 50% biomass experiments (**Appendix D**), approximately 27% of the sulphur content in the fuel is recovered as SO_2. In contrast, approximately 89% and 85% of the sulphur content in the 90% biomass pellets were recovered as SO_2 in the high-power and low-power experiments, respectively.

The low-power experiments generally displayed lower SO_2 emission factors than the high-power experiments, except for the 25% biomass pellets, where the difference between the high-power and low-power experiments was insignificant. Deng, Nie, Lu, et al., (2022) conducted a study on the performance of a solid fuel stove at high-power and low-power settings using bituminous coal and biomass, including wood, as fuel. The SO_2 emission factors resulting from the experiments

decreased under low-power conditions compared to the high-power conditions, similar to the results in this study. The oxygen deficiency in the combustion zone could be a contributing factor, as oxidation is inhibited. The SO_2 emission factors are quantified in **Table 5-9** in $[g/MJ]$. Refer the **Table F-5** in Appendix F for the respective uncertainty analysis.

Table 5-9: SO_2 emission factors of pellets

% Biomass	0	10	25	50	75	90
High-power						
Recovered (%)	24	23	23	27	96	89
EF (g/MJ)	0.22 ± 0.02	0.18 ± 0.02	0.14 ± 0.02	0.11 ± 0.01	0.16 ± 0.02	0.19 ± 0.02
Low-Power						
Recovered (%)	25	18	23	24	44	85
EF (g/MJ)	0.21 ± 0.02	0.15 ± 0.02	0.14 ± 0.02	0.11 ± 0.01	0.13 ± 0.01	0.15 ± 0.02

EF = Emission factor

Meyer et al., (2020) reported similar SO_2 emission factors ranging from 0.33 g/MJ to 0.39 g/MJ while conducting combustion experiments on the same stove design used in this study, using lump coal. Deng, Nie, Lu, et al., (2022) reported SO_2 emission factors ranging from 0.1 g/MJ to 0.16 g/MJ for bituminous and anthracite coal and emission factors ranging from 0.0 g/MJ to 0.04 g/MJ for biomass combustion in a domestic stove. Notably, Deng, Nie, Lu, et al., (2022) attributed the reduced SO_2 emission factors observed in low-power experiments to an oxygen deficit during combustion. Both studies concluded that the primary determinant of SO_2 emission factors is the sulphur content of the fuel. These conclusions align with the findings of the present study. **Table 5-10** summarises emission factors of SO_2 from similar studies.

Table 5-10: Summary of SO_2 emission factors from literature

Study	Fuel	Power setting	SO_2 EF [g/MJ]
This study	0% - 90% biomass pellets	High-power	0.11 – 0.22
		Low-power	0.11 – 0.21
(Sumbane-Prinsloo *et al.*, 2021)	15 mm – 40 mm lump coal	-	1.01 – 4.18
(Meyer *et al.*, 2020)	Grade A and D Lump coal	High-power	0.33 – 0.39
		Low-power	0.32 – 0.39
(Deng, Nie, Lu, *et al.*, 2022)	Biomass pellets	High-power	0.00 – 0.04
		Low-power	0.00 – 0.02
	Lump coal and coal briquettes	High-power	0.09 – 0.16
		Low-power	0.03 – 0.06

The SO_2 emission factors observed in this study align with the studies of Deng, Nie, Lu, et al., (2022) and Meyer et al., (2020).

5.3.4 Particulate Matter Emission Factors

Figure 5-24 shows the levels of PM_{10} emission factors resulting from the combustion of the different pellet blends.

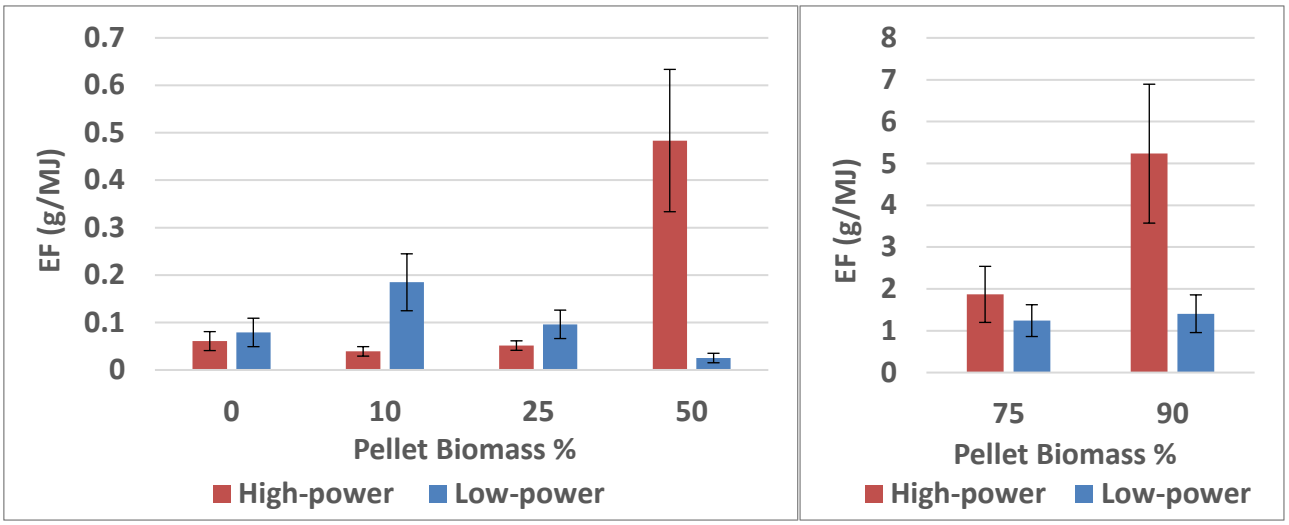

Figure 5-24: PM emission factors of pellet blends (g/MJ)

The low-power experiments produced more PM than the high-power experiments with pellets containing biomass content ranging from 0% to 25%, with the inverse true from 50% to 90% biomass. The trends observed with the PM emission factors regarding biomass content in the pellets are different for high-power and low-power experiments. During high-power experiments, the PM emission factors decreased with the initial addition of biomass from 0% to 10%. With an increase in biomass content greater than 10%, the PM emission factors see a slight increase from 10% to 25% biomass content and a significant increase from 50% to 90% biomass, with the 90% biomass pellets displaying the overall highest PM emission factors during high-power experiments. During low-power experiments, the PM emission factors show an initial increase with the addition of biomass from 0% to 10%. With an increase in biomass content greater than 10%, the PM emission factors exhibit a steady decrease from 10% to 50% biomass, with the 50% biomass pellets resulting in the lowest PM emission factors during low-power experiments. With an increase in biomass content greater than 50%, the PM emission factors rapidly increase from 50% to 90% biomass. Deng et al., (2020) studied the effects of airflow on a force-draft biomass pellet stove and reported that, during biomass combustion, increased airflow to the combustion zone results in an increase in PM emission. This result aligns with the results found in this study. Deng, Nie, Yuan, et al., (2022) investigated the effect of oxygen content in a force-draft biomass pellet stove and reported an increase in $PM_{2.5}$ emissions with an increase in oxygen content in the combustion zone. This trend correlates with the increased PM emissions reported during the high-power experiments of this study. The PM emission factors

are quantified in **Table 5-11** in $[g/MJ]$. Refer the **Table F-7** in Appendix F for the respective uncertainty analysis.

Table 5-11: PM_{10} emission factors of pellets

% Biomass	0	10	25	50	75	90
High-power						
EF (g/MJ)	0.06 ± 0.02	0.04 ± 0.01	0.05 ± 0.01	0.48 ± 0.15	1.9 ± 0.67	5.2 ± 1.66
Low-Power						
EF (g/MJ)	0.08 ± 0.03	0.18 ± 0.06	0.10 ± 0.03	0.03 ± 0.01	1.2 ± 0.38	1.4 ± 0.45

EF = Emission factor

Himanshu et al., (2022) reported PM emission factors of 0.04 g/MJ and 0.03 g/MJ during the combustion of wood pellets in an improved gasifier stove. These results are similar to the 50% biomass pellets during low-power experiments and 25% biomass pellets during high-power experiments. The 75% and 90% biomass pellets exhibit higher PM emission factors than other biomass stoves. A possible explanation for this is the high velocity of the flue gas caused by the pellets' high burn rate (refer to **Table 5-1**), as reported by Deng et al., (2020). Another contributing factor is the thermal degradation of the high biomass content pellets due to their weak structural integrity (Refer to 3.4.3.5: **Compressive Strength**). Strandberg et al., (2018) conducted combustion experiments on biomass pellets and reported that rapid devolatilization compromises the structural integrity of the pellets and creates internal cavities. After the pellets decompose, the high flow rate of the flue gas suspends the decomposed particles in the air. Upon inspection of the inner stove compartments, large amounts of fly ash are observed in the heat exchanger, confirming the generation of fly ash. The inverse is valid for the 50% pellet, low-power experiments. The ash in the stove ash tray seems to keep its original pellet form after combustion, and some ash pellets formed clinkers. Upon closer inspection, the finer ash particles also formed smaller agglomerates, prohibiting fly ash production (Refer to **Appendix E**). This tendency could be a possible explanation for the low PM emission factors of these experiments. **Table 5-12** summarises emission factors of PM from similar studies.

Table 5-12: Summary of PM emission factors from literature

Study	Fuel	Power setting	PM EF [g/MJ]
This study	0% - 90% biomass pellets	High-power	0.06 – 5.2
		Low-power	0.08 – 1.4
(Sumbane-Prinsloo *et al.*, 2021)	15 mm – 40 mm lump coal	-	0.75 – 5.41
(Meyer *et al.*, 2020)	Grade A and D Lump coal	High-power	0.02 – 0.04
		Low-power	0.20 – 0.24
(Deng, Nie, Lu, *et al.*, 2022)	Biomass pellets	High-power	0.01 – 0.05
		Low-power	0.03 – 0.13
	Lump coal and coal briquettes	High-power	0.03 – 0.15
		Low-power	0.16 – 0.26

The PM emission factors on the lower end are comparable to most studies, while those on the higher end are only comparable to the emission factors reported by Sumbane-Prinsloo et al., (2021).

CHAPTER 6: CONCLUSION AND RECOMMENDATIONS

This study investigated the thermal and emissions performance of the NWU semi-continuous stove using coal and torrefied wood blended pellets. This section summarises and concludes the key findings from this study.

6.1 Summary of Findings

Torrefaction of Biomass

The torrefaction process was conducted on wood chips at an operating temperature of 278 °C (± 3 °C) and a residence time of 60 minutes, resulting in a total mass loss of 36.4%. Post-torrefaction, the wood exhibited increased brittleness. Torrefaction reduced the wood's hygroscopic nature, decreasing its moisture absorption tendency. Chemical analysis indicated alterations in wood composition during torrefaction. Oxygen content decreased by 42%, while carbon content decreased by 31%. Torrefaction resulted in a 5% increase in calorific value. Breakdown of hemicellulose during torrefaction occurred at a temperature of 275 °C, with an 81% reduction.

Extrusion of Blended Pellets

The pellets produced through the extrusion process maintained their form, which can be attributed to the compression-based shaping during extrusion. This compression ensured structural integrity for intended applications. However, the compressive strength of the pellets decreased with increasing biomass content. Pellet blend compositions displayed a linear relationship between coal and torrefied biomass, indicating blend homogeneity.

Stove Operation

Pellets with higher biomass content exhibited increased fuel consumption correlated with volatile matter in the fuel, resulting in a proportional decrease in runtime. Notably, pellets with 0% biomass displayed the lowest fuel consumption rate. The relation between burn rate and biomass content was consistent in both high- and low-power experiments. Flue gas volumetric flow rate and velocity initially decrease with low biomass content but significantly increase with higher biomass content. Flue gas volume and velocity were primarily influenced by the burn rate.

The fuel bed temperature consistently exceeded temperatures above the fuel bed, and temperature fluctuations caused by ash detachment occur during grate-shake procedures. As biomass content increases, temperature drops in the fuel bed become less frequent but more pronounced, attributed to pellet thermal degradation. The hopper's temperatures remain below 100 °C, with gradual fuel

ignition closer to the combustion zone. The fuel bed and region above it exhibit parallel temperature trends, with distinct fluctuations during grate-shaking, influencing CO_2 and O_2 concentrations. Grate-shake procedures lead to rapid char oxidation and O_2 shortages, increasing CO production. CO spikes during grate-shakes are higher during low-power experiments due to O_2 taking longer to replenish. Oxygen deficiency occurs in combustion experiments with 75% and 90% biomass pellets, leading to elevated CO production. Fuel bed temperature decreases with rising CO concentration, reflecting the higher heat of formation for CO_2. SO_2 and NO_x formation correlate with combustion zone temperature, indicating potential factors influencing sulphur retention and NO reactions with hydrocarbons.

Thermal Performance

The ignition times of fuels decrease with higher biomass content in both high and low-power experiments. Volatile matter, ash content, and compressive strength influence ignition times. High-power settings accelerate combustion, resulting in shorter ignition times. Pellet composition, structural factors, and power settings collectively influence ignition times. Increasing biomass content leads to a rise in peak temperature until 75%, followed by a decline. Burn rates and peak temperatures increase with a decrease in pellet compressive strength. The stove in this study demonstrates higher biomass consumption rates but maintains a similar coal consumption rate compared to other biomass and coal stoves. Power output increases with biomass content in both high and low-power experiments. The rise in power output corresponds to an increase in burn rate and a decrease in calorific value. The study compares to similar research on coal stoves but notes differences attributable to stove design and fuel characteristics. The mass of fuel needed to raise water temperature increases with biomass content in high-power experiments but decreases beyond 50% in low-power experiments. System efficiency decreases with increasing biomass content. The system efficiency displayed sensitivity to combustion dynamics and oxygen surplus in high-power experiments. In low-power experiments, system efficiency generally improves with biomass content. Cooking energy output and efficiency exhibit an inverse relationship, indicating diminishing returns at higher energy outputs.

Emissions Performance

High-power experiments displayed higher CO and CO_2 emission factors than low-power experiments. CO and CO_2 emissions decreased with pellets containing low biomass content and increased with higher biomass content. The NO_x emission factors exhibited a decrease under low-power conditions, consistent with previous research, and were positively correlated with the nitrogen content of the fuel. The study attributed the low NO_x emission factors to the recycling of flue gas in the stove, potentially reducing NO_x through reactions with hydrocarbons to form N-species. The SO_2

emission factors demonstrated a complex pattern, initially decreasing with biomass content up to 50%, followed by an increase. This trend was attributed to reactions with calcium species in the parent coal and the formation of $CaSO_4$. The low-power experiments generally showed lower SO_2 emission factors. Particulate matter initially decreased with adding biomass and increased with higher biomass content pellets. High-power experiments showed higher PM emissions compared to low-power experiments. The PM emissions displayed sensitivity to flue gas velocity, promoting fly ash generation. High flue gas velocity and weak pellet integrity are the main factors influencing increased PM emissions during the combustion of pellets with high biomass content.

6.2 Conclusion

The torrefaction process proved effective in enhancing biomass's energy density while improving its physical and chemical properties. The effective use of extrusion, facilitated by compressive forces, enabled the production of blended pellets, although those with high biomass content required additional binder for proper agglomeration. However, adding biomass impacted the structural integrity of the pellets, leading to reduced overall stability.

The NWU semi-continuous stove demonstrated high combustion efficiency with coal pellets, surpassing benchmarks found in literature. Furthermore, the stove exhibited comparable fuel consumption rates with low biomass content pellets and extremely high rates with high biomass content pellets. The stove did not effectively regulate airflow and combustion rate with high biomass content pellets.

Challenges arose due to ash accumulation on the grate and the fuel bed. This ash accumulation intensified with increased biomass content. The proximity of the fuel in the hopper to the combustion zone facilitated ignition in the hopper, especially with high biomass pellets. The air supply’s proximity to the hopper promoted combustion of the fuel in the hopper.

Nevertheless, the stove demonstrated effectiveness in boiling water at rates comparable to other stoves in literature, maintaining similar cooking efficiency. Emission performance varied, with lower SO_2 emissions noted for pellets containing less than 50% biomass, low NO_x emissions across all pellet blends, and low CO emissions associated with pellets containing 25% biomass or less. Notably, the stove produced low PM emissions with pellets containing up to 50% biomass but exhibited higher PM emissions with pellets containing more than 50% biomass. In conclusion, the NWU semi-continuous stove effectively burned blended fuel with up to 25% biomass.

6.3 Recommendations

The stove design could be altered to facilitate biomass combustion with the following:

- Relocate air inlet: The fuel in the hopper is in a direct path of the airflow to the combustion zone, leading to hopper combustion and inefficient use of the oxygen supply. Relocating the air inlet to the side of the stove, perpendicular to the combustion chamber, would prevent hopper ignition and decrease oxygen shortages.

- Grate design: The fuel in the hopper rests on a grate that allows air to flow to the hopper. Modifying the grate with a steel plate on the hopper section would inhibit airflow to the hopper and subsequently reduce hopper ignition. This modification would not decrease the grate functionality.

- Utilise an automated grate-shake to minimise human error during laboratory experiments focused on scientific accuracy and manual grate-shakes for experiments focused on the real-life performance of the stove.

- Fuel properties: The fuel properties, such as particle size, can be altered to facilitate slower combustion.

- Utility: The heat exchanger section of the stove is large enough to incorporate an oven utility within. This design should be incorporated while allowing flue gas circulation around the oven.

- Investigate more accurate methods for determining the fuel burn rate regarding fuel temperature and moisture content during combustion experiments.

BIBLIOGRAPHY

Abu Ghalia, M. & Dahman, Y. 2017. Synthesis and utilization of natural fiber-reinforced poly (lactic acid) bionanocomposites. *Lignocellulosic Fibre and Biomass-Based Composite Materials: Processing, Properties and Applications*. (January, 1):313–345.

Adesina, J.A., Piketh, S.J., Burger, R.P. & Mkhatshwa, G. 2022. Assessment of criteria pollutants contributions from coal-fired plants and domestic solid fuel combustion at the South African industrial highveld. *Cleaner Engineering and Technology*. 6:100358.

Adeyemi, K., Lawal, N. & Asere, A. 2017. Thermal Performance of Improved Charcoal Stove as A Clean Development Mechanism Project – A Case Study of Bauchi. *FUOYE Journal of Engineering and Technology*. 2(1).

Agbor, E., Zhang, X. & Kumar, A. 2014. A review of biomass co-firing in North America. *Renewable and Sustainable Energy Reviews*. 40:930–943.

Agenbroad, J., DeFoort, M., Kirkpatrick, A. & Kreutzer, C. 2011. A simplified model for understanding natural convection driven biomass cooking stoves—Part 2: With cook piece operation and the dimensionless form. *Energy for Sustainable Development*. 15(1):169–175.

Ahmad, N. & Zakaria, M.R. 2019. Oligosaccharide From Hemicellulose. *Lignocellulose for Future Bioeconomy*. (January, 1):135–152.

Ahmed, R., P, R., Pemberton-Pigott, C., Abbas, A., Suitan, M. & Nan, Z. 2019. Performance investigation of top-lit updraft gasifier stove using different biomass fuels. *Fresenius Environmental Bulletin*. 28(12):9835–9842.

Ahn, S., Choi, G. & Kim, D. 2014. The effect of wood biomass blending with pulverized coal on combustion characteristics under oxy-fuel condition. *Biomass and Bioenergy*. 71:144–154.

Aich, S., Behera, D., Nandi, B.K. & Bhattacharya, S. 2020. Relationship between proximate analysis parameters and combustion behaviour of high ash Indian coal. *International Journal of Coal Science and Technology*. 7(4):766–777.

Allen, G., Morin, B., Ahmadi, M. & Rector, L. 2022. Online measurement of PM from residential wood heaters in a dilution tunnel. *Journal of the Air & Waste Management Association*. 72(7):662–678.

Andrew, J.E., Johakimu, J., Lekha, P., Gibril, M.E. & Sitholé, B.B. 2016. *Beneficiation of sawdust waste in the context of an integrated forest bio-refinery mill: Kraft and pre-hydrolysis Kraft pulping properties*.

Azom, M.G., Ferdous, J., Hembrom, S., Hossain, M., Islam, M., … Tudu, J.P. 2017. *A preliminary evaluation of ther "Akha" gasifier cookstove by rural households in Bangladesh*.

Bailis, R. 2004. Wood in Household Energy Use. In: *Encyclopedia of Energy*. Elsevier.

Ballard-Tremeer, G. & Jawurek, H.H. 1996. Comparison of five rural, wood-burning cooking devices: Efficiencies and emissions. *Biomass and Bioenergy*. 11(5):419–430.

Ballard-Tremeer, G. & Jawurek, H.H. 1999. The "hood method" of measuring emissions of rural cooking devices. *Biomass and Bioenergy*. 16(5):341–345.

Balmer, M. 2007. Household coal use in an urban township in South Africa. *Journal of Energy in Southern Africa*. 18(3):27–32.

Barnes, B., Mathee, A., Bruce, N. & Thomas, L. 2006. Protecting children from indoor air pollution exposure through outdoor cooking in rural South Africa. *Boiling point*. 52:11–13.

Basu, P. 2018. Torrefaction. *Biomass Gasification, Pyrolysis and Torrefaction: Practical Design and Theory*. (January, 1):93–154.

Basu, P., Butler, J. & Leon, M.A. 2011. Biomass co-firing options on the emission reduction and electricity generation costs in coal-fired power plants. *Renewable Energy*. 36(1):282–288.

Batool, F., Islam, K., Cakiroglu, C. & Shahriar, A. 2021. Effectiveness of wood waste sawdust to produce medium- to low-strength concrete materials. *Journal of Building Engineering*. 44:103237.

Bentson, S., Evitt, D., Still, D., Lieberman, D. & MacCarty, N. 2022. Retrofitting stoves with forced jets of primary air improves speed, emissions, and efficiency: Evidence from six types of biomass cookstoves. *Energy for Sustainable Development*. 71:104–117.

Bergman, P.C.A., Boersma, A., Zwart, R. & Kiel, J.H.A. 2005. Torrefaction for Biomass Co-Firing in Existing Coal-Fired Power Stations. Netherlands: Energy research Centre of the Netherlands (ECN).

Bhuiyan, A.A., Blicblau, A.S., Islam, A.K.M.S. & Naser, J. 2018. A review on thermo-chemical characteristics of coal/biomass co-firing in industrial furnace. *Journal of the Energy Institute*. 91(1):1–18.

Biorefinery Edu. 2018. Chemical overview of wood. 1–9.

Biswas, A.K., Rudolfsson, M., Broström, M. & Umeki, K. 2014. Effect of pelletizing conditions on combustion behaviour of single wood pellet. *Applied Energy*. 119:79–84.

Di Blasi, C. 1997. Influences of physical properties on biomass devolatilization characteristics. *Fuel*. 76(10):957–964.

Bolaji, O.B. & Olalusi, A. 2009. Development of an Improved Coal Stove for Cooking in Developing Countries. *AU Journal of Technology*. 12(3):182–187.

Bowen, B.H. & Irwin, M.W. 2008. Coal Characteristics. *Combustion Engineering Issues for Solid Fuel Systems*. (October 2008):33–81.

Brandelet, B., Rose, C., Rogaume, C. & Rogaume, Y. 2018. Impact of ignition technique on total emissions of a firewood stove. *Biomass and Bioenergy*. 108:15–24.

Brigham, C. 2018. Biopolymers: Biodegradable Alternatives to Traditional Plastics. *Green Chemistry: An Inclusive Approach*. (January, 1):753–770.

Brown, U. 2022. *Illegal Mining*. *Minerals Council of South Africa*.

Buthelezi, S.A., Kapwata, T., Wernecke, B., Webster, C., Mathee, A. & Wright, C.Y. 2019. *Household fuel use for heating and cooking and respiratory health in a low-income, South African coastal community*.

Calvo-Flores, F.G. 2020. Lignin: A Renewable Raw Material. *Encyclopedia of Renewable and Sustainable Materials*. (January, 1):102–118.

Chateigner-Boutin, A.L. & Saulnier, L. 2022. Ferulic and coumaric acids in the cereal grain: Occurrence, biosynthesis, biological and technological functions. *Advances in Botanical Research*. 104:169–213.

Chen, W.H., Lin, B.J., Colin, B., Chang, J.S., Pétrissans, A., … Pétrissans, M. 2018. Hygroscopic transformation of woody biomass torrefaction for carbon storage. *Applied Energy*. 231:768–776.

Chen, W.H., Lin, B.J., Colin, B., Pétrissans, A. & Pétrissans, M. 2019. A study of hygroscopic property of biomass pretreated by torrefaction. *Energy Procedia*. 158:32–36.

Chen, X., Chang, Z. & Peng, Y. 2017. Predicting the degree of surface oxidation on fine coals by measuring the oxygen transfer rate in coal suspensions. *Fuel Processing Technology*. 159:313–319.

Chen, Y., Shen, G., Su, S., Du, W., Huangfu, Y., … Tao, S. 2016. Efficiencies and pollutant emissions from forced-draft biomass-pellet semi-gasifier stoves: Comparison of International and Chinese water boiling test protocols. *Energy for Sustainable Development*. 32:22–30.

Cheng, J., Zhou, F., Si, T., Zhou, J. & Cen, K. 2018. Mechanical strength and combustion properties of biomass pellets prepared with coal tar residue as a binder. *Fuel Processing Technology*. 179:229–237.

Chugh, Y.P. & Behum, P.T. 2014. Coal waste management practices in the USA: an overview. *International Journal of Coal Science & Technology*.

Davidson, R.M. 1982. Molecular Structure of Coal. In: *Coal Science*. Elsevier. pp. 83–160.

Demirbas, A. 2004. Combustion characteristics of different biomass fuels. *Progress in Energy and Combustion Science*. 30(2):219–230.

Deng, M., Li, P., Shan, M. & Yang, X. 2020. Optimizing supply airflow and its distribution between primary and secondary air in a forced-draft biomass pellet stove. *Environmental Research*. 184:109301.

Deng, M., Nie, Y., Yuan, Y., Ma, R., Shan, M. & Yang, X. 2022. The impact of oxygen content in the primary air supply on fuel burning rate and pollutant emissions in a forced-draft biomass stove. *Fuel*. 321:124129.

Deng, M., Nie, Y., Lu, F., Ma, R., Yuan, Y., … Yang, X. 2022. Pollutant emission performances of improved solid fuel heating stoves and future implications in rural China. *Energy and Buildings*. 257:111810.

Department of Energy. 2019. *The South African Energy Sector Report 2019*. *Department of Energy*. http://www.energy.gov.za/files/media/explained/2019-South-African-Energy-Sector-Report.pdf.

Department of Energy. 2021. *South African energy sector report 2021*. http://www.energy.gov.za/files/media/explained/2021-South-African-Energy-Sector-Report.pdf.

Durix, L., Carlsson Rex, H. & Mendizabal, V. 2016. Contextual Design and Promotion of Clean Biomass Stoves. https://openknowledge.worldbank.org/handle/10986/25129.

Easterly, J.L. & Burnham, M. 1996. Overview of biomass and waste fuel resources for power production. *Biomass and Bioenergy*. 10(2–3):79–92.

Energypedia. 2018. *Gasifier Stoves*. *https://energypedia.info/wiki/Gasifier_Stoves#References*.

EPA. 2007. *Methodology for Thermal Efficiency and Energy Input Calculations and Analysis of Biomass Cogeneration Unit Characteristics*.

Eskom. 2021. *CO 0007 Revision 16*. https://www.eskom.co.za/wp-content/uploads/2021/08/CO-0007-Coal-in-SA-Rev-16.pdf.

European commission. 2016. *Production of Solid Sustainable Energy Carriers from Biomass by Means of Torrefaction*. https://cordis.europa.eu/project/id/282826/reporting.

Farrelly, D.J., Everard, C.D., Fagan, C.C. & McDonnell, K.P. 2013. Carbon sequestration and the role of biological carbon mitigation: A review. *Renewable and Sustainable Energy Reviews*. 21:712–727.

Fečko, P., Tora, B. & Tod, M. 2013. Coal waste: handling, pollution impacts and utilization. *The Coal Handbook: Towards Cleaner Production*. 2:63–84.

Felder, R.M., Rousseau, R.W. & Bullard, L.G. 2017. *Felder's Elementary Principles of Chemical Processes*. Global edition ed. John Wiley & Sons.

Ferreira, T., Marques, E., Paiva, J.M. & Pinho, C. 2023. A Study on the Spontaneous Ignition of Some Ligneous Pellets. *Fire*. 6(4):153.

Fleig, D., Normann, F., Andersson, K., Johnsson, F. & Leckner, B. 2009. The fate of sulphur during oxy-fuel combustion of lignite. *Energy Procedia*. 1(1):383–390.

Forest research. 2022. *Typical calorific values of fuels*. https://www.forestresearch.gov.uk/tools-and-resources/fthr/biomass-energy-resources/reference-biomass/facts-figures/typical-calorific-values-of-fuels/.

Gadsby, J., Long, F.J., Sleightholm, P. & Sykes, K.W. 1948. The mechanism of the carbon dioxide-carbon reaction. *Proceedings of the Royal Society of London. Series A. Mathematical and Physical Sciences*. 193(1034):357–376.

Galanakis, C.M. 2017. Energy applications of coffee processing by-products. In: *Handbook of Coffee Processing By-Products*. Elsevier Inc. pp. 323–367.

Gent, S., Twedt, M., Gerometta, C. & Almberg, E. 2017. Introduction to Thermochemical Conversion Processes. *Theoretical and Applied Aspects of Biomass Torrefaction*. (January, 1):1–16.

Gil, S. 2002. *Influence of combustion pressure on fuel-N conversion to NO, N 2O and N2*. Poland. www.intechopen.com.

Glasius, M., Ketzel, M., Wåhlin, P., Jensen, B., Mønster, J., … Palmgren, F. 2006. Impact of wood combustion on particle levels in a residential area in Denmark. *Atmospheric Environment*. 40(37):7115–7124.

González, E., Marzal, F., Miñana, A. & Doval, M. 2008. Influence of exhaust hood geometry on the capture efficiency of lateral exhaust and push-pull ventilation systems in surface treatment tanks. *Environmental Progress*. 27(3):405–411.

Grainger, A. & Smith, G. 2021. The role of low carbon and high carbon materials in carbon neutrality science and carbon economics. *Current Opinion in Environmental Sustainability*. 49:164–189.

Greiner, T.H. 1997. *Carbon Monoxide Poisoning: Checking for Complete Combustion*. *Iowa State University: Department of Agricultural and Biosystems Engineering*.

Grimsby, L.K., Rajabu, H.M. & Treiber, M.U. 2016. Multiple biomass fuels and improved cook stoves from Tanzania assessed with the Water Boiling Test. *Sustainable Energy Technologies and Assessments*. 14:63–73.

Guo, Z., Miao, Z., Guo, F., Guo, Y., Feng, Y., … Zhang, Y. 2022. Parameter optimization of waste coal briquetting and particulate matter emissions test during combustion: A case study. *Environmental Pollution*. 294:118621.

Han, J., Yu, D., Wu, J., Yu, X., Liu, F. & Xu, M. 2023. Effects of torrefaction on ash-related issues during biomass combustion and co-combustion with coal. Part 1: Elemental partitioning and particulate matter emission. *Fuel*. 334:126776.

Havstad, M.R. 2020. Biodegradable plastics. *Plastic Waste and Recycling: Environmental Impact, Societal Issues, Prevention, and Solutions*. (January, 1):97–129.

Hein, K.R.G. & Bemtgen, J.M. 1998. EU clean coal technology—co-combustion of coal and biomass. *Fuel Processing Technology*. 54(1–3):159–169.

Hildemann, L.M., Cass, G.R. & Markowski, G.R. 1989. A Dilution Stack Sampler for Collection of Organic Aerosol Emissions: Design, Characterization and Field Tests. *Aerosol Science and Technology*. 10(1):193–204.

Hill, S.C. & Smoot, L.D. 2000. Modeling of nitrogen oxides formation and destruction in combustion systems. *Progress in Energy and Combustion Science*. 26(4–6):417–458.

Himanshu, Kurmi, O.P., Jain, S. & Tyagi, S.K. 2022. Performance assessment of an improved gasifier stove using biomass pellets: An experimental and numerical investigation. *Sustainable Energy Technologies and Assessments*. 53:102432.

Hueglin, C., Scherrer, L. & Burtscher, H. 1997. An accurate, continuously adjustable dilution system (1:10 to 1:104) for submicron aerosols. *Journal of Aerosol Science*. 28(6):1049–1055.

Hughes, E.E. & Tillman, D.A. 1998. Biomass cofiring: status and prospects 1996. *Fuel Processing Technology*. 54(1–3):127–142.

Islam, A., Roy, H. & Rahman, M.M. 2022. Energy efficiency study of household natural gas burner using pot-bottom shield and modified pot arrangement. *Energy Reports*. 8:12871–12885.

Jayanti, S., Maheswaran, K. & Saravanan, V. 2007. Assessment of the effect of high ash content in pulverized coal combustion. *Applied Mathematical Modelling*. 31(5):934–953.

Jeguirim, M. & Khiari, B. 2022. Green pellets production and applications in energy sector. *Renewable Energy Production and Distribution: Recent Developments*. (January, 1):139–185.

Jiang, Y., Mori, T., Naganuma, H. & Ninomiya, Y. 2022. Effect of the optimal combination of bituminous coal with high biomass content on particulate matter (PM) emissions during co-firing. *Fuel*. 316:123244.

Kalembkiewicz, J. & Chmielarz, U. 2012. Ashes from co-combustion of coal and biomass: New industrial wastes. *Resources, Conservation and Recycling*. 69:109–121.

Kampa, M. & Castanas, E. 2008. Human health effects of air pollution. *Environmental Pollution*. 151(2):362–367.

Kartal, F. & Özveren, U. 2022. Prediction of torrefied biomass properties from raw biomass. *Renewable Energy*. 182:578–591.

Khaniabadi, Y.O., Polosa, R., Chuturkova, R.Z., Daryanoosh, M., Goudarzi, G., … Naserian, P. 2017. Human health risk assessment due to ambient PM10 and SO2 by an air quality modeling technique. *Process Safety and Environmental Protection*. 111:346–354.

Kim, M.H. & Song, H.B. 2014. Analysis of the global warming potential for wood waste recycling systems. *Journal of Cleaner Production*. 69:199–207.

Kole, A.T., Zeru, B.A., Bekele, E.A. & Ramayya, A.V. 2022a. Design, development, and performance evaluation of husk biomass cook stove at high altitude condition. *International Journal of Thermofluids*. 16:100242.

Kole, A.T., Zeru, B.A., Bekele, E.A. & Ramayya, A.V. 2022b. Design, development, and performance evaluation of husk biomass cook stove at high altitude condition. *International Journal of Thermofluids*. 16:100242.

Kopp, O.C. 2022. Coal. *Fossil fual*.

Krawczyk, E. & Zajemska, M. 2013. *The chemical mechanism of SOx formation and elimination in coal combustion process*.

Kühn, T., Bunt, J.R., Neomagus, H.W.J.P., Piketh, S.J., Everson, R.C. & Coetzee, S. 2017. Coal-derived low smoke fuel assessment through coal stove combustion testing. *Journal of Analytical and Applied Pyrolysis*. 126:158–168.

Kumar, N. & Dixit, A. 2021. Management of biomass. *Nanotechnology for Rural Development*. (January, 1):97–140.

Kumar, R. & Singh, R.I. 2016. An investigation in 20 kWth oxygen-enriched bubbling fluidized bed combustor using coal and biomass. *Fuel Processing Technology*. 148:256–268.

Leckner, B. & Karlsson, M. 1993. Gaseous emissions from circulating fluidized bed combustion of wood. *Biomass and Bioenergy*. 4(5):379–389.

Li, C., Ye, K., Mawusi, S., Zhang, W., Xu, Y., … Liu, G. 2020. A 24-h real-time emissions assessment of 41 uncontrolled household raw coal combustion stoves in four provinces of Northern China. *Atmospheric Environment*. 235:117588.

Li, Q., Jiang, J., Zhang, Q., Zhou, W., Cai, S., … Hao, J. 2016. Influences of coal size, volatile matter content, and additive on primary particulate matter emissions from household stove combustion. *Fuel*. 182:780–787.

Liang, B., Bai, H., Fu, L. & Bai, D. 2023. Characteristics of the particulate matter and its toxic substances from different stationary coal-fired sources. *Fuel*. 334:126594.

Liao, L., Zheng, J., Zhang, Y., Li, C. & Yuan, C. 2021. Impact of torrefaction on entrained-flow gasification of pine sawdust: An experimental investigation. *Fuel*. 289:119919.

Lippmann, M. & Leikauf, G.D. 2020. Nitrogen oxides. In: 4th ed. *Environmental Toxicants: Human Exposures and Their Health Effects, Fourth Edition*. John Wiley & Sons Inc.

Liu, S., Zhu, G., Niu, Y., Wen, L., Lei, Y., … Hui, S. 2022. Characteristics of particulate emissions from coal char combustion: Char fragmentation and ash coalescence behaviors. *Fuel*. 310:122283.

Luan, M., Zhang, T., Li, X., Yan, C., Sun, J., … Zheng, M. 2022. Investigating the relationship between mass concentration of particulate matter and reactive oxygen species based on residential coal combustion source tests. *Environmental Research*. 212:113499.

Luo, P., Shen, G., Sun, M., Teng, D., Jia, X. & Zhang, S. 2023. Research on water and waste heat recovery from flue gas using micron ceramic membranes. *Thermal Science and Engineering Progress*. 43:102004.

Madanayake, B.N., Gan, S., Eastwick, C. & Ng, H.K. 2017. Biomass as an energy source in coal co-firing and its feasibility enhancement via pre-treatment techniques. *Fuel Processing Technology*. 159:287–305.

Makonese, T., Masekameni, D.M., Annegarn, H.J. & Forbes, P.B.C. 2017a. Emission factors of domestic coal-burning braziers. *South African Journal of Science*.

Makonese, T., Masekameni, D.M., Annegarn, H.J. & Forbes, P.B.C. 2017b. Emission factors of domestic coal-burning braziers. *South African Journal of Science*. 113(3–4).

Makonese, T., Annegarn, H., Forbes, P. & Masekameni, D. 2015. Influence of fuel-bed temperatures on CO and condensed matter emissions from packed-bed residential coal combustion. *International Conference on the Domestic Use of Energy*. 63–69.

Makonese, T., Ifegbesan, A.P. & Rampedi, I.T. 2018. Household cooking fuel use patterns and determinants across southern Africa: Evidence from the demographic and health survey data. *Energy and Environment*. 29(1):29–48.

Mallakpour, S., Sirous, F. & Hussain, C.M. 2021. Sawdust, a versatile, inexpensive, readily available bio-waste: From mother earth to valuable materials for sustainable remediation technologies. *Advances in Colloid and Interface Science*. 295:102492.

Mastalerz, M., Drobniak, A., Hower, J.C. & O'Keefe, J.M.K. 2011. Spontaneous Combustion and Coal Petrology. *Coal and Peat Fires: A Global Perspective*. 1:47–62.

Maxwell, D., Gudka, B.A., Jones, J.M. & Williams, A. 2020a. Emissions from the combustion of torrefied and raw biomass fuels in a domestic heating stove. *Fuel Processing Technology*. 199:106266.

Maxwell, D., Gudka, B.A., Jones, J.M. & Williams, A. 2020b. Emissions from the combustion of torrefied and raw biomass fuels in a domestic heating stove. *Fuel Processing Technology*. 199:106266.

McNamee, P., Adams, P.W.R., McManus, M.C., Dooley, B., Darvell, L.I., … Jones, J.M. 2016. An assessment of the torrefaction of North American pine and life cycle greenhouse gas emissions. *Energy Conversion and Management*. 113:177–188.

Mekonnen, B.A. 2022. Thermal efficiency improvement and emission reduction potential by adopting improved biomass cookstoves for sauce-cooking process in rural Ethiopia. *Case Studies in Thermal Engineering*. 38:102315.

Meyer, C.W., Neomagus, H.W.J.P., Conradie, F.H., Dreyer, L., Piketh, S.J., … Bunt, J.R. 2020. "Coal Pellets as an Alternative Fuel for a Semi-Continuous Coal Stove. *NACA Conference*.

Middleton, B. 2020. *Hardwood vs Softwood: What's the Difference? National Timber Group*. https://www.laver.co.uk/blog/hardwood-vs-softwood-whats-the-difference/#:~:text=In general%2C hardwood comes from,the wood is usually denser.

Miller, B.G. & Tillman, D.A. 2008. Coal Characteristics. *Combustion Engineering Issues for Solid Fuel Systems*. (January, 1):33–81.

Mishra, R.K. & Mohanty, K. 2018. Pyrolysis kinetics and thermal behavior of waste sawdust biomass using thermogravimetric analysis. *Bioresource Technology*. 251:63–74.

Misra, A., Longnecker, M.P., Dionisio, K.L., Bornman, R.M.S., Travlos, G.S., … Whitworth, K.W. 2018. Household fuel use and biomarkers of inflammation and respiratory illness among rural South African Women. *Environmental Research*. 166:112–116.

Mitchell, E.J.S., Lea-Langton, A.R., Jones, J.M., Williams, A., Layden, P. & Johnson, R. 2016. The impact of fuel properties on the emissions from the combustion of biomass and other solid fuels in a fixed bed domestic stove. *Fuel Processing Technology*. 142:115–123.

Mock, C., Lee, H., Choi, S., Yang, W. & Manovic, V. 2017. Burning characteristics of single particles of coal and wood mixtures for co-firing in an upward-flowing hot gas stream. *Fuel Processing Technology*. 163:20–34.

Montiano, M.G., Barriocanal, C. & Alvarez, R. 2013. Effect of the addition of waste sawdust on thermoplastic properties of a coal. *Fuel*. 106:537–543.

Munawer, M.E. 2018. Human health and environmental impacts of coal combustion and post-combustion wastes. *Journal of Sustainable Mining*. 17(2):87–96.

Neuberger, M., Schimek, M.G., Horak, F., Moshammer, H., Kundi, M., … Hauck, H. 2004. Acute effects of particulate matter on respiratory diseases, symptoms and functions:: epidemiological results of the Austrian Project on Health Effects of Particulate Matter (AUPHEP). *Atmospheric Environment*. 38(24):3971–3981.

Njenga, M., Iiyama, M., Jamnadass, R., Helander, H., Larsson, L., … Sundberg, C. 2016. Gasifier as a cleaner cooking system in rural Kenya. *Journal of Cleaner Production*. 121:208–217.

Nocito, F. & Dibenedetto, A. 2020. Atmospheric CO2 mitigation technologies: carbon capture utilization and storage. *Current Opinion in Green and Sustainable Chemistry*. 21:34–43.

Nunes, L.J.R., Matias, J.C.O. & Catalão, J.P.S. 2014. A review on torrefied biomass pellets as a sustainable alternative to coal in power generation. *Renewable and Sustainable Energy Reviews*. 40:153–160.

Nunes, L.J.R., De Oliveira Matias, J.C. & Da Silva Catalão, J.P. 2018. Future Developments and Derived Fuels. *Torrefaction of Biomass for Energy Applications*. (January, 1):221–229.

Nussbaumer, T. 2003. Combustion and Co-combustion of Biomass: Fundamentals, Technologies, and Primary Measures for Emission Reduction. *Energy & Fuels*. 17(6):1510–1521.

Obata, Y., Takeuchi, K., Soma, N. & Kanayama, K. 2006. Recycling of wood waste as sustainable industrial resources—Design of energy saving wood-based board for floor heating systems. *Energy*. 31(13):2341–2349.

Obi, O.F., Ezeoha, S.L. & Okorie, I.C. 2016. Energetic performance of a top-lit updraft (TLUD) cookstove. *Renewable Energy*. 99:730–737.

Öhman, M., Nordin, A., Skrifvars, B.-J., Backman, R. & Hupa, M. 2000. Bed Agglomeration Characteristics during Fluidized Bed Combustion of Biomass Fuels. *Energy & Fuels*. 14(1):169–178.

De Oliveira Brotto, J., Cruz, T.A., De Oliveira Pereira, I., Ienczak, J.L., Peralta, R.A., … Moreira, R. de F.P.M. 2023. Mechanistic insights and kinetics of torrefaction of pine wood biomasses using solid-state NMR. *Journal of Analytical and Applied Pyrolysis*. 172:106019.

Onuegbu, T.U., Ekpunobi, U.E., Ogbu, I.M., Ekeoma, M.O. & Obumselu, F.O. 2011. *Comparative studies of ignition time and water boiling test of coal and biomass briquettes blend*. www.arpapress.com/Volumes/Vol7Issue2/IJRRAS_7_2_08.pdf.

Ozgen, S., Caserini, S., Galante, S., Giugliano, M., Angelino, E., … Morreale, C. 2014. Emission factors from small scale appliances burning wood and pellets. *Atmospheric Environment*. 94:144–153.

Paraschiv, L.S., Serban, A. & Paraschiv, S. 2020. Calculation of combustion air required for burning solid fuels (coal / biomass / solid waste) and analysis of flue gas composition. *Energy Reports*. 6:36–45.

Parmar, K. 2017. Biomass- An Overview on Composition Characteristics and Properties. *IRA-International Journal of Applied Sciences (ISSN 2455-4499)*. 7(1):42.

Pasha, A.F., Ali, M.A., Roy, H. & Rahman, Md.M. 2023. Designing a modified Tchar stove and evaluation of its thermal performance. *Cleaner Chemical Engineering*. 5:100096.

Patel, J.P. & Parsania, P.H. 2018. Characterization, testing, and reinforcing materials of biodegradable composites. *Biodegradable and Biocompatible Polymer Composites: Processing, Properties and Applications*. (January, 1):55–79.

Pedersen, L.S., Morgan, D.J., van de Kamp, W.L., Christensen, J., Jespersen, P. & Dam-Johansen, K. 1997. Effects on SOx and NOx Emissions by Co-Firing Straw and Pulverized Coal. *Energy & Fuels*. 11(2):439–446.

Pemberton-Pigott, C. 2010. *TLUD Vesto Grasifier*.

Penttinen, P., Timonen, K.L., Tiittanen, P., Mirme, A., Ruuskanen, J. & Pekkanen, J. 2001. Ultrafine particles in urban air and respiratory health among adult asthmatics. *European Respiratory Journal*. 17(3):428–435.

Pisupadti, S. V. 2003. Fuel Chemistry. *Encyclopedia of Physical Science and Technology*. (January, 1):253–274.

Prasad, K.K., Sangen, E. & Visser, P. 1985. Woodburning Cookstoves. *Advances in Heat Transfer*. 17(C):159–317.

Prins, M.J., Ptasinski, K.J. & Janssen, F.J.J.G. 2006a. Torrefaction of wood: Part 1. Weight loss kinetics. *Journal of Analytical and Applied Pyrolysis*. 77(1):28–34.

Prins, M.J., Ptasinski, K.J. & Janssen, F.J.J.G. 2006b. Torrefaction of wood: Part 2. Analysis of products. *Journal of Analytical and Applied Pyrolysis*. 77(1):35–40.

Priyanto, D.E., Ueno, S., Sato, N., Kasai, H., Tanoue, T. & Fukushima, H. 2016. Ash transformation by co-firing of coal with high ratios of woody biomass and effect on slagging propensity. *Fuel*. 174:172–179.

Pundle, A., Sullivan, B., Means, P., Posner, J.D. & Kramlich, J.C. 2019. Predicting and analyzing the performance of biomass-burning natural draft rocket cookstoves using computational fluid dynamics. *Biomass and Bioenergy*. 131:105402.

Rahman, Z. ur, Wang, X., Zhang, J., Yang, Z., Dai, G., … Axelbaum, R.L. 2022. Nitrogen evolution, NOX formation and reduction in pressurized oxy coal combustion. *Renewable and Sustainable Energy Reviews*. 157:112020.

Roberts, M.J., Everson, R.C., Neomagus, H.W.J.P., Van Niekerk, D., Mathews, J.P. & Branken, D.J. 2015. *Influence of maceral composition on the structure, properties and behaviour of chars derived from South African coals*. Vol. 142. *Fuel*.

Le Roux, L. 2009. *Reduction In Air Pollution Using the "Basa Njengo Magogo" Methodology and Applicability to Low-Smoke Fuels*. https://www.researchgate.net/publication/45163221.

Sahu, S.G., Chakraborty, N. & Sarkar, P. 2014. Coal–biomass co-combustion: An overview. *Renewable and Sustainable Energy Reviews*. 39:575–586.

Sami, M., Annamalai, K. & Wooldridge, M. 2001. Co-firing of coal and biomass fuel blends. *Progress in Energy and Combustion Science*. 27(2):171–214.

Sarbassov, Y., Duan, L., Manovic, V. & Anthony, E.J. 2018. Sulfur trioxide formation/emissions in coal-fired air- and oxy-fuel combustion processes: a review. *Greenhouse Gases: Science and Technology*. 8(3):402–428.

Senneca, O. 2017. Oxidation of Carbon: What We Know and What We Still Need to Know. *Energy Procedia*. 120:62–74.

Sermyagina, E., Saari, J., Kaikko, J. & Vakkilainen, E. 2016. Integration of torrefaction and CHP plant: Operational and economic analysis. *Applied Energy*. 183:88–99.

Sh, L., Jeong, T.Y., Jeon, K.T., Park, K.W., Lee, B.H. & Jeon, C.H. 2019. Combustion behaviors of wood pellet fuel and its co-firing with different coals. *Journal of Mechanical Science and Technology*. 33(9):4545–4553.

Shah, A. 2018. Torrefaction: Upgrading biomass to “Green coal”. *Agriculture and Natural Resources*.

Shen, H., Luo, Z., Xiong, R., Liu, X., Zhang, L., … Tao, S. 2021. A critical review of pollutant emission factors from fuel combustion in home stoves. *Environment International*. 157:106841.

Shrestha, P., Zhang, W., Mawusi, S.K., Li, J., Xu, J., … Liu, G. 2021. In-use emissions and usage trend of pellet heating stoves in rural Yangxin, Shandong Province. *Environmental Pollution*. 280:116955.

Singh, S., Wasewar, K.L. & Kansal, S.K. 2020. Low-cost adsorbents for removal of inorganic impurities from wastewater. *Inorganic Pollutants in Water*. (January, 1):173–203.

Skodras, G., Grammelis, P., Samaras, P., Vourliotis, P., Kakaras, E. & Sakellaropoulos, G.P. 2002. Emissions monitoring during coal waste wood co-combustion in an industrial steam boiler. *Fuel*. 81(5):547–554.

Smoot, L.D., Hill, S.C. & Xu, H. 1998. NOx control through reburning. *Progress in Energy and Combustion Science*. 24(5):385–408.

Sondreal, E.A., Benson, S.A., Hurley, J.P., Mann, M.D., Pavlish, J.H., … Zygarlicke, C.J. 2001. Review of advances in combustion technology and biomass cofiring. *Fuel Processing Technology*. 71(1–3):7–38.

Strandberg, A., Thyrel, M., Skoglund, N., Lestander, T.A., Broström, M. & Backman, R. 2018. Biomass pellet combustion: Cavities and ash formation characterized by synchrotron X-ray micro-tomography. *Fuel Processing Technology*. 176:211–220.

Sumbane-Prinsloo, L., Bunt, J., Piketh, S., Neomagus, H., Waanders, F. & Matjie, R. 2021. The influence of particle size on the thermal performance of coal and its derived char in a Union stove. *Energy Geoscience*. 2(2):148–159.

Taha, Y., Benzaazoua, M., Hakkou, R. & Mansori, M. 2017. Coal mine wastes recycling for coal recovery and eco-friendly bricks production. *Minerals Engineering*. 107:123–138.

Taylor, R.P. 2009. The uses of laboratory testing of biomass cookstoves and the shortcomings of the dominant U.S. protocol. Iowa State University.

Thomas, N. 2003. Energy. In: *Field Guide to Appropriate Technology*. Academic Press. pp. 157–275.

Thurston, G.D. 2022. Fossil fuel combustion and PM2.5 mass air pollution associations with mortality. *Environment International*. 160:107066.

Tillman, D.A. 2000. Biomass cofiring: the technology, the experience, the combustion consequences. *Biomass and Bioenergy*. 19(6):365–384.

Trubetskaya, A., Lin, C. & Ovadnevaite, J. 2021. Study of Emissions from Domestic Solid-Fuel Stove Combustion in Ireland. *Energy Fuels*. 35(6):4966–4978.

TSI. 2004. *Combustion Analysis Basics: An Overview of Measurements, Methods and Calculations Used in Combustion Analysis*.

Tumuluru, J.S., Sokhansanj, S., Hess, J.R. & Wright, C.T. 2011. A Review on Biomass Torrefaction Process and Product Properties for Energy Applications. *Industrial Biotechnology*. 7.

Verma, V.K., Bram, S., Delattin, F., Laha, P., Vandendael, I., … De Ruyck, J. 2012. Agro-pellets for domestic heating boilers: Standard laboratory and real life performance. *Applied Energy*. 90(1):17–23.

Vershinina, K., Strizhak, P., Dorokhov, V. & Romanov, D. 2021. Combustion and emission behavior of different waste fuel blends in a laboratory furnace. *Fuel*. 285:119098.

Vitoussia, T., Leyssens, G., Trouvé, G., Brillard, A., Kemajou, A., … Brilhac, J.F. 2020. Analysis of the combustion of pellets made with three Cameroonian biomass in a domestic pellet stove. *Fuel*. 276:118105.

Wagner, N.J. 2021. Geology of Coal. *Encyclopedia of Geology*. (January, 1):745–761.

Wagner, N.J. & Hlatshwayo, B. 2005. The occurrence of potentially hazardous trace elements in five Highveld coals, South Africa. *International Journal of Coal Geology*. 63(3–4):228–246.

Walker, S. 1999. *Uncontrolled fires in coal and coal wastes*. *U.S. Depertment of Energy*.

Wang, Y., Jia, L., Guo, B., Shen, X., Zheng, X., … Jin, Y. 2022. Investigation of interaction mechanisms during co-combustion of sewage sludge and coal slime: Combustion characteristics and NO/SO2 emission behavior. *Science of The Total Environment*. 851:158166.

WCA. 2021. *Coal facts*. https://www.worldcoal.org/coal-facts/.

WHO. 2021a. *WHO Air Quality Guidelines*. https://www.c40knowledgehub.org/s/article/WHO-Air-Quality-Guidelines?language=en_US#:~:text=By reducing air pollution levels,3 - 4 days per year.

WHO. 2021b. *Household air pollution and health*. https://www.who.int/news-room/fact-sheets/detail/household-air-pollution-and-health.

Winans, R.E. & Crelling, J.C. 1983. *Chemistry and characterization of coal macerals*. Washington DC.

Witt, P.J., Solnordal, C.B., Mittoni, L.J., Finn, S. & Pluta, J. 2006. Optimising the design of fume extraction hoods using a combination of engineering and CFD modelling. *Applied Mathematical Modelling*. 30(11):1167–1179.

World Bank. 2014. Clean Stove Initiative Forum Proceedings.

World Bank. 2015. *Overview of Carbon Offset Programs. PMR Technical Note 6, January 2015*. https://www.thepmr.org/system/files/documents/PMR Technical Note 6_Offsets_0.pdf.

Xiao, R. & Song, Q. 2011. Characterization and kinetics of reduction of CaSO4 with carbon monoxide for chemical-looping combustion. *Combustion and Flame*. 158(12):2524–2539.

Xu, M., Yu, D., Yao, H., Liu, X. & Qiao, Y. 2011. Coal combustion-generated aerosols: Formation and properties. *Proceedings of the Combustion Institute*. 33(1):1681–1697.

Yuan, Y., Zuo, H., Wang, J., Gao, Y., Xue, Q. & Wang, J. 2022. Co-combustion behavior, kinetic and ash melting characteristics analysis of clean coal and biomass pellet. *Fuel*. 324:124727.

Zaugg, S.D., Blackham, A.U., Hedman, P.O. & Smoot, L.D. 1989. Sulphur pollutant formation during coal combustion. *Fuel*. 68(3):346–353.

Zeng, F. 2009. Organic and inorganic geochemistry of coal. *Coal, Oil shale, Natural Bitumen, Heavy oil and Peat*. 1.

Zeng, G., Zhou, A., Fu, J. & Ji, Y. 2022. Experimental and numerical investigations on NOx formation and reduction mechanisms of pulverized-coal stereo-staged combustion. *Energy*. 261:125358.

Zhang, X., Li, Y., Wang, L., Zhang, Z. & Dong, Y. 2022. Inhibition of coal-fired condensable particulate matter by addition of biomass. *Fuel*. 310:122461.

Zhou, H., Long, Y., Meng, A., Li, Q. & Zhang, Y. 2013. The pyrolysis simulation of five biomass species by hemi-cellulose, cellulose and lignin based on thermogravimetric curves. *Thermochimica Acta*. 566:36–43.

Zhou, Y., Zi, T., Lang, J., Huang, D., Wei, P., … Cheng, S. 2020. Impact of rural residential coal combustion on air pollution in Shandong, China. *Chemosphere*. 260:127517.

ANNEXURES

APPENDIX A TORREFACTION PRE-TESTS

Thermogravimetric analysis (TGA) was conducted on the raw pine wood to determine the material's thermal degradation and preselect the torrefaction conditions. Non-isothermal torrefaction tests were performed on the pine sawdust in a controlled nitrogen environment.

From literature, torrefaction conditions are often chosen such that a mass loss of 30% to 35% is realised. This mass loss is usually where the hemicellulose breaks down (Kartal & Özveren, 2022; Prins et al., 2006; Zhou et al., 2013). The TGA data is used to investigate the temperature at which the hemicellulose breaks down, and the wood chips lose approximately 35% of their mass.

The residence time was determined by testing larger quantities of wood chips to account for the effect the particles might have on one another. A pyrolysis oven was used to study the effect of time on the mass loss at a constant temperature. The oven schematic and equipment list are displayed in **Figure A-1** and **Table A-1**, respectively.

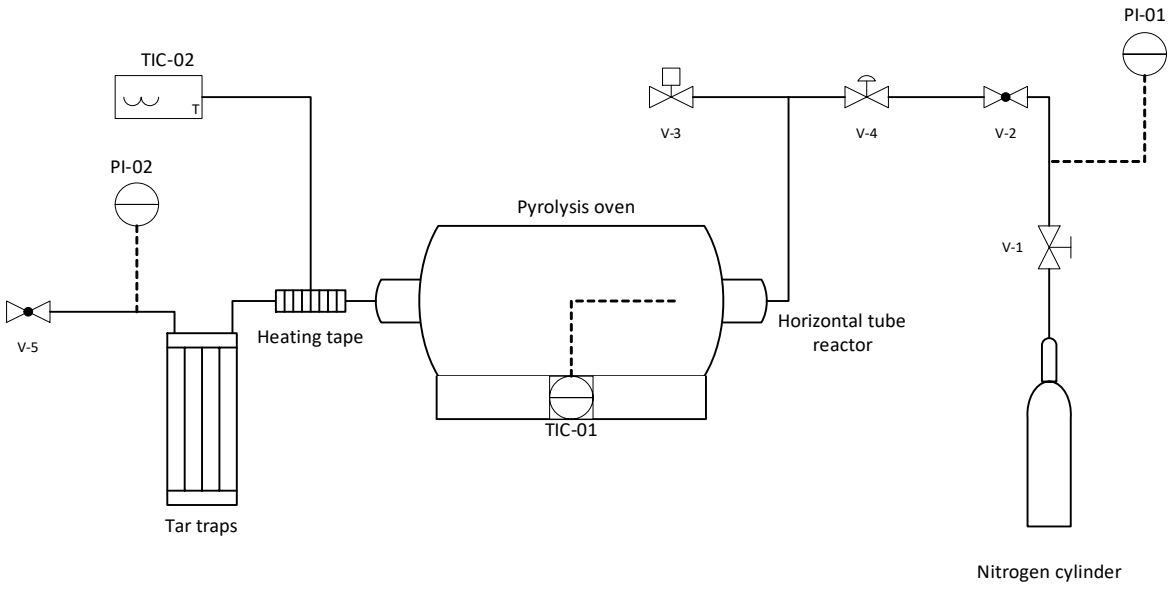

Figure A-1: Schematic of pyrolysis oven

Table A-1: Valve and instrument list of pyrolysis oven

Displayed Text	Description
V-1	Pressure regulator
V-2	Purge valve
V-3	Pressure release valve
V-4	Check valve
V-5	Purge valve
PI-01	Pressure indicator
PI-02	Pressure indicator
TIC-01	Temperature indicator and controller
TIC-02	Temperature indicator and controller

The torrefaction rig employed in the experiments aimed at determining the residence time for the torrefaction process. The oven temperature was maintained at 275 °C, a value established through TGA experiments, while the residence time was varied. Nitrogen was introduced into the oven to establish an inert atmosphere. A sample of wood chips weighing roughly 160 g was placed inside a porcelain sample holder and inserted into the oven. After the designated residence time, the sample was cooled and its mass recorded.

Torrefaction pre-test results

The derived mass loss from the TGA experiments is displayed in **Figure A-2**.

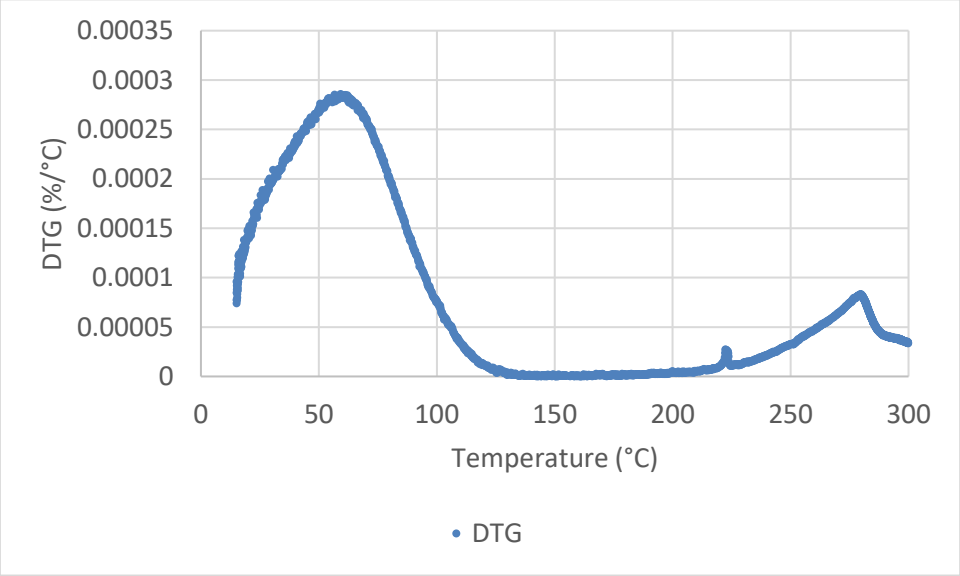

Figure A-2: DTG analysis of raw pine sawdust

Thermogravimetric analysis was performed on the raw pine sawdust, and the resulting mass loss, expressed as percentage loss per degree Celsius (%/°C), was recorded. **Figure A-3** shows a peak at approximately 275 °C, indicating a sufficient breakdown of hemicellulose and devolatilization.

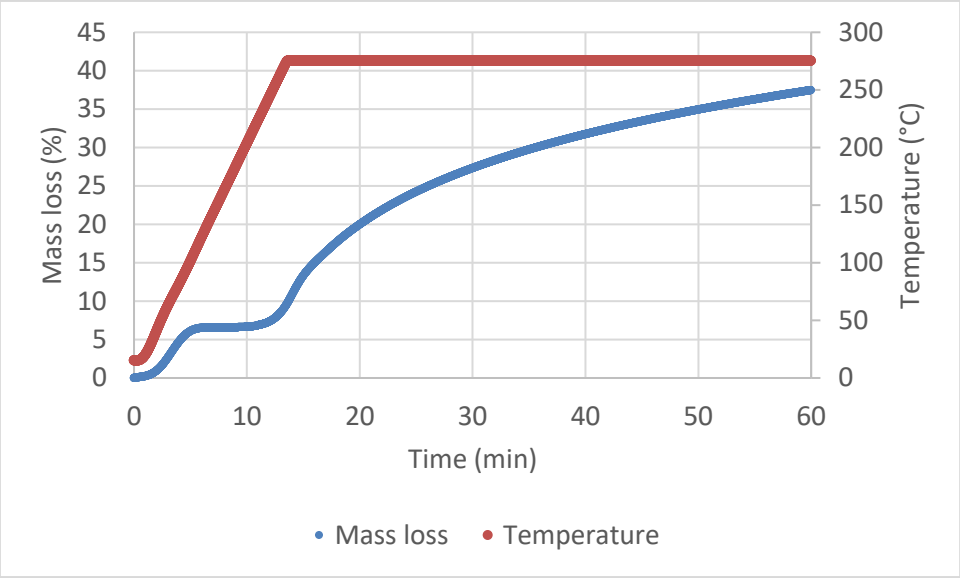

Figure A-3: Mass loss of raw pine sawdust during TGA

Consequently, the torrefaction operating temperature was set at 275 °C to ensure a mass loss of approximately 35%. Zhou et al., (2013) conducted thermogravimetric analysis on hemicellulose and reported that peak breakdown occurred at 274 °C.

Table A-2 displays the total mass reduction observed after torrefaction at specific residence times.

Table A-2: Residence time and mass loss correlation

Residence time (min)	Final mass loss (%)
30	26.7
45	31.3
60	35.5
75	36.1

The experiments demonstrated that a 60-minute residence period was ample for achieving full torrefaction. Consequently, based on these findings, the bulk torrefaction process was standardized to a 60-minute residence time.

APPENDIX B PELLETISATION PRE-TESTS

Various lab-scale techniques were employed to produce pellets from the coal-biomass blends. This endeavour aimed to assess and determine the most suitable method for large-scale pellet production.

The agglomeration method involves a rotating drum set to a specific RPM and angle. Water is incrementally added to the blends until the moisture content reaches approximately 10%. The fine particles from each blend are introduced into the drum, where centrifugal forces, coupled with gravity, promote the agglomeration of particles into spherical pellets. The angle and rotational speed of the drum are adjusted to control pellet size.

The 100% coal blend pelletisation was successful with the drum pelletisation technique. However, it was observed that this technique was incompatible with the blends containing biomass. The dissimilarity in the physical properties of coal and torrefied wood led to an unfavourable outcome; only the coal particles successfully agglomerated within the drum, while the torrefied wood particles remained unagglomerated. This outcome compromised the intended biomass-to-coal ratio within the resulting pellets, deviating from the desired composition.

Table B-1 shows the compressive strength of coal pellets produced via drum pelletisation and extrusion.

Table B-1: Compressive strength of drum coal pellets and coal extrudates

Method	Compressive strength (MPa)
Drum pellets	6.9 ± 0.8
Extrudates	12.8 ± 0.9

The extrudates show higher compressive strength compared to the drum pellets. This difference is due to extrusion using compression to produce pellets, whereas drum pelletisation relies on the agglomerative ability of the material.

APPENDIX C CARBON BALANCE

The following carbon and mass balance is conducted on the 0% biomass, high-power combustion experiment. **Figure C-1** shows the mass loss detected by the scale over time ($\frac{dm_{a.f}}{dt}$).

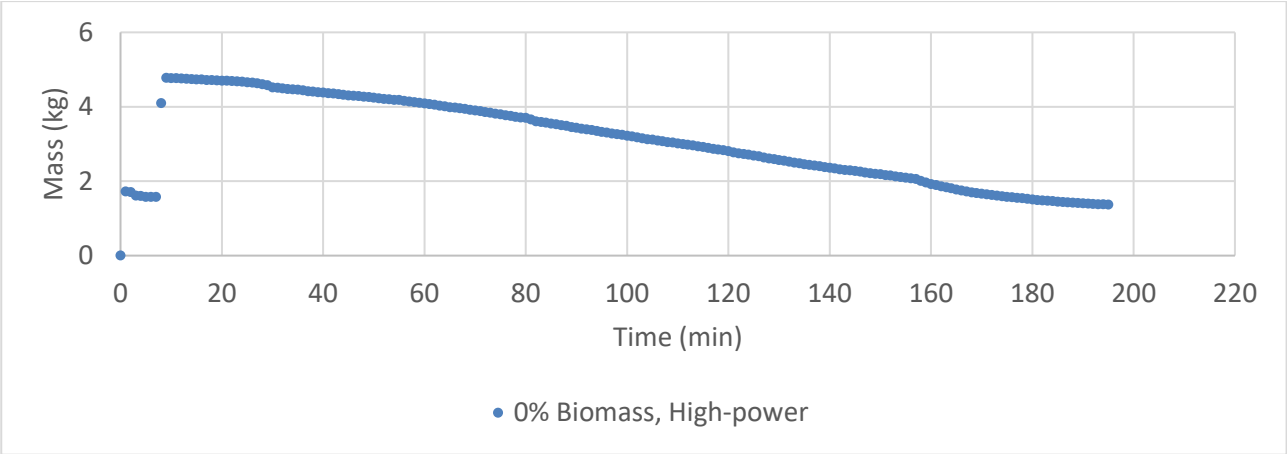

Figure C-1: dm/dt raw data

The mass loss detected on an ash-free basis is retrieved from the scale recordings as raw data. The detected mass loss and fuel composition are then used to determine the carbon consumption rate ($\frac{dm_C}{dt}$) in fuel due to combustion using Equation 4-12. **Figure C-2** shows the mass rate of carbon oxidising due to combustion.

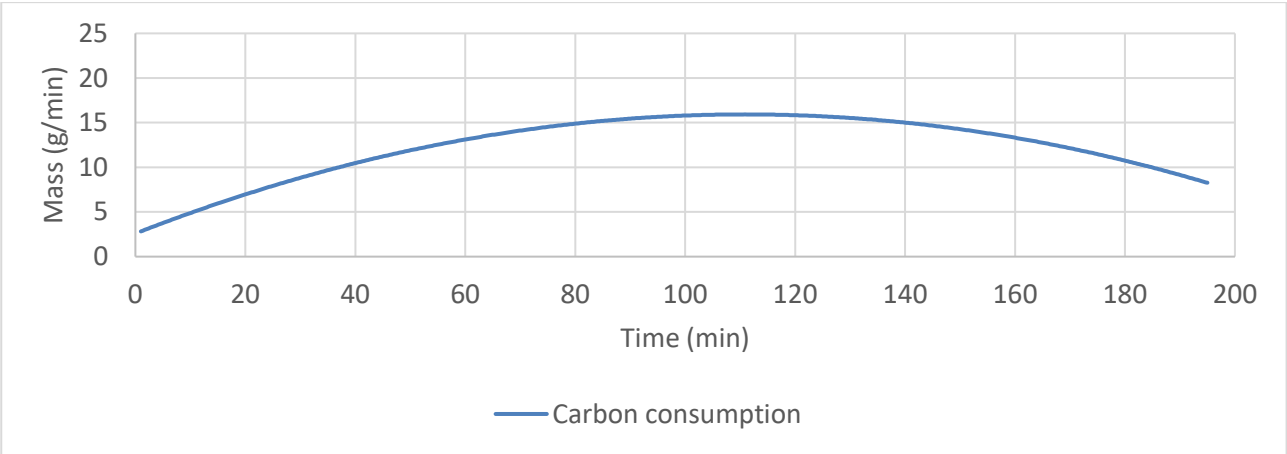

Figure C-2: Mass carbon consumption rate of fuel

The mass consumption of the carbon is then converted to mole flowrate of carbon ($\frac{dn_C}{dt}$) using Equation 4-13. **Figure C-3** shows the mol rate of carbon oxidising due to combustion.

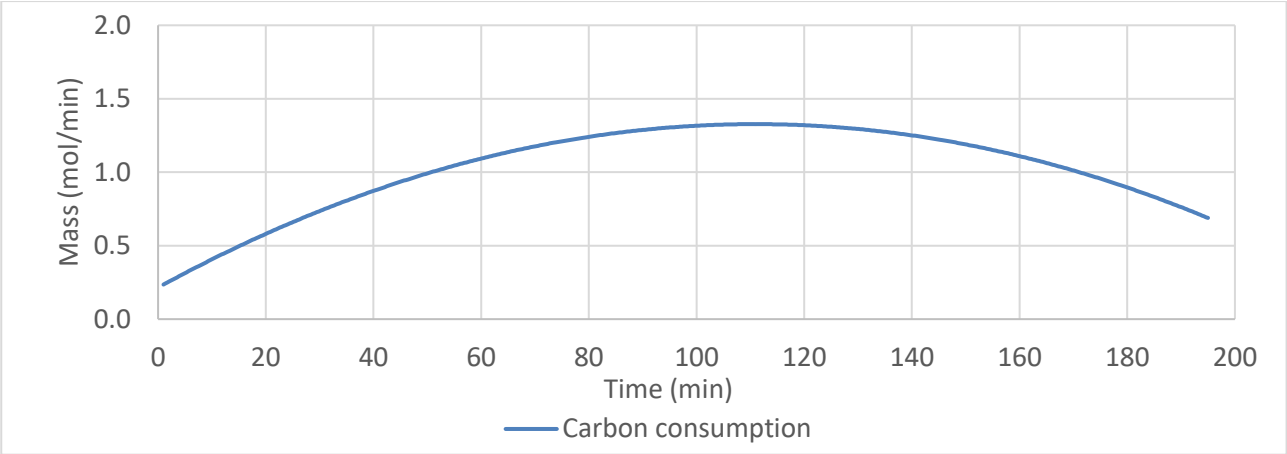

Figure C-3: Mol carbon consumption rate of fuel

Assuming that the carbon consumed in combustion only converts to CO_2 and CO and that the carbon in the fuel is the only source, then the molar flow rate of the flue gas ($\frac{dn_{fg}}{dt}$) is determined using Equation 4-14. **Figure C-4** shows the molar flow rate of the flue gas.

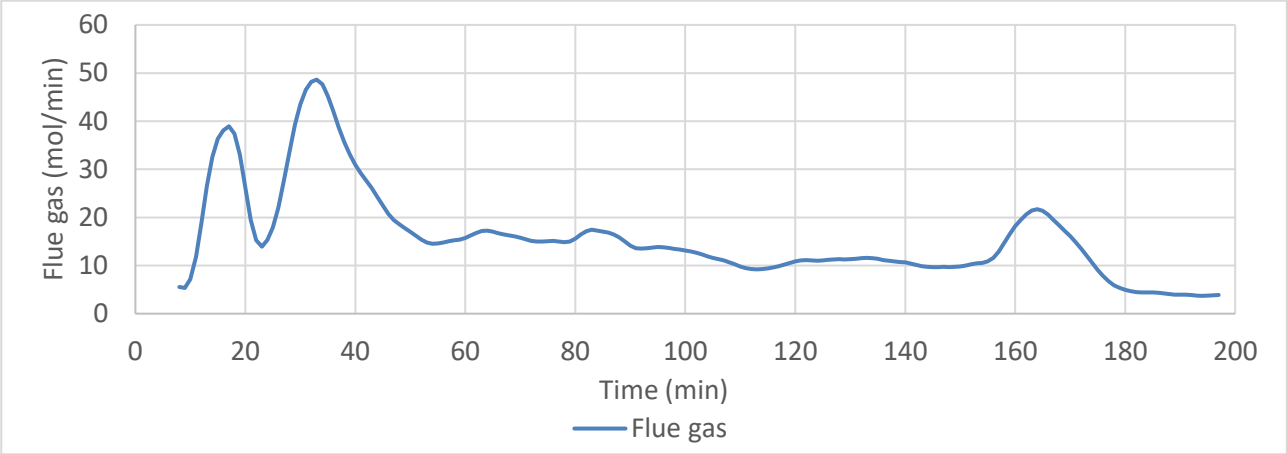

Figure C-4: Mol flow rate of flue gas

The molar flow rate of the flue gas is then used to determine the molar flow rates of the pollutants using Equation 4-15.

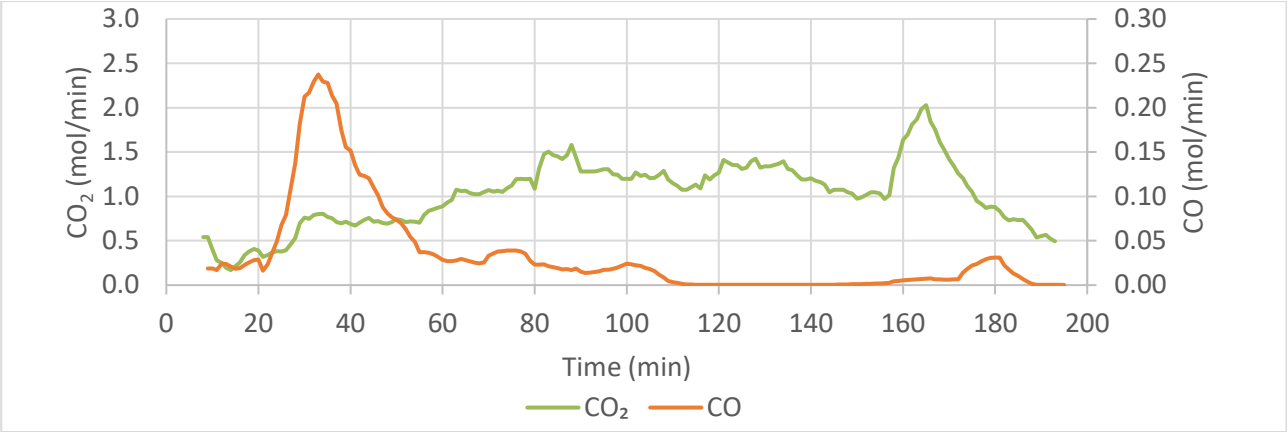

Figure C-5 displays the molar flow rates of CO_2, CO, NO_x, and SO_2 in the flue gas.

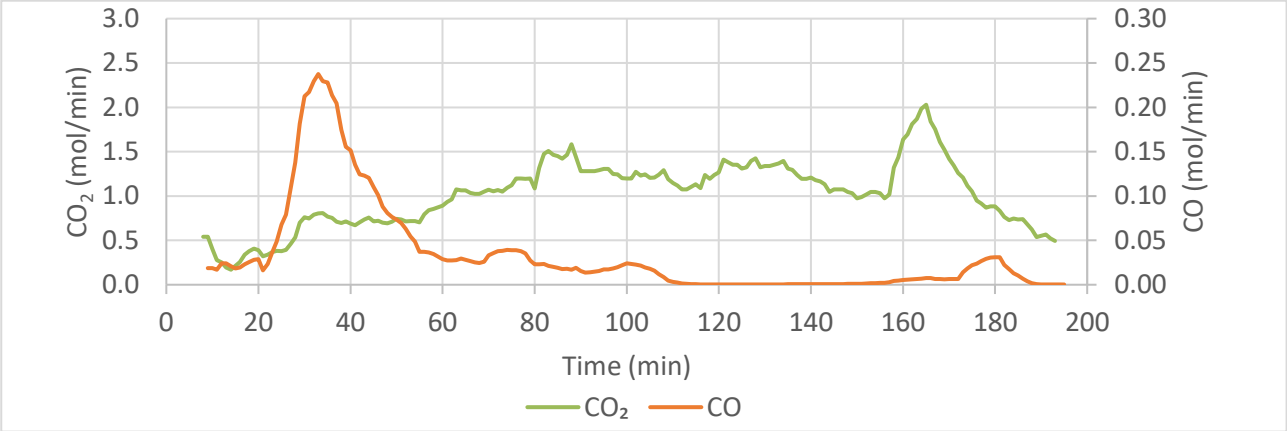

Figure C-5: Molar flow rates of CO_2, CO, NO_x, and SO_2 in flue gas

Integrating over the CO and CO_2 curves results in the total mole CO and CO_2 detected in the flue gas throughout the entire experiment. The total mole carbon in the flue gas during this period can be determined using stoichiometry. The mole carbon is converted to mass using Equation 4-16. The unreacted carbon in the ash is quantified in Appendix E: **Table E-2**. The carbon recovery is determined by Equation C-1:

$$\%Recovery = \frac{m_{C,flue} + m_{C,ash}}{m_{C,fuel}} \cdot 100 \quad \text{(C-1)}$$

Where $\boldsymbol{m_{C,flue}}$ is the mass of carbon detected in the flue gas, $\boldsymbol{m_{C,ash}}$ is the mass carbon in the ash post-combustion, and $\boldsymbol{m_{C,fuel}}$ is the mass of carbon in the fuel. **Table C-1** shows the carbon balance over the fuel, ash, and flue gas of the combustion experiments of all pellet blends.

Table C-1: Carbon balance over the fuel, ash, and flue gas example

Mass Carbon Observed (g)				
% Biomass	Fuel	Ash	Flue gas	%Recovery
High-power				

0	2409	11.7	2564	107
10	2372	3.4	2341	99
25	2431	0.9	2494	103
50	2405	0.6	2518	105
75	2226	0.5	2310	104
90	1576	0.4	1520	96
Low-power				
0	2382	11.9	2466	104
10	2532	3.5	2313	91
25	2284	1.0	2296	101
50	2268	0.6	2283	101
75	2080	0.5	2013	97
90	1434	0.4	1389	97

APPENDIX D MASS BALANCE

Table D-1 summarises the mass balance conducted in the combustion experiments. The carbon, sulphur, and nitrogen detected in CO2, CO, SO2, and NO_x are displayed.

Table D-1: Mass balance recovery through flue

	% Recovery		
% Biomass	C	S	N
High-power			
0	107	24	8
10	99	23	8
25	103	23	10
50	105	27	11
75	104	96	9
90	96	89	9
Low-power			
0	104	25	6
10	91	18	8
25	101	23	8
50	101	24	8
75	97	44	7
90	97	85	10

APPENDIX E ASH BEHAVIOUR

Figure E-1 shows the ash tray after the high-power combustion experiment using 0% (a), 25% (b), and 75% (c) biomass pellets.

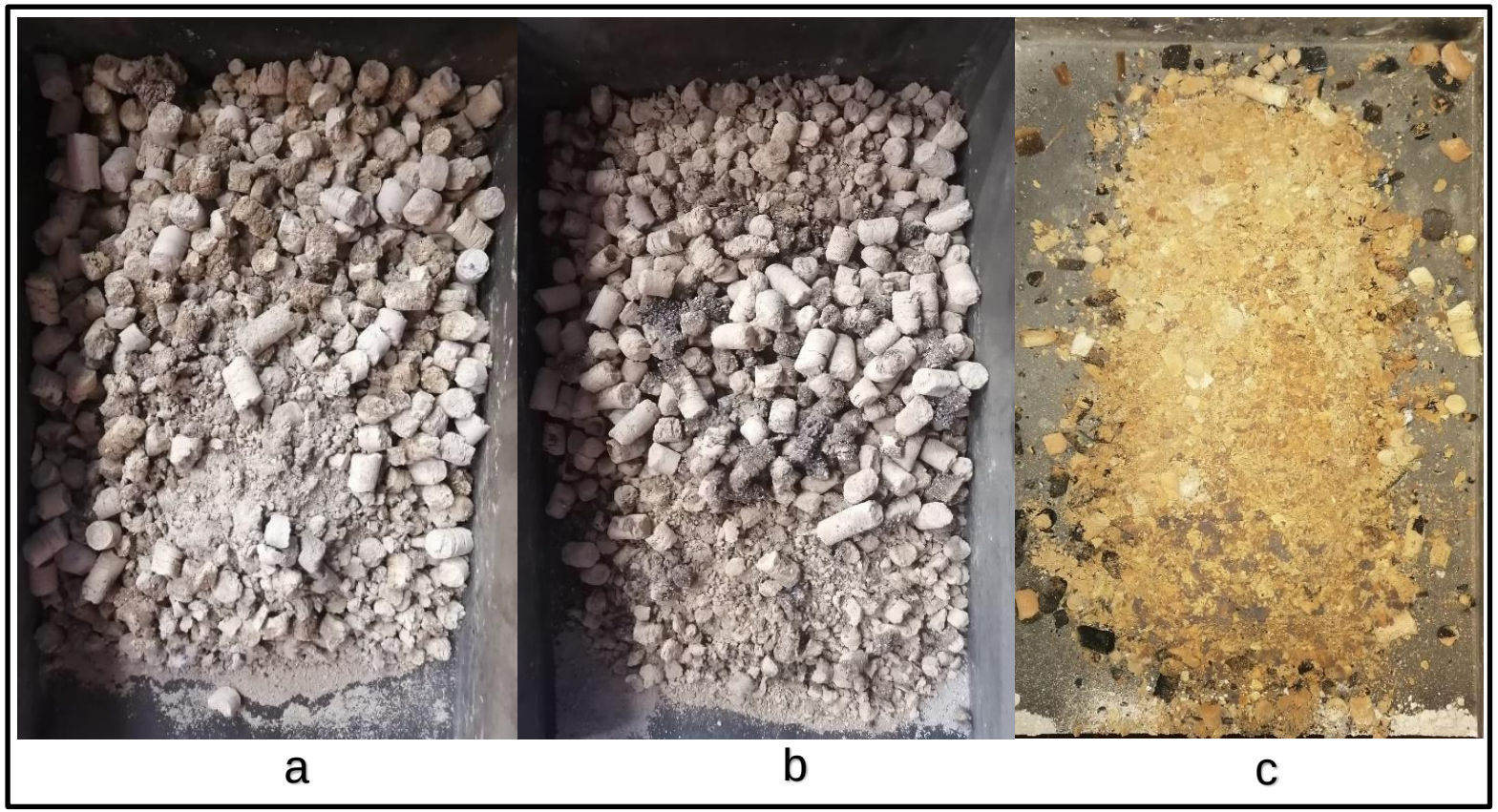

Figure E-1: Ash tray after high-power combustion experiments using 0%, 25%, and 75% biomass pellets

The 0% biomass to 50% pellets maintain their pellet form after combustion, as the ash appears to have agglomerative characteristics. The ash's tendency to agglomerate inhibits the production of fly ash, producing less fly ash production. The 90% biomass pellets disintegrated during combustion. The ash of these pellets displayed no resemblance to their original pellet form. Following the combustion of the 90% biomass pellets, the ashtray contained wood chips that were used as fire starters.

Table E-1 shows the proximate analysis results on the ash post-combustion of the pellets on a dry-basis.

Table E-1: Proximate analysis of pellet ash post-combustion (d.b)

% Biomass	0	10	25	50	75	90
Volatile matter	1.6	2.1	1.9	2.9	3	3.3
Ash yield	90.0	95.3	97.2	96.2	95.6	93.8
Fixed carbon	8.4	2.7	1.0	0.9	1.4	2.9

The volatile matter in the ash increases with pellets containing increased biomass. The fixed carbon in the ash initially decreases with the addition of biomass and increases with pellets containing high biomass content. The unreacted carbon in the ash is determined with the proximate analysis of the ash in **Table E-1** with Equation E-1:

$$m_{ash} = \frac{m_f \cdot x_{ash.f}}{x_{ash.a}} \quad \text{(E-1)}$$

Equation E-1 determines the ash mass in the tray after each combustion experiment using the ash yield of the pellets (refer to **Table 3-15**) and the ash yield of the ash samples collected post-combustion (**Table E-1**). This method accounts for the ash lost due to fly ash generation and avoids detecting other materials in the ashtray, like wood chips used as fire starters. The carbon in the volatile matter is assumed to be negligible in small quantities, as seen in the ash's proximate analysis.

Table E-2 shows the mass unreacted carbon in the post-combustion ash for all pellet blends.

Table E-2: Mass unreacted carbon in post-combustion ash for each pellet blend

Mass unreacted carbon in ash (g)						
% Biomass	0	10	25	50	75	90
High-power	11.7	3.4	0.9	0.6	0.5	0.4
Low-power	11.9	3.5	1.0	0.6	0.5	0.4

APPENDIX F EXPERIMENTAL UNCERTAINTY

To determine the experimental repeatability, experiments were repeated at the same operating conditions.

Fuel Consumption

Figure F-1 and **Figure F-2** display the fuel consumption of 10% biomass pellets at high-power and low-power with their respective repeats.

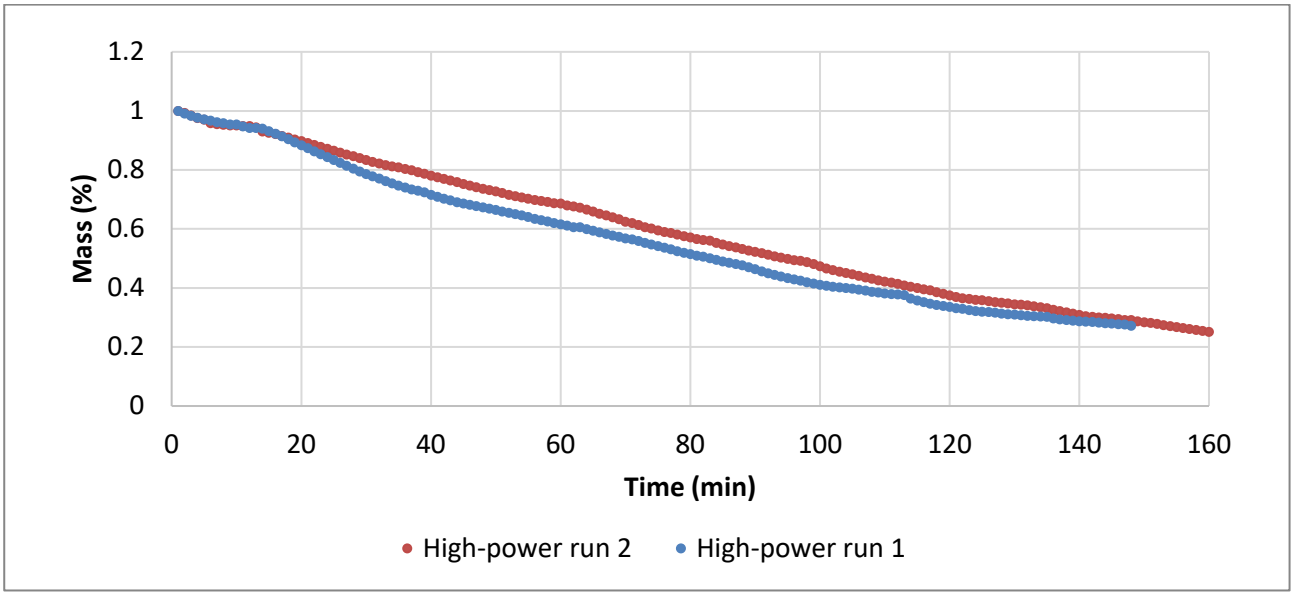

Figure F-1: Fuel consumption of 10% biomass pellets as a function of time at high-power

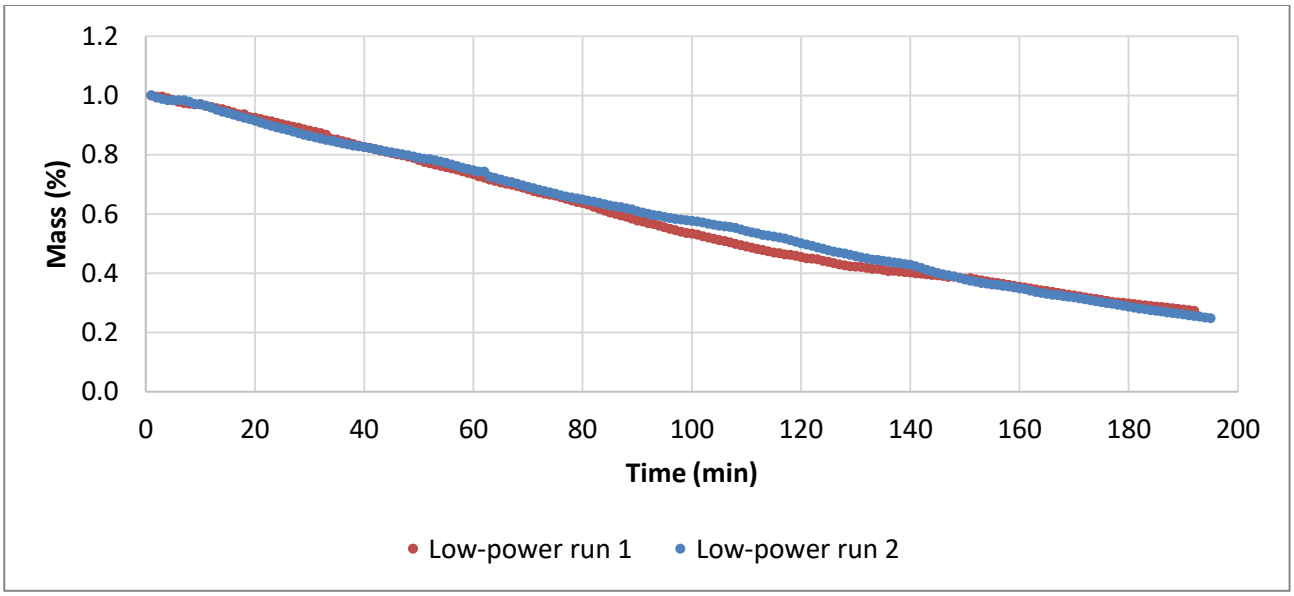

Figure F-2: Fuel consumption of 10% biomass pellets as a function of time at low-power

The mean mass loss recorded during the high-power experiments using 10% biomass pellets was 0.51 %/min and 0.48 %/min (ash-free), respectively. This translates to a mean fuel consumption rate of 32 g/min and 30 g/min. The two experiments show a 0.03 %/min difference in mass loss and a 2 g/min difference in fuel consumption rate. The deviation for these two experiments is 6.5%. The mean mass loss recorded during the low-power experiments using 10% biomass pellets was 0.38 %/min and 0.40 %/min (ash-free), respectively. This translates to a fuel consumption rate of 23 g/min and 25 g/min. The two experiments show a 0.02 %/min difference in mean mass loss and a 2 g/min difference in fuel consumption. The deviation for these two experiments is then 8.3%.

Stove temperature

Figure F-3 displays the fuel bed temperature (T-07) during the high-power experiments using 0% biomass pellets.

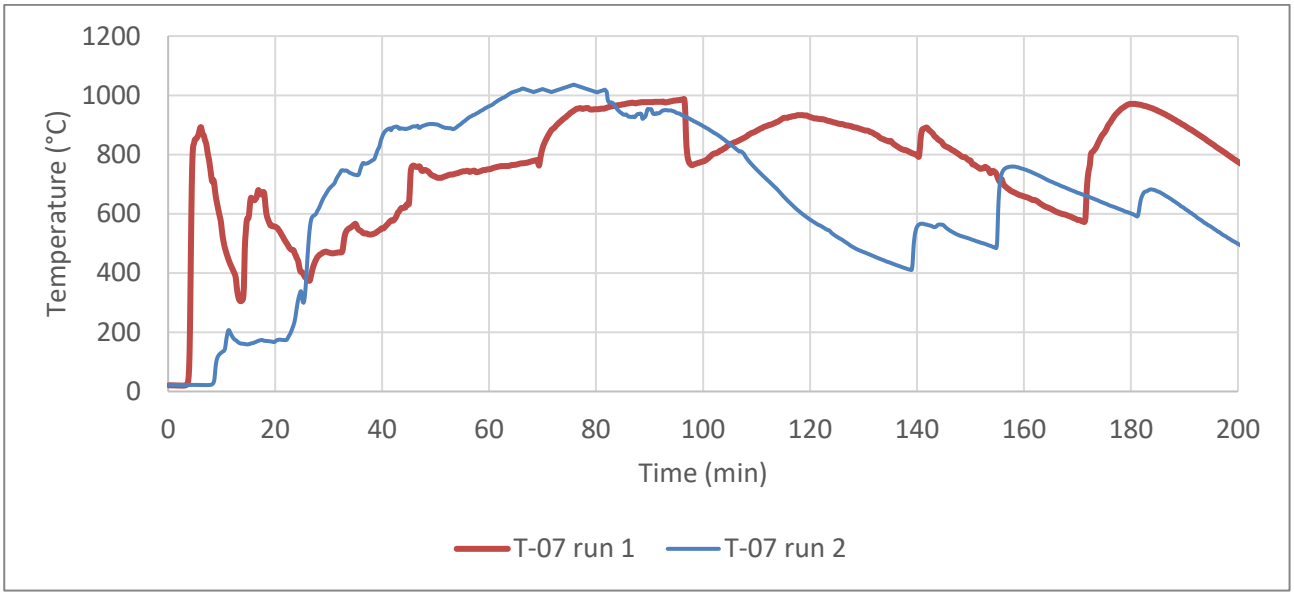

Figure F-3: Fuel bed temperature of high-power experiment using 0% biomass pellets.

The temperatures of the two experiments show similar trends. The first grate-shake of run 2 was done during the second grate-shake of run 1 and, therefore, shows a larger temperature drop between 100 minutes and 140 minutes. Furthermore, the temperature spikes due to the grate-shake procedure are similar. Run 1 displayed a peak temperature of 987 °C, and run 2 displayed a peak temperature of 1032 °C. The deviation between the peak temperature of the two experiments is 4.5%. This comparison, excluding the peak temperature, is used qualitatively and, therefore, does not have a deviation.

Ignition times

Table F-1 shows the ignition times of the repeat experiments for 0%, 10%, 75%, and 90% biomass pellets.

Table F-1: Ignition times of repeated experiments

		Ignition Time (min:sec)			
% Biomass	Run	0	10	75	90
High-power	1	36:20	24:10	06:20	03:50
	2	34:10	22:50	06:50	04:30
	Deviation	6.1%	5.7%	7.6%	16%
Low-power	1	47:30	38:30	-	-
	2	50:10	40:30	-	-
	Deviation	5.5%	5.1%	-	-

The 90% biomass pellets displayed the largest difference deviation. This can be attributed to the highly volatile nature of the pellets. Outside factors can easily influence the ignition time, significantly affecting the ignition time.

Power output

Figure F-4 displays the power output of the high-power combustion experiments using 0% biomass pellets as a function of the mass fuel used (ash-free).

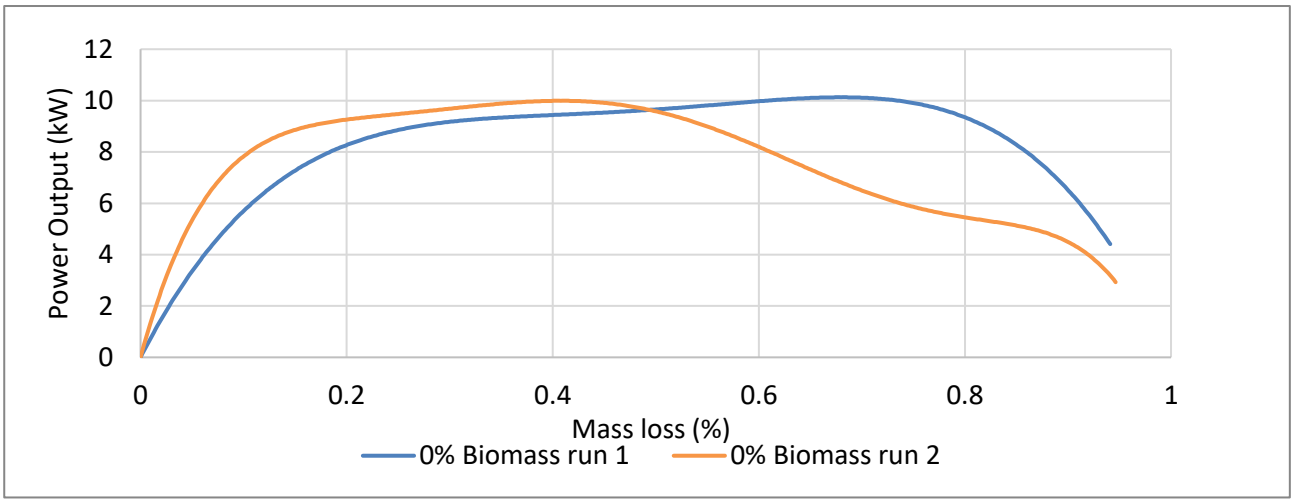

Figure F-4: Power output of 0% biomass pellets over mass loss (a.f.b)

The experiments show similar power output throughout the experiment until 50% of the fuel has been consumed. Run 2 exhibits a steady decrease in power output. This corresponds with the drop in temperature seen in the combustion chamber of run 2. This drop in power output was due to the

grate-shake procedure not being administered on time. This comparison is used qualitatively and does not have a value for a deviation.

Water boiling test

Table F-2 shows the water boiling times for the repeat experiments and their deviation.

Table F-2: Water boiling test times of repeated experiments

		Boiling time		
% Biomass	Run	0	10	50
High-power	1	11	8	6
	2	13	8	6
	Deviation	16.7%	0%	0%
Low-power	1	17	14	-
	2	20	11	-
	Deviation	16.2%	24%	-

The boiling times for the water boiling test show increased deviations for longer boiling times and decreased deviations for shorter boiling times.

Emission factors

Table F-3 shows the deviation determined for CO_2 emission factors from various pellet blends.

Table F-3: Deviation of CO_2 emission factors

% Biomass		0	10	25	50
		High-power			
EF (g/MJ)	1	97	90	89	90
	2	95	88	91	92
	Deviation	2%	2%	2%	2%
		Low-Power			
EF (g/MJ)	1	95	90	-	-
	2	92	84	-	-
	Deviation	3%	7%	-	-

Table F-4 shows the deviation determined for CO emission factors from various pellet blends.

Table F-4: Deviation of CO emission factors

% Biomass		0	10	25	50
		High-power			
EF (g/MJ)	1	1.41	0.90	0.87	0.77
	2	1.24	1.11	0.73	0.94
	Deviation	13%	20%	18%	17%
		Low-Power			
EF (g/MJ)	1	2.05	0.57	-	-
	2	2.26	0.72	-	-
	Deviation	10%	23%	-	-

The deviation for CO is relatively high and inconsistent. This is due to the various factors that influence the combustion efficiency of the stove. The main contributing factor is the form of the pellets. The fuel bed differs for each combustion experiment, causing the airflow between the pellets to differ. This has a significant influence on the production of CO throughout the experiment.

Table F-5 shows the deviation for SO_2 emission factors from various pellet blends.

Table F-5: Deviation of SO_2 emission factors

% Biomass		0	10	25	50
		High-power			
EF (g/MJ)	1	0.22	0.18	0.14	0.11
	2	0.20	0.20	0.15	0.12
	Deviation	9%	10%	7%	9%
		Low-Power			
EF (g/MJ)	1	0.21	0.15	-	-
	2	0.22	0.18	-	-
	Deviation	5%	18%	-	-

Table F-6 shows the deviation for NO_x emission factors from various pellet blends.

Table F-6: Deviation of NO_x emission factors

% Biomass		0	10	25	50
		High-power			
EF (g/MJ)	1	0.10	0.11	0.10	0.11
	2	0.11	0.09	0.10	0.08
	Deviation	9%	20%	0%	31%
		Low-Power			
EF (g/MJ)	1	0.09	0.10	-	-
	2	0.10	0.08	-	-
	Deviation	9%	20%	-	-

Table F-7 shows the deviation for PM emission factors from various pellet blends.

Table F-7: Deviation of PM emission factors

% Biomass		0	10	25	50
		High-power			
EF (g/MJ)	1	0.06	0.04	0.05	0.48
	2	0.07	0.09	0.07	0.40
	Deviation	15%	77%	33%	18%
		Low-Power			
EF (g/MJ)	1	0.08	0.18	-	-
	2	0.10	0.23	-	-
	Deviation	22%	24%	-	-

The deviations for the SO_2 and NO_x emission factors are high due to the emission factors being relatively small. Equipment accuracy becomes a contributing factor when readings are low.

APPENDIX G CALIBRATION CURVES

Table G-1 shows the calibration data of two consecutive experiments.

Table G-1: Calibration data of two consecutive experiments

Run	NOx	SO2	CO	CO2	O2
Span Calibration					
1	1.0743	1.1762	1.1412	1.0095	0.9878
2	1.0615	1.2066	1.1496	1.0062	0.9881
Zero Calibration					
1	1	1	0	5	4
2	1	0	0	4	3

The calibration data only differs slightly after experimenting.

APPENDIX H COMBUSTION EXPERIMENT TEMPERATURE DATA

Combustion chamber temperatures

Figure H-1 and **Figure H-2** show the combustion chamber temperature of the high-power and low-power experiments using 0% biomass pellets.

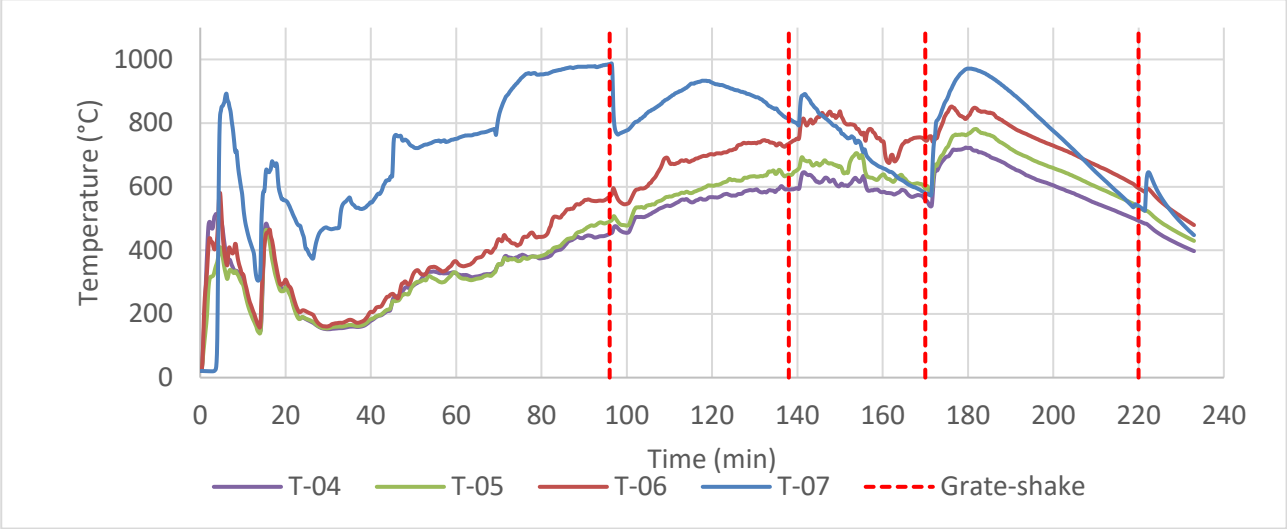

Figure H-1: Combustion chamber temperatures (0% biomass, high-power experiment)

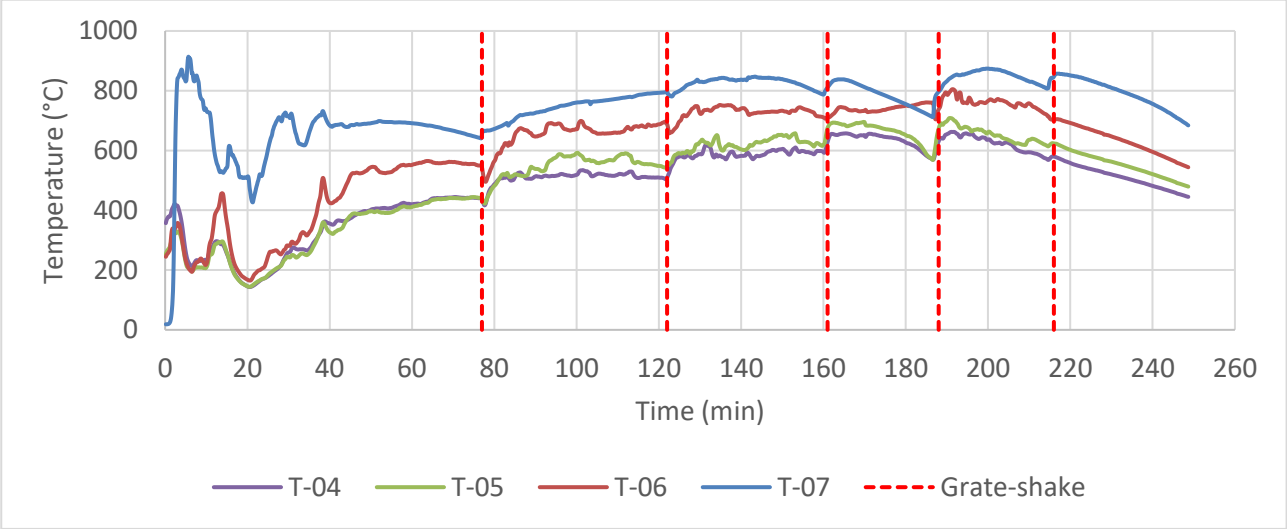

Figure H-2: Combustion chamber temperatures (0% biomass, Low-power experiment)

Figure H-3 and **Figure H-4** show the combustion chamber temperature of the high-power and low-power experiments using 10% biomass pellets.

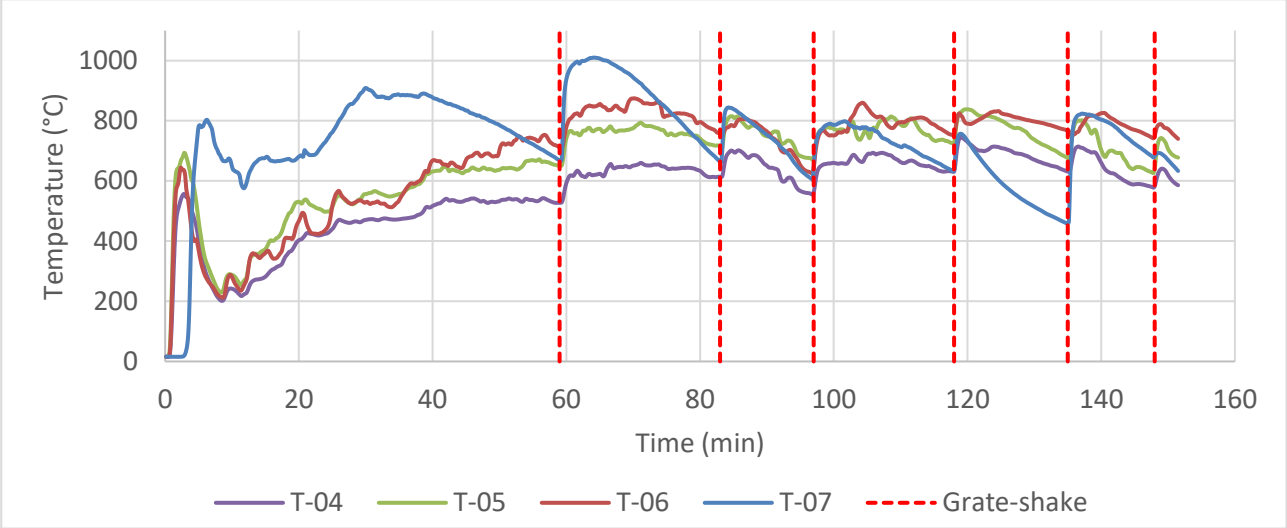

Figure H-3: Combustion chamber temperatures (10% biomass, high-power experiment)

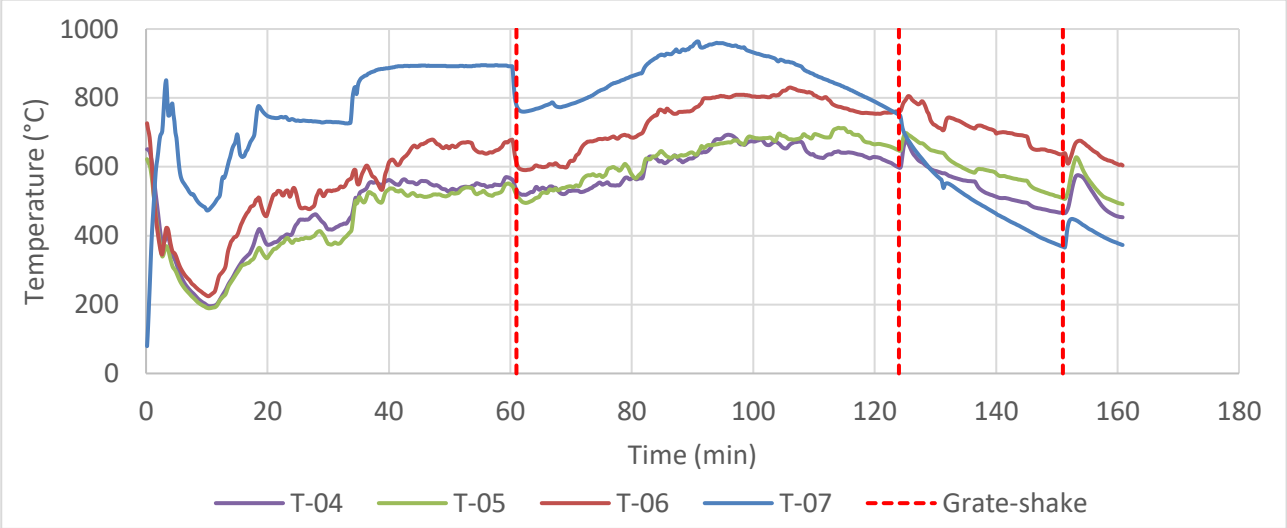

Figure H-4: Combustion chamber temperatures (10% biomass, low-power experiment)

Figure H-5 and **Figure H-6** show the combustion chamber temperature of the high-power and low-power experiments using 25% biomass pellets.

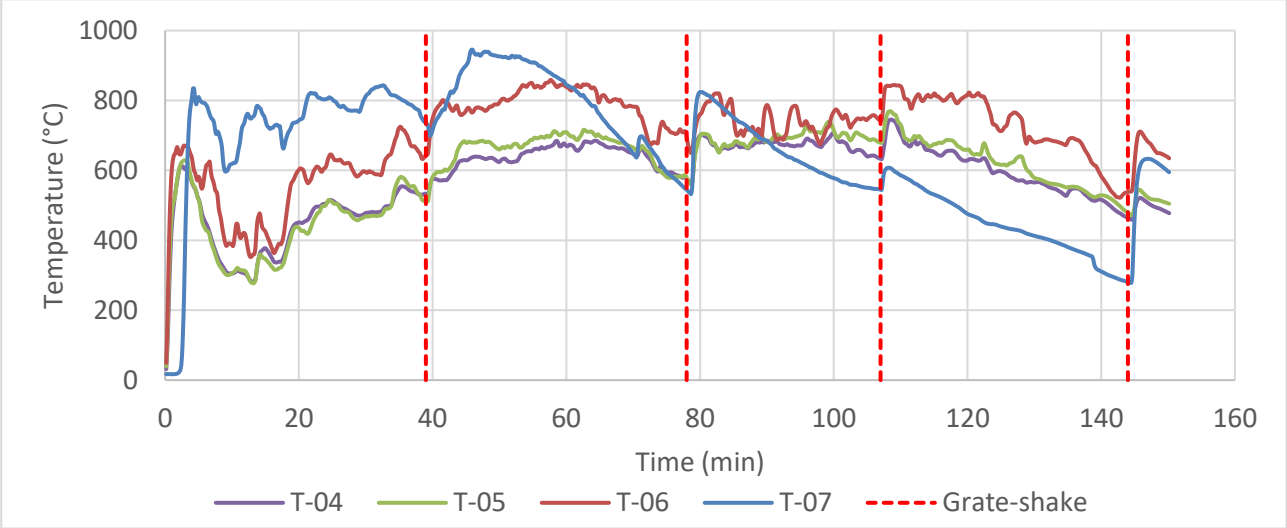

Figure H-5: Combustion chamber temperatures (25% biomass, high-power experiment)

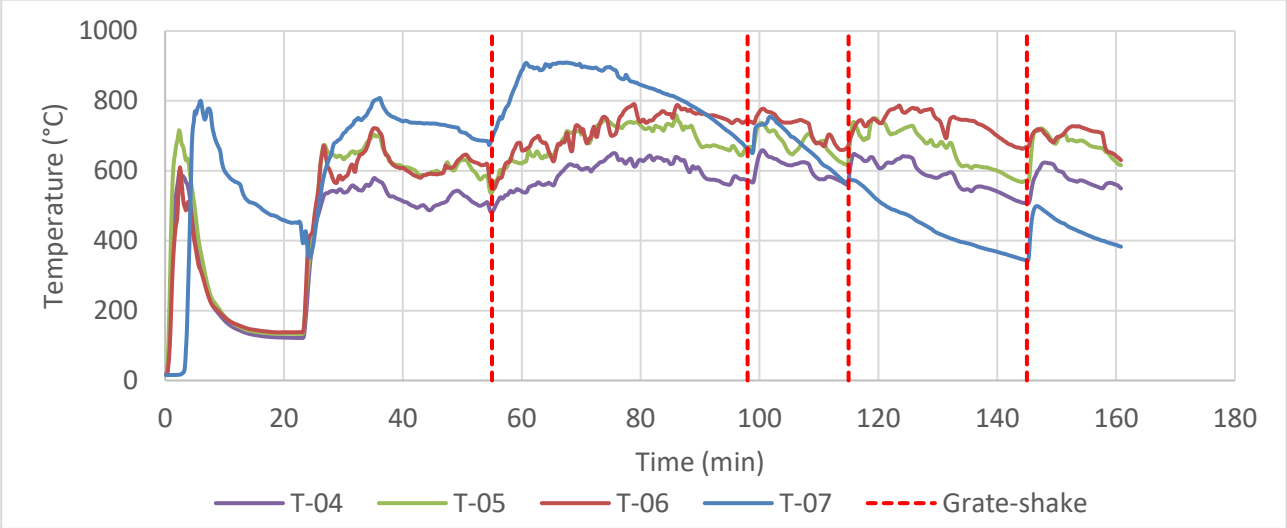

Figure H-6: Combustion chamber temperatures (25% biomass, low-power experiment)

Figure H-7 and **Figure H-8** show the combustion chamber temperature of the high-power and low-power experiments using 50% biomass pellets.

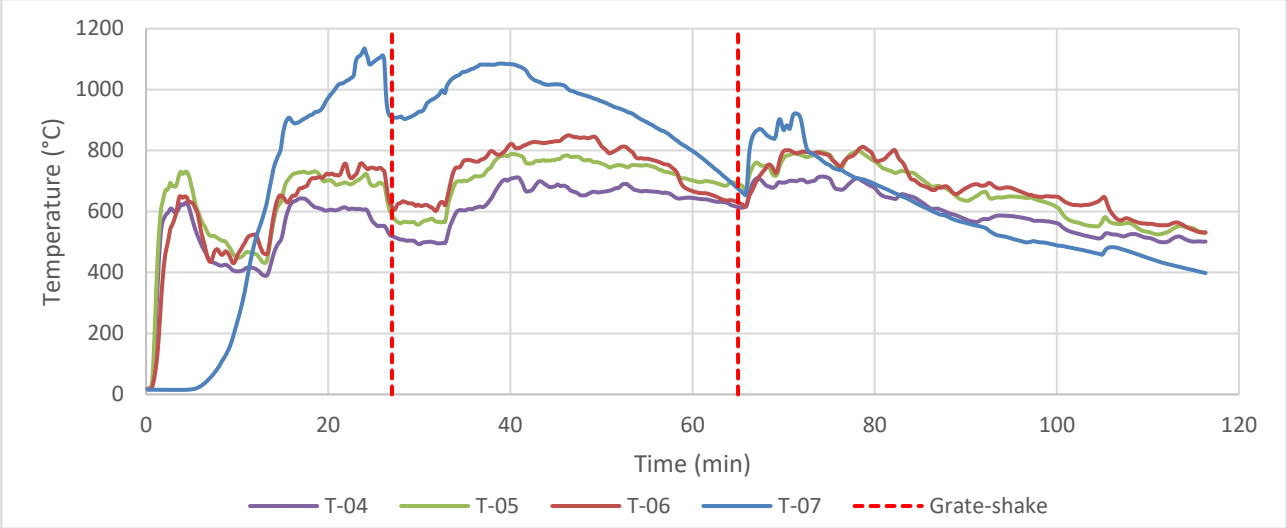

Figure H-7: Combustion chamber temperatures (50% biomass, high-power experiment)

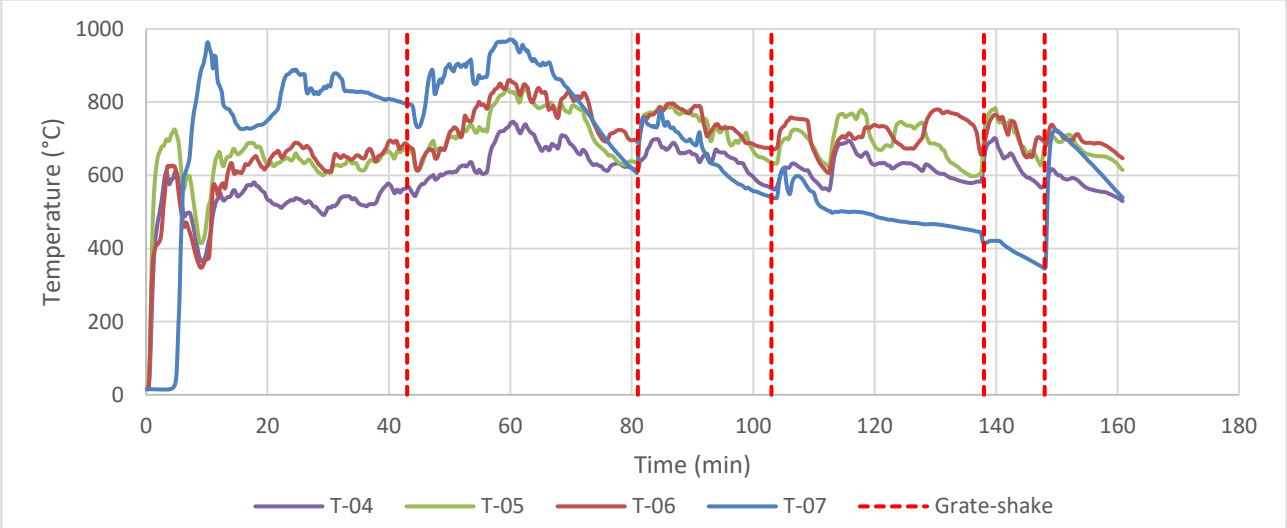

Figure H-8: Combustion chamber temperatures (50% biomass, low-power experiment)

Figure H-9 and **Figure H-10** show the combustion chamber temperature of the high-power and low-power experiments using 75% biomass pellets.

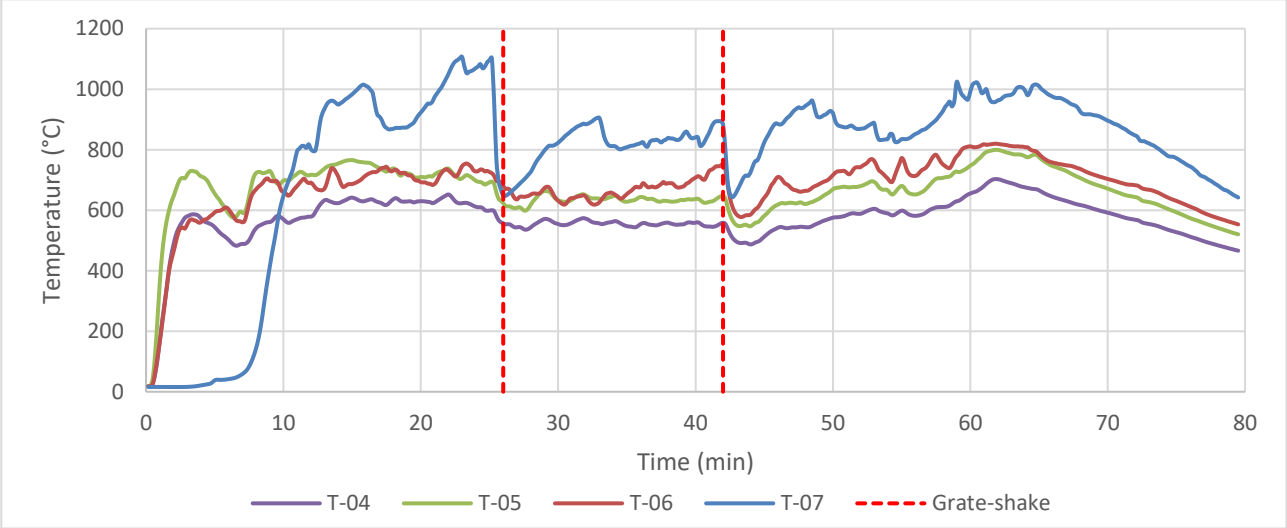

Figure H-9: Combustion chamber temperatures (75% biomass, high-power experiment)

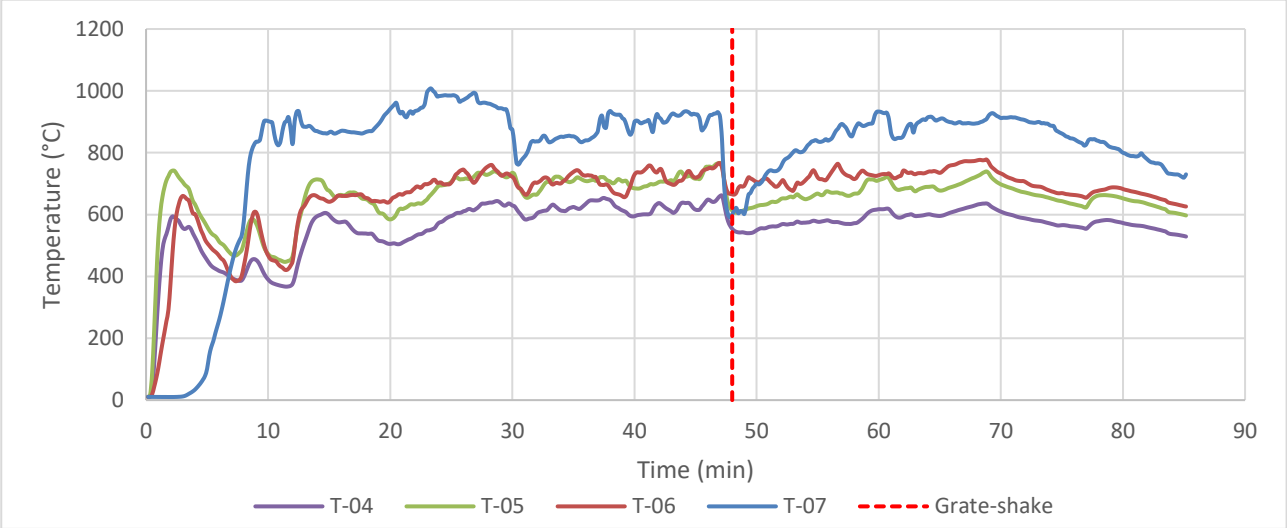

Figure H-10: Combustion chamber temperatures (75% biomass, low-power experiment)

Figure H-11 and **Figure H-12** show the combustion chamber temperature of the high-power and low-power experiments using 90% biomass pellets.

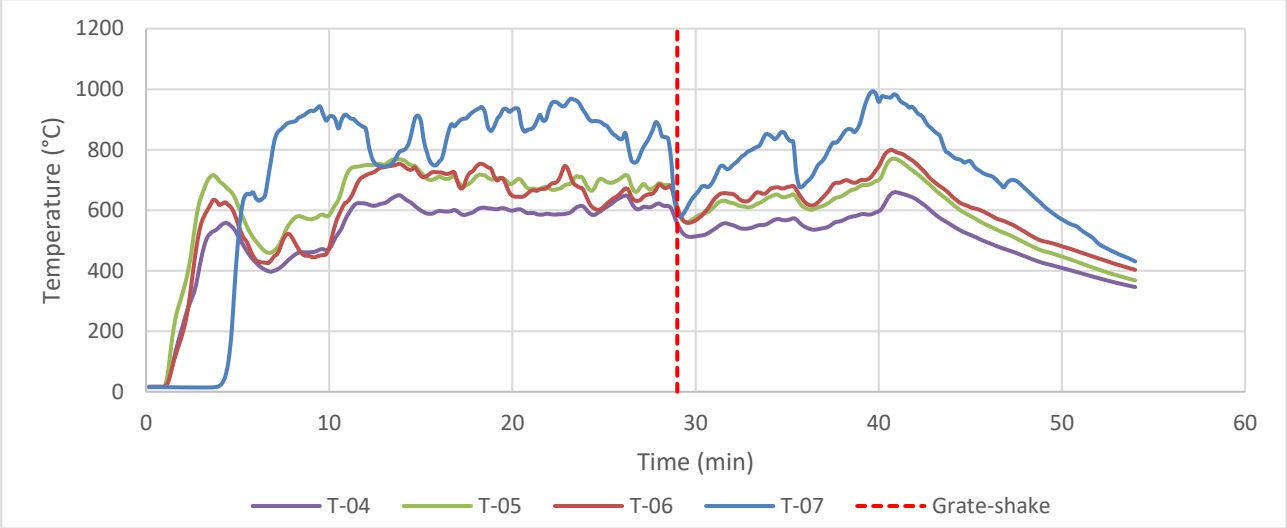

Figure H-11: Combustion chamber temperatures (90% biomass, high-power experiment)

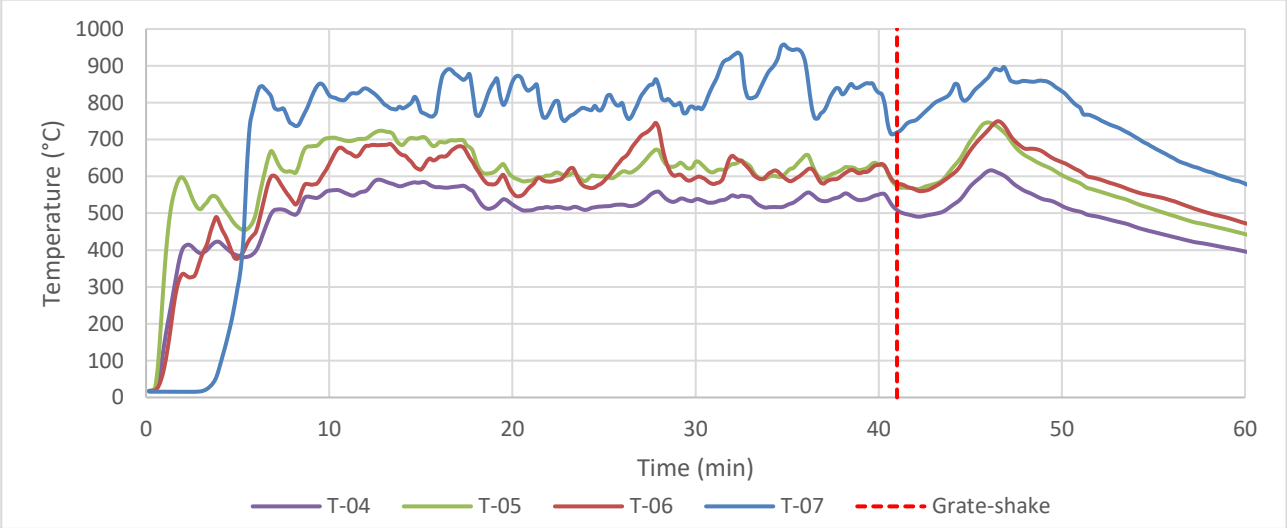

Figure H-12: Combustion chamber temperatures (90% biomass, low-power experiment)

Hopper temperatures

Figure H-13 and **Figure H-14** show the hopper temperatures for the high-power and low-power experiments using 0% biomass pellets.

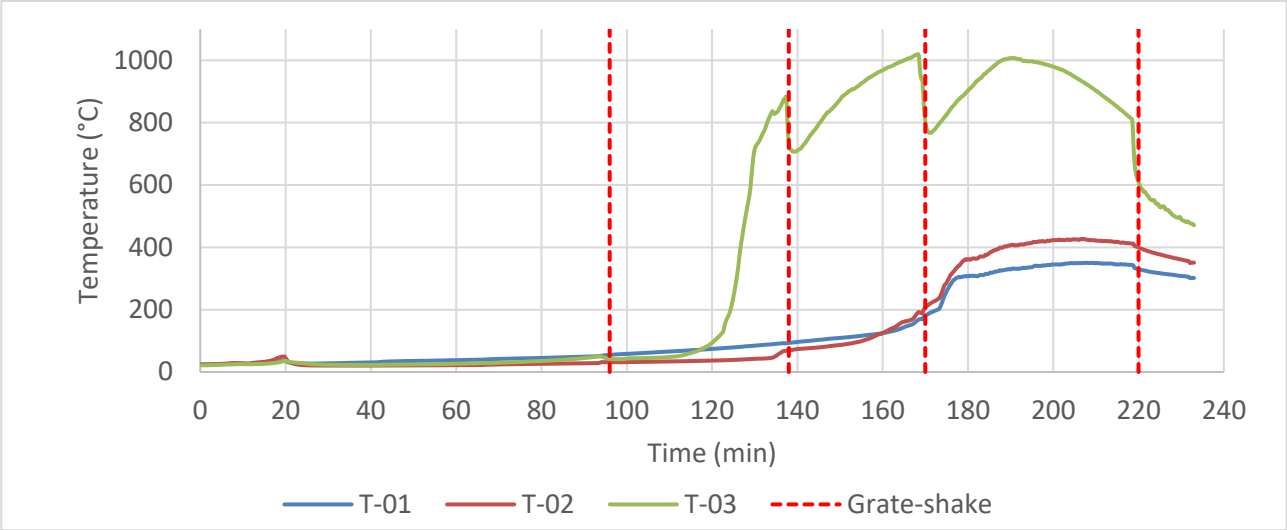

Figure H-13: Hopper temperatures (0% biomass, high-power experiment)

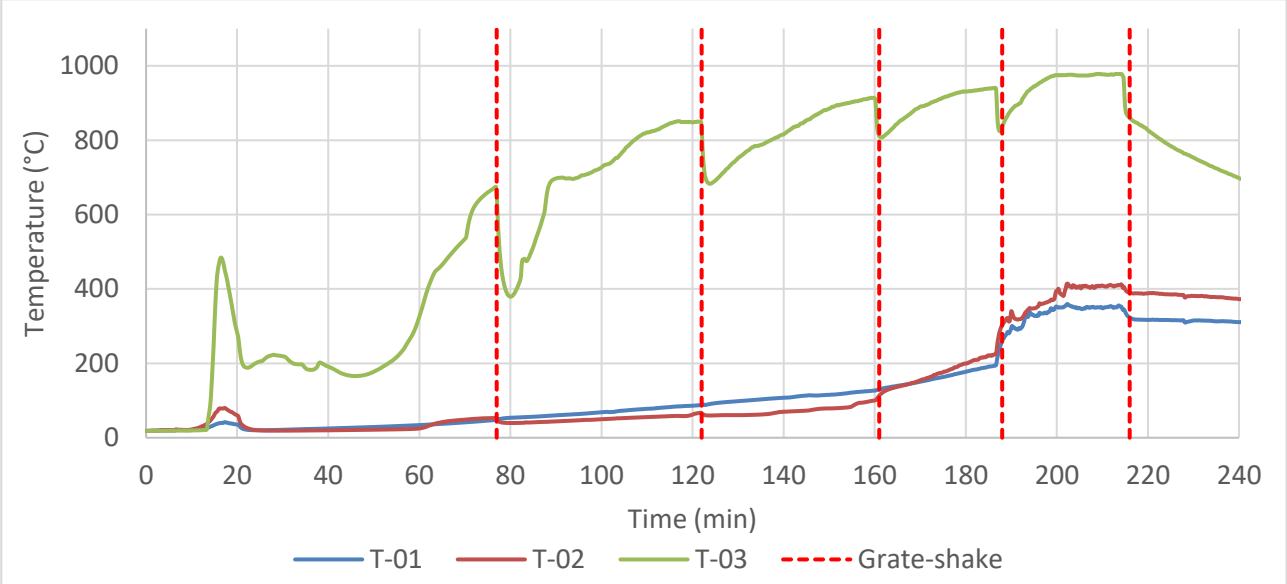

Figure H-14: Hopper temperatures (0% biomass, low-power experiment)

Figure H-15 and **Figure H-16** show the hopper temperatures for the high-power and low-power experiments using 10% biomass pellets.

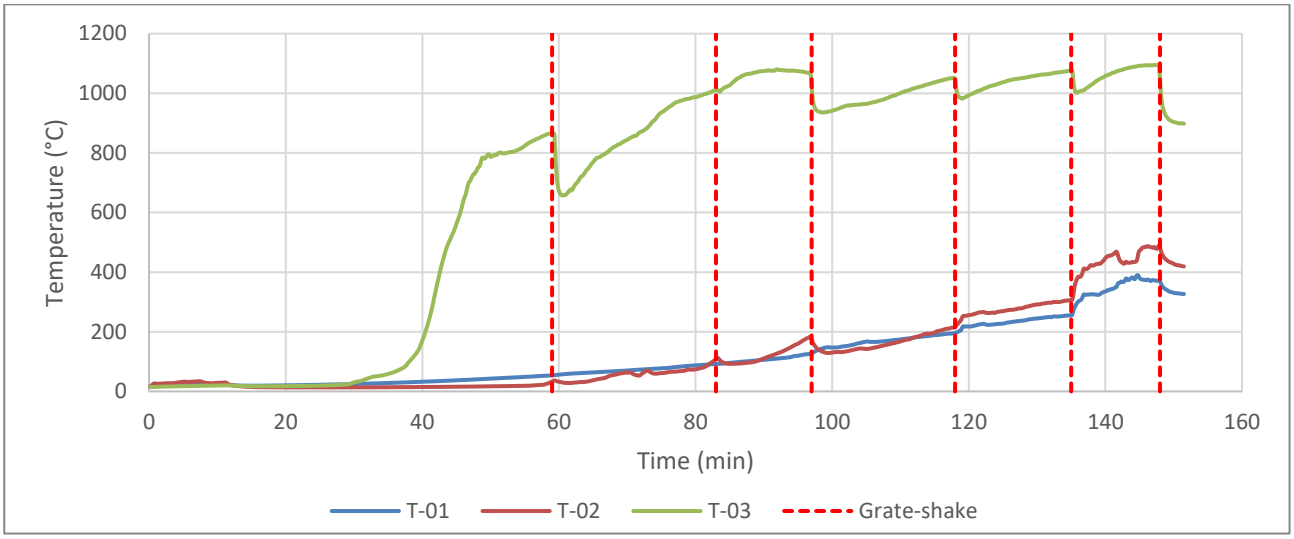

Figure H-15: Hopper temperatures (10% biomass, high-power experiment)

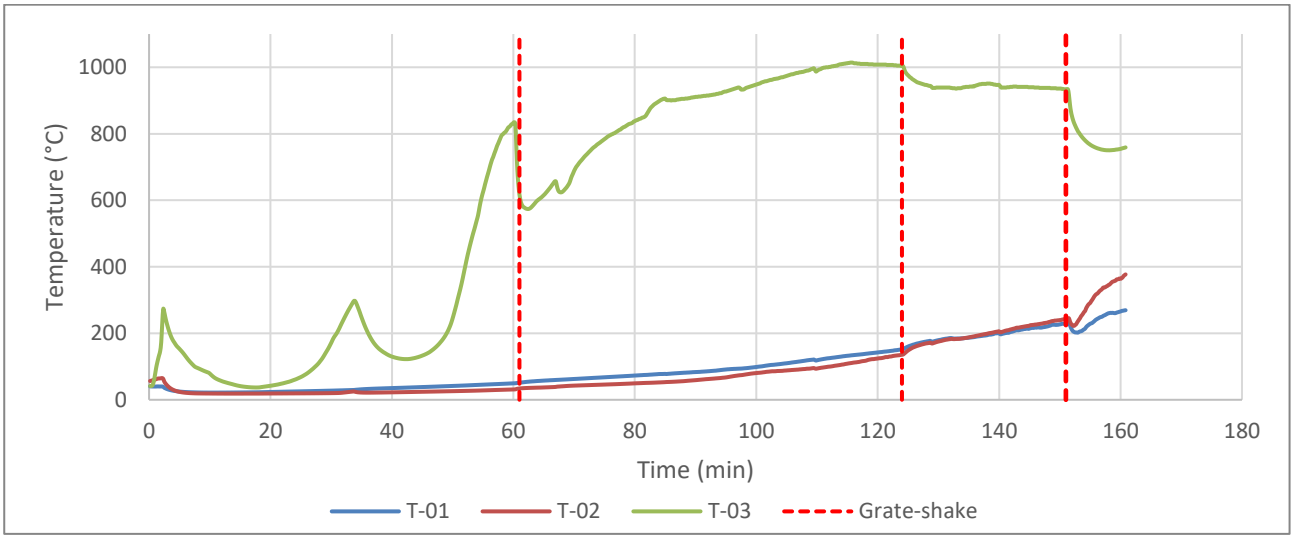

Figure H-16: Hopper temperatures (10% biomass, low-power experiment)

Figure H-17 and **Figure H-18** show the hopper temperatures for the high-power and low-power experiments using 25% biomass pellets.

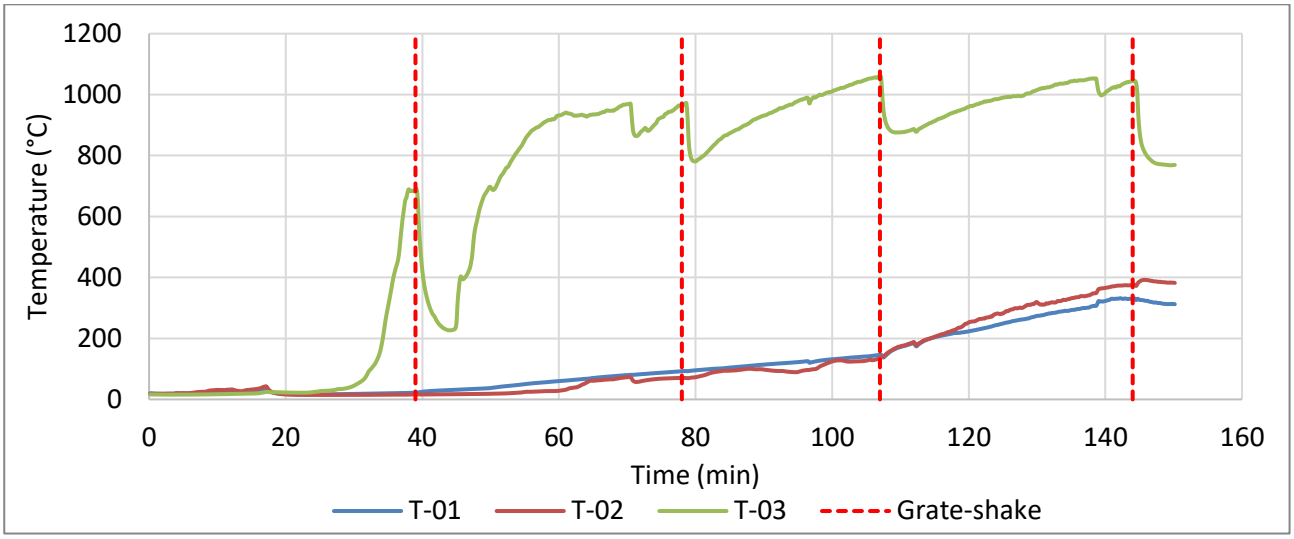

Figure H-17: Hopper temperatures (25% biomass, high-power experiment)

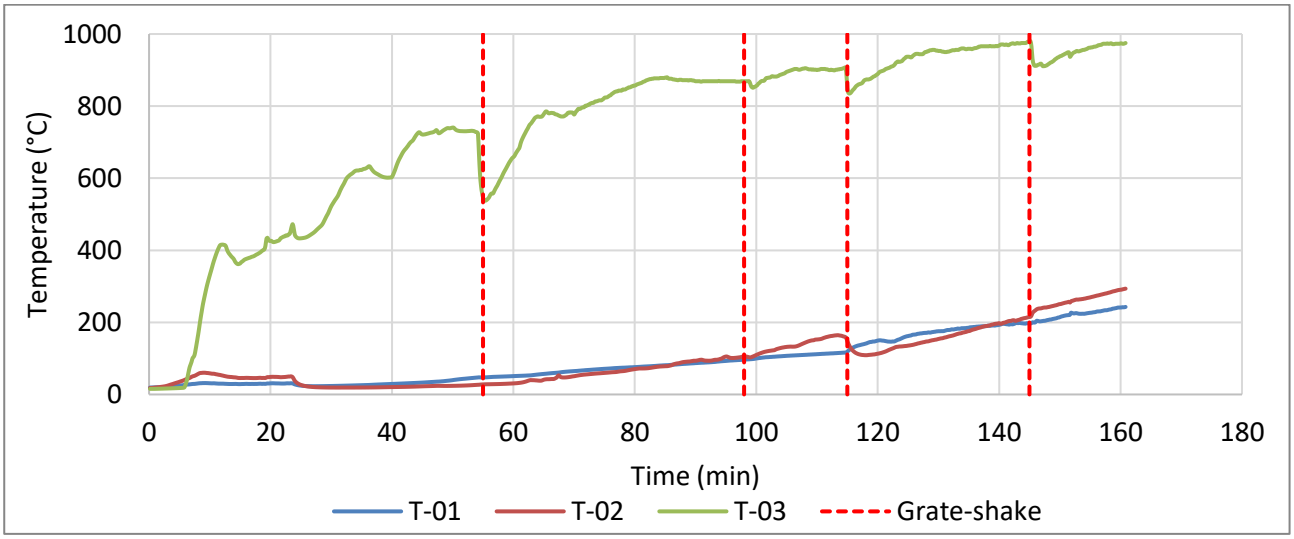

Figure H-18: Hopper temperatures (25% biomass, low-power experiment)

Figure H-19 and **Figure H-20** show the hopper temperatures for the high-power and low-power experiments using 50% biomass pellets.

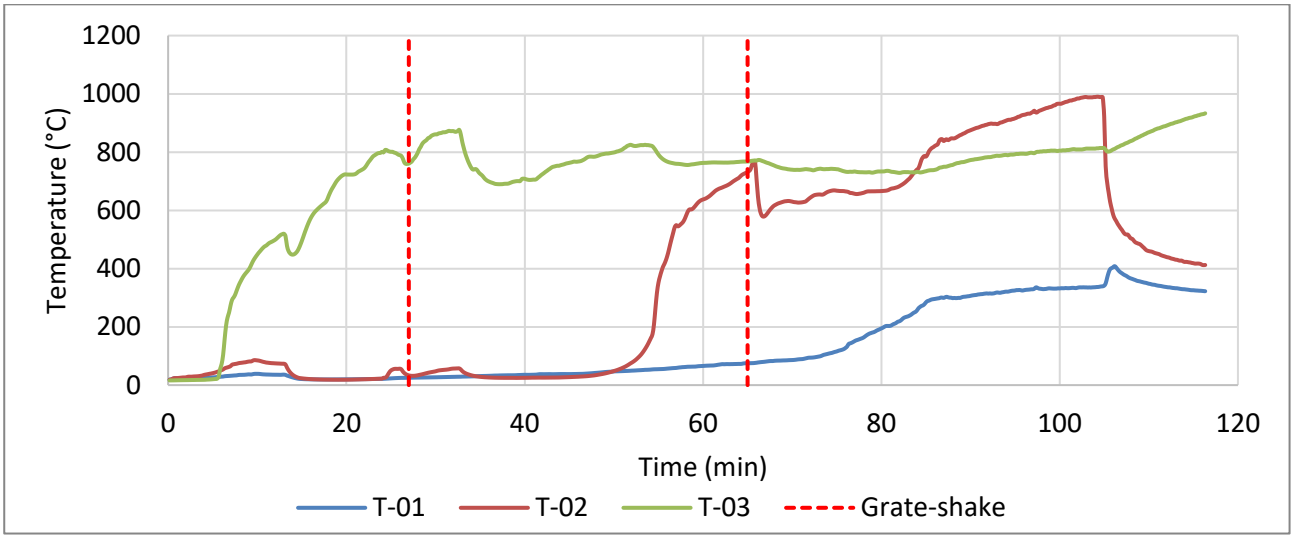

Figure H-19: Hopper temperatures (50% biomass, high-power experiment)

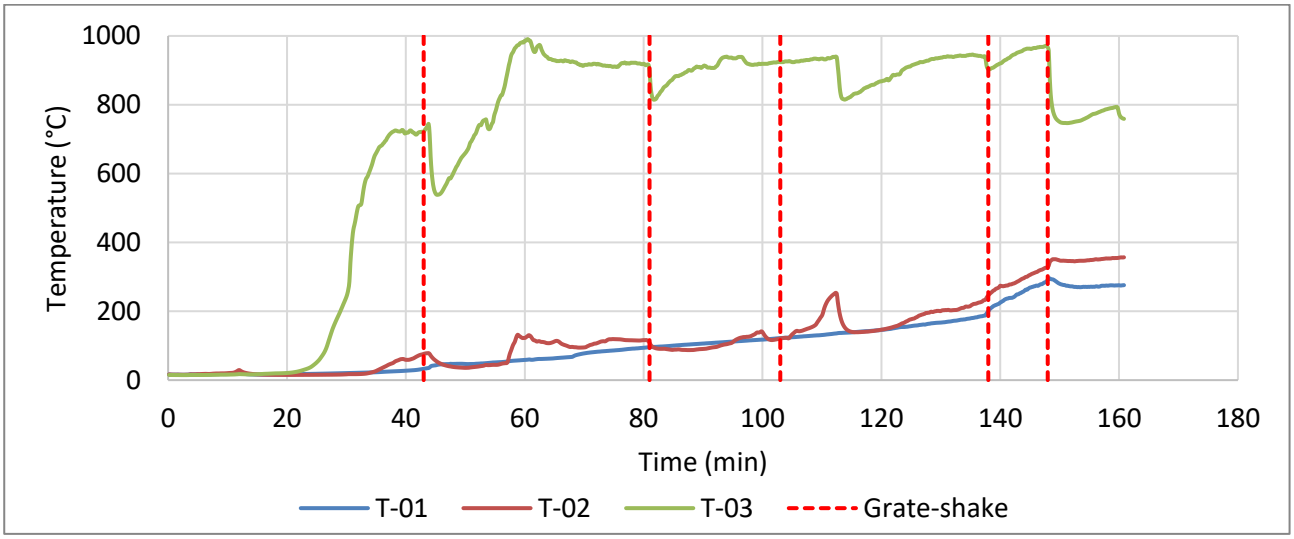

Figure H-20: Hopper temperatures (50% biomass, low-power experiment)

Figure H-21 and **Figure H-22** show the hopper temperatures for the high-power and low-power experiments using 75% biomass pellets.

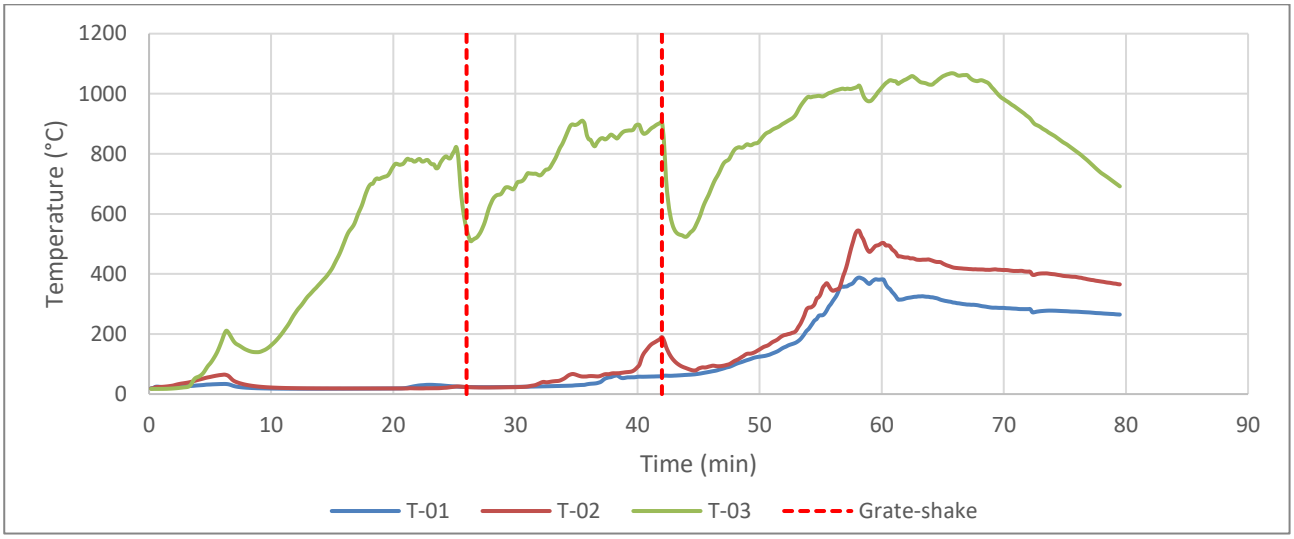

Figure H-21: Hopper temperatures (75% biomass, high-power experiment)

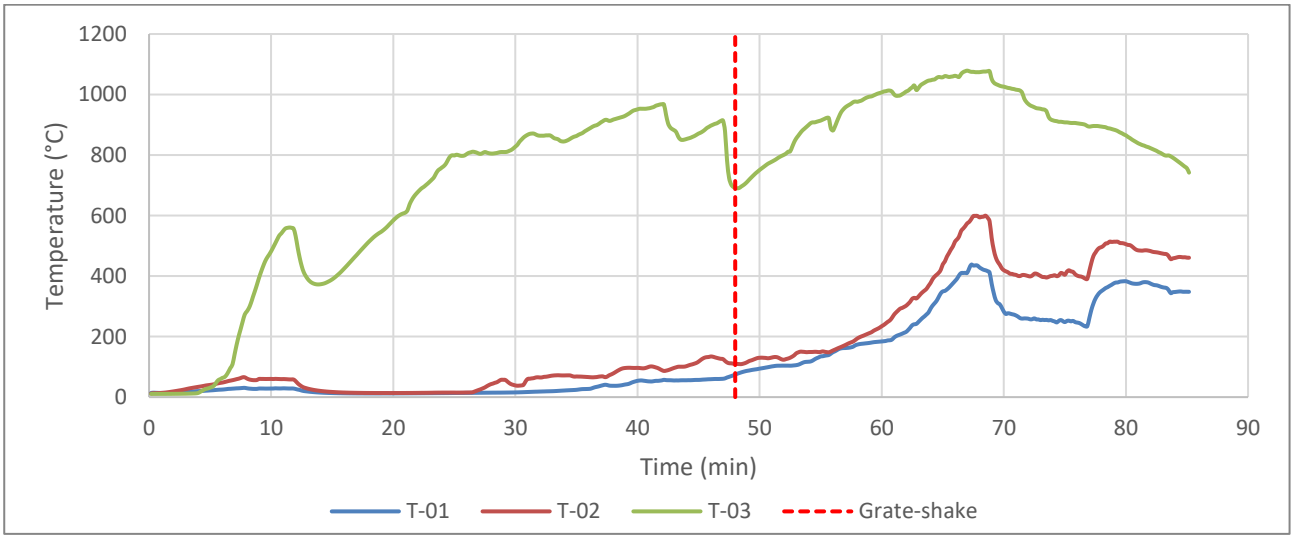

Figure H-22: Hopper temperatures (75% biomass, low-power experiment)

Figure H-23 and **Figure H-24** show the hopper temperatures for the high-power and low-power experiments using 90% biomass pellets.

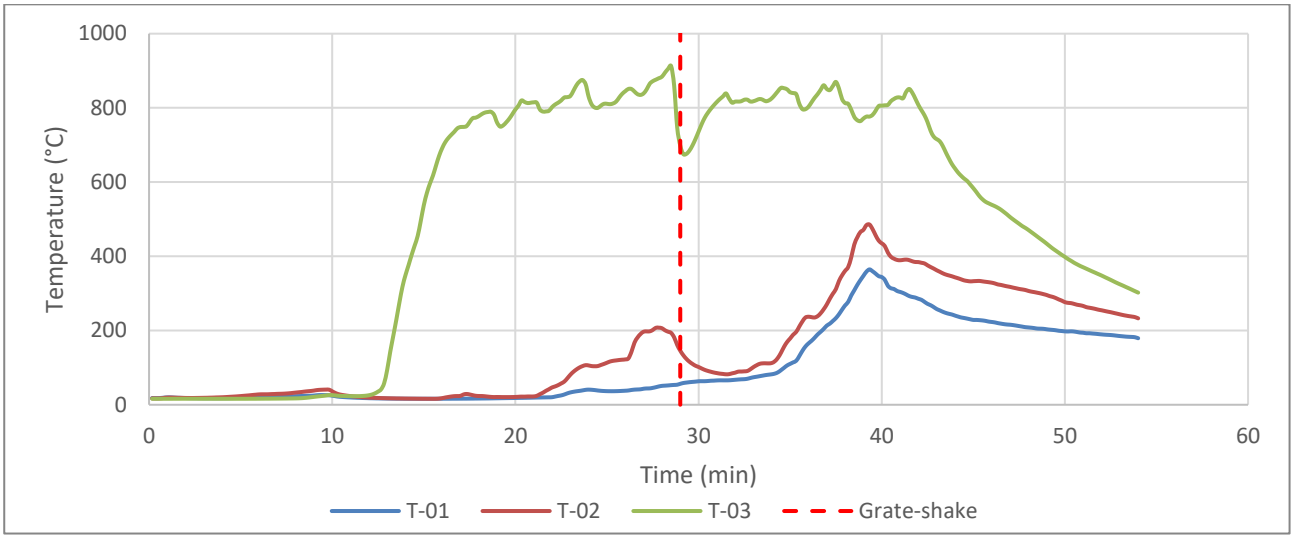

Figure H-23: Hopper temperatures (90% biomass, high-power experiment)

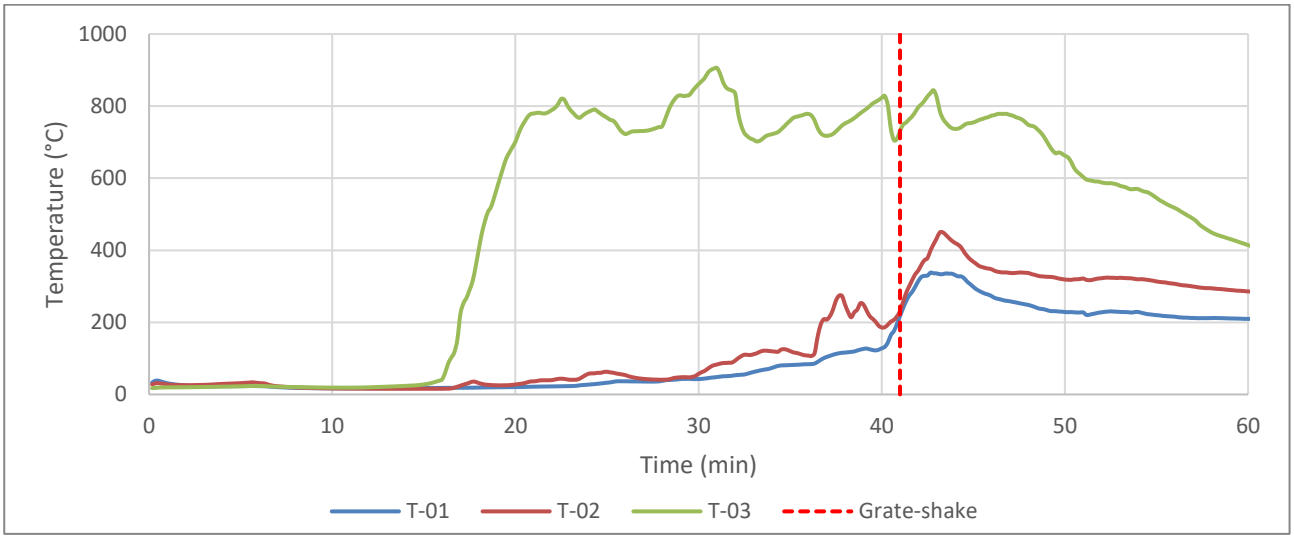

Figure H-24: Hopper temperatures (90% biomass, low-power experiment)

APPENDIX I OBSERVED FLUE GAS COMPOSITION

Figure I-1 and **Figure I-2** display the CO_2, O_2, and CO concentrations in the flue gas during the high-power and low-power combustion experiments of the 0% biomass pellets.

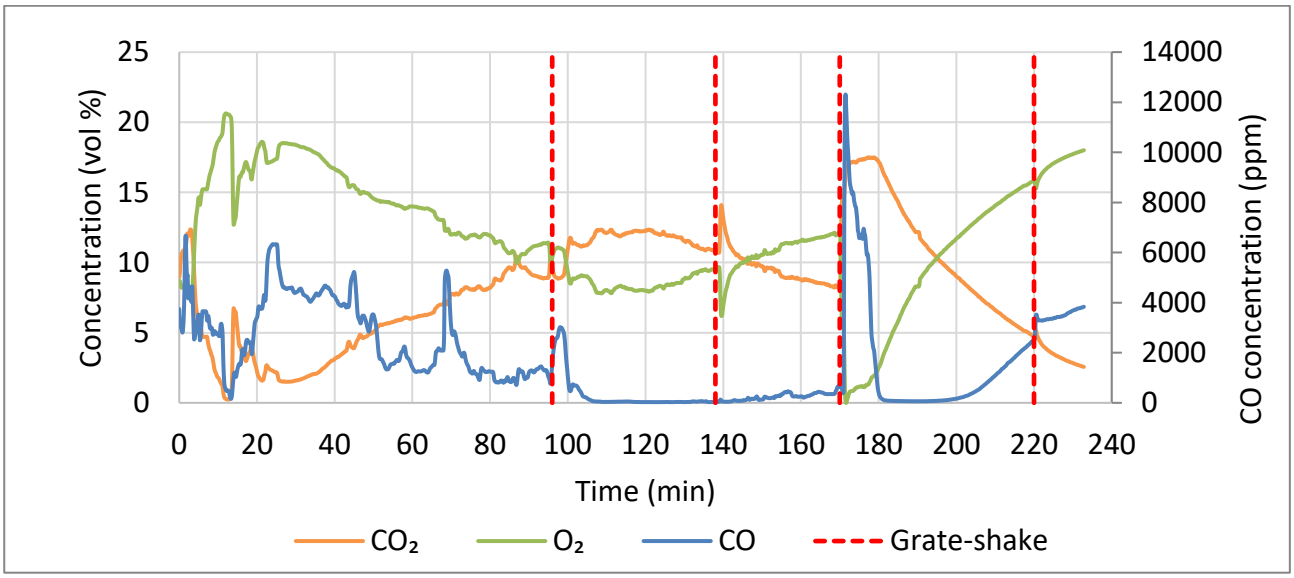

Figure I-1: CO_2, O_2, and CO concentrations over time (0% biomass, high-power experiment)

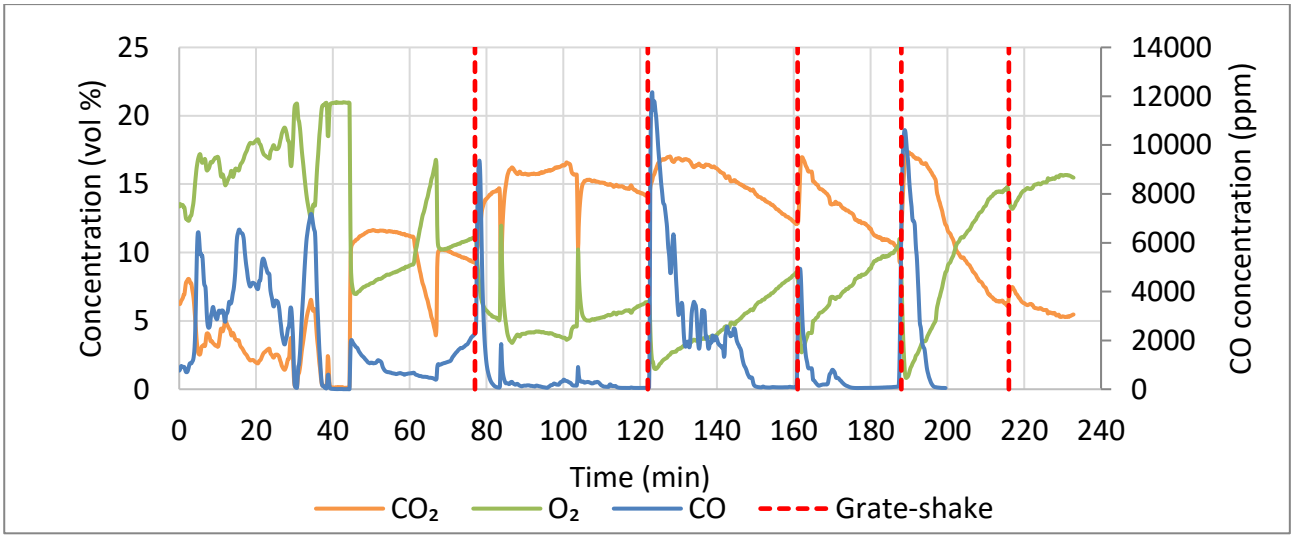

Figure I-2: CO_2, O_2, and CO concentrations over time (0% biomass, low-power experiment)

Figure I-3 and **Figure I-4** display the CO_2, O_2, and CO concentrations in the flue gas during the high-power and low-power combustion experiments of the 10% biomass pellets.

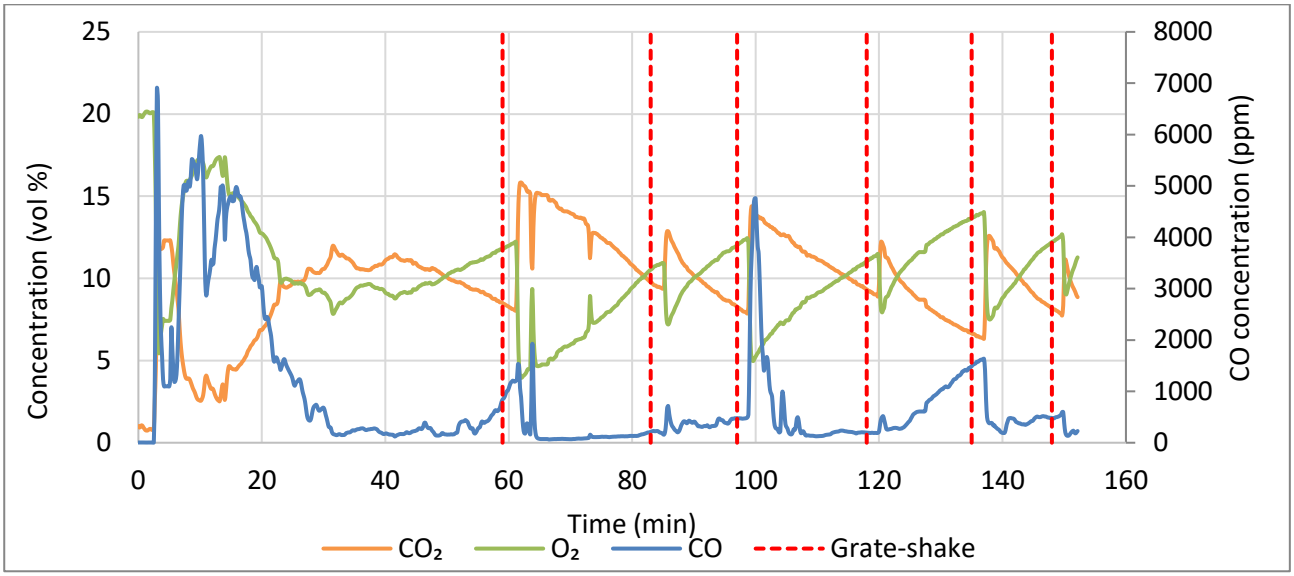

Figure I-3: CO_2, O_2, and CO concentrations over time (10% biomass, high-power experiment)

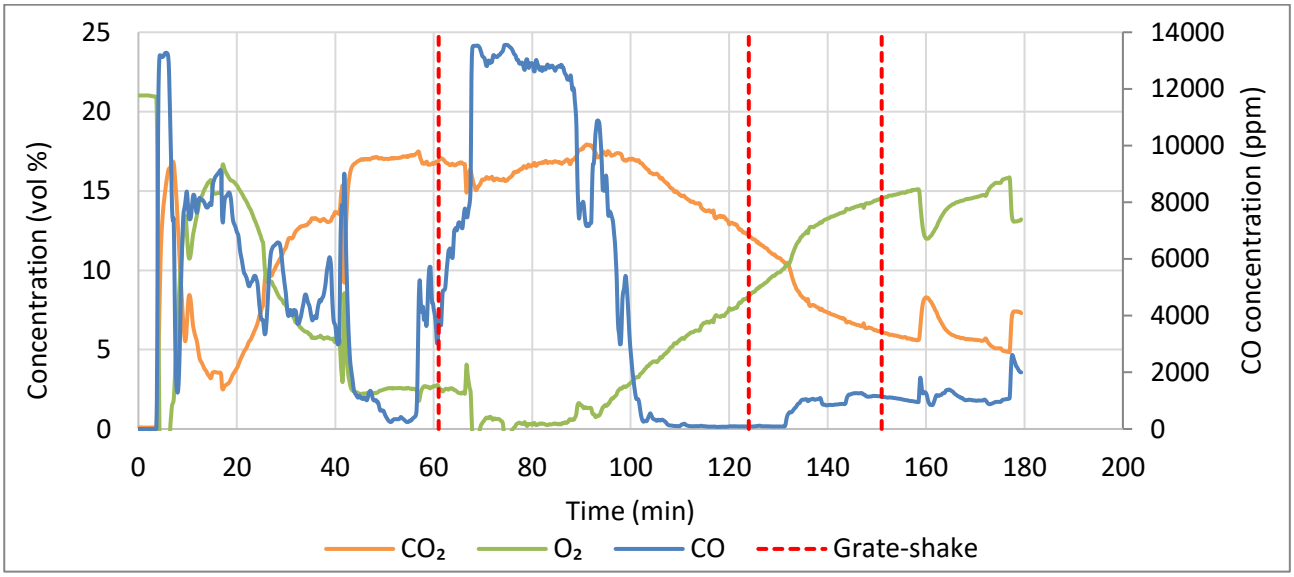

Figure I-4: CO_2, O_2, and CO concentrations over time (10% biomass, low-power experiment)

Figure I-5 and **Figure I-6** display the CO_2, O_2, and CO concentrations in the flue gas during the high-power and low-power combustion experiments of the 25% biomass pellets.

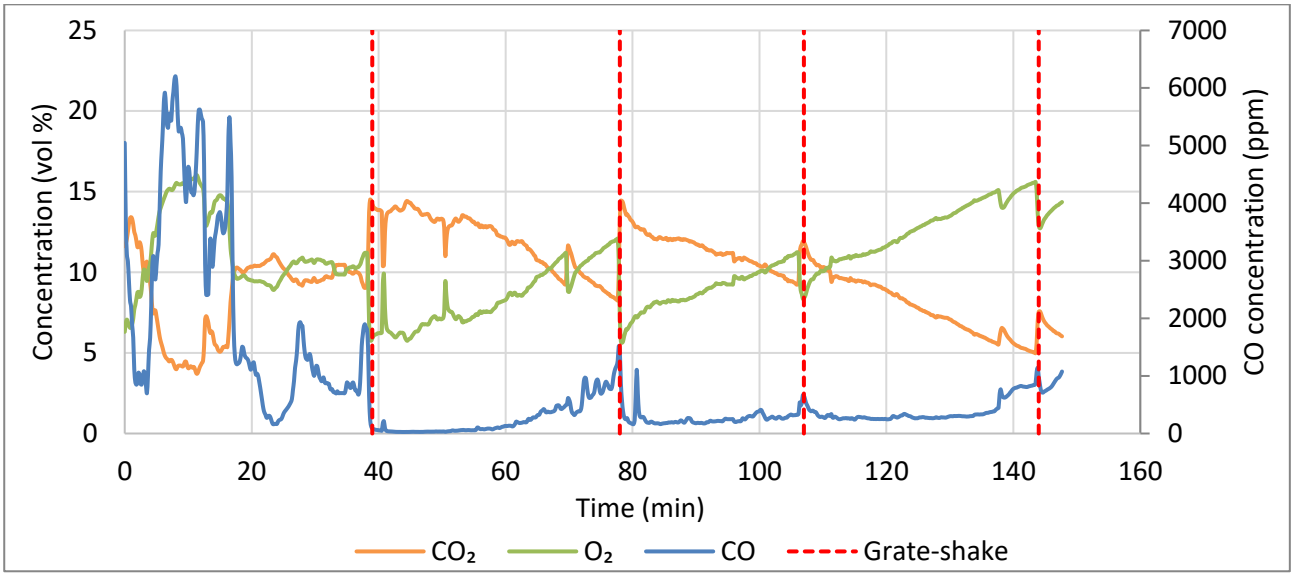

Figure I-5: CO_2, O_2, and CO concentrations over time (25% biomass, high-power experiment)

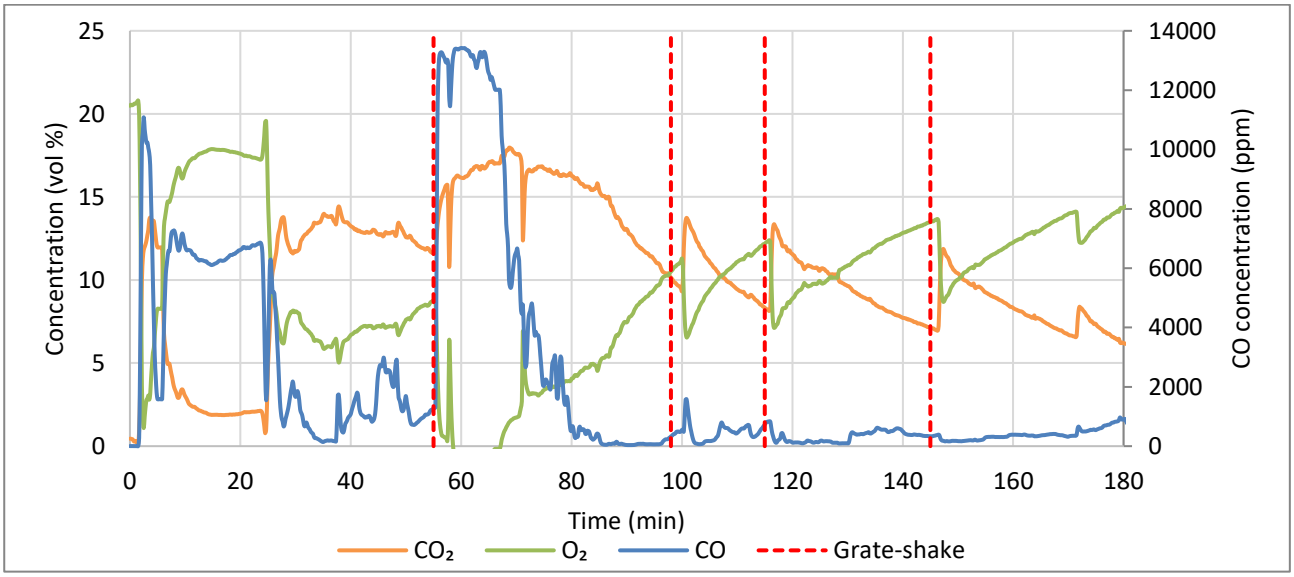

Figure I-6: CO_2, O_2, and CO concentrations over time (25% biomass, low-power experiment)

Figure I-7 and **Figure I-8** display the CO_2, O_2, and CO concentrations in the flue gas during the high-power and low-power combustion experiments of the 50% biomass pellets.

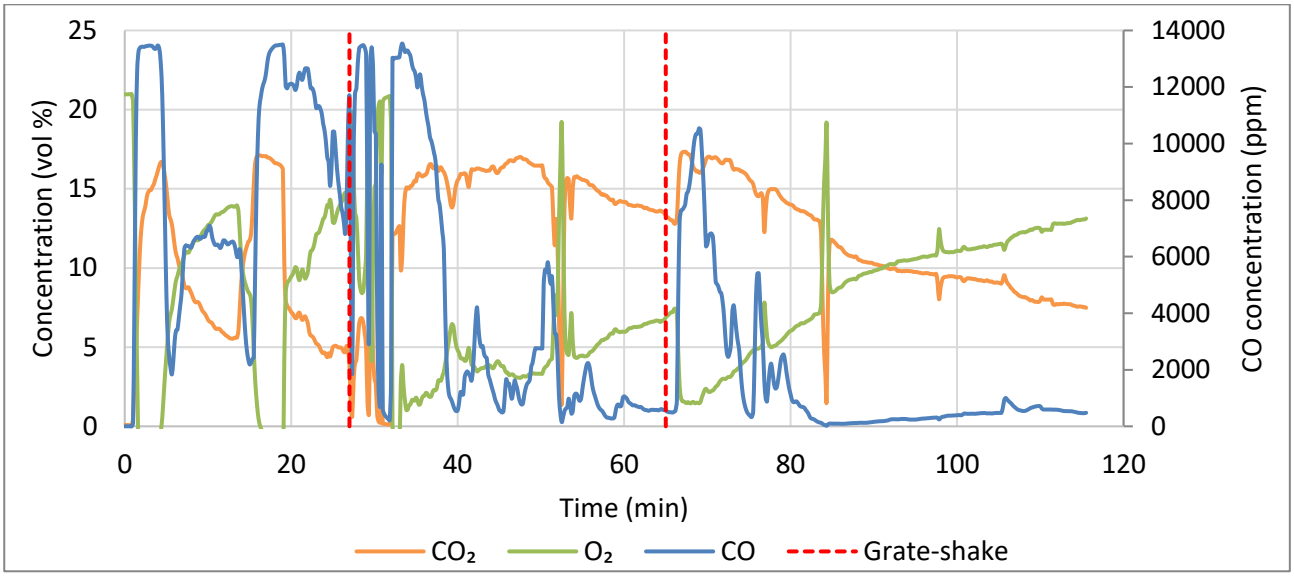

Figure I-7: CO_2, O_2, and CO concentrations over time (50% biomass, high-power experiment)

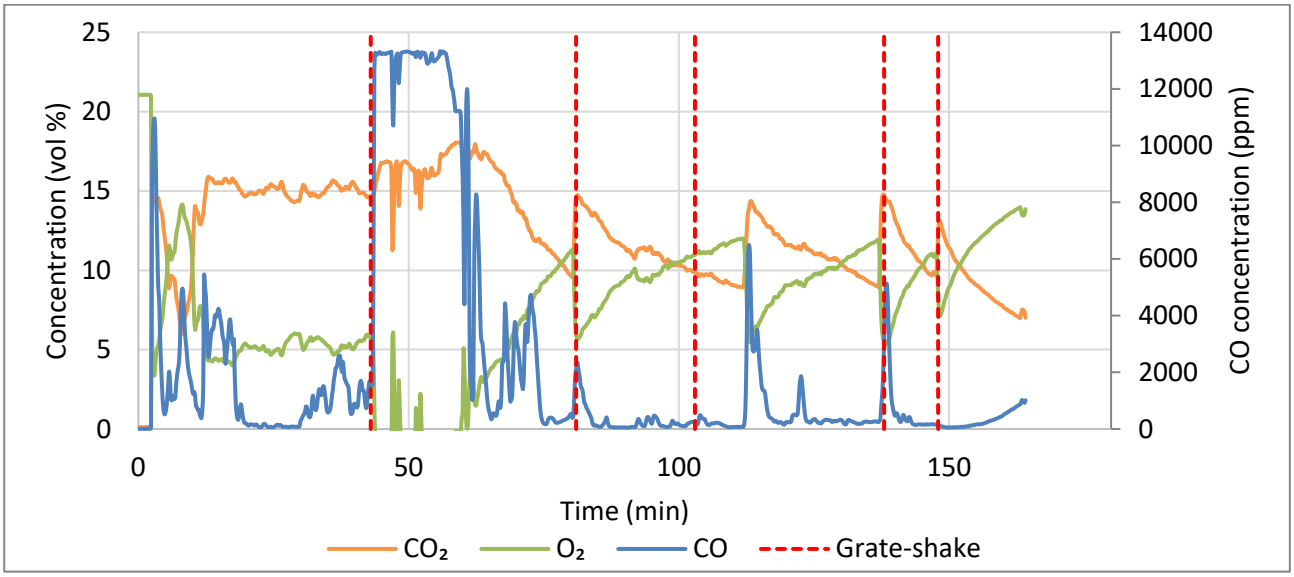

Figure I-8: CO_2, O_2, and CO concentrations over time (50% biomass, low-power experiment)

Figure I-9 and **Figure I-10** display the CO_2, O_2, and CO concentrations in the flue gas during the high-power and low-power combustion experiments of the 75% biomass pellets.

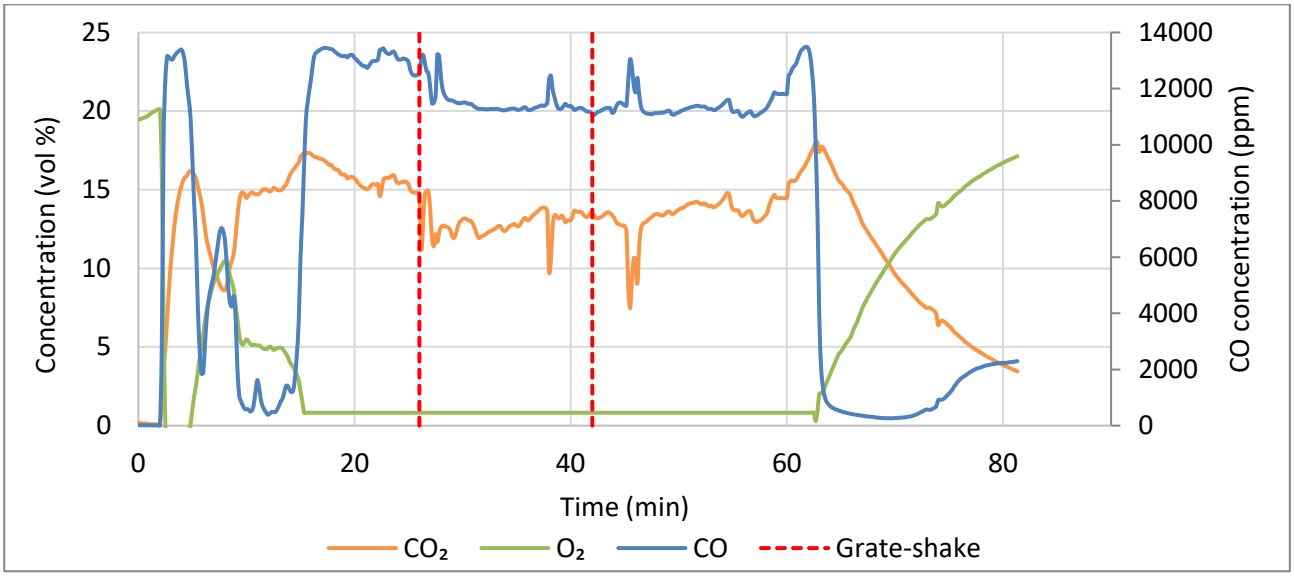

Figure I-9: CO_2, O_2, and CO concentrations over time (75% biomass, high-power experiment)

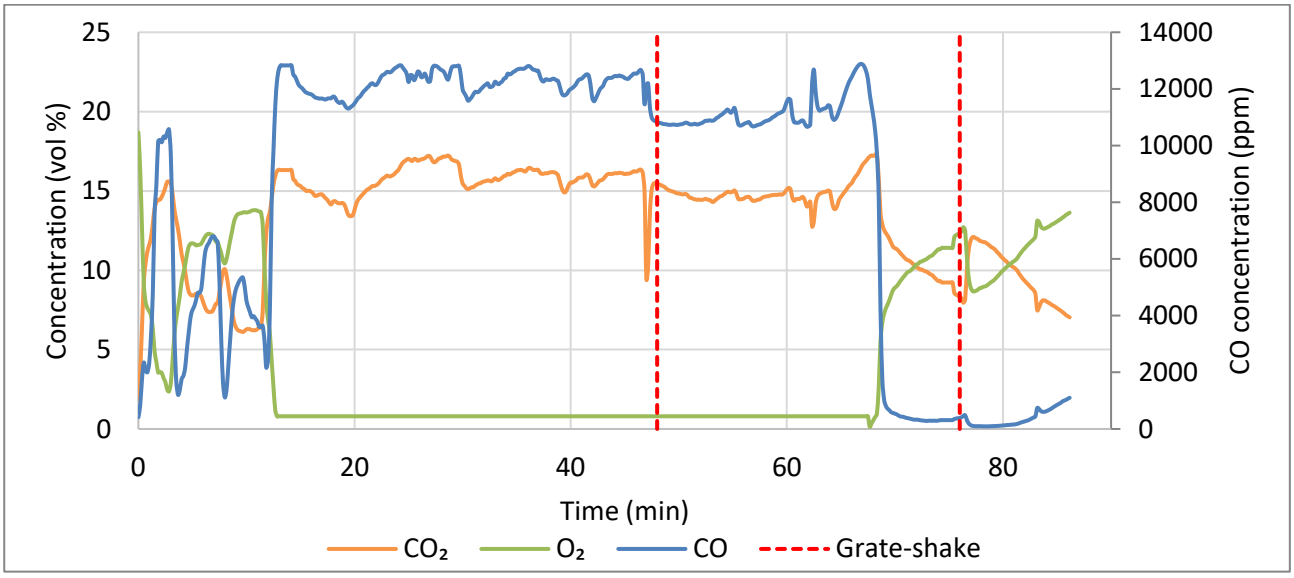

Figure I-10: CO_2, O_2, and CO concentrations over time (75% biomass, low-power experiment)

Figure I-11 and **Figure I-12** display the CO_2, O_2, and CO concentrations in the flue gas during the high-power and low-power combustion experiments of the 90% biomass pellets.

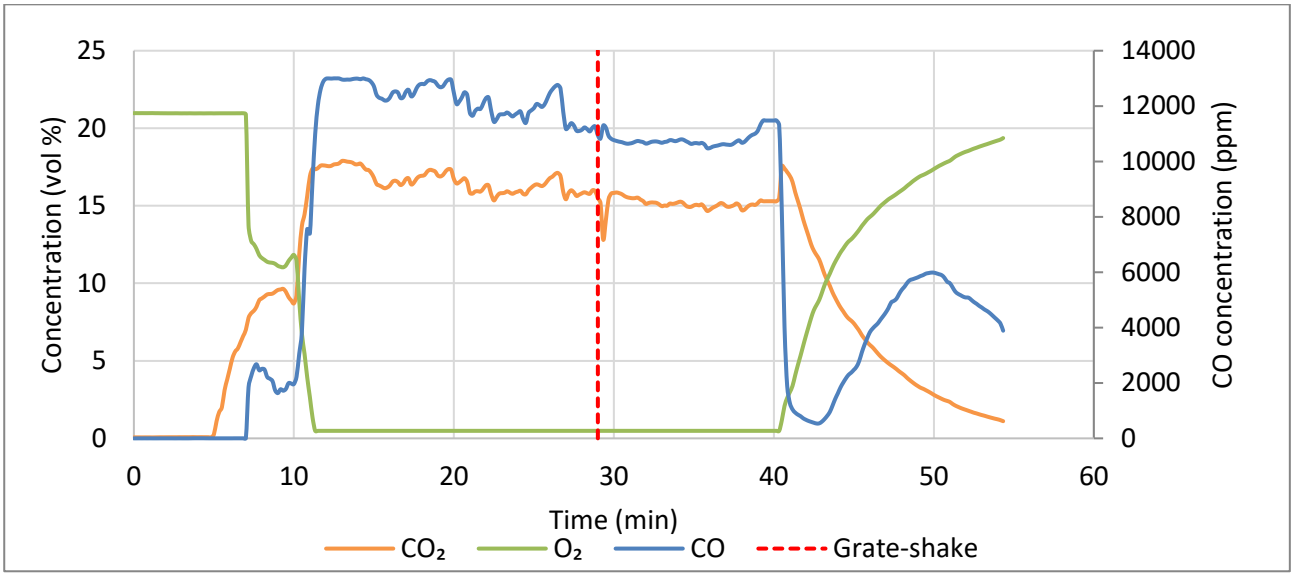

Figure I-11: CO_2, O_2, and CO concentrations over time (90% biomass, high-power experiment)

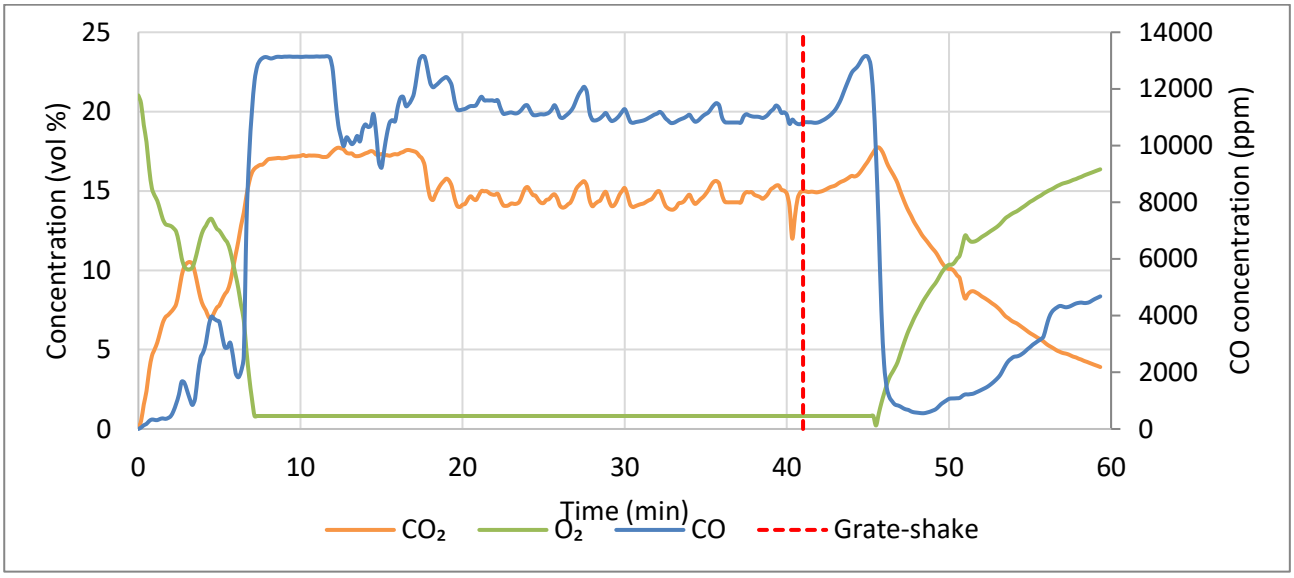

Figure I-12: CO_2, O_2, and CO concentrations over time (90% biomass, low-power experiment)

APPENDIX J COMBUSTION TEMPERATURE AND CO/SO_2/NO_X

Figure J-1 shows the CO, SO_2, and NO_x concentration and combustion temperature during high-power combustion experiments using 0% biomass pellets.

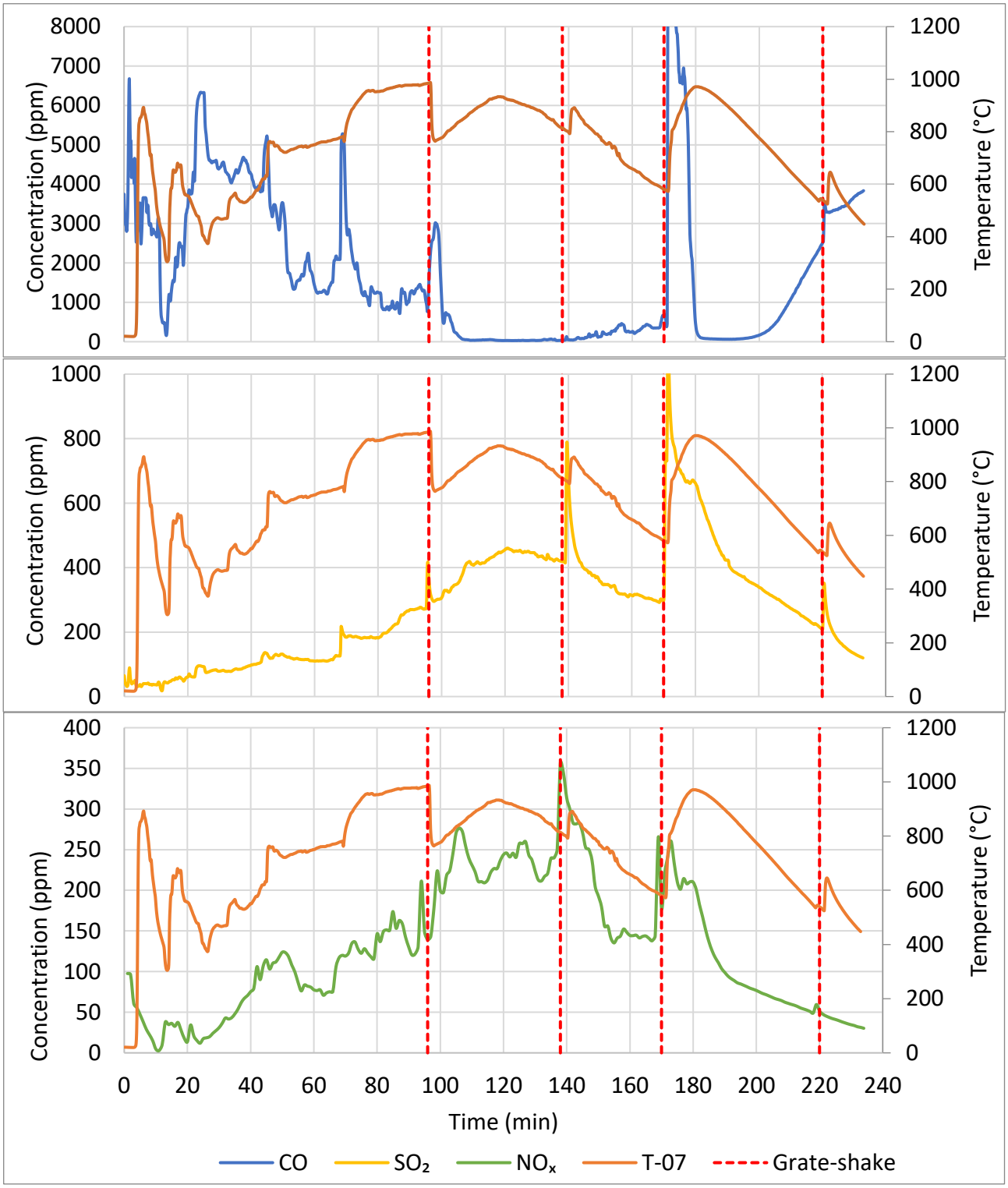

Figure J-1: CO, SO_2, and NO_x concentration and combustion zone temperature over time (0% biomass, high-power experiment)

Figure J-2 shows the CO, SO_2, and NO_x concentrations and combustion temperature during low-power combustion experiments using 0% biomass pellets.

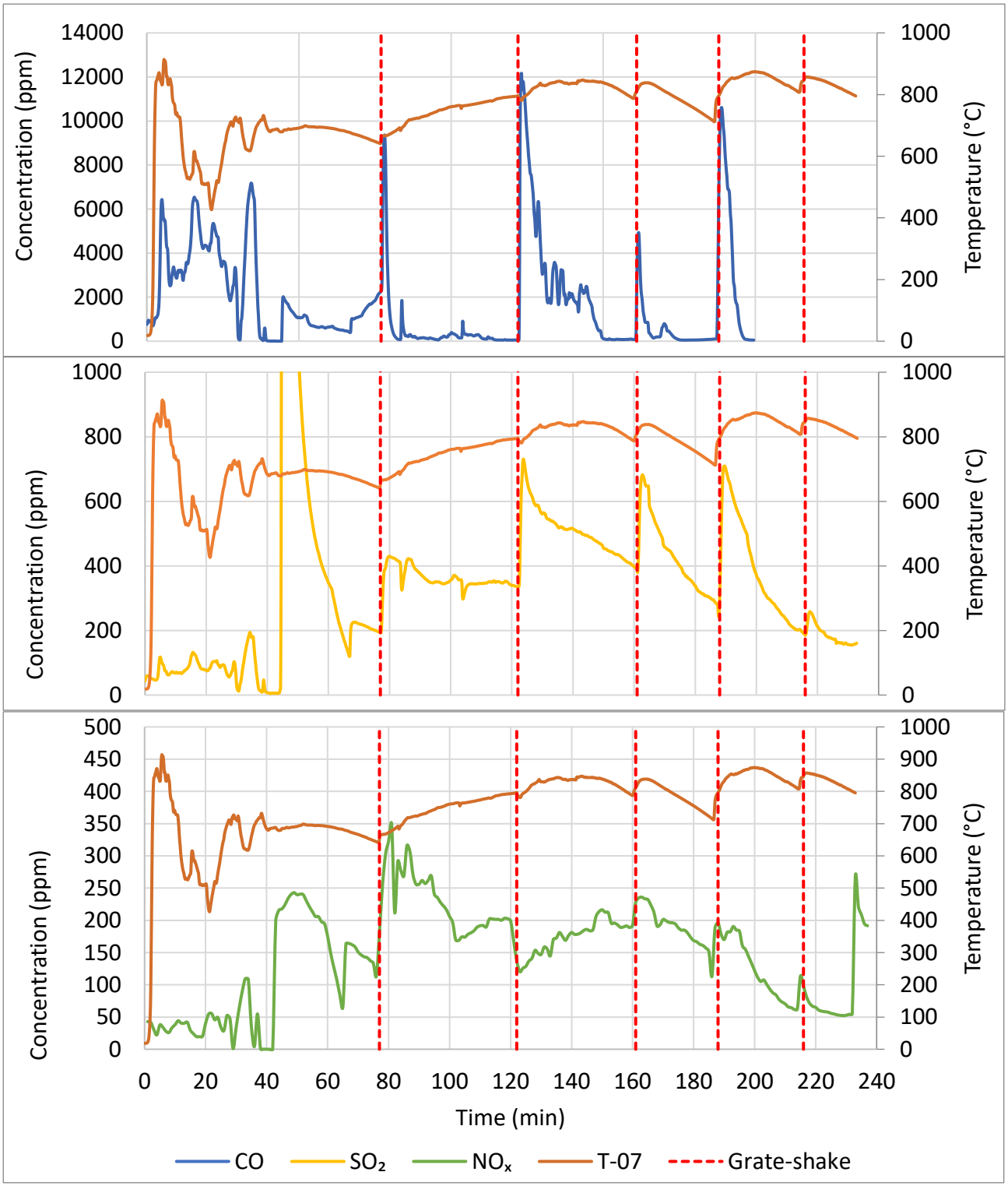

Figure J-2: CO, SO_2, and NO_x concentration and combustion zone temperature over time (0% biomass, low-power experiment)

Figure J-3 shows the CO, SO_2, and NO_x concentrations and combustion temperature during high-power combustion experiments using 10% biomass pellets.

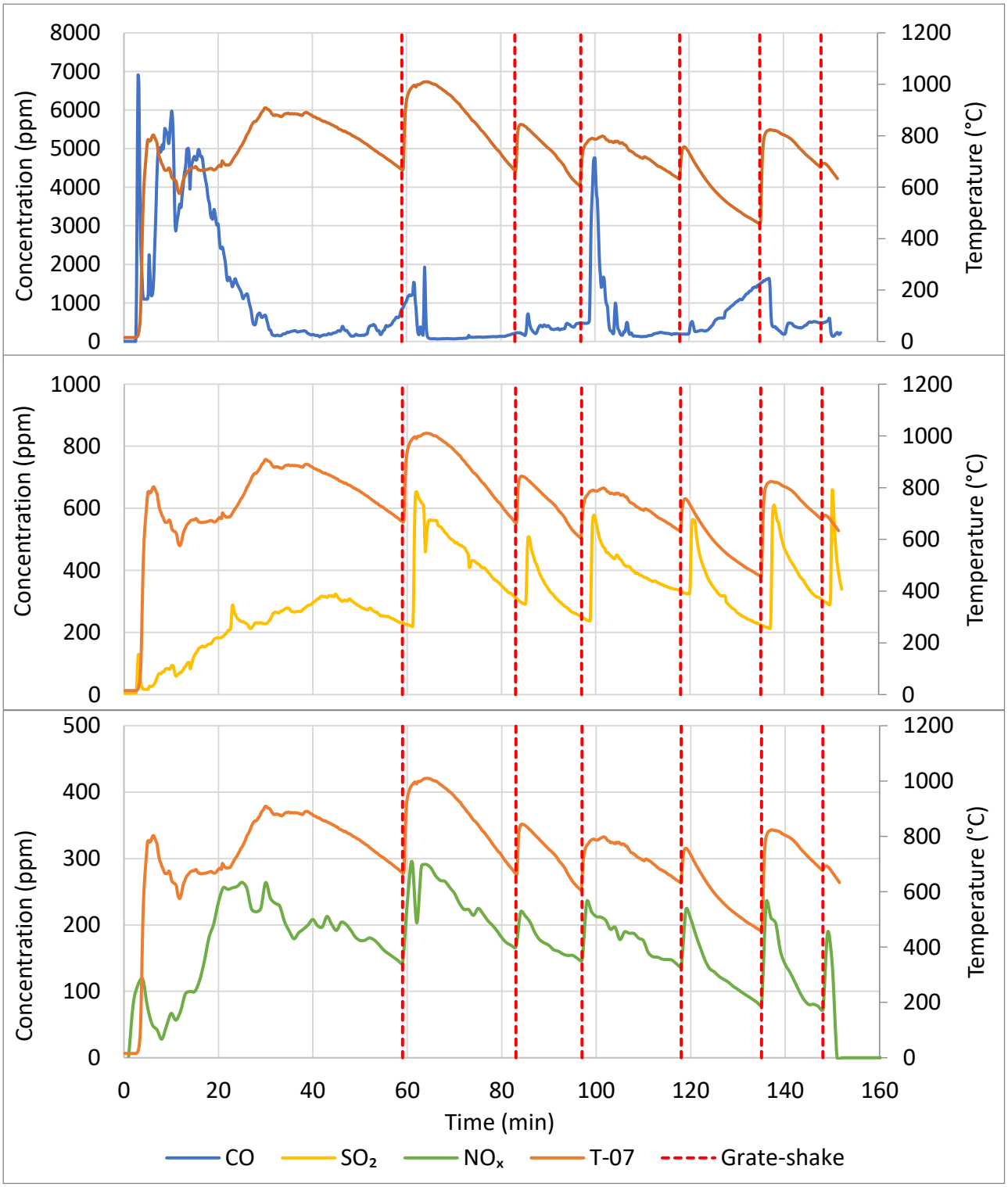

Figure J-3: CO, SO_2, and NO_x concentration and combustion zone temperature over time (10% biomass, high-power experiment)

Figure J-4 shows the CO, SO_2, and NO_x concentrations and combustion temperature during low-power combustion experiments using 10% biomass pellets.

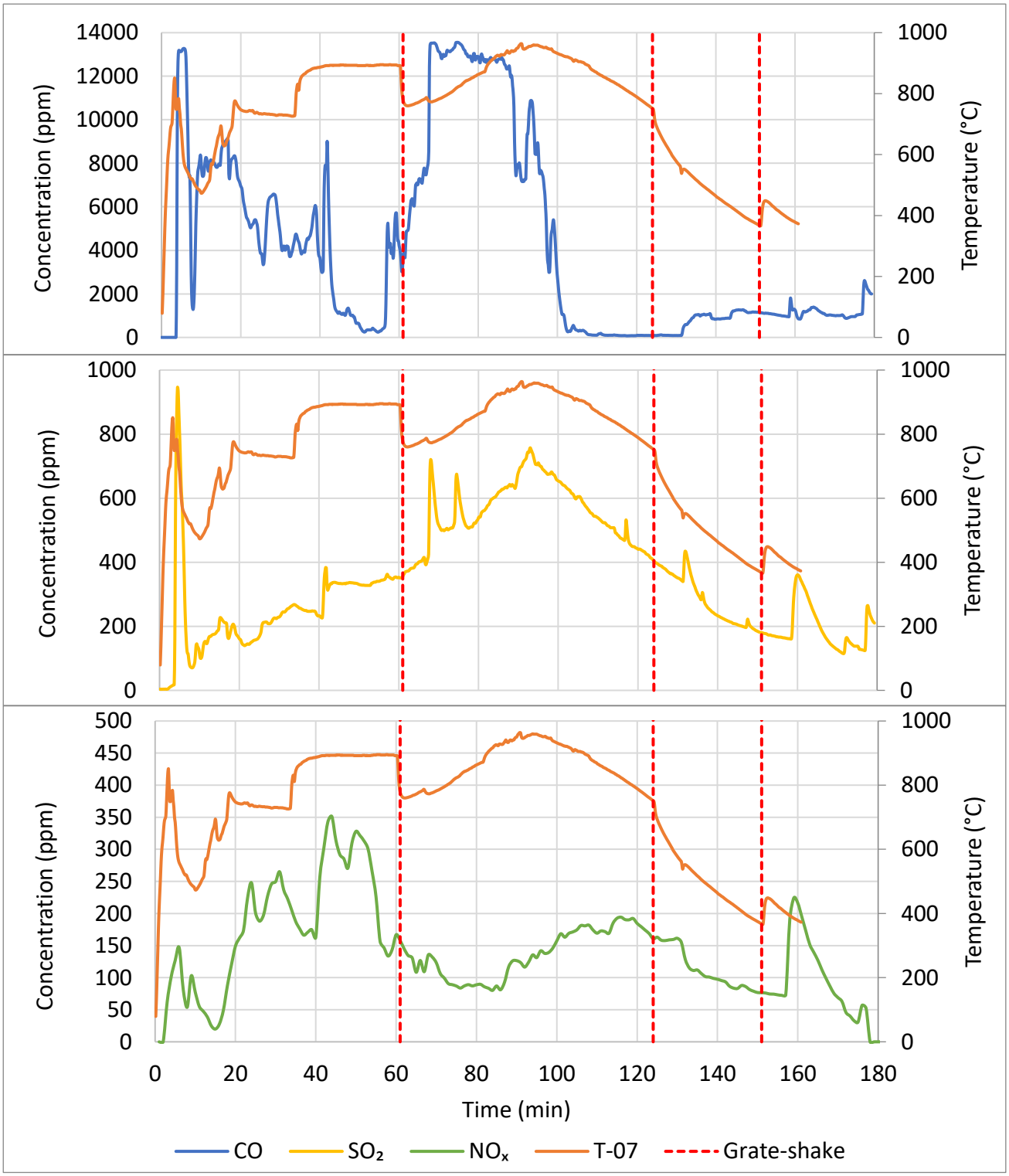

Figure J-4: CO, SO_2, and NO_x concentration and combustion zone temperature over time (10% biomass, low-power experiment)

Figure J-5 shows the CO, SO_2, and NO_x concentrations and combustion temperature during high-power combustion experiments using 25% biomass pellets.

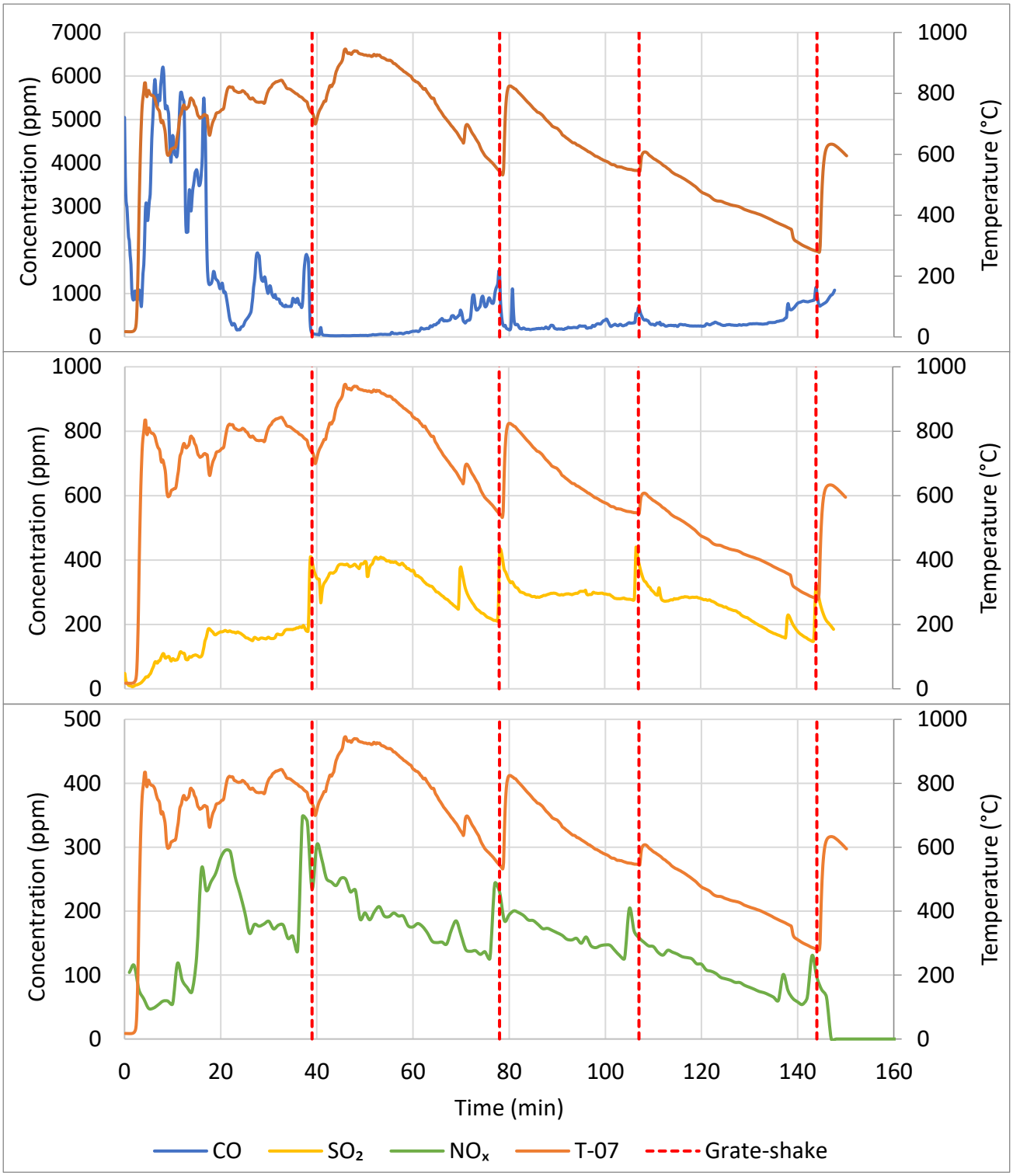

Figure J-5: CO, SO_2, and NO_x concentration and combustion zone temperature over time (25% biomass, high-power experiment)

Figure J-6 shows the CO, SO_2, and NO_x concentrations and combustion temperature during low-power combustion experiments using 25% biomass pellets.

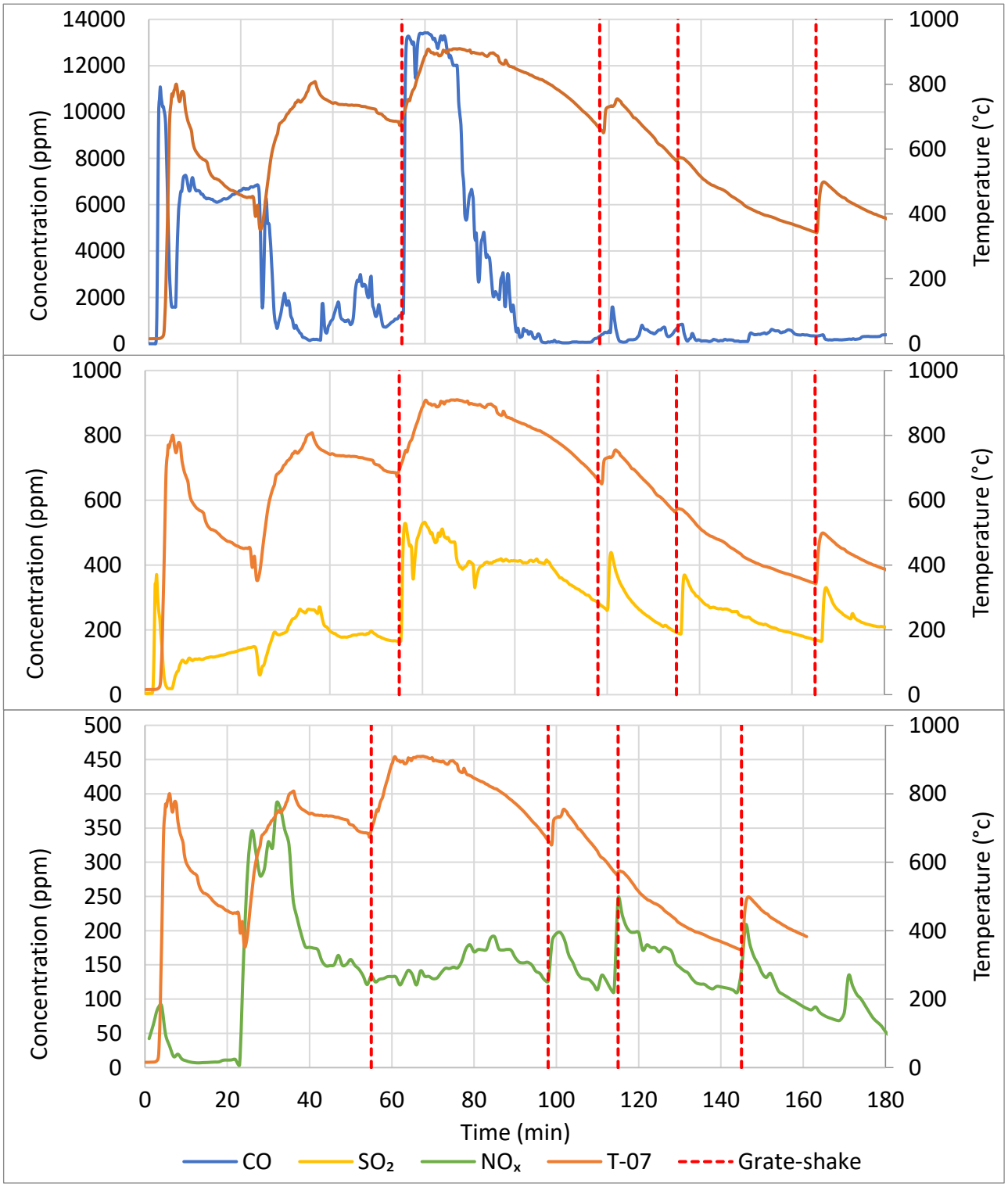

Figure J-6: CO, SO_2, and NO_x concentration and combustion zone temperature over time (25% biomass, low-power experiment)

Figure J-7 shows the CO, SO_2, and NO_x concentrations and combustion temperature during high-power combustion experiments using 50% biomass pellets.

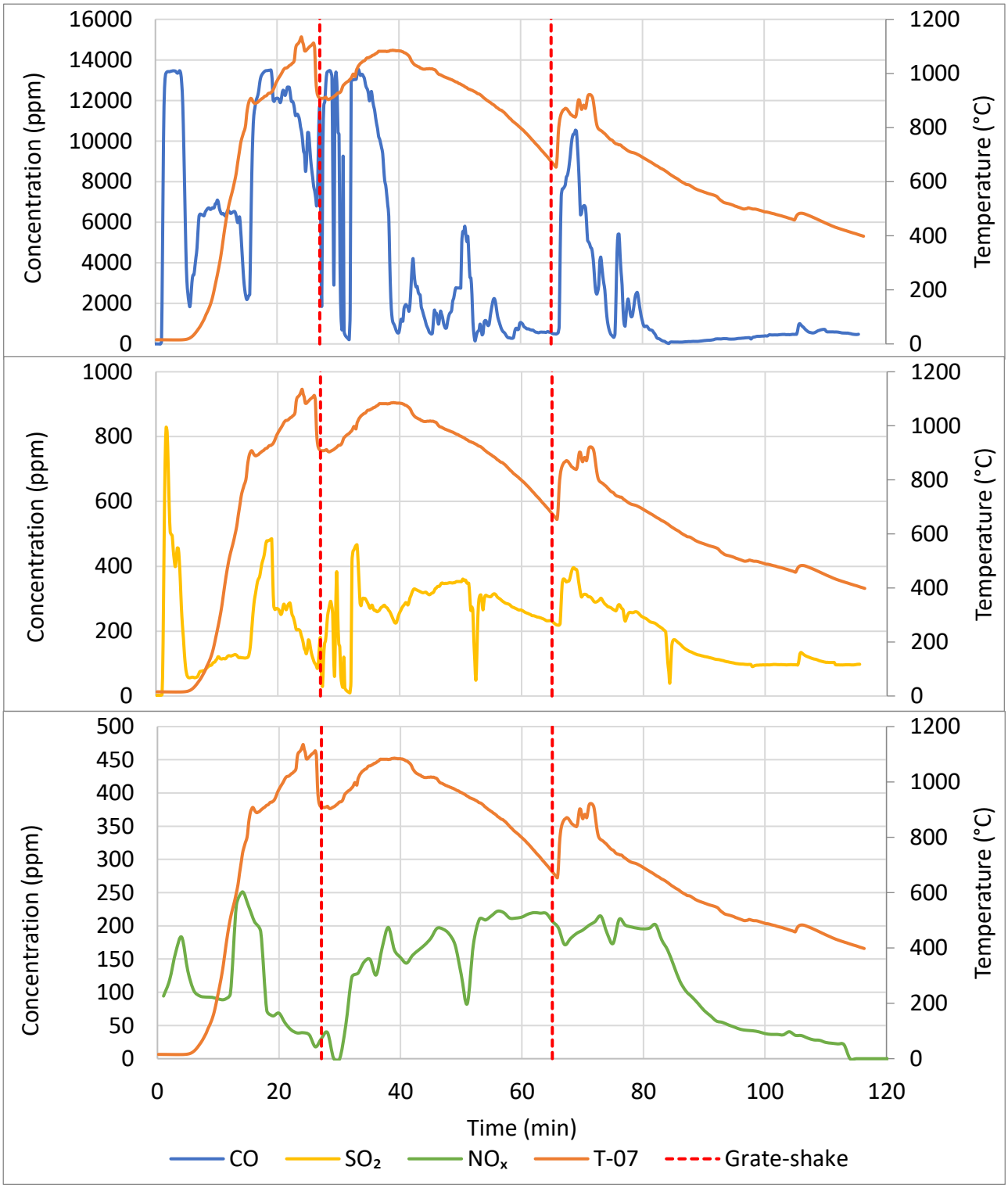

Figure J-7: CO, SO_2, and NO_x concentration and combustion zone temperature over time (50% biomass, high-power experiment)

Figure J-8 shows the CO, SO_2, and NO_x concentrations and combustion temperature during low-power combustion experiments using 50% biomass pellets.

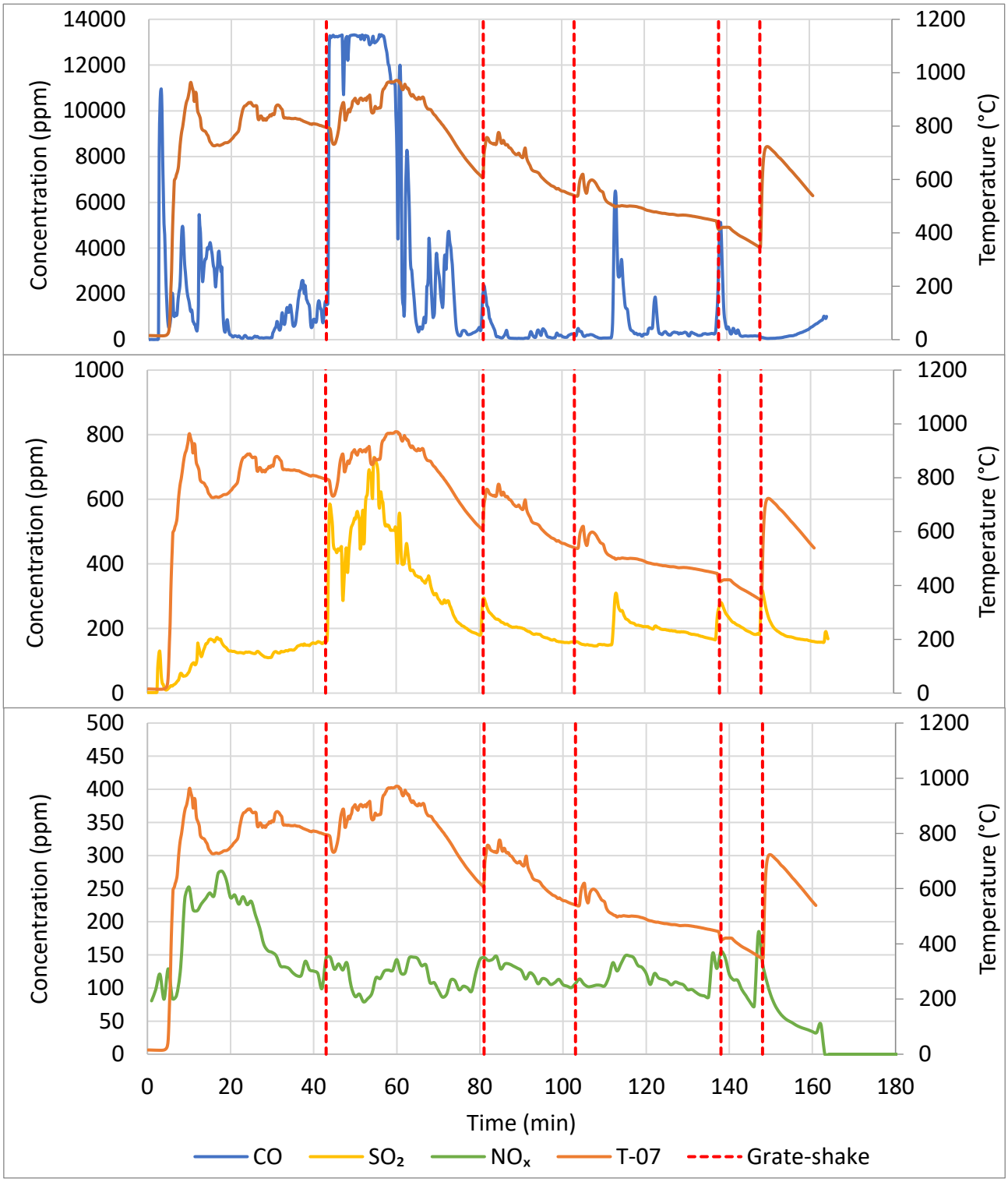

Figure J-8: CO, SO_2, and NO_x concentration and combustion zone temperature over time (50% biomass, low-power experiment)

Figure J-9 shows the CO, SO_2, and NO_x concentrations and combustion temperature during high-power combustion experiments using 75% biomass pellets.

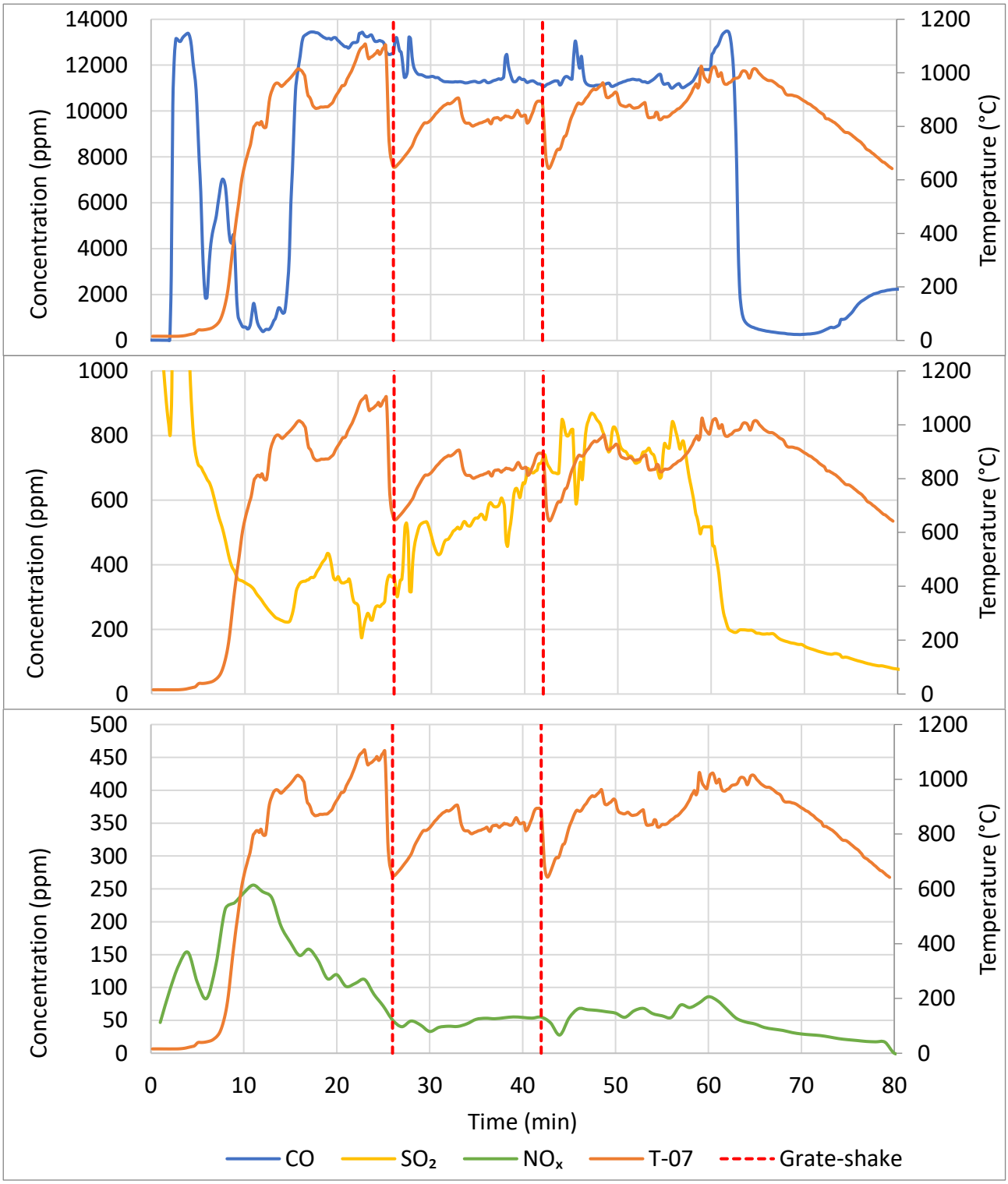

Figure J-9: CO, SO_2, and NO_x concentration and combustion zone temperature over time (75% biomass, high-power experiment)

Figure J-10 shows the CO, SO_2, and NO_x concentrations and combustion temperature during low-power combustion experiments using 75% biomass pellets.

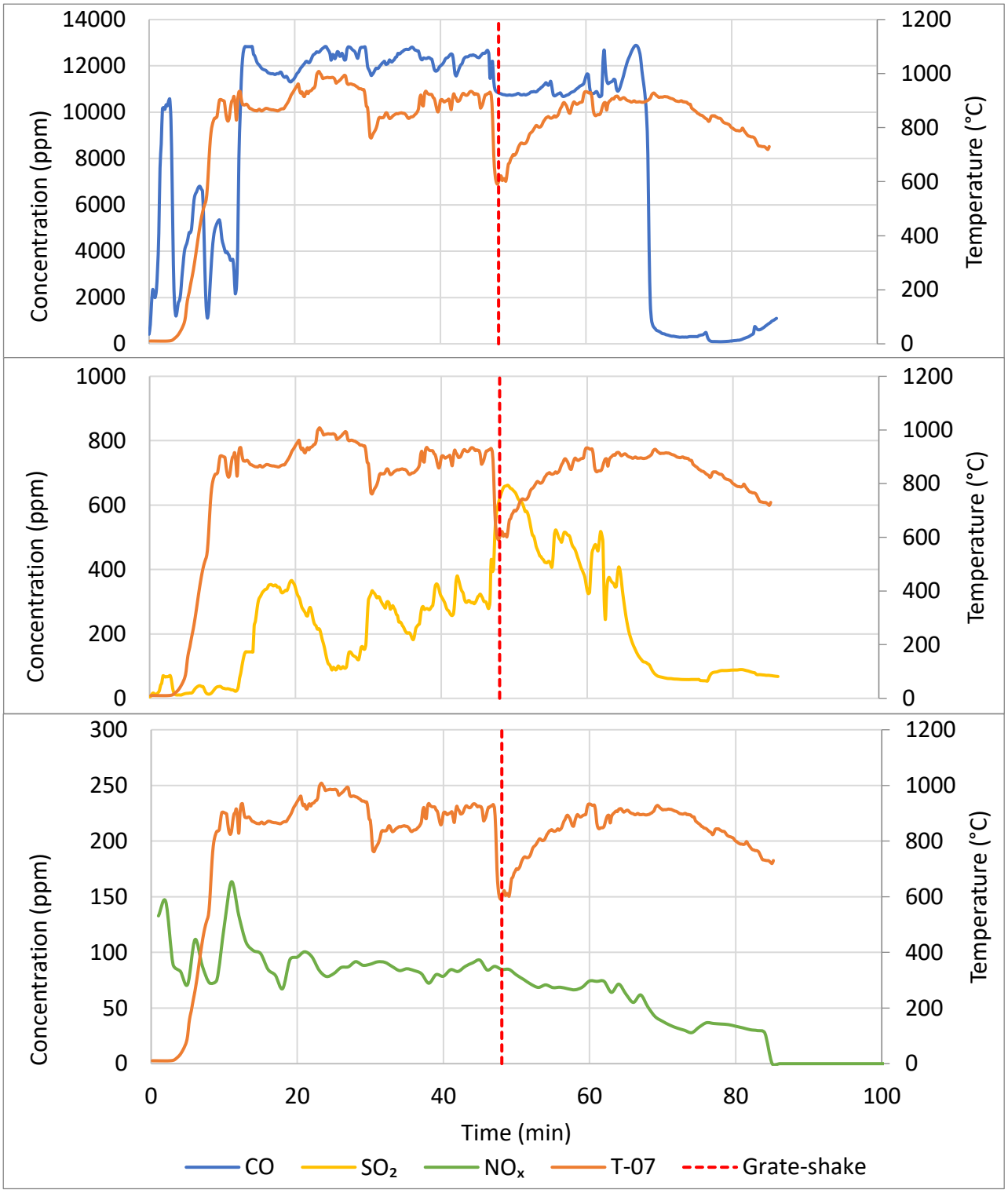

Figure J-10: CO, SO_2, and NO_x concentration and combustion zone temperature over time (75% biomass, low-power experiment)

Figure J-11 shows the CO, SO_2, and NO_x concentrations and combustion temperature during high-power combustion experiments using 90% biomass pellets.

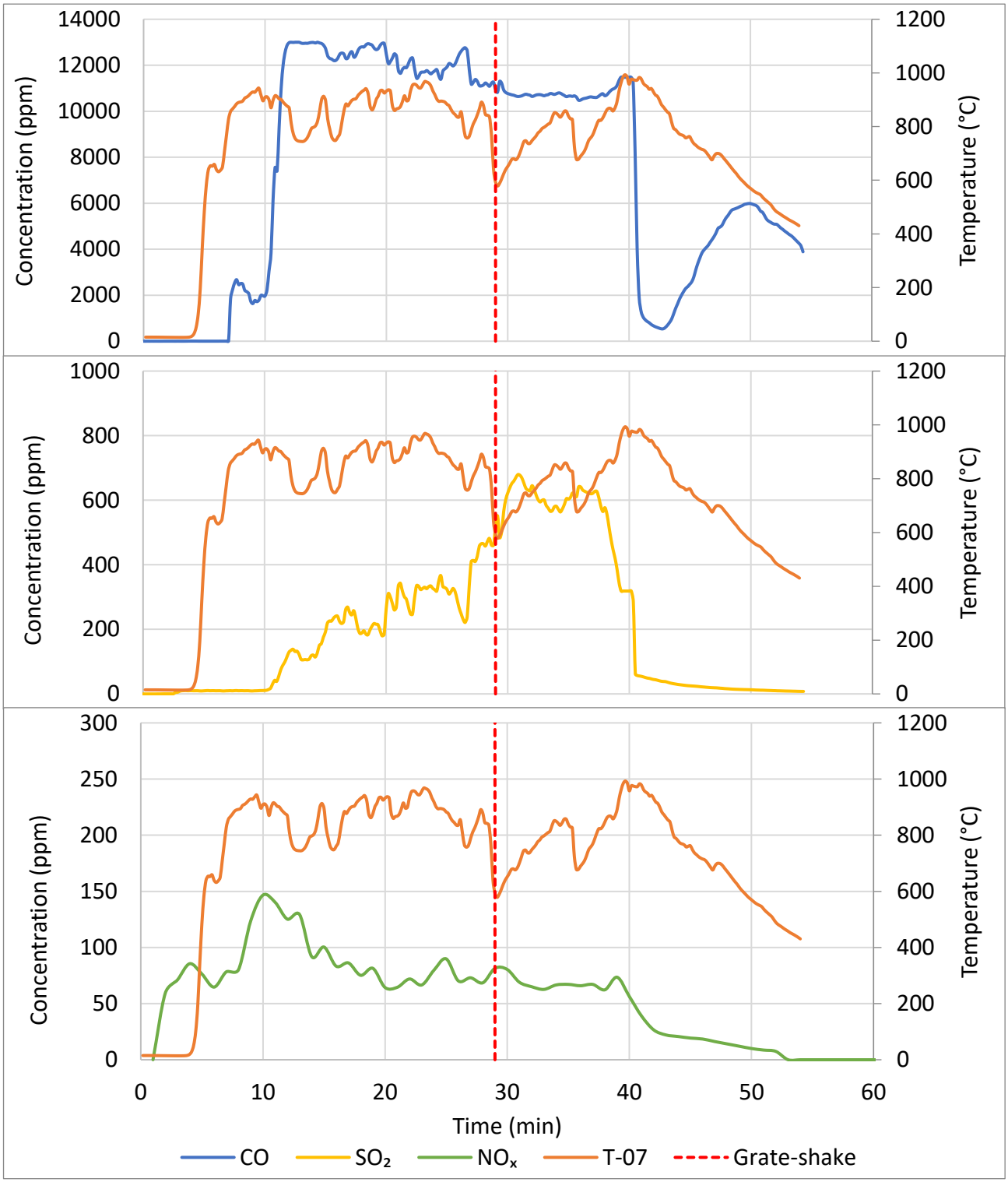

Figure J-11: CO, SO_2, and NO_x concentration and combustion zone temperature over time (90% biomass, high-power experiment)

Figure J-12 shows the CO, SO_2, and NO_x concentrations and combustion temperature during low-power combustion experiments using 90% biomass pellets.

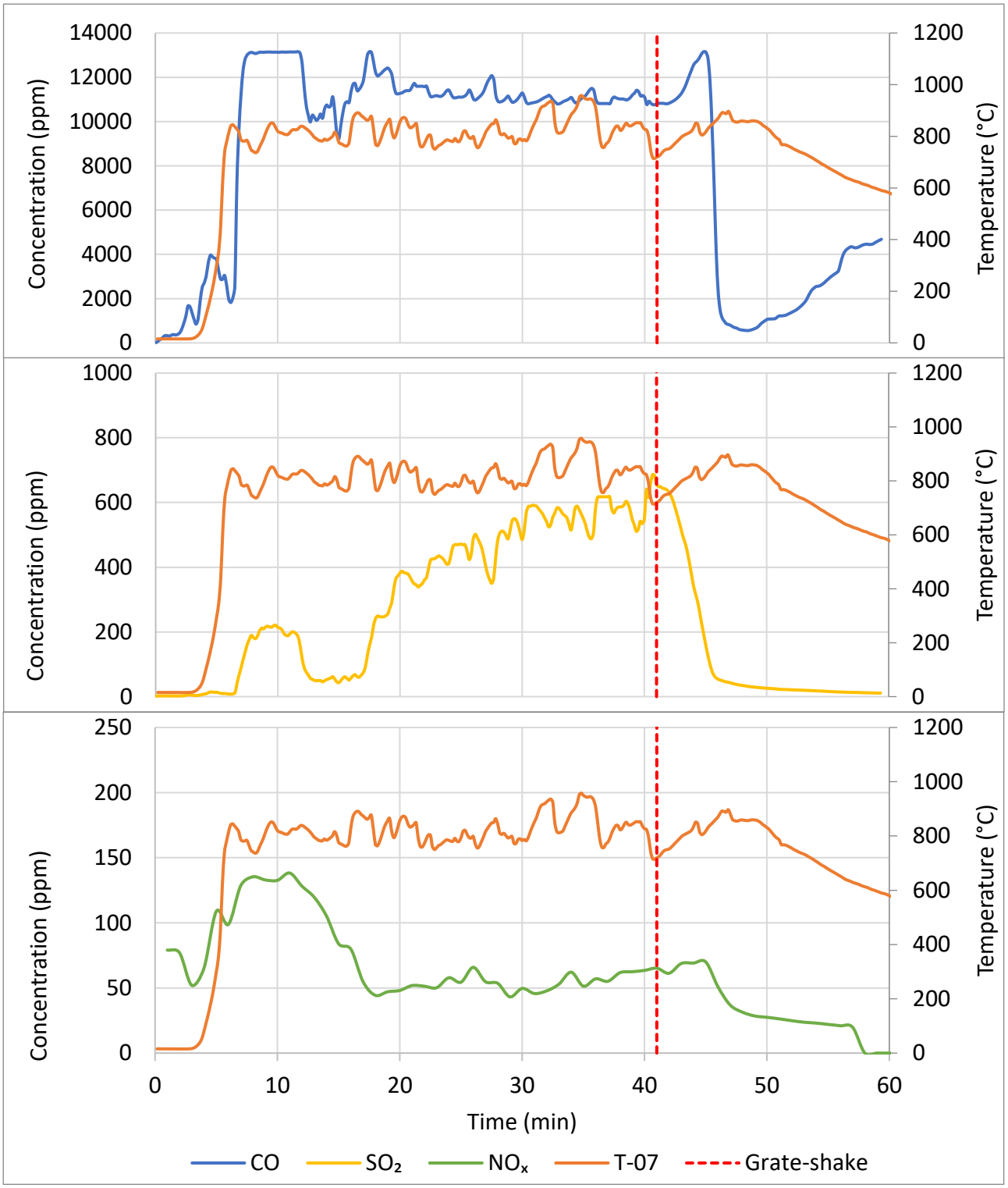

Figure J-12: CO, SO_2, and NO_x concentration and combustion zone temperature over time (90% biomass, low-power experiment)